TRANSPORTATION RESEARCH RECORD 1022

Analysis and Testing of Granular Bases and Subbases

TRB
TRANSPORTATION RESEARCH BOARD
NATIONAL RESEARCH COUNCIL
WASHINGTON, D.C. 1985

Transportation Research Record 1022
Price $17.90
Editor: Elizabeth W. Kaplan
Compositor: Harlow A. Bickford
Layout: Theresa L. Johnson

modes
1 highway transportation
3 rail transportation
4 air transportation

subject areas
61 soil exploration and classification
62 soil foundations
63 soil and rock mechanics

Transportation Research Board publications are available by ordering directly from TRB. They may also be obtained on a regular basis through organizational or individual affiliation with TRB; affiliates or library subscribers are eligible for substantial discounts. For further information, write to the Transportation Research Board, National Research Council, 2101 Constitution Avenue, N.W., Washington, D.C. 20418.

Printed in the United States of America

Library of Congress Cataloging in Publication Data
National Research Council. Transportation Research Board.
Analysis and testing of granular bases and subbasses.

(Transportation research record ; 1022)
1. Roads–Base courses–Addresses, essays, lectures.
2. Roads–Subgrades–Addresses, essays, lectures.
3. Road materials–Testing–Addresses, essays, lectures.
4. Granular materials–Testing–Addresses, essays, lectures. I. National Research Council (U.S.). Transportation Research Board. II. Series.
TE7.H5 no. 1022 380.5 s [625.7'35] 85-25829
[TE212]
ISBN 0-309-03911-8 ISSN 0361-1981

Sponsorship of Transportation Research Record 1022

GROUP 2–DESIGN AND CONSTRUCTION OF TRANSPORTATION FACILITIES
Robert C. Deen, University of Kentucky, chairman

Soil Mechanics Section
Raymond A. Forsyth, California Department of Transportation, chairman

Committee on Soils and Rock Instrumentation
William H. Hansmire, Parsons, Brinckerhoff, Quade and Douglas, Inc., chairman
Stephen F. Brown, Jerry C. Chang, John B. Gilmore, Gordon E. Green, Joseph B. Hannon, Robert D. Holtz, Richard H. Ledbetter, Verne C. McGuffey, Vincent G. Miller, Gregory N. Richardson, Ernest T. Selig, Anwar E. Z. Wissa

Committee on Mechanics of Earth Masses and Layered Systems
Robert D. Stoll, Columbia University, chairman
S. S. Bandyopadhyay, Walter R. Barker, Richard D. Barksdale, Jerry C. Chang, J. M. Duncan, Kingsley Harrop-Williams, John S. Horvath, T. Kuppusamy, Zenon G. Kyfor, Michael S. Mamlouk, Gerald P. Raymond, Robert L. Schiffman, H. J. Siriwardane, Harry E. Stewart, Kenneth H. Stokoe II, Harvey E. Wahls, John L. Walkinshaw, T. H. Wu

Committee on Subsurface Drainage
Gary L. Hoffman, Pennsylvania Department of Transportation, chairman
Gordon R. Benson, Robert G. Carroll, Jr., Barry J. Dempsey, Wilbur M. Haas, Kent A. Healy, S. Bennett John, Gary L. Klinedinst, Donald C. Long, Robert H. Manz, Vernon J. Marks, C. Robert McQuary, Lyle K. Moulton, Edwin C. Novak, Jr., Willard G. Puffer, Hallas H. Ridgeway, George W. Ring III, L. David Suits, William D. Trolinger, Hugh L. Tyner, Walter C. Waidelich, David C. Wyant, Thomas F. Zimmie

Geology and Properties of Earth Materials Section
Wilbur M. Haas, Michigan Technological University, chairman

Committee on Exploration and Classification of Earth Materials
Martin C. Everitt, Louis Berger International, chairman
Robert K. Barrett, P. J. Beaven, John A. Bischoff, H. Allen Gruen, Robert K. H. Ho, Robert B. Johnson, Jeffrey R. Keaton, C. William Lovell, B. Sen Mathur, Donald E. McCormack, Jim McKean, Olin W. Mintzer, Zvi Ofer, Harold T. Rib, Lawrence C. Rude, James Chris Schwarzhoff, Berke L. Thompson, Sam I. Thornton, J. Allan Tice, A. Keith Turner, Gilbert Wilson, Duncan C. Wyllie

Neil F. Hawks, Transportation Research Board staff

Sponsorship is indicated by a footnote at the end of each paper. The organizational units, officers, and members are as of December 31, 1984.

Contents

Addresses of Authors

Alexander, Don R., USAE Waterways Experiment Station, P.O. Box 631, Vicksburg, Miss. 39180-0631
Aziz, Cecep N., Department of Civil Engineering, North Carolina State University, Raleigh, N.C. 27695-7908
Borden, Roy H., Department of Civil Engineering, North Carolina State University, Raleigh, N.C. 27695-7908
Brown, S. F., Department of Civil Engineering, University of Nottingham, University Park, Nottingham NG7 2RD, England
Bush, Albert J., III, USAE Waterways Experiment Station, P.O. Box 631, Vicksburg, Miss. 39180-0631
Davies, Trevor G., Department of Civil Engineering, State University of New York at Buffalo, Buffalo, N.Y. 14260
Diyaljee, Vishnu A., Alberta Transportation, 4999 98th Avenue, Edmonton, Alberta T6B 2X3, Canada
Gabr, Muhammed A., Department of Civil Engineering, North Carolina State University, Raleigh, N.C. 27607
Garrick, Norman W., School of Civil Engineering, Purdue University, West Lafayette, Ind. 47907
Greenstein, Jacob, Louis Berger International, Inc., 100 Halsted Street, East Orange, N.J. 07019
Jenkins, James L., System Research Laboratory, 2800 Indian Ripple Road, Dayton, Ohio 45440
Khedr, Safwan A., Department of Civil Engineering, University of Kansas, Lawrence, Kans. 66045
Khosla, N. Paul, Department of Civil Engineering, North Carolina State University, Raleigh, N.C. 27695-7908
Kraft, David C., Department of Civil Engineering, University of Kansas, Lawrence, Kans. 66045
Lowder, Wesley M., Department of Civil Engineering, North Carolina State University, Raleigh, N.C. 27695-7908
Mamlouk, Michael S., Department of Civil Engineering, Arizona State University, Tempe, Ariz. 85287
Motan, E. Sabri, Department of Civil and Environmental Engineering, Clarkson University, Potsdam, N.Y. 13676
Norman-Gregory, Gillian M., Department of Civil Engineering, University of Massachusetts, Amherst, Mass. 01002
Pappin, J. W., Ove Arup Partnership, 13 Fitzroy Street, London W1P 6BQ, England
Raad, Lutfi, Department of Civil Engineering, American University of Beirut, 850 Third Avenue, New York, N.Y. 10022
Raymond, Gerald P., Department of Civil Engineering, Queen's University, Kingston, Ontario K7L 3N6, Canada
Roesset, Jose M., Department of Civil Engineering, The University of Texas at Austin, Austin, Tex. 78712
Scholer, Charles F., School of Civil Engineering, Purdue University, West Lafayette, Ind. 47907
Selig, Ernest T., Department of Civil Engineering, University of Massachusetts, Amherst, Mass. 01002
Shao, Ko-Young, Department of Civil Engineering, The University of Texas at Austin, Austin, Tex. 78712
Sharp, Richard W., Department of Main Roads, Robinson Street, Goulburn, New South Wales 2580, Australia
Stewart, Harry E., School of Civil and Environmental Engineering, Cornell University, Ithaca, N.Y. 14853
Stubstad, R. N., Dynatest Consulting, Inc., P.O. Box 71, Ojai, Calif. 93023
Ullidtz, P., The Technical University of Denmark, Lyngby 2800, Denmark
Uzan, Jacob, Faculty of Civil Engineering, Technion-Israel Institute of Technology, Haifa 32000, Israel
Wiseman, Gdalyah, Faculty of Civil Engineering, Technion-Israel Institute of Technology, Haifa 32000, Israel
Yandell, W. O., School of Civil Engineering, University of New South Wales, P.O. Box 1, Kensington 2033, Australia

Theoretical Response of Multilayer Pavement Systems to Dynamic Nondestructive Testing

TREVOR G. DAVIES and MICHAEL S. MAMLOUK

ABSTRACT

Nondestructive testing of highway and airport pavements has become increasingly popular. Although dynamic loading devices have become the method of choice because their field operation is relatively simple, fast, and economical, analysis of the test data remains problematic. Using a rigorous elastodynamic formulation, it is demonstrated in this paper that the dynamic phenomena of resonance and inertial damping within the subgrade may result in significant differences in pavement response to static and dynamic loading. Because static analyses are currently used to analyze the latter, significant errors may arise in back-calculating layer stiffnesses, particularly because the iterative schemes used in such analyses are ill-conditioned. Examination of the data obtained from a study of the response of four-layer flexible pavements to excitation by the Road Rater device for a wide range of frequencies suggests that no simple correlation between dynamic and static deflections can be developed. Some improvement in current practice may be effected by carrying out tests over the entire operating range of frequencies to ensure that the measured deflections are not corrupted by spurious subgrade resonances.

Nondestructive testing has been extensively used in the last few decades for evaluation of the load-deformation response of highway and airfield pavement systems. The results of such surveys have significant impact on the operation and maintenance of these facilities and, therefore, accurate interpretation of the test data is important.

Nondestructive testing can be divided into two main types: seismic techniques (associated with time measurements) and surface loading tests (associated with deflection measurements). Extraction of layer stiffnesses from these data is the crux of the problem, which has not yet been fully resolved.

The seismic techniques normally employed in highway engineering are based on measurement of the velocities of the Rayleigh waves (surface waves) of the pavement system (1,2). Such techniques have not gained wide acceptance, partly as a consequence of the relative sophistication required in field operation and in interpretation of the test data. Surface loading tests, on the other hand, have been extensively used by many highway agencies because of their simplicity and their ability to model real traffic load intensities and durations. Thus the stiffnesses computed from surface deflection measurements are more nearly representative of field conditions.

Surface deflection measurement devices can be categorized as static (e.g., Benkelman Beam, California Traveling Deflectometer) and dynamic [e.g., Dynaflect, Road Rater, various vibratory devices (3), falling weight deflectometer]. The Dynaflect, the Road Rater, and the vibratory devices impart steady-state dynamic (harmonic) loading to loading plates, whereas the falling weight deflectometer imparts an impulsive load developed by a weight falling on a spring-loaded single plate. Most of the vibratory devices are capable of generating a wide range of loading frequencies and for that reason are preferred to the single frequency Dynaflect. Although the falling weight deflectometer simulates traffic loading somewhat better than do harmonic loading devices, a high degree of correlation between the test data obtained from the Road Rater and the falling weight deflectometer has been reported (4).

Analyses of the data obtained from dynamic loading devices have hitherto been based on either empirical approaches or elastostatic and viscoelastostatic models (5-9). Obviously, empirical correlations are restricted to conditions similar to those in which such correlations were originally developed, and, in the static analyses, the inertia of the pavement is neglected. In other words, it is assumed that the dynamic response of pavement structures is no different from the static response.

Experimental work performed by others emphasizes the difference between static and dynamic responses of pavement systems. For example, Hoffman and Thompson (4) operated a circular plate Road Rater at peak-to-peak loads of 2, 4, 6, and 8 kips and driving frequencies of between 6 and 30 Hz at 2-Hz intervals for each load. The results of those tests are shown in Figure 1 for three pavement sections with various layer thicknesses and material properties. The experimental results show that resonant frequencies (natural vibration frequencies) of 10, 18, and 16 Hz existed for the three pavement sections, respectively. These resonant frequencies were almost independent of load intensity and were within the normal range of operating frequencies. The resonant frequencies were different from one pavement section to another depending on layer thicknesses and material properties. The resonant frequencies of the pavement systems cannot be explained by any static analysis.

In this paper, an elastodynamic solution is used to show that the static and dynamic responses of pavements may be significantly different even at low frequencies (Figure 2). This rather complex approach is necessary because one-degree of freedom approximations [e.g., Weiss (10)] cannot reproduce all

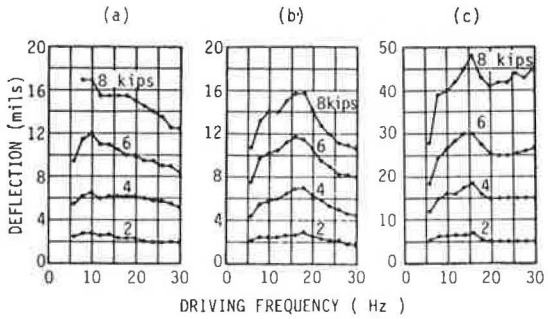

FIGURE 1 Experimental peak-to-peak deflection versus driving frequency of the Road Rater at three pavement sections (a) Sherrard: 4 in. AC, 14 in. crushed stone, (b) Monticello: 3.5 in. AC, 8 in. plant CAM, and (c) Deland: surface treatment, 8 in. granular base B *(4)*.

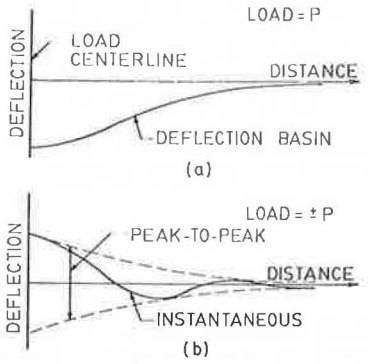

FIGURE 2 Surface deflection profiles for (a) static loading and (b) dynamic loading.

facets of the dynamic behavior of multi-degree of freedom pavement systems.

An analysis of the Road Rater device is presented. Similar results are to be expected for harmonic loading devices such as the Dynaflect and impulsive loading devices such as the falling weight deflectometer.

INTERPRETATION OF DEFLECTION DATA

Although empirical rules for assessing the integrity of pavements on the basis of nondestructive test data are commonly employed, in practice there is an increasing trend toward adoption of methods based on theoretical models of pavements. However, the inverse problem of determining material properties from pavement deflections caused by prescribed loads is difficult even if the assumption of linear elastic behavior of isotropic layers is valid. Given limited data, no unique solution can be determined although in practice the range of admissible solutions may be relatively narrow. The problem is compounded because it is necessary to employ iterative schemes [e.g., Kilareski and Anani (7)] to solve the inverse problem. Although the stiffness of the subgrade can often be determined reasonably accurately, the iterative schemes employed in practice are necessarily ill-conditioned and inevitably magnify the data and modeling errors. Thus, for the upper layers, the predicted stiffnesses may be considerably in error.

In principle, nonlinear elastic models of pavement structures (5) would appear to offer some improvement over the simpler linear analyses commonly used. Unfortunately, there are grave difficulties in applying such analyses in practice. Among these are the uncertainties in determining the in situ stress state, selection of an appropriate constitutive law, and determination of the material parameters. Subgrade response may depend on whether loading takes place under drained or undrained conditions, which in turn is dependent on soil type and loading rate.

Moreover, potentially grave modeling errors result from neglecting the inertial response of pavements to dynamic excitation. In the following sections, a brief description of an elastodynamic algorithm for harmonic loading of horizontally layered strata is described. The deflections predicted by this model are quite different from those of an equivalent static analysis. Thus the solution of the inverse problem using a static analysis may be subject to significant error.

METHOD OF ANALYSIS

The governing equation for steady-state elastodynamics (i.e., harmonic motion) is the well-known Helmholtz equation (11)

$$C_p^2 \, \text{grad}(\text{div}\, \underset{\sim}{u}) - C_s^2 \, \text{curl}(\text{curl}\, \underset{\sim}{u}) + \rho^2 \omega^2 \underset{\sim}{u} = 0 \qquad (1)$$

where C_p and C_s are the pressure and shear wave velocities, respectively; $\underset{\sim}{u}$ is the displacement vector; and ω is the circular frequency of excitation. The displacement vector in Equation 1 can be expressed in the form:

$$\underset{\sim}{u}(t) = \underset{\sim}{u}^* e^{i\omega t} \qquad (2)$$

in which $\underset{\sim}{u}^*$ are the (complex) amplitudes of the displacement vector, t denotes time, and i is the unit imaginary number. The wave velocities are related to the stiffness and mass density of the solid by the equations:

$$C_p = \{[E(1 - \mu)]/[(1 + \mu)(1 - 2\mu)\rho]\}^{1/2} \qquad (3)$$

$$C_s = \{E/[2(1 + \mu)\rho]\}^{1/2} \qquad (4)$$

where E, μ, and ρ are the Young's modulus, Poisson's ratio, and mass density, respectively.

Clearly, integration of Equation 1 for any but the simplest boundary conditions is impossible by analytical means. The only closed-form solution available is for a point load excitation in an infinitely extensive homogeneous medium. Solutions for the present (layered) problem must therefore be obtained by numerical means. In this analysis, the usual assumptions of material linearity and isotropy are invoked. Soil and pavement layers are assumed to be unbounded laterally but are underlain by a rigid (reflective) bedrock layer at a finite depth, and full interface bonding (no slip) conditions are assumed at the layer interfaces.

The numerical solution of Kausel and Peek (12), which is used here, involves subdivision of the given layered system into thin artificial sublayers. For each sublayer, a stiffness matrix in the so-called frequency-wave number (transform) domain may be found:

$$\begin{bmatrix} \bar{P}_1 \\ \bar{P}_2 \end{bmatrix} = [K] \begin{bmatrix} \bar{U}_1 \\ \bar{U}_2 \end{bmatrix} \qquad (5)$$

in which the superscript bar indicates transformed quantities; $\bar{P}$ and $\bar{U}$ are interface forces and displacements; subscripts 1 and 2 denote the upper and lower interfaces, respectively; and [K] is a matrix whose elements are simple algebraic functions of the mass densities and elastic moduli of the layer and the frequency of excitation. The simple form of [K] follows from the assumption that the displacements vary linearly (in the direction of layering) between adjacent interfaces. It is important, therefore, that sufficiently thin layers be specified to preserve accuracy. Stiffness matrices for each layer can then be assembled, in the finite element sense, to form a global stiffness matrix. The relative simplicity of this approximate method, in comparison with the "exact" methods that involve numerical evaluation of highly oscillatory infinite integrals (13), renders the layered pavement structure problem tractable.

PAVEMENT PROPERTIES

Material Damping

Material damping refers to the internal energy dissipation that occurs in real materials subjected to dynamic loading. Granular pavement materials (e.g., gravels) exhibit hysteretic damping behavior manifested by a frequency-invariant damping ratio; typical values for the damping ratio for such soils are approximately 5 percent (14). This value is adopted in the numerical study that follows. It should be noted, however, that by far the major component of energy dissipation in pavements results from radiation (geometric) damping; that is, the dispersion of energy from the source of excitation to the far field. Using the correspondence principle of viscoelasticity, material damping can be easily incorporated in the analysis by replacing Young's modulus in Equations 3 and 4 by its complex counterpart; that is,

$$E^* = E(1 + 2i\beta) \tag{6}$$

where β is the damping ratio.

Resilient and Dynamic Moduli

The stress-strain relations of isotropic elastic materials are, in classical formulations, expressed in terms of fundamental material parameters (e.g., Young's modulus and Poisson's ratio). But in highway engineering it has become common to define state-dependent parameters such as the resilient modulus and the dynamic modulus. These parameters are often used to interpret the nonlinear and the time-dependent response of pavement materials. The resilient modulus is obtained by subjecting a specimen to repeated stress reversals and measuring the recoverable strain after a number of load applications, as shown in Figure 3. The resilient modulus, therefore, is the Young's modulus of the material after many load repetitions (i.e., the shake-down modulus of the material), which is normally different from the initial value. On the other hand, the dynamic modulus is obtained by subjecting a finite specimen to harmonic loading: it is simply the ratio of the stress amplitude to the corresponding strain amplitude as shown in Figure 4.

Clearly, the resilient modulus is relevant in analyses of pavement deflections in that field data reflect the current stiffness of pavements. However, the dynamic modulus is irrelevant (except as noted later) to dynamic analyses of pavement deflections notwithstanding the apparently widely held contrary

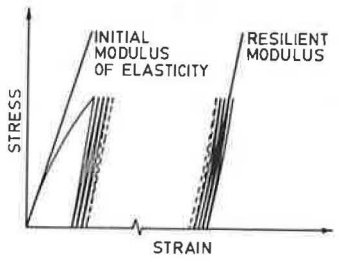

FIGURE 3 Definition of resilient modulus.

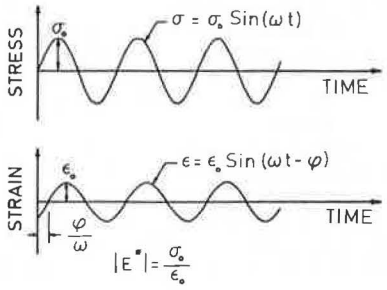

FIGURE 4 Definition of dynamic modulus.

view. Clearly, because the elastodynamic equations of equilibrium cannot be recovered from the corresponding static equations by substituting frequency-dependent moduli, analyses based on such methods must be inconsistent and often yield completely erroneous results. Such analyses cannot, for example, predict a resonant condition.

Laboratory measured values of complex moduli can, however, yield valuable information on the fundamental material parameters (stiffness, internal damping) provided that these tests are properly interpreted (e.g., with due recognition of the inertia of the specimen itself). Such data, combined with a rigorous elastodynamic theory for the pavement structure, offer the greatest promise for real progress in evaluating the response of pavements to moving loads.

ANALYSIS AND RESULTS

The theoretical analysis of the twin-plate Road Rater device (Figure 5) involved idealization of the loading platens by two flexible circular plates 3 in. in radius spaced 10.5 in. center-to-center. The geophones were assumed to be located 12 in. apart with the first one located midway between the two platens. Surface deflections were computed at each of the four geophones for a number of representative

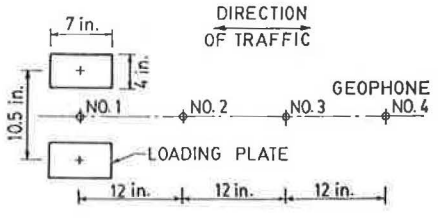

FIGURE 5 Schematic diagram of the Road Rater.

TABLE 1 Properties of Pavement Layers

Layer	Thickness H(in.)			Young's Modulus E(ksi)			Poisson's Ratio	Mass Density
	Thin	Medium	Thick	Soft	Medium	Stiff	μ	(lbm/ft^3)
Surface	1	2	4	100	500	2,000	0.35	150
Base	3	6	12	50	100	200	0.40	145
Subbase	6	12	24	10	20	40	0.40	135
Subgrade	150	150	150	4	8	16	0.45	120

pavement structures (Table 1) for frequencies of excitation of 0 to 50 Hz, which broadly encompass the capability of the Road Rater.

Figure 6 shows the displacement at the first geophone as a function of layer thickness and stiffness under static and harmonic (25 Hz) loading conditions of unit stress intensity. For both static and dynamic loading conditions, deformations are greatest for the thin, soft pavements. Moreover, in all cases the static displacements are greater than the dynamic displacements. For the thick, soft pavement, the static displacements are 50 percent greater than the dynamic displacements.

Typical data illustrating the influence of increasing frequency on the deflections measured at the geophones are shown in Figure 7. These data are normalized with respect to the static deflections. For each geophone, the dynamic deflections initially increase sharply with increasing frequency but thereafter decay. A medium thickness, stiff pavement was analyzed to obtain these data although similar results were obtained for pavements with the same geometry but consisting of medium stiffness and soft materials, respectively.

The initial increase in deflection at low frequencies is due to excitation of resonance in the subgrade (a phenomenon that is explored in more detail subsequently), and the relatively low deflections at higher frequencies are a manifestation of inertial effects. Neither of these phenomena can be reproduced by static analyses of this problem. Although the trend of the results is similar for pavements of different stiffnesses and geometries, the numerical data are sensitive to these parameters. Moreover, the deflections at different locations from the load are correlated only very approximately. This observation is evident from Figure 6, which shows that the deflection ratios at a typical frequency employed in practice (25 Hz) are sensitive to both geophone location and layer geometry. Whereas for thick pavement the deflection ratios are virtually equal at all geophones, the static displacement exceeds the dynamic displacement by approximately 30 percent. Consequently, pavement moduli would be overestimated by a similar margin if deflection data were analyzed by a static analysis. Such an analysis of pavement deflections for the thin pavement (Figure 8) raises greater difficulties because the deflection ratios are not the same for each geophone. In most iterative-solution schemes, the stiffness of the subgrade, which is assumed to be primarily a function of the deflection at the outermost geophone, would be underestimated by approximately 35 percent in this case. The relatively low deflection ratios at the geophones nearest the Road Rater would in consequence yield anomalously high moduli for the upper pavement layers (despite the virtually identical static and dynamic deflections for these geophones).

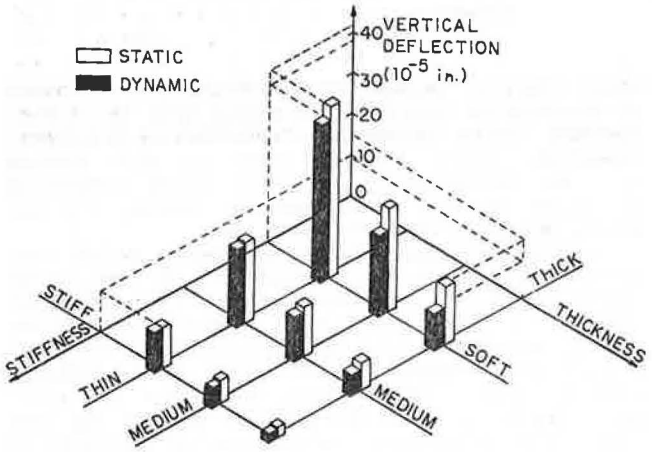

FIGURE 6 Surface deflections at geophone 1 under unit static and 25 Hz dynamic loading conditions.

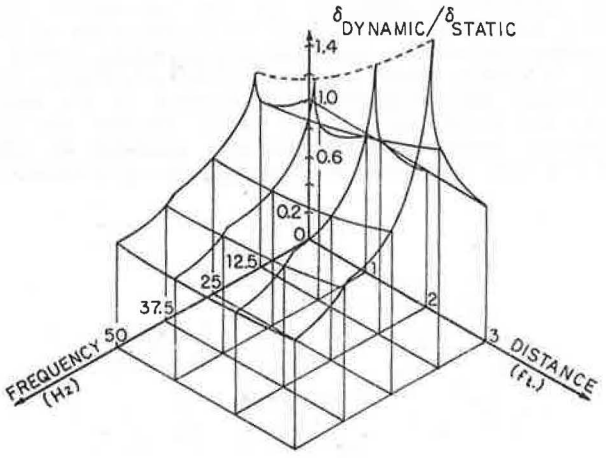

FIGURE 7 Dynamic-to-static surface deflection ratios for medium thickness, stiff pavement.

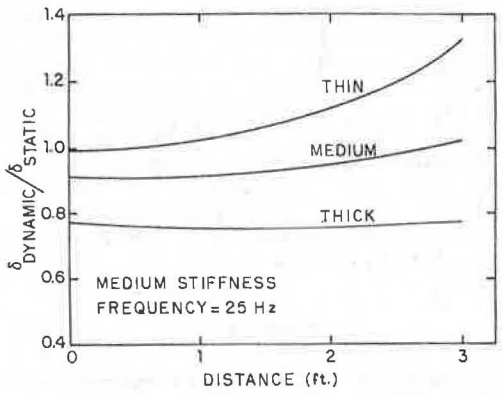

FIGURE 8 Dynamic-to-static surface deflection ratios at various geophone locations.

The effect of pavement stiffness on the dynamic response of pavements is shown in Figure 9. The plots for the soft, medium-stiff, and stiff pavements exhibit similar trends. Most noteworthy is that the peak deflection ratios (at resonance) are virtually the same for each of the three pavements, but the resonance frequencies are distinctly different. Examination of the data reveals that these resonant frequencies are proportional to the square root of the pavement stiffness and are, therefore, proportional to the wave velocities. Figure 10 shows the effect of the depth of subgrade on the dynamic response of the pavement. If the subgrade is shallow, marked resonances may occur and the dynamic deflections may greatly exceed those obtained under static loading conditions. The fundamental frequency when the first resonant mode is excited is almost inversely proportional to the depth of the subgrade, which lends credence to the supposition that resonance occurs principally in the subgrade. The deflection ratios at resonance are greatest for the most shallow subgrade. Clearly, at resonance a static analysis of deflection data will yield erroneous results. In practice, if a resonance condition is suspected, perhaps because of fluctuating geophone readings (9), then the Road Rater's frequency of excitation can be changed by the field operators. However, as Figure 10 shows, because the deflection ratios are unity at only one frequency, selection of an arbitrary frequency of operation will not in general prove satisfactory. Finally, it is worth noting that second harmonics are excited at frequencies approximately twice that of the fundamental. These resonances are, however, relatively small.

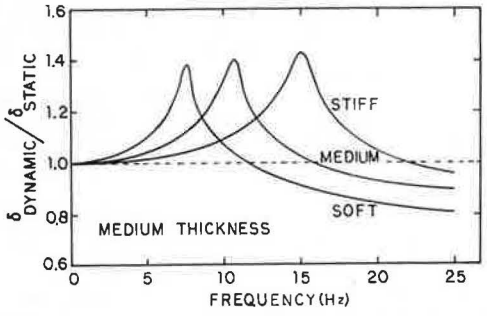

FIGURE 9 Influence of pavement stiffness on the pavement resonant response recorded at geophone 1.

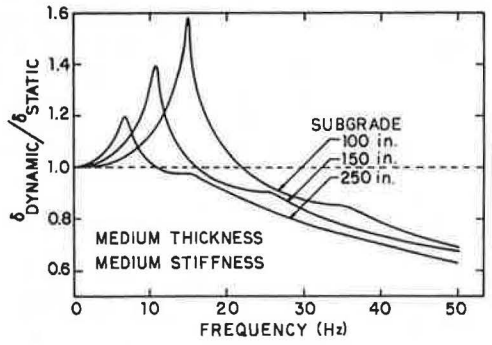

FIGURE 10 Influence of subgrade thickness on the pavement resonant response recorded at geophone 1.

As a working hypothesis, the evidence of Figures 9 and 10 suggests that resonance occurs when the frequency of excitation of the Road Rater satisfies the semiempirical equation:

$$f = 0.4\ C_S/H \tag{7}$$

where H is the thickness of the subgrade and C_S is the shear wave velocity of the subgrade.

If the frequency of excitation of the Road Rater is increased by 50 percent above the resonant frequency, obtained either by means of Equation 7 or by field observation, then the dynamic displacements measured at this higher frequency correspond closely to the static displacement, at least for the range of pavement structures considered in this study. Figures 11 and 12 are plots of the in-phase and 90-degree out-of-phase displacements relative to the Road Rater loading cycle for a typical pavement. The data are plotted as components of the complex amplitude of the deflection (u*) in which the real part Re(u) signifies the in-phase displacement and the imaginary part Im(u) signifies the out-of-phase displacement. Clearly, at low frequencies, the out-of-phase displacements are zero. The trend of the data is the same for all geophones (resonance occurs at approximately 11 Hz) but at high frequencies the geophones' responses become increasingly out-of-phase not only with the load but also with each other, which is manifested by differences in the ratios of Im(u) to Re(u) among the geophones. In reality, this implies that the wavelength of the surface waves generated by the Road Rater at high frequencies is of the same order of magnitude as the separation of the geophones. Therefore, only at low

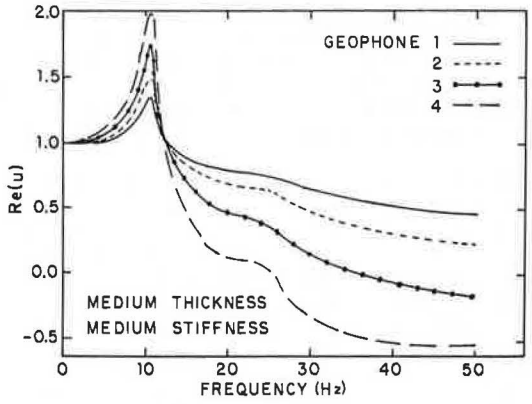

FIGURE 11 In-phase components of displacement.

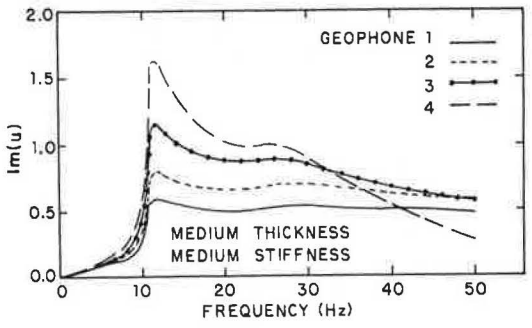

FIGURE 12 Out-of-phase components of displacement.

frequencies, or under static loading, is the notion of a dish-shaped deflection basin valid.

DISCUSSION

The numerical results of this study indicate that the response of pavements to dynamic loading may be significantly different from their response to static loading. These differences are principally the result of the inertial forces that resist the motion of the pavement and, at certain frequencies, excite resonances, not the result of the dynamic properties of the pavement materials themselves. Because static analyses cannot be used to predict these phenomena, back-calculation of the stiffness of pavement materials from deflection measurements gained under dynamic loading conditions should be undertaken with caution. Unfortunately, there does not appear to be any simple procedure for determining the deflection ratios as a function of frequency of excitation, pavement stiffness and geometry, and geophone location. Even for a given pavement, the deflection ratios are not the same at each geophone. The evidence suggests that deflection ratios tend to increase with increasing subgrade stiffness and decreasing pavement stiffness but tend to decrease at high frequencies (beyond the resonant frequency). The latter trend is simply a consequence of the inertial forces that increase rapidly with increasing frequency.

Perhaps the most interesting result obtained from this study is the observation that resonances may be excited in the subgrade. At or near these resonant frequencies, the dynamic deflections may be substantially higher than the corresponding static deflections. Thus, at some higher frequency, because the deflection ratios tend to decrease with increasing frequency, the dynamic and static deflections become equal. As a consequence, under these conditions a static analysis of the dynamic deflections will yield the correct values of the pavement layer stiffnesses. As a good first approximation it can be assumed that resonance occurs simultaneously at all geophones although this is not a necessary assumption.

On the basis of this study, it would appear reasonable to suggest that Road Rater deflection measurements should be secured at a number of different frequencies in order to determine the displacement-frequency response. From these data it should be possible to make a good estimate of the static deflection response. The evidence of this study suggests that a frequency of excitation 50 percent higher than the resonant frequency will yield deflection ratios of unity, but caution should be exercised in applying this result in practice because field conditions obviously depart in many ways from the idealized model analyzed here. Devices such as the Dynaflect, which operates at a fixed frequency (8 Hz) and cannot offer the flexibility necessary to explore the frequency response of pavements, should be used with caution.

CONCLUSIONS

Pavement deflections generated by such vibratory loading devices as the Road Rater may be substantially different from those obtained under static loading conditions.

Static analyses of dynamic pavement deflections may yield misleading results if the operating frequency of the loading device is approximately equal to the resonant frequency of the pavement system or is so high that inertial forces become dominant.

Resonance arises principally in the subgrade and may be quite marked if the subgrade is shallow. In practice, a resonant condition may be detected in extreme cases by unsatisfactory operation of the data acquisition devices although, more generally, deflection frequency plots may be constructed for this purpose.

ACKNOWLEDGMENTS

The authors gratefully acknowledge the generosity of E. Kausel of the Massachusetts Institute of Technology who provided the computer program used in this study. Computational and other facilities were furnished by courtesy of the Department of Civil Engineering at the State University of New York at Buffalo.

REFERENCES

1. W. Heukelom and C.R. Foster. Dynamic Testing of Pavements. Journal of Soil Mechanics and Foundation Division, ASCE, Vol. 86, No. SM1, Feb. 1960, pp. 1-28.
2. S. Nazarian and K.H. Stokoe II. Nondestructive Testing of Pavements Using Surface Waves. In Transportation Research Record 993, TRB, National Research Council, Washington, D.C., 1984, pp. 67-79.
3. W.M. Moore, D.I. Hanson, and J.W. Hall. An Introduction to Nondestructive Structure Evaluation of Pavements. Transportation Research Circular 189, TRB, National Research Council, Washington, D.C., 1978, 33 pp.
4. M.S. Hoffman and M.R. Thompson. Comparative Study of Selected Nondestructive Testing Devices. In Transportation Research Record 852, TRB, National Research Council, Washington, D.C., 1982, pp. 32-41.
5. M.S. Hoffman and M.R. Thompson. Backcalculating Nonlinear Resilient Moduli from Deflection Data. In Transportation Research Record 852, TRB, National Research Council, Washington, D.C., 1982, pp. 42-51.
6. L.H. Irwin. Determination of Pavement Layer Moduli from Surface Deflection Data for Pavement Performance Evaluation. Proc., Fourth International Conference on the Structural Design of Asphalt Pavements, University of Michigan, Ann Arbor, Aug. 1977, Vol. 1, pp. 831-840.
7. W.P. Kilareski and B.A. Anani. Evaluation of In-situ Moduli and Pavement Life from Deflection Basins. Proc., Fifth International Conference on the Structural Design of Asphalt Pavements, Delft University of Technology, The Netherlands, Aug. 1982, Vol. 1, pp. 349-366.
8. B.F. McCullogh and A. Taute. Use of Deflection Measurements for Determining Pavement Material Properties. In Transportation Research Record 852, TRB, National Research Council, Washington, D.C., 1982, pp. 8-14.
9. G.W. Sharpe, H.F. Southgate, and R.C. Deen. Dynamic Pavement Deflections. Journal of the Transportation Engineering Division, ASCE, Vol. 107, No. TE2, March 1981, pp. 167-181.
10. R.A. Weiss. Pavement Evaluation and Overlay Design: A Method that Combines Layered-Elastic Theory and Vibratory Nondestructive Testing. In Transportation Research Record 700, TRB, National Research Council, Washington, D.C., 1979, pp. 20-34.
11. A.C. Eringen and E.S. Suhubi. Elastodynamics: Vol. 2, Linear Theory. Academic Press, New York, 1975.

12. E. Kausel and R. Peek. Dynamic Loads in the Interior of a Layered Stratum: An Explicit Solution. Bulletin of the Seismological Society of America, Vol. 72, No. 5, Oct. 1982, pp. 1459-1481.
13. R.J. Apsel. Dynamic Green's Functions for Layered Media and Applications to Boundary-Value Problems. Ph.D. dissertation. University of California at San Diego, 1979.
14. F.E. Richart, Jr., J.R. Hall, Jr., and R.D. Woods. Vibrations of Soils and Foundations. Prentice-Hall, Inc., Englewood Cliffs, N.J., 1970.

Publication of this paper sponsored by Committee on Mechanics of Earth Masses and Layered Systems.

Dynamic Interpretation of Dynaflect and Falling Weight Deflectometer Tests

JOSE M. ROESSET and KO-YOUNG SHAO

ABSTRACT

The Dynaflect and the falling weight deflectometer are commonly used for nondestructive testing of pavements. In both cases a dynamic load is imparted, and the determination of the mechanical properties of the pavement, the base, and the subbase is normally performed by comparing the measured deflections at various points along the surface to results of static analyses that consider the subbase as a homogeneous, elastic half-space. In this paper, the displacements obtained from dynamic analyses are compared to those provided by conventional static programs when the subbase is a homogeneous soil stratum of finite depth resting on a much stiffer rocklike material and when the soil properties increase smoothly with depth, as is often the case. The results of these comparisons indicate that for certain ranges of depth to bedrock a static interpretation of the Dynaflect and falling weight deflectometer tests may lead to substantial errors. Situations in which these errors are important are more likely to be encountered with the Dynaflect than with the falling weight deflectometer.

The Dynaflect and the falling weight deflectometer are commonly used for nondestructive testing of pavements. The Dynaflect consists of a force generator and five geophones housed in a small trailer, which is towed by a light vehicle. The loading system consists of two counterrotating eccentric masses. The resulting vertical force varies harmonically with time. At a frequency of 8 Hz, a 1,000-lb peak-to-peak oscillating force and a base load of 1,000 lb are transmitted to the pavement through the loading wheels. The resulting deflection basin is measured by five geophones that are mounted on the trailer draw bar at 12-in. intervals. The positions of the geophones (ST1 through ST5) with respect to the wheels are shown schematically in Figure 1.

The falling weight deflectometer has a 330.7-lb (150-kg) weight mounted on a vertical shaft and housed in a compact trailer that can easily be towed by most conventional passenger cars. The weight is hydraulically lifted to a predetermined height (ranging from 0 to 15.7 in. or 0 to 400 mm). It is then dropped onto a rubber pad 11.8 in. (300 mm) thick, that helps to distribute the load uniformly over the loading area. The resulting load is a force impulse with a duration of approximately 30 msec and a peak magnitude ranging from 9 to 14,000 lbs (0 to 60 000 N) depending on the drop height. The peak force and maximum deflections at various points along the surface are measured by load cells and velocity transducers. The applied pressure is measured in kilopascals and the deflections in micrometers.

In the case of the Dynaflect the deflections measured at the various stations represent the amplitudes of the steady-state displacements at a given frequency (8 Hz). For the falling weight deflectometer they are the peak displacements under a transient-type excitation. In both cases the tests are dynamic in nature, but the interpretation of their results to estimate the elastic properties of the pavement, base, and subbase relies on static analyses. Furthermore, these analyses assume that the soil in the subbase is an elastic, homogeneous, and isotropic half-space. In many cases soil properties

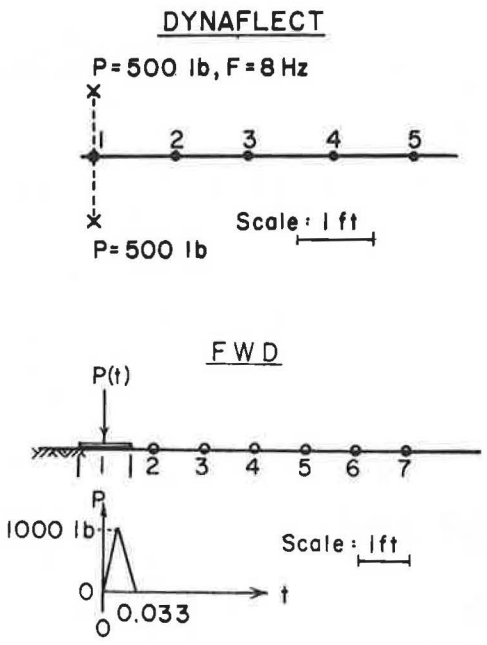

FIGURE 1 Geometric configuration of loads and stations for Dynaflect and falling weight deflectometer.

will vary with depth and the soil will be underlain at some depth by stiffer, rocklike material.

The purpose of this work is to determine the dynamic displacements at points along the surface of a pavement excited by forces simulating the excitation of the Dynaflect and the falling weight deflectometer. These displacements are compared for various depths to bedrock with those resulting from static analyses for the same soil profile and assuming an elastic half-space (the normal assumption). The dynamic deflection bulbs obtained from the analyses are then used as input for the standard backfiguring process to estimate the elastic moduli of the pavement, base, and subbase in order to assess the errors induced by neglecting dynamic effects.

FORMULATION

Consider a soil deposit that consists of horizontal layers. The mass density and the elastic moduli of the soil may change with depth, from layer to layer, but are assumed to be constant over each layer. For the present application the top layer would represent the pavement (assuming that it extends to infinity in both horizontal directions), the second layer would be the base, and the remaining layers would represent the soil of the subbase. An accurate solution would require consideration of the finite width of the pavement. Even so, for the purposes of this study, these simplifying assumptions should not be unreasonable. The determination of the response of this soil deposit to dynamic loads applied at the surface (or at any point within the soil mass) falls mathematically into the area of wave propagation theory.

The formulation of these problems always starts by considering steady-state harmonic forces and displacements at a given frequency. For a harmonic excitation, as caused by a vibrating machine rotating at a specified velocity (case of the Dynaflect), the solution at the corresponding frequency provides directly the desired results. For an arbitrary transient excitation (case of the falling weight deflectometer), the time history of the specified forces must be decomposed into different frequency components using a Fourier series, or more conveniently a Fourier transform. Results are then obtained for each term of the series (each frequency) and combined to obtain the time history of displacements (inverse Fourier transform).

For an isolated layer with uniform properties, the stresses and displacements along the top and bottom surfaces can be expanded in a double Fourier series (or Fourier transform) in the two horizontal directions for Cartesian coordinates, or in a Fourier series in the circumferential direction and a series of modified Bessel functions in the radial direction for cylindrical coordinates. For each term of these series, corresponding to a given wave number, there can be determined closed-form analytical expressions in the form of a transfer matrix relating amplitudes of stresses and displacements at the bottom surface to the corresponding quantities at the top (or vice versa). This approach [Thomson (1) and Haskell (2)] has served as the basis for most studies on wave propagation through layered media in the last 30 years. An alternative is to relate the stresses at both surfaces to the displacements, obtaining a dynamic stiffness matrix for the layer (3), which can be used and understood in much the same way as those in structural analysis. For a half-space, the stiffness matrix relates directly stresses and displacements at the top surface because the bottom surface is pushed to infinity. Assembling the stiffness matrices of the different layers, there can be obtained a stiffness matrix for the complete soil deposit, which relates forces per unit of area applied at the free surface, or the interfaces between the layers, to the displacements at the same elevations.

The terms of the transfer or stiffness matrices of each layer are transcendental functions (complex exponentials). In addition, results must be obtained for each term of the Fourier series decomposition (each wave number), then combined, normally by numerical integration, to obtain the solution for a specified load distribution. On the other hand, the thickness of the layers is controlled only by physical considerations and the assumption of uniform properties. This makes the procedure particularly convenient when dealing with a homogeneous half-space or a small number of layers but extremely expensive when a large number of layers are needed to reproduce properly the variation of soil properties with depth. Formulations along these lines have been implemented by Gazetas (4) in Cartesian coordinates and by Apsel (5) in cylindrical coordinates.

When the layers are extremely thin, the transcendental functions representing the variation of displacements with depth can be approximated over each layer by a straight line (or higher order polynomial expansions). The solution (displacements and stresses) is then expressed in terms of the exact analytical expressions in the two horizontal (or radial and circumferential) directions and in terms of simpler polynomial expansions in the vertical direction (as in a finite element formulation). This approximation leads to much simpler algebraic expressions for the terms of the transfer or stiffness matrices of the layers. In addition, when the soil is underlain by a much stiffer, rocklike material, which can be considered rigid, it is possible to determine the wave numbers (eigenvalues) and the mode shapes (eigenvectors) of the waves propagating through the soil deposit by solving an algebraic eigenvalue problem (6,7). Expressing the solution in terms of these mode shapes (eigenfunction expansion), Kausel (8) was able to obtain explicit solutions for the displacements caused by harmonic dy-

namic loads in a layered soil deposit. Kausel's formulation is particularly efficient from the point of view of computation, but the layers must be sufficiently thin to reproduce accurately the variation of the displacements with depth with a piecewise linear approximation.

Because the purpose of this work was to investigate the effects of depth to bedrock and variation of soil properties with depth on the dynamic response of a pavement, it was decided to use Kausel's formulation. The formulation was implemented in a computer program and the results were compared with those published by Kausel (8) with excellent agreement. Because of the discrete nature of the formulation, before it is applied, an appropriate mesh size (thickness of the sublayers) to guarantee an accurate solution must be determined.

Studies were conducted first for static loads (zero frequency), a homogeneous soil deposit of finite depth, and a vertical load on the surface uniformly distributed over a circular area with a radius (r_o) of 1 in. (simulating the loading in the Dynaflect) or 6 in. (approximate dimensions of the loading plate of the falling weight deflectometer). The properties of the soil deposit are shown in Figure 1. This represents another approximation because the load distribution for the Dynaflect will be more nearly elliptical. This simplification appears to be justified for the purposes of this study. A model with all layers of the same thickness was initially considered. Figure 2 shows typical results for a deposit 40 ft deep. The displacements at the center of the loaded area and at distances (d) of 2 and 4 ft from this point are divided by the exact solution and plotted versus the inverse of the number of layers. Ten layers correspond, therefore, to a layer thickness of 4 ft. It can be seen from this figure that excellent results are obtained at distances of 2 and 4 ft even with the coarser mesh (10 layers). The error for a distance of 2 ft is slightly larger for the small loaded area (radius of 1 in.), but it is only 2 percent with the coarse mesh. Results at the center of the loaded area are, on the other hand, extremely poor even when taking

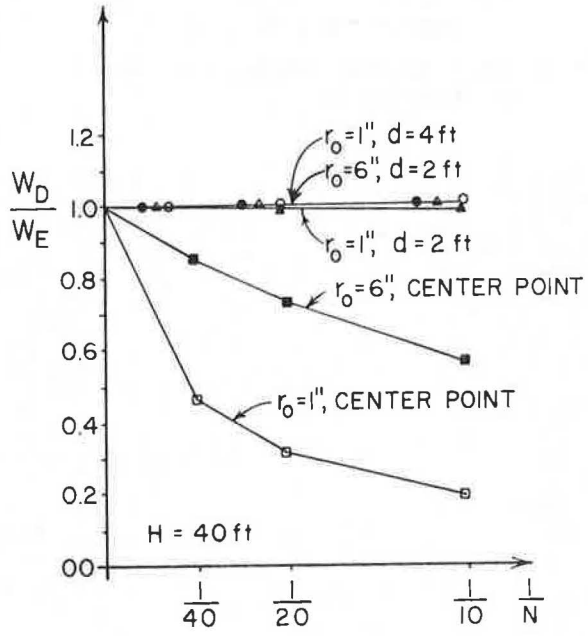

FIGURE 2 Variation of displacements with number of layers at H = 40 ft, W_E = exact solution.

40 layers (thickness of 1 ft for each layer), and they are much worse for the small loaded area. This indicates that for static loads the thickness of the layers has to decrease with decreasing distance between the load and the point where displacements are computed.

Figure 3 shows the ratio (w_H/w_∞) where w_H is the displacement for a stratum of depth H and w_∞ is the displacement for a half-space. The displacements are computed at the center of the loaded area and at distances (d) of 2 and 4 ft. They are plotted versus the inverse of the stratum thickness to better illustrate the convergence rate. The results indicate that the displacement is nearly inversely proportional to H. It is interesting to note that at the center of the loaded area the displacements for a stratum with a depth of only 8 ft are already within 1 percent of the results for a half-space with a radius of 1 in. and within 5 percent for the 6-in. radius. The depth needed to reproduce a half-space increases clearly with increasing distance between the load and the point where displacements are computed. This suggests also that close to the load the static displacements are affected only by the soil properties near the surface, whereas for increasing distances the soil properties at larger depths will influence the results more significantly.

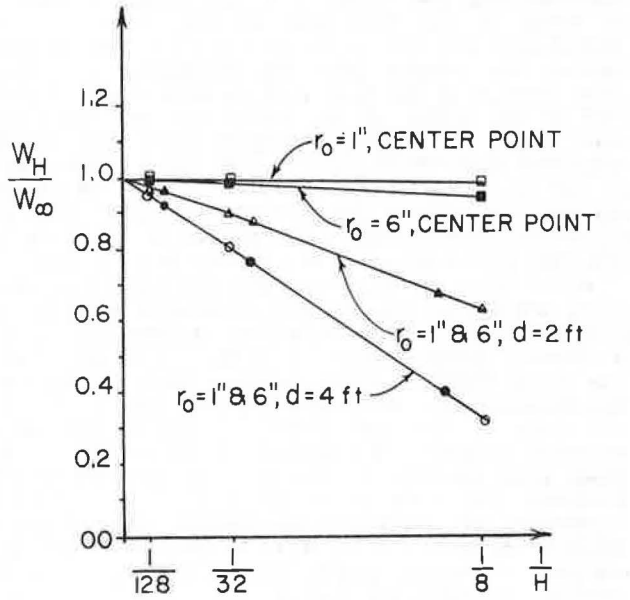

FIGURE 3 Variation of displacements with depth to bedrock.

On the basis of the observations from these two series of studies, it was decided that an improvement in the accuracy and the economy of the computations could be obtained by taking thin sublayers near the surface and gradually increasing their thickness with depth. The distance from the center of the loaded area to the point where the displacements are computed was designated D, and a rule was derived to automatically generate a desired mesh. According to this rule the first D ft are divided into 2N sublayers of equal thickness, and the next D ft are divided into N sublayers. N sublayers are then used for the following 2D ft, the next 4D ft, and so forth. When results are desired under the loaded area the distance D is replaced by the radius of the loaded area. For a nonhomogeneous soil deposit (such as a pavement), the thickness of each

TABLE 1 Displacements for Different Meshes (10^{-8} ft)

Radius of Disk (in.)	Center Point				d = 2 ft				d = 4 ft			
	H (ft)	Fine	Standard	Coarse	H (ft)	Fine	Standard	Coarse	H (ft)	Fine	Standard	Coarse
6					2							
	8	35.27	34.88	33.48	8	2.971	2.970	2.909	8	0.7609	0.7664	0.7613
	32	36.58	36.20	34.78	32	4.237	4.230	4.148	32	1.887	1.884	1.847
	128	36.92	36.53	35.10	128	4.566	4.557	4.472	128	2.214	2.209	2.168
1	5.33	219.6	217.3	208.7	8	2.932	2.930	2.873	8	0.7553	0.7607	0.7560
	21.33	221.6	219.2	210.7	32	4.200	4.192	4.113	32	1.883	1.879	1.843
	85.33	222.1	219.8	211.2	128	4.529	4.519	4.437	128	2.209	2.205	2.164

sublayer is the smaller of the value suggested by the rule or the actual physical dimension of the layer. When the physical thickness controls, the mesh generated according to the rule is subdivided automatically to accommodate this criterion. Finally, when the results are obtained simultaneously at various points, the smallest D (or the radius of the loaded area) controls.

This rule was used to construct meshes with values of N equal to 4, 2, and 1. These will be referred to as fine, standard, and coarse mesh, respectively. Results were then obtained for a homogeneous soil deposit with a Young's modulus (E) of 20 ksi and a Poisson's ratio of 0.4. The displacements obtained with the coarse mesh are within 5 percent of those of the fine mesh at the center of the loaded area and improve in accuracy for greater distances. The results with the standard mesh differ from those with the fine mesh by less than 1.5 percent at the center of the loaded area and are again even closer for greater distances (Table 1). It was concluded from these results that the standard mesh should be sufficiently accurate for most practical applications. Given the various approximations and uncertainties involved in all phases of these analyses, the coarse mesh may be adequate in many cases.

Using these three meshes and the same soil profile, parametric studies were conducted next for a dynamic excitation and different frequencies. It is a commonly accepted rule of thumb, in dynamic studies using finite element models, that the size of the elements must be of the order of one-quarter to one-sixth of the wavelength to obtain reasonably accurate results. The wavelength is equal to the shear wave velocity of the material divided by the frequency for shear waves and the P wave velocity divided by the frequency for compressional or dilatational waves. If E is Young's modulus of the material, υ its Poisson's ratio, and ρ its mass density, the shear modulus is

$$G = E/2(1 + \upsilon) \quad (1)$$

and the constrained modulus is

$$\lambda + 2G = E(1 - \upsilon)/(1 + \upsilon)(1 - 2\upsilon) \quad (2)$$

The shear wave velocity (v_S) is then given by

$$v_S^2 = G/\rho \quad (3)$$

and the P wave velocity is

$$v_S^2 = (\lambda + 2G)/\rho = v^2\, 2(1 - \upsilon)/(1 - 2\upsilon) \quad (4)$$

The Rayleigh wave velocity, associated with surface waves generated by a surface loading, is only slightly smaller than the shear wave velocity (v_S).

Figure 4 shows the amplitude of the steady-state displacements obtained with the fine and standard meshes at a point 5 ft from the center of the loaded area. The displacements are plotted versus a dimensionless frequency. A value of the dimensionless frequency of 1 corresponds to an actual frequency of 16 Hz and a wavelength of approximately 32 ft. The maximum layer thickness, at the bottom of the soil profile, in the standard mesh is 8 ft and in the fine mesh 4 ft. It can be seen that the results are in good agreement up to a dimensionless frequency of about 1, corresponding to a wavelength equal to four times the maximum layer thickness of the standard mesh. For higher frequencies the results of the standard mesh exhibit a series of sharp peaks that are not present in the more refined solution. Figure 5 shows similar results using the fine mesh and a mesh with twice the number of layers (each layer half the thickness of those in the fine mesh). The two solutions are almost identical up to a dimensionless frequency of about 2, corresponding to a wavelength equal to four times the maximum layer thickness of the fine mesh. In both cases the agreement is even better when the displacements at closer distances are considered. The distances involved in the Dynaflect and falling weight deflectometer tests are smaller than or equal to 6 ft.

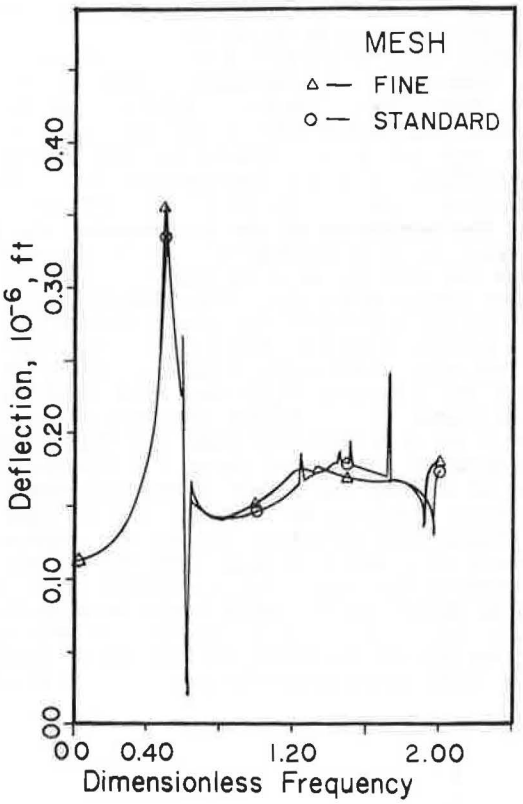

FIGURE 4 Amplitude of displacements at Point 7, fine and standard meshes.

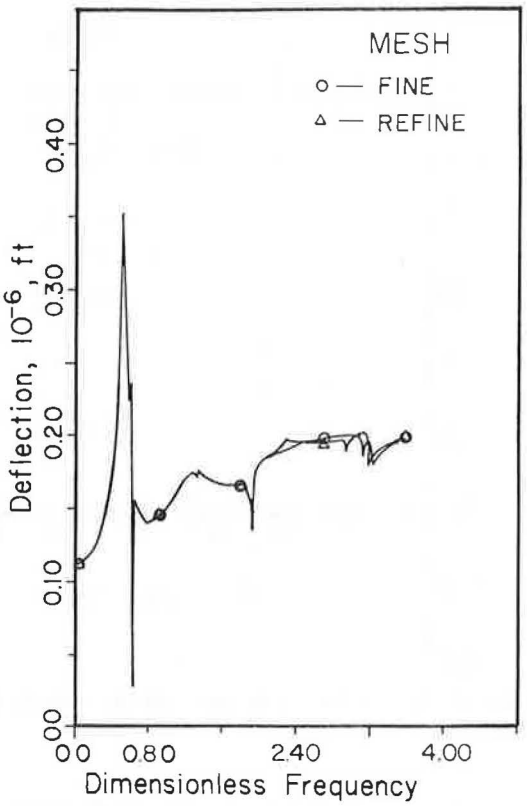

FIGURE 5 Amplitude of displacements at Point 7, fine and refined meshes.

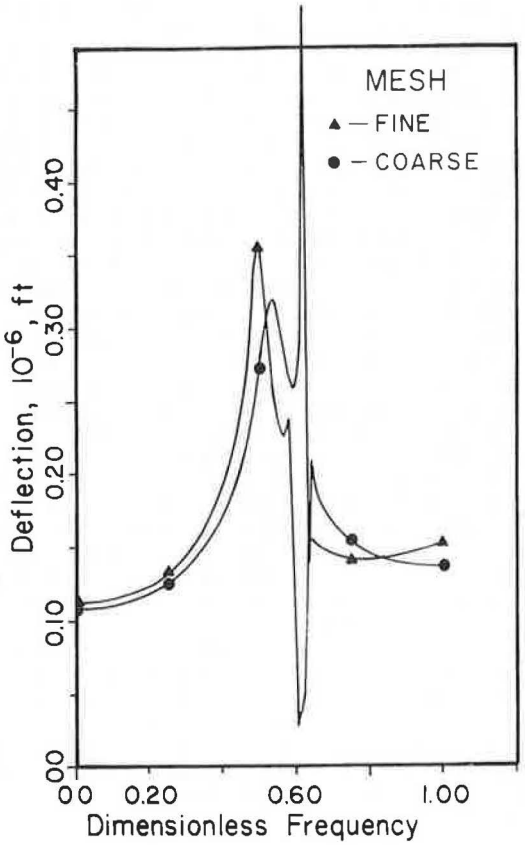

FIGURE 6 Amplitude of displacements at Point 7, fine and coarse meshes.

Figure 6 shows the results using the fine and coarse meshes. The differences in this case are of the same order of magnitude as those reported for static loads in the low-frequency range, but they become much more pronounced for dimensionless frequencies greater than 0.4 (wavelengths less than 5 times the maximum layer thickness).

These results appear to confirm the validity of the rule of thumb commonly used in practice. The standard mesh will provide good results for the dynamic case as long as the wavelengths are longer than four times the maximum thickness of any layer. For higher frequencies the mesh must be modified to satisfy this additional constraint (reducing the thickness of the bottom layers).

SIMULATION OF DYNAFLECT TESTS

A pavement system was selected to evaluate the importance of dynamic effects on the results of the Dynaflect tests (Figure 7). The pavement has a thickness of 2.5 in. and a Young's modulus of 200 ksi; the base has a thickness of 15 in. and a modulus of 78.5 ksi. The soil of the subbase was considered homogeneous with a Young's modulus of 29 ksi and with a modulus starting with this value at the top and increasing with depth. Different depths to bedrock were used in the range from 10 to 110 ft. Displacements were computed at the points corresponding to the stations of the Dynaflect for a static load and for a frequency of 8 Hz.

Figure 8 shows the variation of the static displacements with depth to bedrock at the five stations. Figure 9 shows the corresponding results for a frequency of 8 Hz, typical of Dynaflect tests.

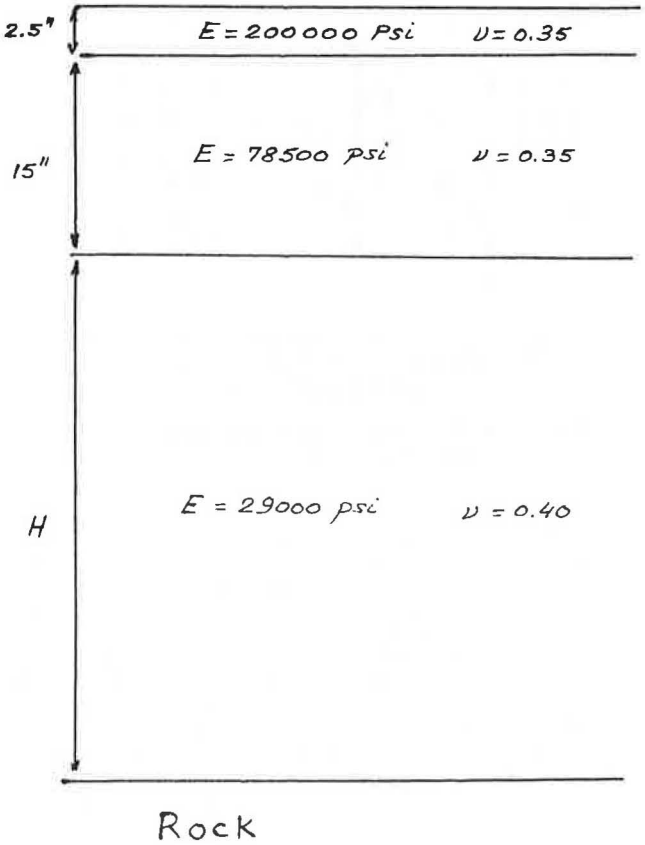

FIGURE 7 Profile of pavement used for studies.

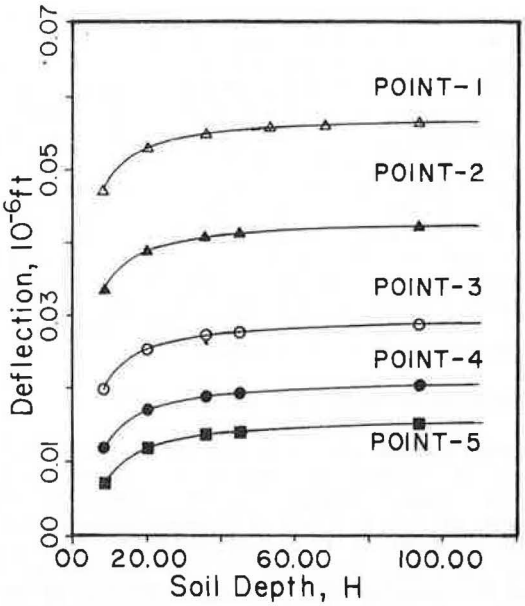

FIGURE 8 Variation of static displacements with depth to bedrock—Dynaflect.

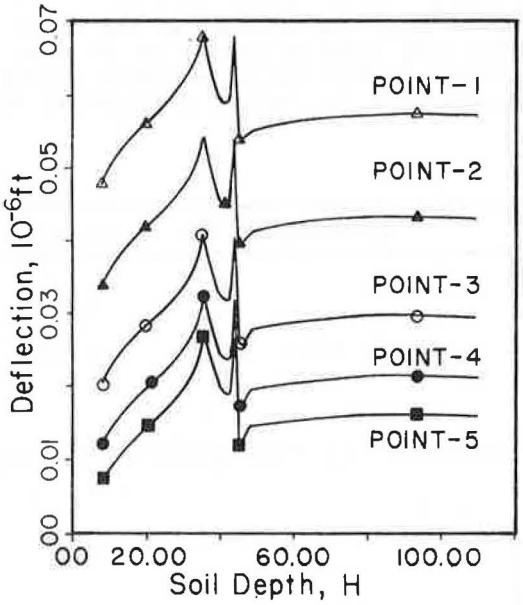

FIGURE 9 Variation of dynamic displacements with depth to bedrock—Dynaflect.

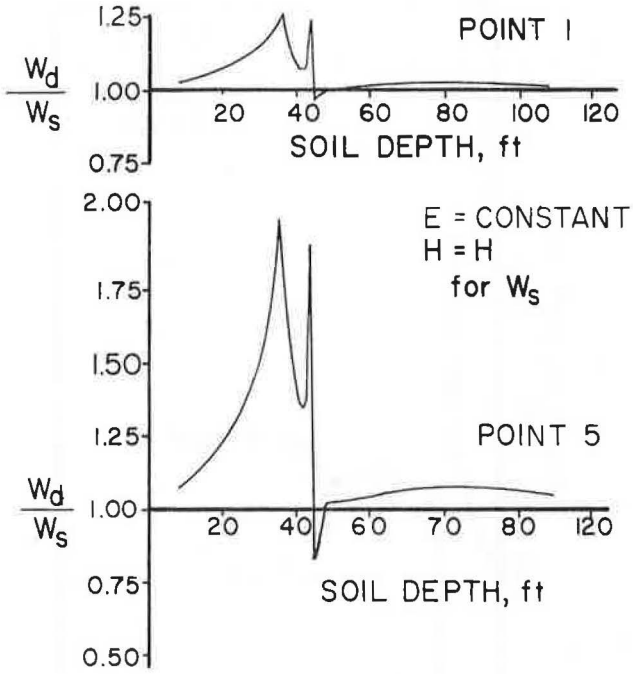

FIGURE 10 Ratio of dynamic to static deflections, Points 1 and 5—Dynaflect.

Figure 10 shows, finally, the ratio of the dynamic to the static displacements at Points 1 (between two wheels) and 5 (farthest from the loads). As the depth to bedrock increases so does the ratio of dynamic to static deflections, reaching a peak for a depth of approximately 35 ft and a second, much sharper peak for a depth of about 42 ft and exhibiting a sharp valley immediately after. As the depth to bedrock continues to increase the ratio appears to tend to 1 from above. Additional studies assuming 2 and 3 percent internal damping in the soil indicated that the first peak was only slightly affected by the existence of a small amount of material damping (which can always be expected) but that the second peak and the following trough disappeared almost entirely. The range of depths over which there is a substantial dynamic amplification of the deflections is closely associated with the depths for which a frequency of 8 Hz represents the natural frequencies of the soil deposit in shear and dilatation. These would be 20 and 48 ft, respectively.

Because the elastic properties of the pavement, base, and subbase are normally determined by comparing the measured deflections to those resulting from static analyses assuming that the subbase is an elastic half-space, it is perhaps more interesting to compare the dynamic results to the static deflections for an infinite depth to bedrock. The ratio of these deflections for Points 1 and 5 is shown in Figure 11. These results indicate that for shallow depths to bedrock (less than 20 or 25 ft) the dynamic deflections are smaller than the static deflections for a half-space (although they are larger than the static deflections for the same soil profile with a finite depth). For a range of depths of from 25 to 40 ft the dynamic results are larger than the static ones because the dynamic amplification is more pronounced as the distance to the load increases. For depths greater than 50 or 60 ft the ratio of dynamic to static displacements is close to 1. It is thus for depths to bedrock of less than 40 ft that the errors committed by the present interpretation procedures can be most serious for this particular profile. (Greater depths would be significant if the soil of the subbase were stiffer than the one selected for this study.)

Determination of the characteristics of the profile from the measured deflections falls into the general category of system identification problems (sometimes referred to as the inverse problem). Because only five deflections are available, it is often assumed that the thickness of the pavement and the base are known and that the only unknowns are the moduli of elasticity. These moduli are normally estimated by a trial and error procedure, assuming a set of values, computing the corresponding static deflections, comparing them to the measured values, and iterating until the differences are smaller than

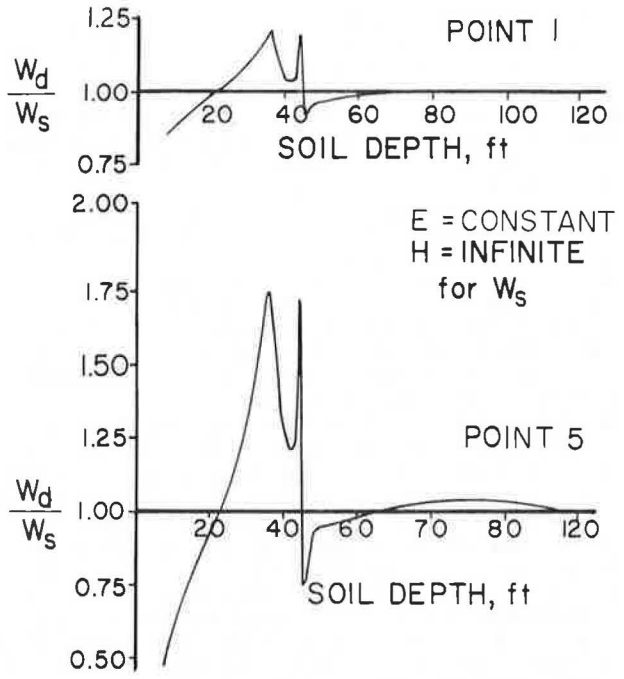

FIGURE 11 Ratio of dynamic to static (H = ∞) displacements, Points 1 and 5—Dynaflect.

an acceptable tolerance. Unfortunately, uniqueness of the solution cannot be guaranteed and different sets of elastic moduli can produce results that are within the specified tolerance.

To get a better feeling for the significance of the difference between static and dynamic displacements, the deflection bulbs computed for depths to bedrock of 10, 20, 35, and 110 ft were used as input to the identification procedure. The exact values of the elastic moduli were used as initial guesses and a gradient search technique was used in an attempt to converge to an optimum match using the computer program BASSD2 (9). The results of these studies are given in Table 2. Listed in the table are the computed deflections, the estimated values of the elastic moduli, and the errors in these moduli. It can be seen that for a depth to bedrock of only 10 ft the stiffness of the subbase is badly overestimated, whereas the modulus of elasticity of the base as well as the modulus of the pavement are underestimated. This occurs because the dynamic and finite layer effects are more pronounced for the farthest stations, the deflections of which are heavily influenced by the soil properties at greater depths. For a depth to bedrock of 20 ft the properties of the base and the soil are accurately determined, but the modulus of the pavement is badly overestimated. For a depth of 35 ft the moduli of the pavement and the base are both overestimated and the stiffness of the subbase is underestimated. This situation is the reverse of that encountered for a depth of 10 ft. When the depth of bedrock is 110 ft the results are more reasonable although the estimated modulus of the pavement is still 24 percent too high.

It is important to keep in mind that these results are not unique and that another person might obtain different values of the moduli with the same quality of fit. Even so, it is believed that the results illustrate reasonably well the type of errors and the variation in estimated properties that can be expected.

The same series of studies was conducted assuming that the soil properties increased gradually with depth. Figure 12 shows the ratio of the dynamic deflections for the soil profile with bedrock at a finite depth to the static deflections assuming that the subbase is homogeneous and extends to infinity. Notice that in this case the range of depths over which there is a substantial dynamic amplification is somewhat larger (from 20 to 60 ft approximately) because the subbase is effectively stiffer. An amplification effect is still apparent for a depth to bedrock of 110 ft whereas for the homogeneous soil the ratio of dynamic to static deflections is close to 1 for these depths.

SIMULATION OF FALLING WEIGHT DEFLECTOMETER TESTS

Because the loads applied by the falling weight deflectometer are transient in nature, it is necessary, to simulate the results of this test, to decompose the time history of the force into frequency components using the Fourier transform. Analyses must then be conducted for a large number of different frequencies to obtain the transfer functions of the deflections at each point (station). These transfer functions are then multiplied by the Fourier transform of the input and the resulting functions are converted back to time using the inverse Fourier transform. The final results are the time histories of the deflections at the various points. The complete analysis is clearly much more expensive than is the case of the Dynaflect where only one frequency is involved. Therefore the studies were

TABLE 2 Deflection Bulbs and Estimated Elastic Moduli for Homogeneous Subbase and Different Depths to Bedrock—Dynaflect

	H	Displacement (mils)					Young's Modulus	Error
	(ft)	Point 1	Point 2	Point 3	Point 4	Point 5	(lb/in^2)	(%)
Static	∞	0.70	0.52	0.36	0.26	0.20	200,000	
							78,500	
							29,000	
Dynamic	10	0.61	0.44	0.28	0.17	0.11	150,000	25.0
							30,000	61.8
							45,000	55.2
Dynamic	20	0.68	0.51	0.35	0.24	0.18	340,500	70.3
							78,000	0.6
							29,837	2.8
Dynamic	35	0.82	0.65	0.48	0.38	0.31	350,000	75.0
							98,500	25.5
							20,000	31.0
Dynamic	110	0.69	0.52	0.35	0.25	0.18	248,370	24.0
							78,500	0.0
							29,833	2.9

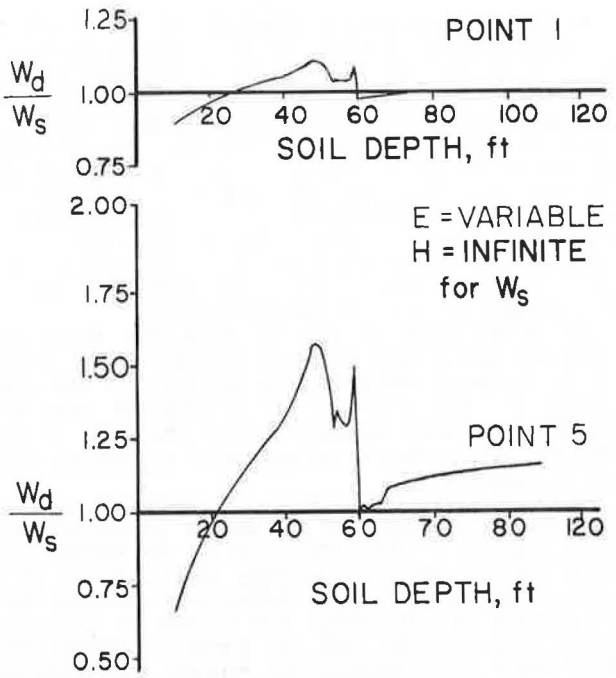

FIGURE 12 Ratio of dynamic to static (H = ∞) displacements, variable soil profile—Dynaflect.

limited to depths to bedrock of 10, 20, 40, and 80 ft.

The continuous Fourier transform involves an integral over time (direct transform) or frequency (inverse transform) extending from minus infinity or zero to infinity. In practice, however, a discrete transform, referred to as the fast Fourier transform, is used. In this case a finite number of points (power of 2) are selected to reproduce the function of time at equal time intervals (Δt). The total duration is $T = N\Delta t$ if N is the number of points. Notice that for an impulse-type load the values of the function will be nonzero for only a few points. The Fourier transform is then calculated at N/2 points with a frequency interval $\Delta f = 1/T$ and a maximum frequency (f_{max}) equal to $1/2\Delta t$. Proper selection of these parameters is important to guarantee the accuracy of the final results. A small time interval (Δt) is desirable to reproduce properly the time variation of the forcing function and to ensure that the peak response displacement is not missed. The total duration (T) should be several times larger than the actual duration of the load to ensure that spurious free vibration terms have attenuated; the appropriate value depends on the fundamental period of the system and the amount of damping (in the present case no internal damping is assumed for the soil and the only source of energy dissipation results from radiation or geometric spreading of the waves above the fundamental frequency of the soil stratum). The frequency increment Δf [fixed when the duration (T) has been selected] should be small to reproduce properly the transfer function, particularly if it exhibits some sharp peaks (typical of lightly damped systems). All these considerations point out the desirability of a small Δt and a large number of points N. It should be noticed, however, that as the number of points increases so do the cost of computation and the number of frequencies for which analyses must be conducted. As Δt decreases, the maximum frequency (f_{max}) increases. This requires more refined meshes and a larger number of layers because of the dynamic limitation on the thickness of the layers.

A number of preliminary studies were conducted to assess the values of Δt and N required to obtain reasonably accurate results. It was concluded from these studies that a value of N equal to 2,048 and a time interval of approximately 0.002 sec were appropriate for these applications. Figure 13 shows a typical transfer for the center of the loaded area and a depth to bedrock of 20 ft. (The transfer function is actually complex; the amplitude of the function is shown.) It can be seen that for frequencies larger than 20 Hz the function is relatively smooth without any pronounced peaks. It was decided, therefore, to calculate the values of the transfer functions at frequency intervals of approximately 0.25 Hz in the range from 0 to 20 Hz, 2 Hz from 20 to 60 Hz, and 4 Hz from 60 to 120 Hz. Because the Δf required is of the order of 0.25 Hz the values of the transfer functions at intermediate points are evaluated by interpolation between the computed values. Finally, because f_{max} should be approximately 240 Hz the values between 120 and 240 Hz were obtained by extrapolation. The preliminary studies indicated that the results obtained with these simplifications (leading to considerable savings in computer time) were in good agreement with those obtained using a constant frequency increment of 0.25 Hz over the complete range of freqencies.

Figure 14 shows typical time histories of the displacements at Point 1 (center of the loaded area) and Point 7 (farthest station) for a depth to bedrock of 20 ft. From these figures the peak deflection was computed at each station and the deflection bulb was obtained. Figure 15 shows the ratio of the dynamic to the static deflections considering both a finite layer and a half-space for the static analyses. It can be seen that a small amount of dynamic amplification takes place particularly as the distance to the load increases although dynamic effects are much less pronounced than in the case of the Dynaflect.

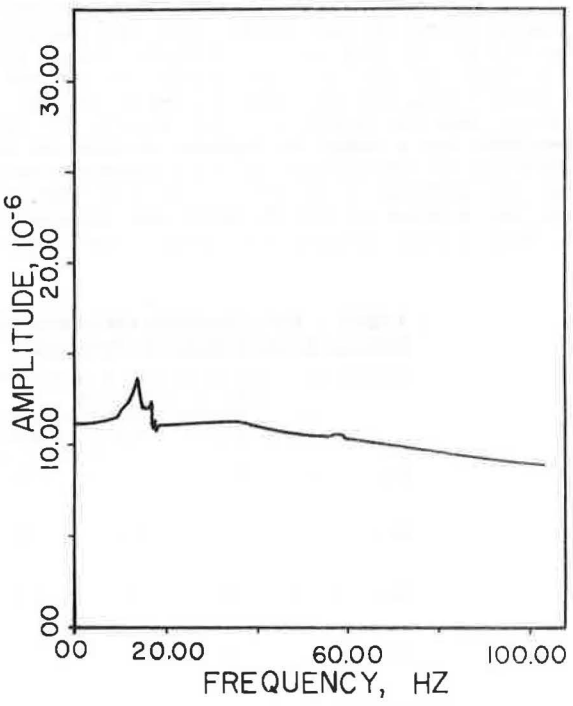

FIGURE 13 Transfer function at Point 1 (center of load) at H = 20 ft—falling weight deflectometer.

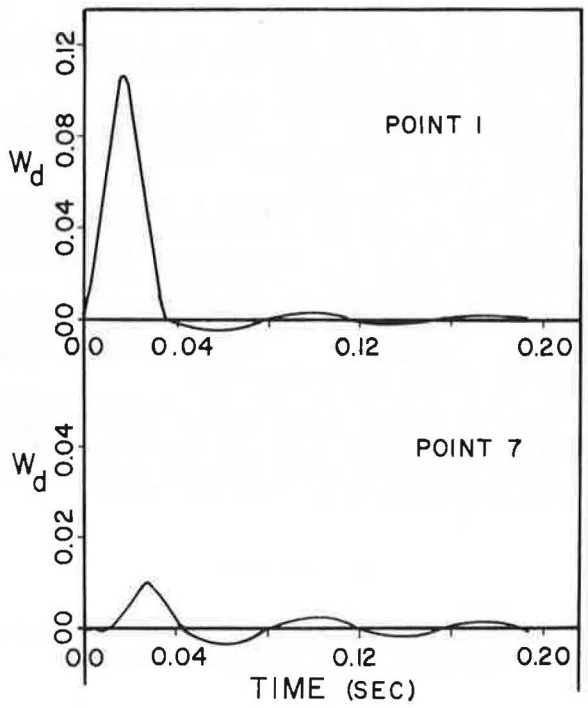

FIGURE 14 Time history of deflections at Points 1 and 7—falling weight deflectometer.

The computed deflections and the estimated moduli of the pavement, base, and subbase for the cases studied are summarized in Table 3. Although the errors are now much smaller, there are still some significant differences for shallow soil deposits (i.e., 10 ft) where the stiffness of the subbase is overestimated and for some intermediate depths (40 ft) where the modulus of the subbase is underestimated but that of the pavement is overestimated by 40 percent.

CONCLUSIONS

The results of the studies conducted to date indicate that a static interpretation of the deflections measured in the Dynaflect tests may be reasonable when dealing with a homogeneous soil (subbase) extending to depths of 60 ft or more. When much stiffer bedrock is encountered at shallower depths important dynamic amplification can occur. The elastic properties backfigured for the pavement system using standard techniques can then be substantially in error. The situation is aggravated when the soil of the subbase is not homogeneous but its stiffness increases with depth.

Dynamic effects are less important for the falling weight deflectometer because a broad range of frequencies is excited instead of a single one. Even so there are still some ranges of depth to bedrock for which the differences in dynamic effects at the various stations (distorting the shape of the de-

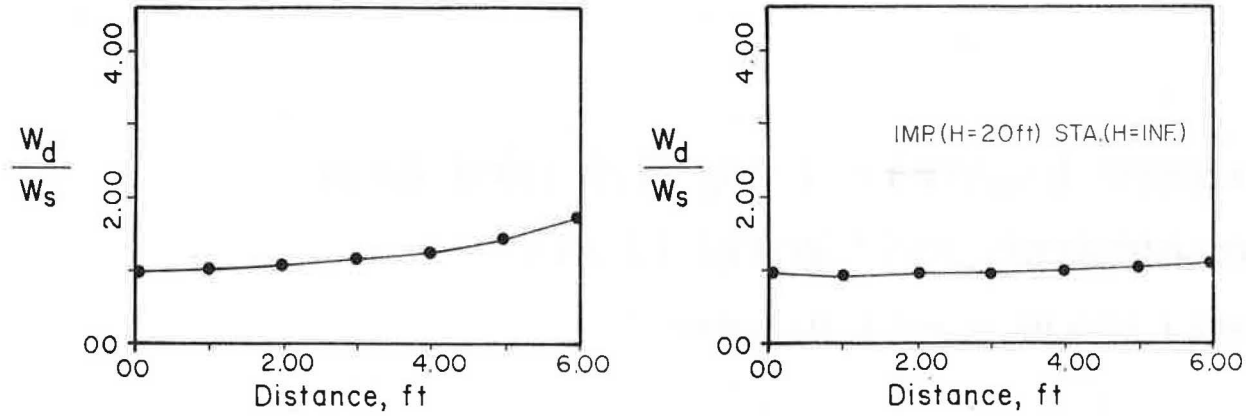

FIGURE 15 Ratio of dynamic (IMP) to static (H = ∞) deflections at H = 20 ft—falling weight deflectometer.

TABLE 3 Deflection Bulbs and Estimated Elastic Moduli for Homogeneous Subbase and Different Depths to Bedrock, Falling Weight Deflectometer (displacement x 10^{-8} ft)

		Distance to the Center (ft)								
	H (ft)	0	1	2	3	4	5	6	Estimated (lb/in^2)	Errors (%)
Static	∞	11.54	5.139	3.141	2.180	1.611	1.253	1.015	200,000	
									78,500	
									29,000	
Dynamic	10	10.60	4.622	2.842	1.923	1.317	0.9094	0.7214	200,000	
									78,500	0.0
									35,539	
Dynamic	20	11.06	4.652	3.013	2.073	1.538	1.280	1.090	200,000	0.0
									82,200	4.7
									28,790	0.7
Dynamic	40	10.74	4.860	3.008	2.111	1.590	1.288	1.086	287,200	43.6
									87,375	11.3
									28,331	2.3
Dynamic	80	11.08	4.733	3.073	2.109	1.608	1.311	1.044	200,000	0.0
									89,131	13.5
									29,245	0.8

flection bulb) may lead to erroneous estimates of the elastic moduli.

ACKNOWLEDGMENTS

The work described in this paper was conducted at The University of Texas at Austin under a research grant from the Texas State Department of Highways and Public Transportation.

REFERENCES

1. W.T. Thomson. Transmission of Elastic Waves Through a Stratified Soil Medium. Journal of Applied Physics, Vol. 21, Feb. 1950.
2. N.A. Haskell. The Dispersion of Surface Waves on Multilayered Media. Bulletin of the Seismological Society of America, Vol. 43, No. 1, Feb. 1953.
3. E. Kausel and J.M. Roesset. Stiffness Matrices for Layered Soils. Bulletin of the Seismological Society of America, Vol. 71, No. 6, Dec. 1981.
4. G. Gazetas. Dynamic Stiffness Functions of Strip and Rectangular Footings on Layered Soils. S.M. thesis. Massachusetts Institute of Technology, Cambridge, 1975.
5. R.J. Apsel. Dynamic Green's Functions for Layered Media and Applications to Boundary Value Problems. Ph.D. dissertation. University of California, San Diego, 1979.
6. G. Waas. Linear Two-Dimensional Analysis of Soil Dynamics Problems on Semi-Infinite Layered Media. Ph.D. dissertation. University of California, Berkeley, 1972.
7. E. Kausel. Forced Vibrations of Circular Foundations on Layered Media. Research Report R74-11. Department of Civil Engineering, Massachusetts Institute of Technology, Cambridge, 1974.
8. E. Kausel. An Explicit Solution for the Green Functions for Dynamic Loads in Layered Media. Research Report R81-13. Massachusetts Institute of Technology, Cambridge, 1981.
9. W. Uddin, W.R. Meyer, and K.H. Stokoe. Project-Level Structural Evaluation of Pavements Based on Dynamic Deflections. In Transportation Research Record 1007, TRB, National Research Council, Washington, D.C., 1985, pp. 37-45.

Publication of this paper sponsored by Committee on Mechanics of Earth Masses and Layered Systems.

Pavement Evaluation Using Deflection Basin Measurements and Layered Theory

ALBERT J. BUSH III and DON R. ALEXANDER

ABSTRACT

Recent developments through research efforts at the Waterways Experiment Station (WES) have produced a pavement evaluation procedure that uses deflection basin measurements from nondestructive test devices. These deflections are input for a layered elastic program (BISDEF) that predicts elastic moduli for each pavement layer for up to a four-layer system. The approach has been verified through comparison of predicted moduli from the computer program to moduli from laboratory modulus tests. The moduli determined from the deflection basin and BISDEF are then used with limiting strain criteria and a layered elastic program (AIRPAVE) to determine allowable aircraft loads, strengthening overlay requirements, and so forth. The use of a single evaluation procedure that employs test results from six different nondestructive testing devices to determine the allowable aircraft load on flexible airfield pavements is evaluated. Test data presented here were obtained from a side-by-side comparative study conducted in October 1982 at MacDill Air Force Base on three different pavements (two asphalt concrete and one composite of asphalt concrete over portland cement concrete). Test devices considered in this paper are the WES 16-kip vibrator, three falling weight deflectometers, a Road Rater, and a Dynaflect. Allowable loads determined using data from each device compare favorably with the standard evaluation procedure. The moduli values for the base course materials are higher when a preload is applied as in the case of the WES 16-kip vibrator.

The U.S. Army Engineer Waterways Experiment Station (WES) has been performing research in nondestructive pavement evaluation since the early 1960s. The procedures for evaluating load-carrying capacity have used data collected from a single device, the WES 16-kip vibrator. This device is unique and not presently available in the private sector. A need exists for an evaluation procedure that is device independent.

Nondestructive testing (NDT) offers many advantages over conventional pavement evaluation testing. The main advantage is the ability to collect data at many locations on a runway or taxiway in a short time. Ample test results can be collected in a few hours instead of the day or more required for test pit construction and repair. Nondestructive testing can be conducted at night to provide the least interference with traffic, or in some cases between aircraft operations on a particular airport feature, thus reducing costly delays in airline operations normally associated with test pits.

During the past 20 years several types of NDT equipment have been developed and used in the evaluation of roads and airfields. Most equipment applies a load, either vibratory or impulse, to the pavement and measures the resulting pavement surface deflection. Deflection is obtained with most devices by integrating the surface velocity measured with velocity transducers. The force generators for the vibratory equipment are either counterrotating masses or electrohydraulic systems that produce a sinusoidal loading. The impulse load devices use a falling weight dropped on a set of cushions to dampen the impulse for a loading time to simulate a moving wheel. The magnitude of the load is measured on some devices and calculated on others.

A study was conducted to evaluate the use of a single evaluation procedure employing the results from six nondestructive testing devices to determine the allowable aircraft load on flexible airfield pavements. Results on three pavement areas will be compared. Results will be presented to illustrate the applicability of the layered elastic evaluation procedure for those devices. Comparisons of allowable aircraft loads determined from NDT and destructive evaluation procedures will be presented.

ANALYTICAL MODEL AND APPROACH

A nondestructive evaluation procedure using a layered elastic method of analysis has been developed by WES for light aircraft pavements (1). The reported procedure used only one device, the Model 2008 Road Rater. In this method, a computer program developed to backcalculate the modulus for the measured deflections, CHEVDEF, uses the Chevron (2) layered elastic program. Chevron does not allow variable interface conditions. Therefore, a program called BISDEF, which uses the BISAR (3) program as a subroutine, was developed to handle multiple loads and to consider different layer interface conditions. This procedure is device independent. The routine for determining the modulus values is the same as that presented by Michelow (2). To determine the modulus values, the pavement system is modeled as a layered system. Poisson ratios are assumed for each layer. The modulus of any surface layer may be assigned or computed. If assigned, the value will be based on the type of material, or properties of the material, at the time of testing. For example, the assigned modulus will be a function of pavement temperature for flexible pavements. For BISDEF, a range of modulus values is input with an estimated initial modulus value for each layer for which modulus values are to be computed (variable layer). The number of layers with unknown modulus values cannot exceed the number of measured deflections. Best results are obtained when not more than three layers are allowed to vary. A rigid layer is placed 20 ft from the pavement surface.

Figure 1 is a simplified illustration of how the deflection basins are matched. This illustration is

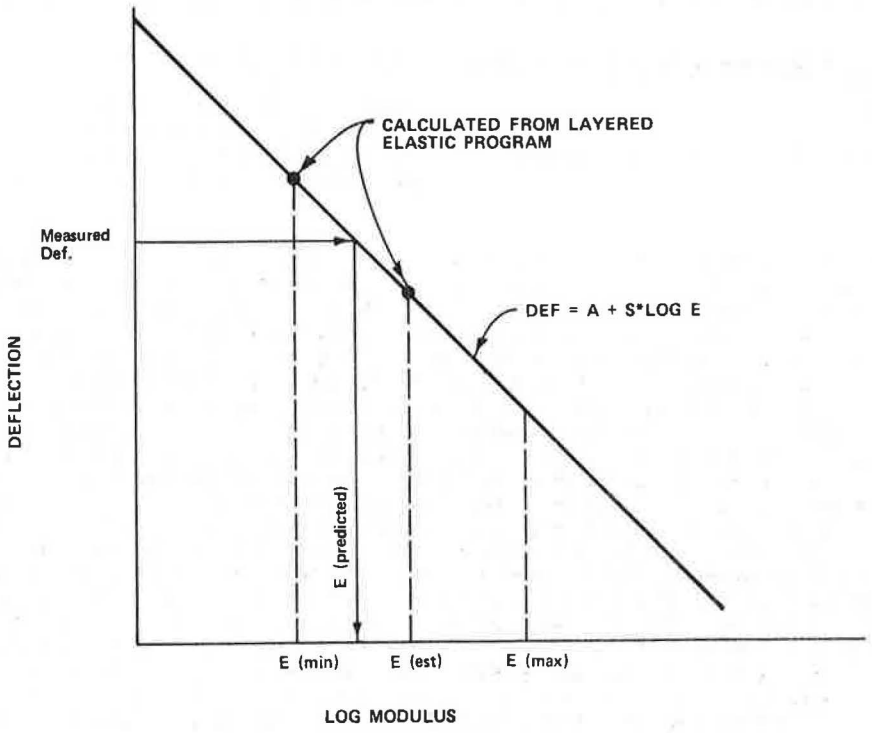

FIGURE 1 Simplified description of how deflection basins are matched in BISDEF.

for one deflection and one layer. For multiple deflections and layers, the solution is obtained by developing a set of equations that define the slope and intercept for each deflection and each variable layer modulus as follows:

$$Def_j = A_{ji} + S_{ji}(\log E_i) \quad (1)$$

where

A = intercept,
S = slope,
j = 1 to the number of deflections, and
i = 1 to the number of variable layers.

Errors are minimized by weighting deflections so that the smaller deflections away from the applied load contribute as much as do those near the load. Normally three iterations within the program produce a set of modulus values that yield a deflection basin that is within an average of 3 percent of each of the measured deflections. This accuracy appears to be well within the accuracy of most NDT deflection measuring sensors.

Allowable load-carrying capacities were evaluated using the WES-developed computer program AIRPAVE. For a particular aircraft (gear configuration, load, pass intensity level, and so forth), AIRPAVE uses the modulus values determined from BISDEF and the BISAR program to compute strains (for flexible pavement) that will occur in the pavement system. AIRPAVE then calculates the limiting strain values on the basis of present Corps of Engineers design and evaluation criteria (4,5). The allowable load for the aircraft is determined by comparing the predicted stress or strain to the limiting value.

The horizontal tensile strain at the bottom of the asphalt concrete (AC) and the vertical strain on top of the subgrade are both considered in the evaluation of flexible pavements. The allowable AC strain criterion used is as follows (4):

$$\varepsilon_{All}(AC) = 10^{-A} \quad (2)$$

where

$A = \{N + 2.665\ [\log_{10}(E_{AC}/14.22)] + 0.392\}/5.0$,
$N = \log_{10}$ (aircraft coverages), and
E_{AC} = AC modulus.

The allowable subgrade strains (5) are computed using the following:

$$N = 10{,}000\ [(A/\varepsilon_{All_{subg}})^B] \quad (3)$$

where

$A = 0.000247 + 0.000245 \log E_{subgrade}$,
$B = 0.0658\ (E_{subgrade})^{0.559}$, and
N = repetitions.

DESCRIPTION OF MacDILL AFB TESTS

WES was sponsored in 1982 by the Air Force Engineering and Services Center (AFESC), Tyndall AFB, Florida, to conduct a study of pavement evaluation techniques based on NDT.

The scope of the project involved comparisons of selected NDT equipment and procedures on representative airfield pavements and a comparison of the NDT results to those obtained from the standard AF evaluation procedures based on test pit measurements. WES selected six private firms with demonstrated NDT capabilities each of which represented a different approach. In addition, WES demonstrated three NDT schemes that it had developed, and the AFESC demonstrated its NDT methodology. The field demonstrations were conducted on five selected test areas at MacDill Air Force Base, Tampa, Florida, during October and November 1982. The test areas at MacDill AFB had been evaluated in March 1980 through test pit measurements in each of the five test areas.

Each participant made an evaluation of the test areas that consisted of determining allowable gross aircraft loadings and overlay thickness requirements and independently submitted a report to WES. A final report (6) presented all test data, a description of each evaluation methodology, and comparisons of the various results. Field test data extracted from this report for six different test devices are presented in this paper. A layout of the airfield at MacDill AFB indicating the five test areas, which consisted of two rigid, two flexible, and one composite pavement, is shown in Figure 2. Results from the two flexible and one composite pavement (Areas 2, 3, and 4) will be presented in this paper.

Description of Test Areas

Each of the test areas contained approximately 50,000 ft² of pavement. This size was selected to be large enough to provide a representative amount of pavement and yet small enough so the five test

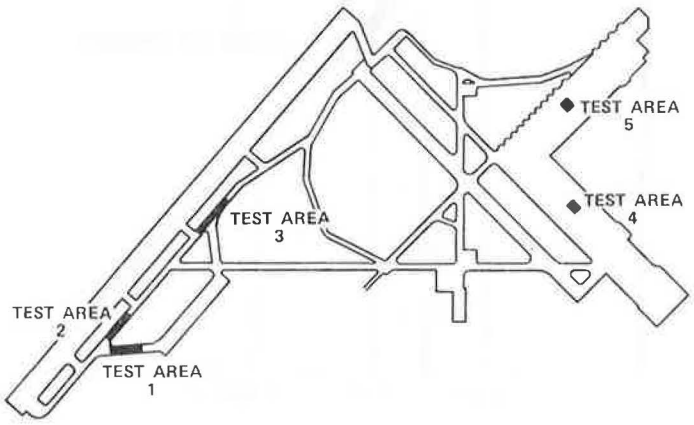

FIGURE 2 Airfield layout at MacDill AFB showing location of test areas.

areas would not require more than 1 full day of testing for each participant. The test areas were selected so as to provide the least interference with MacDill AFB's daily aircraft operations. Each test area was outlined and marked so that the location of all tests could be identified. A summary of the pavement properties as determined by test pit methods for each area is as follows:

Test Area	Pavement Properties
2	10 in. AC 8 in. limerock base CBR = 80 7 in. stabilized subbase CBR = 30 Subgrade (SP) CBR = 30
3	5.5 in. AC 8.0 in. limerock base CBR = 80 7.0 in. stabilized subbase CBR = 30 Subgrade (SP) CBR = 30
4	7.5 in. AC 6.0 in. portland cement concrete (PCC) R = 650 psi Subgrade (SP) k = 250 pci

where

CBR = California bearing ratio,
R = flexural strength of PCC (psi), and
k = modulus of subgrade reaction (pci).

Test Area 2

Test Area 2 was located on the taxiway parallel (Taxiway 3B) to the main runway and was constructed in 1943. The pavement consists of a 10-in. asphaltic concrete surface, an 8-in. limerock base, and a 7-in. subbase of limerock-stabilized sand over the sand subgrade (SP-SM). The pavement was in good condition but contained longitudinal and transverse cracking. This test area was 75 ft wide and 700 ft long.

Test Area 3

Test Area 3 was along the same parallel taxiway as Test Area 2 but farther north. This pavement was also constructed in 1943 and was originally identical to Test Area 2. The original 3-in. asphalt surface had been overlaid to the present thickness of 5.5 in. Beneath the AC surface is an 8-in. limerock base over a 7-in. subbase of limerock-stabilized sand over the sand subgrade. This area, considered in fair condition, exhibited considerable distress in the form of block cracking. This test area was 40 ft by 1,000 ft. The tests were confined to the 40-ft width because the pavement outside this width was not the same thickness.

Test Area 4

Test Area 4 was a composite section located in Apron 1-A-1. The original 6-in. PCC pavement placed on the sand subgrade was constructed in 1941. The slabs were 25 ft by 25 ft, and the design was for 8-in. thickened edges. A 7.5-in. AC overlay was placed on this pavement in 1952 followed by a slurry seal in 1966. There was a considerable amount of reflective cracking of the joints and from cracks in the underlying slabs. The overall condition was considered good. The area was 200 ft by 250 ft.

Description of Test Equipment

The six NDT devices included in this paper are WES 16-kip vibrator, WES falling weight deflectometer (FWD) (15-kip Dynatest Model 8000), 24-kip Dynatest Model 8000 FWD, Shell FWD, Road Rater Model 2000, and Dynaflect. A general description of each is provided in the following paragraphs.

WES 16-Kip Vibrator

The WES 16-kip vibrator is an electrohydraulic steady-state vibratory loading system. The unit is contained in a 36-ft semitrailer along with supporting power supplies and automatic data recording equipment. A 16,000-lb preload is applied to the pavement with a superimposed dynamic load ranging up to 30,000 lb peak-to-peak. The dynamic load can be applied over a frequency range of from 5 to 100 Hertz (Hz), but the standard test frequency is 15 Hz. The dynamic load is measured with a set of three load cells mounted on an 18-in.-diameter load plate. Velocity transducers, which are located on the load plate and at points away from the plate, are calibrated to measure elastic deflection. Test results are recorded on X-Y plotters and a digital printer. Data collected with the WES 16-kip vibrator are the dynamic stiffness modulus (DSM) and deflection basins. DSM is obtained from the slope (load/deflection) of the dynamic load versus deflection data obtained by sweeping the force to maximum at a constant frequency of 15 Hz. This slope is taken at the higher force levels. Deflection basins are obtained by measuring deflections at distances of 18, 36, and 60 in. away from the center of the load plate.

WES FWD

The FWD used by WES was a Dynatest Model 8000 (15 kip). A dynamic force is applied to the pavement surface by dropping a 440-lb weight on a set of rubber cushions, which results in an impulse loading. The applied force and pavement deflections are measured with load cells and velocity transducers. The drop height can be varied from 0 to 15.7 in. to produce an impact force of from 0 to 15,000 lb. The load is transmitted to the pavement through a plate 11.8 in. (30 cm) in diameter. The signal conditioning equipment displays the resulting average pressure in kilopascals and the maximum peak displacement in micrometers. Results presented in this paper were converted to pounds force and mils. Readings from as many as three displacement sensors may be recorded at one time by this data acquisition equipment.

FWD data collected were deflection basin measurements. Displacements were measured on the load plate and at distances of 12, 24, 36, and 48 in. away from the center of the load plate. Because this particular model has only two transducers for deflection basin measurement, the four deflection points were obtained by dropping the weight twice at each location and shifting the transducers to the additional spacings.

Dynatest FWD

The 24-kip Dynatest Model 8000 is a newer version FWD that has several features not found on the WES FWD. The adjustable load was set to its capacity of approximately 24,000 lb, and a loading plate of approximately 6-in. (150-mm) radius was used to simulate the stress level of a heavily loaded jet aircraft. The resulting stress level was somewhat in excess of 200 psi under the loading plate.

The FWD load is transient (as opposed to vibratory), having a time of loading of some 25 to 30 msec, thus corresponding to the effect of a moving aircraft wheel load. Both the load level and a se-

ries of seven simultaneous deflections are monitored for each FWD test, with the deflections measured at the surface of the pavement from the center of the loading plate (through a small hole in the middle of it) to a distance of more than 7 ft (2 m) from the center.

Shell FWD

The Shell device is a heavy FWD, and all tests were performed at a force level of 22,400 lb (100 kN). With this machine, a mass falls on a base plate that is connected to a foot plate by means of a set of springs, thus exerting a pulse load on the pavement surface. The duration of the pulse load is comparable to the duration of the pulse load exerted by actual traffic. The force level can be changed by adjusting the drop height. The deflection of the pavement is measured by four velocity transducers (geophones)--on the center of the foot plate and at three other radial distances. At MacDill AFB the radial distances were 0, 24, 39, and 79 in. (0, 60, 100, and 200 cm). The deflection signals are obtained by a single integration of the velocity signals from the geophones, which is performed electronically by integrated circuits.

Road Rater

The Model 2000 Road Rater is a trailer-mounted, electrohydraulic vibrator that has a variable force and frequency capability. A peak-to-peak cyclic load of 4,500 lb at a frequency of 25 Hz can be obtained. Deflection sensors were placed either 12, 24, and 36 in. or 12, 24, and 60 in. from the center of the load plate. One sensor is mounted at the center of the 18-in.-diameter plate.

Dynaflect

The Dynaflect is an electromechanical system for measuring the dynamic deflection of a pavement caused by an oscillatory load. The trailer-mounted device applies a 1,000-lb (4448-N) peak-to-peak sinusoidal load to the pavement. This load is generated by two counterrotating masses that are rotating at a constant frequency of 8 Hz. The force is transmitted to the pavement through two polyurethane-coated steel wheels that are 4 in. (10.2 cm) wide and 16 in. (40.6 cm) in outside diameter. The wheels are spaced 20 in. (50.8 cm) apart. The Dynaflect applies a 2,000-lb (907-kg) static weight to the pavement.

The pavement response to the dynamically applied load is measured with 210-ohm, 4.5-Hz geophones that are shunted to a damping factor of approximately 0.7. One geophone was located directly between the two steel wheels. The other four geophones were spaced at 12-in. (30.5-cm) intervals at the front of the trailer.

A summary of the most important characteristics of each test device and the location of displacement sensors for the MacDill tests is given in Table 1.

Field Tests

The field tests, conducted between October 26 and November 3, 1982, were coordinated with MacDill AFB operations. Each participant in the project was provided a full day to test all five areas. Only one participant was on the field on any given day of the demonstration. Also, each was free to choose the number and location of tests to be performed within each area. However, they were each asked to perform one test at or near a designated location within each area near the test pits. Test Area 4 became the parking apron for F-111 aircraft on November 2. This resulted in much of the area not being available for tests.

Data Analysis

The three test areas at MacDill AFB were evaluated in terms of the Allowable Gross Aircraft Load (AGAL) using deflection data from each of the six NDT devices and the previously described layered elastic methodology. These results were then compared to each other on a relative basis in an attempt to evaluate the device dependency of the procedure. The

TABLE 1 Characteristics of NDT Equipment

	WES 16-Kip	WES FWD	Dynatest FWD	Shell FWD	Road Rater	Dynaflect
Type of load applied	Vibratory	Impulse	Impulse	Impulse	Vibratory	Vibratory
Type of deflection output	Peak-to-peak	Peak	Peak	Peak	Peak-to-peak	Peak-to-peak
Contact area (in.^{2})	254	110	110	110	254	8.6
Peak-to-peak maximum dynamic/impulse force (lb)	30,000	15,000	24,000	22,400	4,500	1,000
Static weight (lb)	16,000	–	–	–	3,800	2,067
Test frequency (Hz)	15	–	–	–	25	8
Loading time (msec)	–	25-30	25-30	–	–	–
Number of displacement sensors	4	3	7	4	4	5
Location of displacement sensors, distance from center of loaded area (in.)						
0	x	x	x	x	x	x
8			x			
12		x	x		x	x
18	x					
24		x	x	x	x	x
36	x	x	x[a]		x[a]	x
39				x		
48		x	x			x
60	x		x[a]		x[b]	
71			x[c]			
79				x		
96			x[b]			

Note: Dashes indicate data were not applicable or were unavailable.

[a] Flexible and composite pavements only.
[b] Rigid and composite pavements only.
[c] Rigid pavements only.

TABLE 2 Deflection Data from Six NDT Devices

Nondestructive Test Device	Force (lb)	Deflection (mils) at Distance from Center of Loaded Area (in.) 0	8	12	18	24	36	39	48	60	71	79	96
Test Area 2													
WES 16-kip	28,960	13.26	–	–	9.18	–	4.480	–	–	2.74	–	–	–
WES FWD	14,206	8.68	–	6.08	–	3.880	2.480	–	1.770	–	–	–	–
Dynatest FWD	23,473	16.30	13.50	11.60	–	7.600	5.100	–	3.600	2.60	–	–	–
Shell FWD	22,400	13.11	–	–	–	6.650	–	3.46	–	–	–	1.69	–
Road Rater	4,510	1.83	–	1.35	–	0.800	0.570	–	–	–	–	–	–
Dynaflect	1,000	0.40	–	0.35	–	0.255	0.207	–	0.177	–	–	–	–
Test Area 3													
WES 16-kip	28,428	24.96	–	–	14.74	–	5.800	–	–	3.96	–	–	–
WES FWD	14,055	23.84	–	14.68	–	5.120	2.580	–	1.870	–	–	–	–
Dynatest FWD	22,043	43.90	31.40	23.40	–	9.800	4.900	–	3.400	2.80	–	–	–
Shell FWD	22,400	37.16	–	–	–	9.960	–	3.94	–	–	–	2.09	–
Road Rater	4,470	4.55	–	3.43	–	1.810	1.180	–	–	–	–	–	–
Dynaflect	1,000	0.90	–	0.60	–	0.380	0.225	–	0.189	–	–	–	–
Test Area 4													
WES 16-kip	28,934	9.80	–	–	8.30	–	5.940	–	–	4.14	–	–	–
WES FWD	14,098	5.09	–	4.57	–	3.860	3.290	–	2.560	–	–	–	–
Dynatest FWD	23,390	8.94	8.35	7.91	–	7.200	5.470	–	–	3.54	–	–	1.89
Shell FWD	22,400	9.80	–	–	–	8.190	–	5.83	–	–	–	3.27	–
Road Rater	3,666	1.23	–	1.22	–	1.000	–	–	–	0.54	–	–	–
Dynaflect	1,000	0.45	–	0.43	–	0.390	0.350	–	0.310	–	–	–	–

Note: Dashes indicate data not applicable.

results were also compared to the results obtained using the standard Air Force evaluation procedure (7). The B-52 (maximum gross load = 490,000 lb) was selected as the design aircraft, and the evaluations of each area were based on 15,000 aircraft passes.

Selection of Deflection Data and Layered Evaluation

To evaluate these pavement areas using the layered elastic methodology, a representative deflection basin for each test area had to be selected for each test device. However, this selection of a representative basin would have been quite complicated for the MacDill data because no two participants used the same test pattern or test frequency. Also, the magnitude of the deflections measured on the flexible pavements varied considerably in the transverse direction across the test areas. Therefore, only the data collected at the one designated location near the test pit in each area were considered in this work. The deflection basins used in determining the layer modulus values for each test area are given in Table 2 and presented graphically in Figures 3-5.

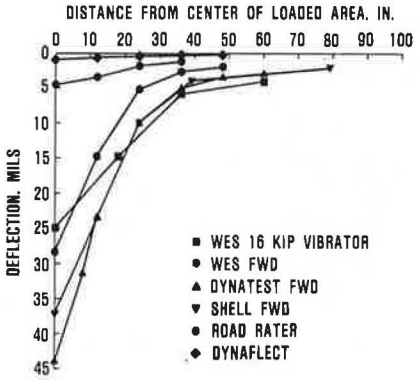

FIGURE 4 Comparison of measured deflection basins on Test Area 3.

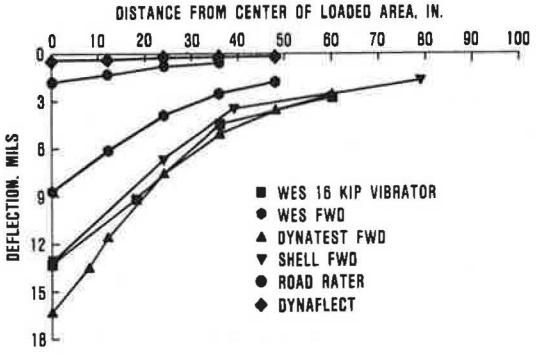

FIGURE 3 Comparison of measured deflection basins on Test Area 2.

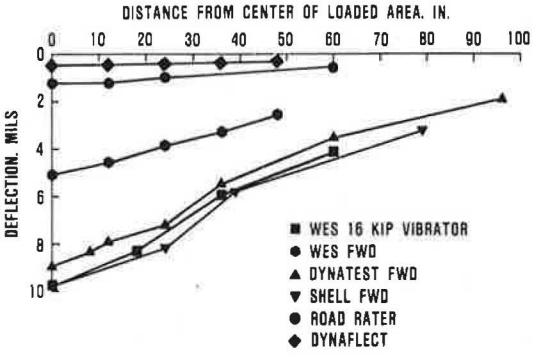

FIGURE 5 Comparison of measured deflection basins on Test Area 4.

These values were input to the computer program BISDEF from which the modulus values were computed for each layer in the pavement system (including the surface AC). Results are summarized in Table 3 for each test area and all six NDT devices. Poisson's Ratios of 0.35, 0.15, 0.35, and 0.40 were assumed for the AC, PCC, base course, and subgrade materials, respectively.

The AGAL was then determined by inputting the base course and subgrade modulus values from BISDEF into the evaluation program AIRPAVE. For evaluation, the modulus values for the AC surface layers were assigned at 300,000 psi. The resulting AGALs are given in Table 4. It is important to note that the composite pavement (Area 4) was evaluated using flexible pavement criteria.

Standard Evaluation

The standard evaluation was performed using the previously stated physical properties for each area. Here, Area 4 was again evaluated as a flexible pavement. The PCC layer beneath the AC was assigned a CBR value of 80. Results of the standard evaluation are given in Table 4.

Analysis of Area 2

A graphic comparison of the modulus values for the base and the subgrade of Area 2 is shown in Figures 6 and 7. The Dynaflect values are high for the limerock base material and low for the subgrade. There is some variability in the values from the other equipment. Because the WES 16-kip device and the Road Rater both apply a static load to the pavement, higher modulus values may be expected for granular materials. The allowable aircraft loads from the AIRPAVE program are shown in Figure 8. This evaluation considered the limiting strain in both the asphalt layer and the subgrade. All devices with the exception of the 15-kip WES FWD and the 24-kip Dynatest FWD indicated that the area could support a fully loaded B-52. When only the subgrade strain was

TABLE 3 Moduli Predicted from Deflection Basins from Different NDT Equipment

		Layer 1			Layer 2			Layer 3		
Test Area	Nondestructive Test Device	Thickness (in.)	Material	Elastic Modulus (psi)	Thickness (in.)	Material	Elastic Modulus (psi)	Thickness (in.)	Material	Elastic Modulus (psi)
2	WES 16-kip	10.0	AC	680,279	15.0	Limerock-stabilized base	59,740	Subgrade	Sand	37,209
	WES FWD			572,022			40,116			37,438
	Dynatest FWD			538,205			36,649			29,799
	Shell FWD			559,951			65,255			31,818
	Road Rater			452,499			90,633			50,928
	Dynaflect			154,052			403,405			22,579
3	WES 16-kip	5.5	AC	691,229	15.0	Limerock-stabilized base	40,926	Subgrade	Sand	26,573
	WES FWD			185,244			16,241			31,738
	Dynatest FWD			185,952			20,682			20,375
	Shell FWD			332,768			18,244			27,155
	Road Rater			537,513			35,074			24,344
	Dynaflect			52,175			40,381			23,872
4	WES 16-kip	7.0	AC	1,440,817	6.0	PCC	3,227,078	Subgrade	Sand	25,157
	WES FWD			1,982,381			2,047,265			23,242
	Dynatest FWD			1,903,426			1,841,818			22,108
	Shell FWD			2,334,218			1,387,285			17,160
	Road Rater			6,878,414			248,228			23,376
	Dynaflect			12,030,469			716,925			10,687

TABLE 4 Allowable Loads for the B-52 Determined Using AIRPAVE and the Standard Air Force Evaluation Procedure

					Allowable Load (kips)		
					AIRPAVE		
Test Area	Test Device	Design Aircraft	Design Pass Level	Design Load	Subgrade Criteria	Both Criteria	Standard Evaluation
2	WES 16-kip	B-52	15,000	490	490+	490+	490+
	WES FWD				490+	446	
	Dynatest FWD				490+	414	
	Shell FWD				490+	490+	
	Road Rater				490+	490+	
	Dynaflect				490+	490+	
3	WES 16-kip	B52	15,000	490	370	370	400
	WES FWD				421	211	
	Dynatest FWD				269	234	
	Shell FWD				358	223	
	Road Rater				334	334	
	Dynaflect				335	335	
4	WES 16-kip	B-52	15,000	490	490+	490+	333
	WES FWD				490+	490+	
	Dynatest FWD				490+	490+	
	Shell FWD				490+	490+	
	Road Rater				490+	490+	
	Dynaflect				351	351	

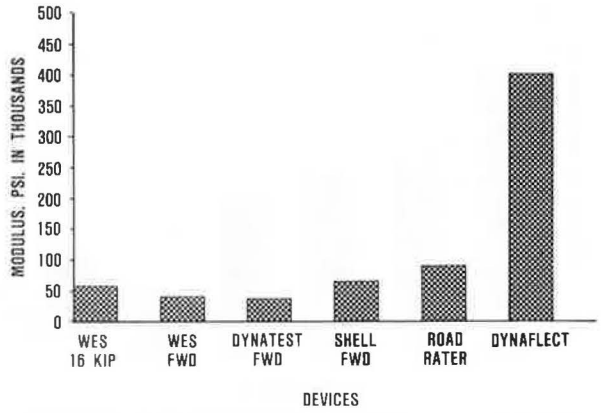

FIGURE 6 Comparison of the modulus values computed for the base course of Test Area 2.

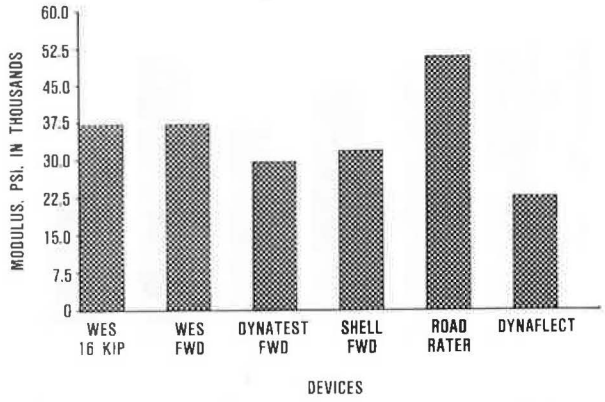

FIGURE 7 Comparison of the modulus values computed for the subgrade of Test Area 2.

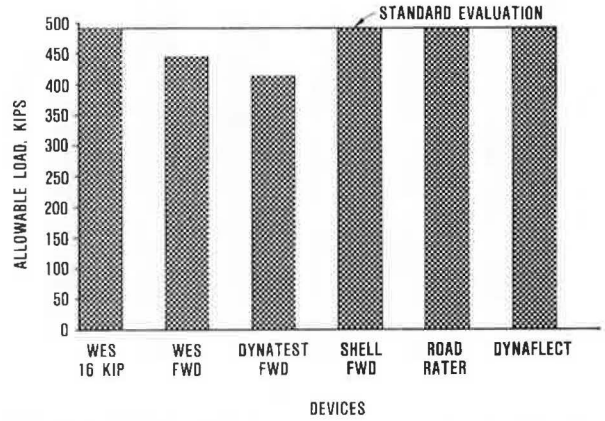

FIGURE 8 Allowable aircraft loads from AIRPAVE for Test Area 2.

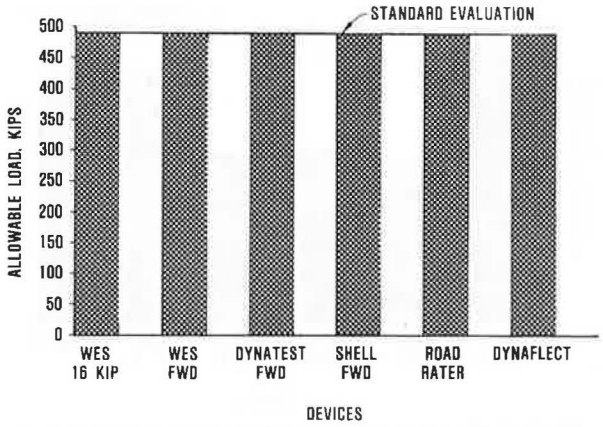

FIGURE 9 Allowable aircraft loads from AIRPAVE for Test Area 2 with only the subgrade strain criteria considered.

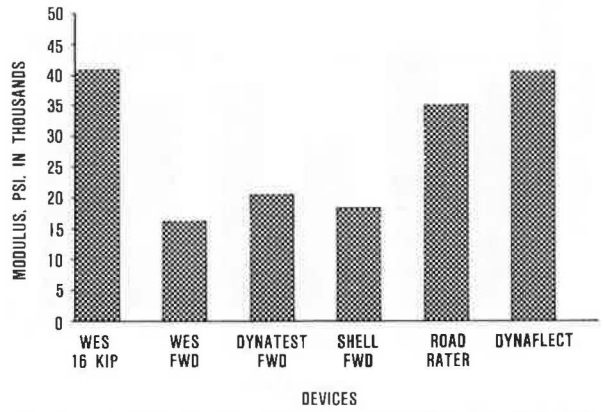

FIGURE 10 Comparison of the modulus values computed for the base course of Test Area 3.

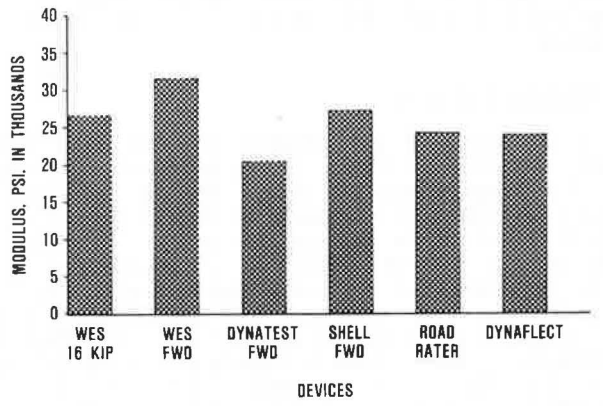

FIGURE 11 Comparison of the modulus values computed for the subgrade of Test Area 3.

considered, all devices yielded the maximum allowable load (490 kips as shown in Figure 9). This agrees with the standard evaluation that is based on the CBR design procedure and does not account for strain in the surface layer.

Analysis of Area 3

Modulus values for the base and the subgrade of Area 3 are shown in Figures 10 and 11. For the base course modulus, the values of the vibratory devices--the WES 16-kip, the Road Rater, and the Dynaflect--are higher than those of the FWDs. The values for the subgrade are similar.

The allowable aircraft loads using both asphalt and subgrade strain criteria are lower than the standard evaluation (Figure 12). When only the subgrade strain criteria are used, the allowable loads are near the standard evaluation (Figure 13). The differences in allowable load between the FWDs and the vibratory devices may be due to the lower base

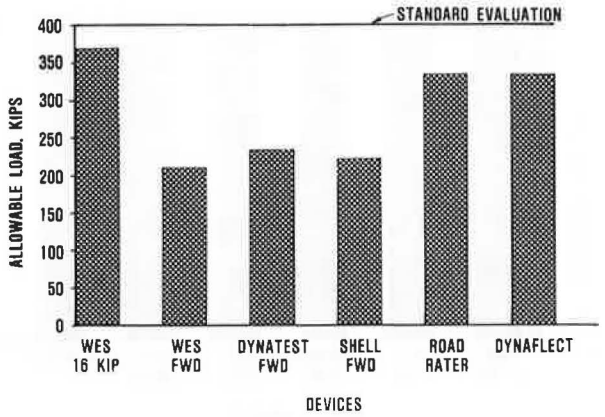

FIGURE 12 Allowable aircraft loads from AIRPAVE for Test Area 3.

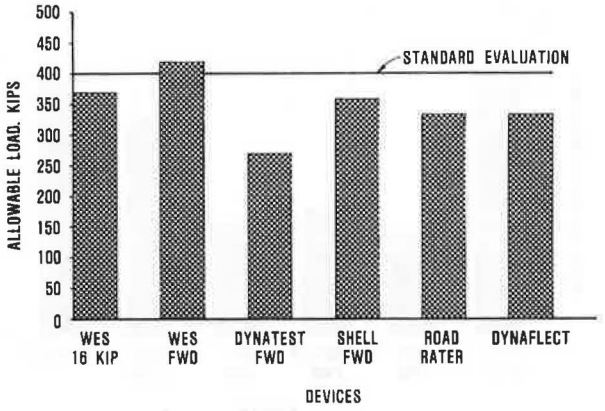

FIGURE 13 Allowable aircraft loads from AIRPAVE for Test Area 3 with only the subgrade strain criteria considered.

course modulus obtained from the FWD deflections, particularly when both strain criteria are considered.

Analysis of Area 4

A large variation was obtained for the base (PCC) layer for Area 4 (Figure 14). Some variation is seen in the subgrade modulus values (Figure 15). Evaluation of composite pavements is difficult when the thickness of the AC overlay is near the thickness of the PCC. A failure criterion (flexible or rigid) must be selected in a layered system evaluation. The flexible pavement criterion was selected for this area because the standard evaluation is for flexible pavement. Allowable aircraft loads are shown in Figure 16. The evaluation using Dynaflect data is nearer the standard evaluation than is the evaluation using all other devices. This may be discredited because the layer modulus values do not appear reasonable for the PCC and the sand subgrade.

CONCLUSIONS

An evaluation procedure based on layered elastic analysis was presented, and comparisons were made using deflection data from six different NDT devices on three pavement sections. The NDT testing data were taken from a study in which leaders in the field of NDT airfield evaluation were asked to evaluate pavements. These firms were allowed to test at

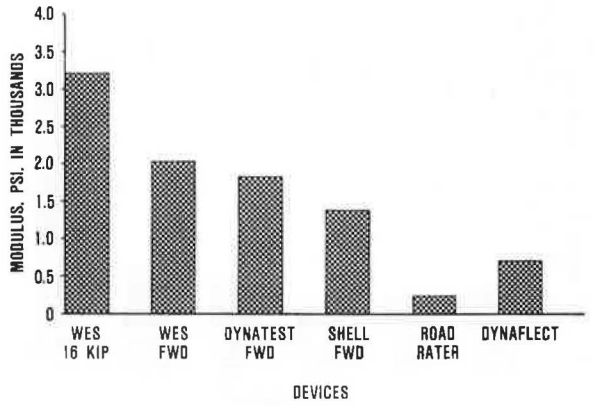

FIGURE 14 Comparison of the modulus values computed for the base course (PCC) of Test Area 4.

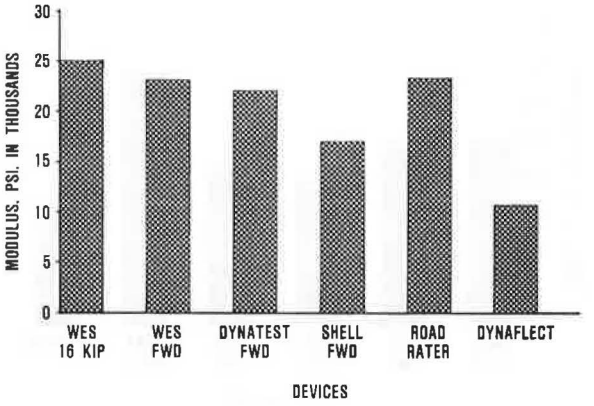

FIGURE 15 Comparison of the modulus values computed for the subgrade of Test Area 4.

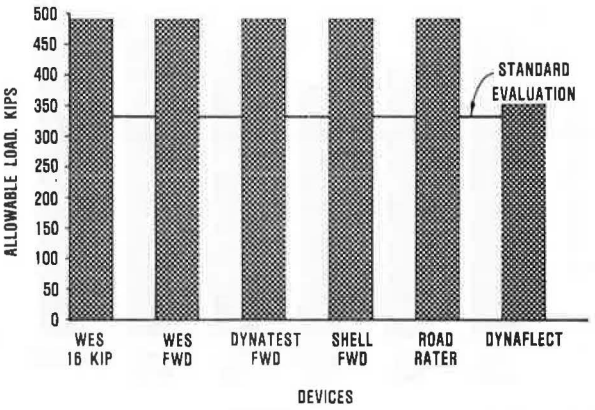

FIGURE 16 Allowable aircraft loads from AIRPAVE for Test Area 4.

any location within specified test areas; therefore, it was difficult to find test locations that were common to all devices. The following conclusions are presented:

1. Results from each device compare favorably with the standard evaluation procedure in terms of allowable gross aircraft loads.
2. The computed moduli of the base course materials are higher when a preload is applied as in the case of the WES 16-kip vibrator.

3. A study would be more beneficial in determining the differences in NDT equipment if it were conducted on a site where tests with all devices were conducted at the same test locations.

4. The allowable gross aircraft load for two of the three pavements evaluated was at the maximum for the B-52 aircraft, which is one of the most critical aircraft in terms of pavement evaluation. If further research is conducted, it is recommended that a site with fine grained subgrades, where design loads are less than maximum for the evaluated aircraft, be selected.

ACKNOWLEDGMENT

This paper was based on an Air Force Engineering and Services Center (AFESC) research project conducted by the U.S. Army Engineer Waterways Experiment Station (USAEWES). The authors gratefully acknowledge the support of the engineers at AFESC and USAEWES who were actively involved in this work.

The views expressed in this paper are those of the authors who are responsible for the facts and accuracy of the data. The contents do not necessarily reflect the official views or policies of the AFESC or USAEWES. This paper does not constitute a standard, specification, or regulation. The use of the following trade or manufacturing names was considered essential because they appear in the Air Force report on which this paper is based: Dynatest FWD, Shell FWD, Road Rater, and Dynaflect. Mention of the products listed does not constitute USAEWES endorsement or rejection of the products.

Discussion

Waheed Uddin, Phil Smith, and Harvey J. Treybig*

The authors are to be congratulated for carrying out this study on a large scale as reported by Hall (6). Direct comparison of different nondestructive devices by testing at the same locations on in-service pavement is undoubtedly an appropriate approach for a comparative study of these devices along with their respective evaluation methodologies. The Air Force report (6), from which the authors have extracted contents for their paper, is based on two objectives: (a) comparison of NDT devices and results from different evaluation procedures and (b) comparison of allowable load rating and overlay thickness predictions from these procedures with the standard test pit rating. However, the paper focuses only on some selected data from this large report. Unfortunately, the presentation of the data and results in this paper are out of context. A reader who has not reviewed the report (6) may misinterpret the results presented in the paper and form a biased opinion about the results.

Unfortunately, the results in the paper are not those that compare the results of a particular device and its analysis methodology. Instead data are taken from several devices and a single analysis package is misapplied. The discussion presented here centers around the following key points:

*ARE, Inc., 2600 Dellana Lane, Austin, Tex. 78746

1. The results reported by each of the participants in the overall study (6) were available to the authors of the paper but were not reported in the paper; thus the major thrust of the overall study was omitted.

2. The authors used the participants' field measured deflection data as inputs to their own analysis and evaluation methodology. This is not the best systematic technique for comparing devices because it ignores proven methodology developed by each participant on the basis of the participant's NDT device.

3. The Dynaflect load and sensor configuration was improperly modeled by the authors, which results in inaccurate deflection basins and moduli predictions.

COMPARISON OF DYNAMIC DEFLECTION BASINS

There is no explanation in the paper of why results from only three of the five test areas are reported. Only one basin measured by each NDT device on each of Areas 2, 3, and 4 is used for pavement evaluation; the full report is much broader in scope.

The deflection basins given in Table 2 and shown in Figures 3-5 do not properly represent the Dynaflect loading and geophone configuration. A more rational approach to comparing deflection basins from different NDT devices suggests a plotting of normalized deflections versus radial distances of sensors from the center of the test load (8) as shown in Figure 17. The radial distances of the

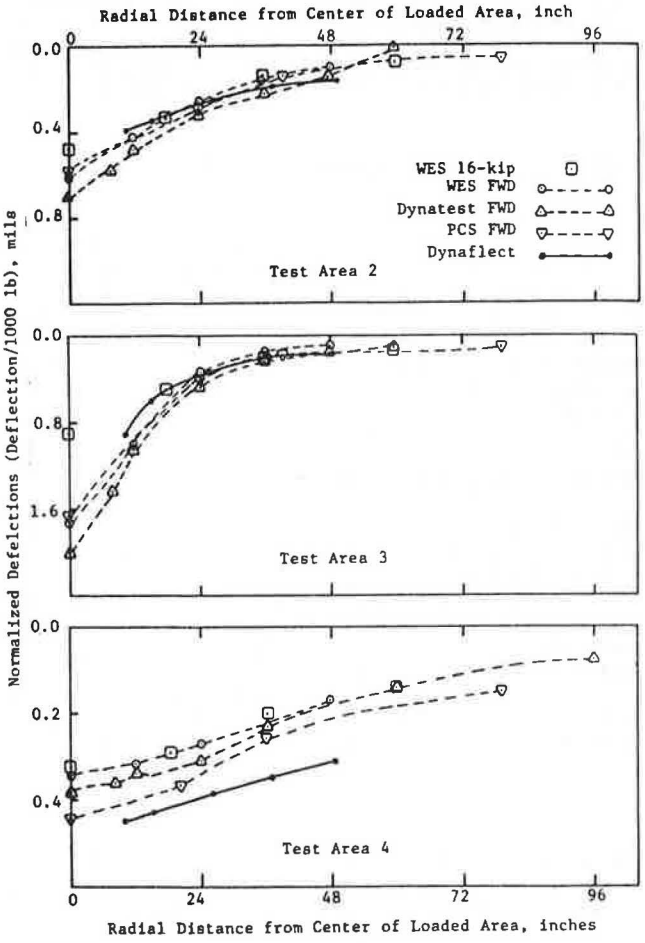

FIGURE 17 Normalized deflection basin plots for different NDT devices.

TABLE 5 Summary of Estimated Young's Moduli Based on Evaluation Methodologies of Participants

Test Area	NDT Device	Moduli Reported by Participants *(6)* in psi			Percentage Difference in Modulus from BISDEF and Participants {100 x [Modulus (BISDEF) − Modulus (participant)] ÷ Modulus (participant)}		
		Surface	Base	Subgrade	Surface	Base	Subgrade
2	WES 16-kip	250,000	51,000	39,000	+172.1	+17.1	−4.6
	WES FWD	250,000	36,000	39,000	+128.8	+11.4	−4.0
	Dynatest FWD	348,000	32,000	26,000	+54.6	+14.5	+14.6
	PCS FWD	635,000	35,300	51,200	−11.8	+84.8	−37.8
	Berger Profiler	400,000	100,000	37,000	+13.1	−9.4	+37.6
	Dynaflect	500,000	120,000 (60,000)[a]	34,500	−69.2	+236.2	−34.5
3	WES 16-kip	250,000	44,000	24,000	+176.5	−7.0	+10.7
	WES FWD	250,000	13,500	24,000	+176.5	+20.3	+32.2
	Dynatest FWD	401,000	16,000	20,000	−53.6	+29.3	+1.9
	PCS FWD	635,000	10,000	41,000	−47.6	+82.4	−33.8
	Berger Profiler	300,000	50,000	24,000	+79.2	−29.9	+1.4
	Dynaflect	200,000	60,000 (35,000)[a]	27,000	−73.9	−32.7	−11.6
4[b]	WES 16-kip	250,000	500,000	19,000	+476.3	+545.4	+32.4
	WES FWD	250,000	500,000	18,000	+693.0	+309.4	+29.1
	Dynatest FWD	533,000	4,500,000	26,200	+257.1	−59.1	−15.6
	PCS FWD	635,000	900,000	30,600	+267.6	+54.1	−43.9
	Berger Profiler	800,000	4,000,000	24,000	+759.8	−93.8	−2.6
	Dynaflect	300,000	6,000,000	21,000	+3910.2	−88.1	−49.1

[a] Subbase modulus.
[b] Base in Text Area 4 is a PCC layer.

Dynaflect sensors are 10.0, 15.6, 26.0, 37.4, and 49.0 in. from the center of the loaded area under each loading wheel. It can be seen from the normalized plots (Figure 17) that (a) the pavement response is affected by the loading mode and (b) the response is device dependent, as is apparent from variations in the data of the three FWD units.

EVALUATION OF PAVEMENT MODULI

The authors have not chosen in this paper to report results of the pavement evaluations made independently by the participants. Each participant has used an evaluation methodology to analyze data from its respective NDT device. The paper inaccurately implies that the Dynaflect does a poor job; the full report shows excellent correlation of the Dynaflect results, based on the participant's analysis and evaluation.

Pavement Evaluation by Participants

Table 5 gives the results extracted from the full report (6), as well as a comparison with the moduli reported by the authors.

The moduli from WES 16-kip and WES FWD devices are in most cases identical, although considerable differences exist in the normalized deflection basins from the two devices.

It is to be appreciated that the results from the methodologies of the participants are in general similar and within a reasonable margin of error (Figures 18-20).

BISDEF Methodology

The authors provide only a cursory description of their BISDEF program. Its parent program, CHEVDEF, was specifically designed for Road Rater model 2008 (1). Ample explanation of the following points is needed.

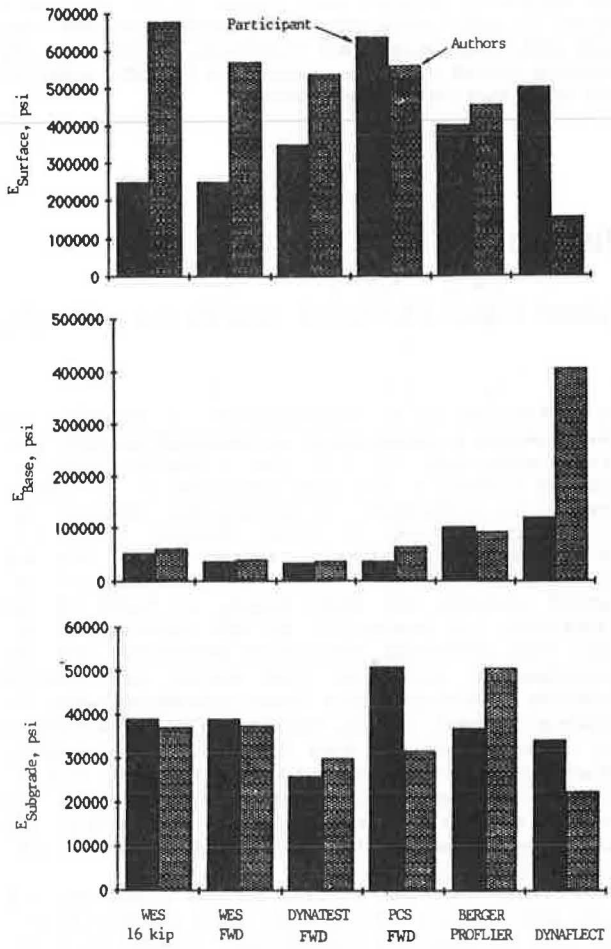

(Black indicates the results reported by an individual participant. Grey shows the results of the authors.)

FIGURE 18 Comparison of pavement evaluation results for Test Area 2.

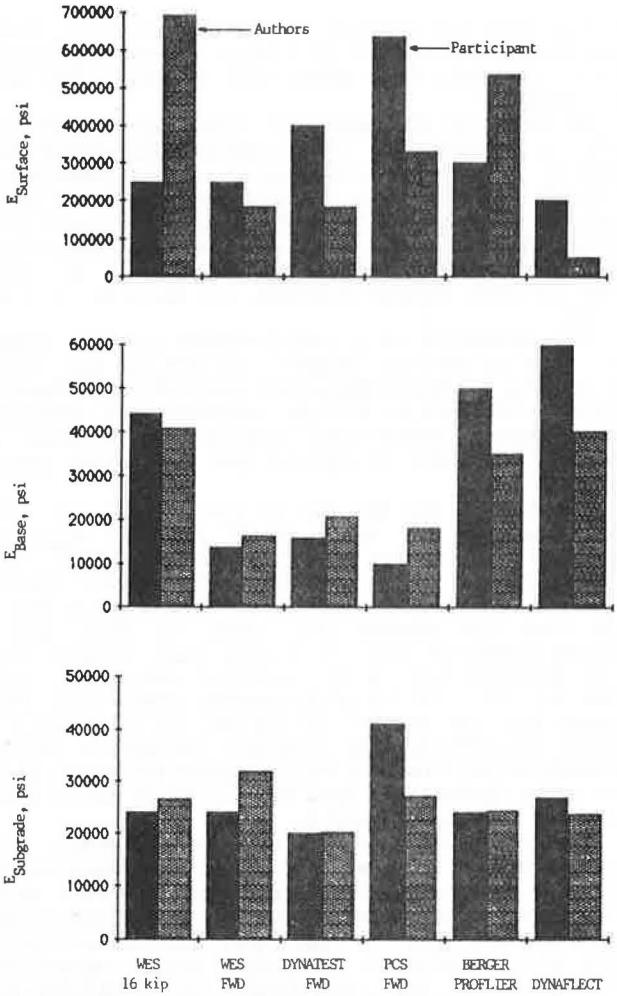

(Black indicates the results reported by an individual participant. Grey shows the results of the authors.)

FIGURE 19 Comparison of pavement evaluation results for Test Area 3.

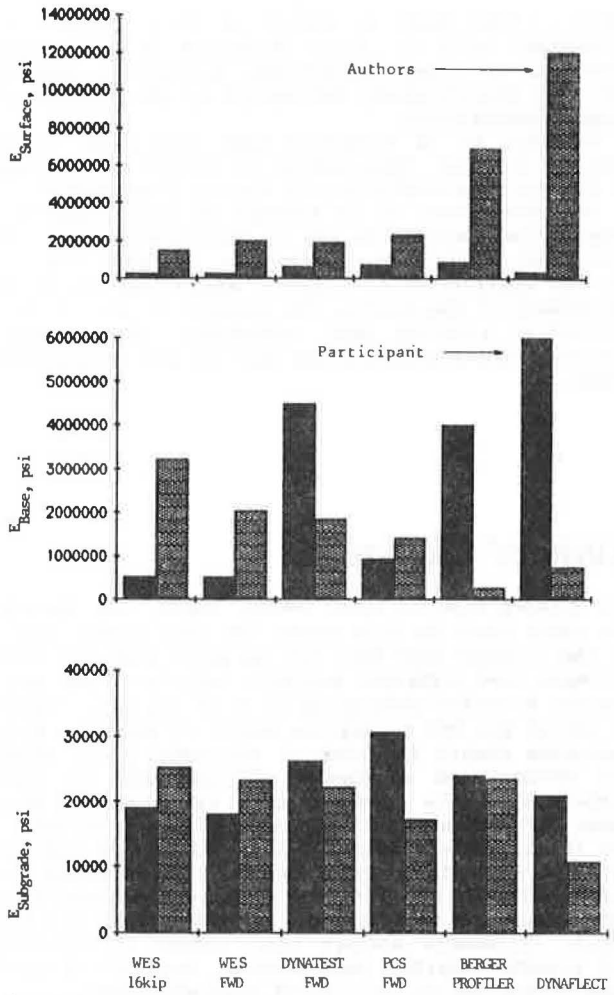

(Black indicates the results reported by an individual participant. Grey shows the results of the authors.)

FIGURE 20 Comparison of pavement evaluation results for Test Area 4.

1. Assumptions used in applying BISDEF to NDT data.
2. Using an arbitrary value of 20 ft for the depth to an assumed rock layer is a debatable point. Bush (1) found 20 ft to be a good assumption for obtaining a better fit for measured Road Rater 2008 deflections at the Pennsylvania test road facility. The authors apply the 20 ft assumption to all other NDT devices and geological conditions and to rigid pavements.
3. The basin-fitting technique in BISDEF is a function of an initial input estimate of moduli and a reasonable range defined by maximum and minimum values (E_{max} and E_{min}). A table that gives these values should have been provided by the authors.

Test Area 4

This is a composite pavement site. Independent evaluations from the participants (Table 5 and Figure 20) show moduli of all layers in reasonable agreement. In contrast, BISDEF produces unreasonably high values of AC modulus for all NDT devices. These high values are practically not possible in the climatic conditions of Florida. It would be interesting to know the E_{max} value of AC layer used in the analysis. Evidently this value must be more than 12 million psi.

On the basis of the BISDEF results, the authors discredit the Dynaflect for unreasonable values of PCC layer (716,925 psi) and subgrade (10,687 psi). The authors do not comment on the 12 million psi value for AC modulus. However, the in situ moduli (Table 5 and Figures 18-20) and allowable aircraft loads, evaluated by the discussants and presented in detail in the report (6), clearly demonstrate that the discussants' methodology does an excellent job: the results for allowable loads and overlay thickness are consistently reasonable.

COMMENTS ON AUTHORS' CONCLUSIONS

For the benefit of readers who do not have access to the report (6), the moduli evaluated by each participant should have been reported in this paper.

It is inferred in the second conclusion that a preload will result in a higher base modulus. This is apparently in error. The BISDEF program has computed a high base modulus (65,255 psi) for PCS FWD with no preload, which is not significantly different from the base modulus (59,740 psi) for the WES 16-kip device.

Conclusion 3 is quite true and timely, but there should be some independent measurement of in situ dynamic moduli (e.g., using different wave propagation techniques). Comparison with results of static

tests or laboratory M_R values is always debatable. Laboratory tests can never duplicate in situ environmental or stress conditions. Laboratory results are also significantly influenced by the effects of sample disturbances.

Finally, it is suggested that this paper could then be retitled "Application of BISDEF Methodology to NDT Data for Evaluation of Airport Pavements."

The main lesson to be learned is that compatible comparisons involve the use of the procedure and the analytical techniques appropriate to each device, not the application of a common analytical technique regardless of the device. The concept of system compatibility requires that compatible measurements, analyses, and predictions be used in any engineering study.

Authors' Closure

The authors wish to thank Uddin, Smith, and Treybig for their input to this paper. The discussants point to the results from Hall (6) in which each NDT participant used different analysis techniques for each device. A stated conclusion of Hall (6) was, "Based on use of the NDT evaluation method at MacDill, wide variation occurs in terms of allowable loads among the results and substantial disagreement of some methods with the standard test set method." This paper was presented to illustrate that the variability in allowable load could be significantly reduced by using a single analysis technique. This would allow an airport owner to use different equipment or consultants and be reasonably confident that the end result (allowable airport load, passes to failure, and possible overlay requirements) would be consistent regardless of the type of equipment used.

It was demonstrated, contrary to what the discussants say, that a single analysis technique can be used with different devices to produce consistent results.

The authors agree that a footnote should be added to Tables 1 and 2 to indicate that for the Dynaflect device the distance from the center of the load area is the distance from the midpoint of the loading wheels. The Dynaflect device was correctly modeled in the BISDEF program using two loaded areas and a deflection measurement centered between the loaded areas and four other deflections spaced at 1-ft intervals away from the first sensor.

Two methods can be used to compare deflection basins. One method, illustrated in the paper, shows differences in magnitude. The method used by the discussants is also acceptable. The selection depends on the point to be made. In the case of this paper, the authors were illustrating the relative magnitudes as shown.

In the prediction of moduli, the method presented by the authors produces the best fit of measured deflections to those determined from the layered theory. The moduli values reported in this paper are given in Table 10 of Hall (6). The differences given by the discussants in Table 5 and shown in Figures 18-20 are from values used for evaluation by each participant. The values that the discussants report were determined from a large number of tests over the entire pavement area and not from points where tests were conducted with all devices. Those values were also adjusted for design environmental conditions and were not the actual values that were determined from field data. For example, the modulus of the asphalt surface layer was adjusted to represent a value for a design pavement temperature. Moduli values reported in this paper are as determined from field data at a given test location with all NDT devices.

As stated in the paper, the BISDEF program is the same as CHEVDEF with the exception that BISAR was used as the multilayered elastic routine instead of CHEVRON. The advantages to using BISAR are that multiple loads can be evaluated, as in the case of the Dynaflect, and different layer interface conditions can be considered. The assumptions, which are the same for most layered programs, are the same in both cases.

The assumption of a semi-infinite subgrade layer can also be debated. Research at WES on test sections with surface deflections measured by different means in addition to NDT has indicated that measured and computed deflections compare better when a boundary condition is applied such as a rigid layer at 20 ft.

Research at the WES and as reported by Bush (1) indicates that the magnitude or range of E_{max} or E_{min} has little effect on the predicted moduli.

Discussants' questions about the moduli values from the Dynaflect deflections on Site 4 again deviate from the purpose and intent of this paper. Values presented are the values that produce the best possible fit to the measured deflections and were not adjusted to environmental conditions. The reason for the unusual values may be explained by Figure 17. Whereas the Dynaflect deflection basin, normalized for load, is significantly different from the other devices for Test Area 4, it is quite similar for Test Areas 2 and 3.

The conclusion that the base course moduli are greater when a preload is applied was questioned. This was true eight times out of nine when the FWDs were compared to the WES 16-kip vibrator (also eight of nine times when the Road Rater and the Dynaflect were each compared to the FWDs). Other comparative studies at the WES have shown this condition to occur in nearly all cases.

The authors believe that a single approach must be developed for each major airport authority such as the FAA, Air Force, Army, Navy, or state to ensure that reasonable comparisons of structural capacity can be obtained from different evaluations. The MacDill study concluded that variation could be expected from different procedures. The variation is due in part to the different models and different failure criteria that are used.

The development of pavement NDT equipment during the last 10 years has provided excellent tools for determining in situ material properties under simulated design loading conditions. Understanding the results from different devices can improve the overall assessment of pavement capacities and life.

REFERENCES

1. A.J. Bush III. Nondestructive Testing of Light Aircraft Pavements, Phase II: Development of the Nondestructive Evaluation Methodology. Report FAA-RD-80-9-II. Federal Aviation Administration, U.S. Department of Transportation, 1980.
2. J. Michelow. Analysis of Stresses and Displacements in an N-Layered Elastic System Under a Load Uniformly Distributed on a Circular Area. California Research Corporation, Richmond, Calif., 1963.
3. Koninilijke/Shell Laboratorium. BISAR Users Manual: Layered System Under Normal and Tangential Loads. Amsterdam, The Netherlands, 1972.
4. W. Heukelom and A.J.G. Klomp. Dynamic Testing as a Means of Controlling Pavements During and

After Construction. Proc., First International Conference on the Structural Design of Asphalt Pavements, Ann Arbor, Mich., 1975.
5. W.R. Barker and W.N. Brabston. Development of a Structural Design Procedure for Flexible Airport Pavements. Report FAA-RD-74-199. Federal Aviation Administration, U.S. Department of Transportation, 1975.
6. J.W. Hall, Jr. Comparative Study of Nondestructive Pavement Testing--MacDill Air Force Base. U.S. Air Force Engineering and Services Center, Tyndall AFB, Florida, 1984.
7. J.W. Hall, Jr. Flexible Airfield Pavement Evaluation. TM 5-827-2/AFM 88-24, Chapter 2. U.S. Air Force, Washington, D.C., April 1981.
8. W. Uddin, A.H. Meyer, W.R. Hudson, and K.H. Stokoe II. Project-Level Structural Evaluation for Pavements Based on Dynamic Deflections. In Transportation Research Record 1007, TRB, National Research Council, Washington, D.C., 1985, pp. 37-45.

Publication of the paper sponsored by Committee on Mechanics of Earth Masses and Layered Systems.

Application of Simplified Layered Systems to NDT Pavement Evaluation

GDALYAH WISEMAN, JACOB GREENSTEIN, and JACOB UZAN

ABSTRACT

Presented are nondestructive testing (NDT) deflection measurements on flexible, rigid, and composite pavements obtained with two vibratory devices, the Pavement Profiler and the WES 16-kip vibrator, and one impulse loading device, the falling weight deflectometer (FWD). The deflection bowls are analyzed in terms of the elastic parameters of layers using the Hogg, the Burmister, and the Odemark-Ullidtz approximation to linear layered elastic system models. The results are compared with those obtained using more exact solutions and are found to be satisfactory. The evaluated elastic parameters were found to be similar for all three NDT devices for the subgrade and the surface layers of the pavement. Lower elastic moduli were found for the base course with deflection bowls produced by the FWD than for those produced by the other two vibratory devices. Most pavement evaluation is done on pavements that have been in service for many years and have a varied history of maintenance and overlaying. The resulting lack of homogeneity must be considered in developing a strategy for meaningful pavement evaluation. It is therefore necessary to examine a large number of test points. The use of simplified layered system models for NDT pavement evaluation is, therefore, recommended. This makes it economically feasible to analyze each test point with respect to the relative contribution of the strength of the subgrade and the condition of the pavement structure to the overall performance of the pavement. It is also possible to examine material variability for each of the layers. Results of such computations given in this paper show higher variability in the asphaltic concrete and the base course layers than in the concrete or the subgrade.

Pavement evaluation is most frequently done on pavements that have been in service for many years and have a varied history of maintenance and overlaying. The resulting lack of homogeneity must be considered in developing a strategy for meaningful pavement evaluation. A large number of test points are therefore mandatory, so that the responsible engineer can make intelligent decisions with due regard to the statistical nature of the problems of pavement evaluation and rehabilitation.

Nondestructive testing (NDT) and deflection measurements are now universally recognized methods for the structural evaluation of road and airfield pavements. In many cases use is still made of empirical correlations between deflection under a test load and pavement performance. There is, however, general recognition that the maximum benefit is derived from NDT deflection measurements if the deflection bowl is interpreted in terms of the material parameters of the various component layers of pavement structure and subgrade.

The results of NDT deflection measurements on

flexible, rigid, and composite pavements obtained with both impulse and vibratory loading are presented here. The deflection bowls are analyzed in terms of the elastic parameters of layers using simplified approximations of the more exact linear layered elastic models. The results are compared with those obtained using the more exact solutions. The deflection bowls for the various pavements were measured with three different NDT devices and the computed moduli are compared and examined for variability.

Variability in deflection measurements has been extensively documented in the technical literature. Here an attempt is made to examine the variability in the evaluated moduli of elastic layers on the basis of measured deflections.

The use of simplified layered system models for NDT pavement evaluation makes it feasible to analyze each test point with respect to the relative contribution of the strength of the subgrade and the condition of the pavement structure to the overall performance of the pavement.

TESTING PROGRAM

The pavements tested were two rigid pavements 10.5 in. and 20 in. thick, two flexible pavements, and one composite pavement at MacDill Air Force Base in Tampa, Florida. The pavement elevations were from 5 to 10 ft above sea level and the water table was about 4 ft below ground surface. The subgrade soils were poorly graded sand with in situ California bearing ratio (CBR) values that ranged from 10 to 45. The two flexible pavements had base courses of Florida limerock with less than 30 percent retained on the No. 4 sieve, which classifies as a silty sand. This material is nonplastic but quite sensitive to moisture. It is customarily assigned a CBR of 80. The concrete pavements were placed directly on the poorly graded sand subgrade. The pavements tested were in five different areas and are numbered 1 to 5. Pavement types and thicknesses for each test area are shown in Figure 1.

Three different NDT devices were used. They are well known and will be only briefly described:

- A model 2000 Pavement Profiler (PP) applying a peak-to-peak force of 4,500 lb at a frequency of 25 Hz on an 18-in.-diameter plate.
- The Waterways Experiment Station (WES) 16-kip vibrator applying a peak-to-peak force of 29,200 lb at a frequency of 15 Hz on an 18-in.-diameter plate.
- A falling weight deflectometer (FWD) applying a peak impulse force of 14,200 lb on a 12-in.-diameter plate.

Testing with the 16-kip vibrator and the FWD was performed by WES and the field test records were made available.

Overall structural condition of pavement is sometimes described by the dynamic load required to produce a unit deflection and is termed stiffness. In the case of the Pavement Profiler and the 16-kip vibrator, stiffness is the peak-to-peak vibratory force (P) on an 18-in.-diameter plate divided by the peak-to-peak displacement of the pavement at the center of load application (Δ_o). In the case of the falling weight deflectometer, stiffness is the transient peak impulse force on a 12-in.-diameter plate divided by the maximum transient deflection at the center of load application.

The average pavement stiffness for each of the three NDT devices for all five test areas is shown in Figure 1. The lower pavement stiffness for FWD test results on the flexible pavements in Test Areas 2 and 3 is possibly due in part to the smaller diameter plate (12 in.) than that used for both the Pavement Profiler and the 16-kip vibrator (18 in.). This matter will be clarified further when the evaluated layer moduli are examined.

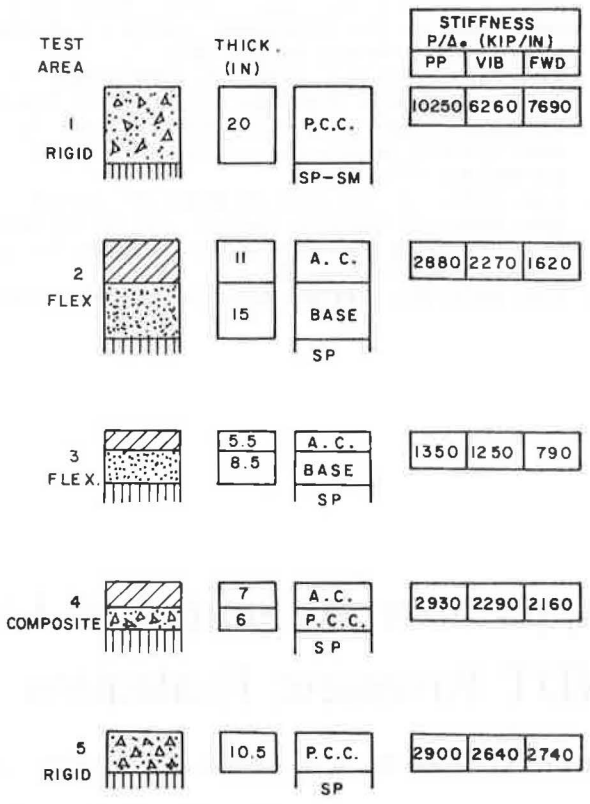

FIGURE 1 Description of five test pavements.

DEFLECTION BOWLS

With each of the NDT devices, in addition to measurements of the center deflection (Δ_o), measurements were made of the offset deflections (Δ_r) at various distances (r) from the center of load application. After examination of the measured deflection bowls, 15 sets of deflection bowl measurements (three NDT devices at each of five test areas) were created for subsequent analysis. For each test area care was taken to include only data from test points that had known pavement layer thicknesses. For the flexible pavements of Test Areas 2 and 3 it was therefore necessary to exclude test data from outer portions of the pavement close to the pavement edge, which apparently had layer thicknesses less than those given in Table 1. In Test Areas 1, 4, and 5 all the measured data were used. The average measured deflection per unit load as a function of offset distance for each of the three NDT devices for the 10.5-in. rigid pavement of Test Area 5 is shown in Figure 2.

Because, at least in the first approximation, pavement systems are linear, this presentation of the data (deflection per unit load) for three devices with applied loads of 4.5, 14.2, and 29.2 kips, respectively, allows an easier comparison of the deflection bowls than does a direct comparison of the actual measured deflections.

It should be noted that, for Test Area 5 with the 10.5-in. concrete pavement, all three devices had almost identical average deflection bowls when normalized with respect to load. (This pavement would

TABLE 1 Coefficients of Variation of Deflection Measurements

No. of Test Points	Equipment	Coefficient of Variation (percentage) for Sensor 1	2	3	4
Test Area 1					
28	WES vibrator	11	8	8	9
27	FWD	9		9	7
8	PP	12	12	14	18
Test Area 2					
8	WES vibrator	10	13	14	12
8	FWD	13	12	12	15
8	PP	11	13	16	19
Test Area 3					
11	WES vibrator	9	9	9	9
11	FWD	14	12	11	11
11	PP	13	13	15	15
Test Area 4					
12	WES vibrator	13	14	16	21
11	FWD	14		10	9
10	PP	28	28	38	38
Test Area 5					
35	WES vibrator	7	8	9	10
34	FWD	7		7	8
22	PP	11	13	13	14

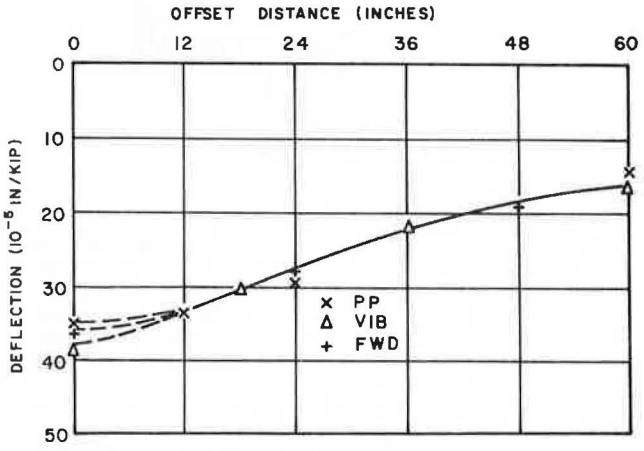

FIGURE 2 Deflection bowls, Test Area 5.

be expected to exhibit the most linear behavior of all the pavements tested.) The comparative results for this pavement establish a high degree of confidence in both the load and the deflection measuring instrumentation for all three NDT devices.

Shown in Figures 3 and 4 are the average deflection ratios (Δ_r/Δ_o) as a function of offset distance (r) for each of the five test areas for the Pavement Profiler and the falling weight deflectometer, respectively. The overall pavement stiffness, based on center deflection alone, is shown in Figure 1. It may be observed that the stiffest pavement is the 20-in. concrete pavement of Test Area 1 and the pavement with the lowest stiffness is the asphalt concrete pavement of Test Area 3. The relative load distribution capabilities of these pavements may be seen in Figures 3 and 4. Also shown in Figures 3 and 4 are the computed deflection ratios for the Hogg model of a thin plate on a finite elastic subgrade

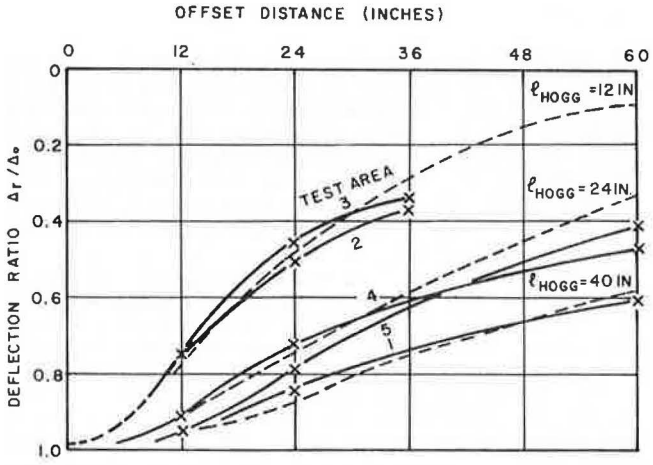

FIGURE 3 Deflection ratios, Test Areas 1-5 (Pavement Profiler).

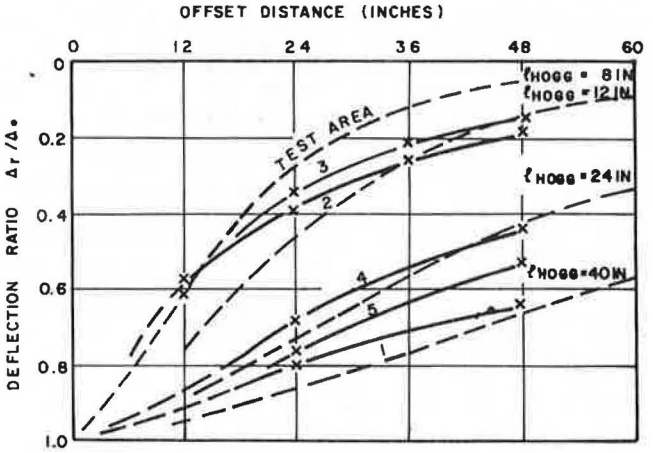

FIGURE 4 Deflection ratios, Test Areas 1-5 (FWD).

for various values of the characteristic length of the deflection bowl (ℓ). These curves are for an elastic subgrade of thickness (h) 10 times the characteristic length of the deflection bowl (ℓ). Pavement models are discussed in greater detail next.

PAVEMENT MODELS

The cases considered subsequently are all for a uniform applied vertical load on a circular area on the surface of a layered isotropic linear elastic medium. Generally, it is assumed that the thickness and number of the layers comprising the pavement system are known and that Poisson's ratio can be estimated. An exact solution can be obtained for surface deflection bowls for given moduli of elasticity using various available computer programs that require the use of at least a minicomputer. One such program has been used as a standard against which to compare the results obtained with simpler models and computational routines.

In all cases a finite subgrade thickness was assumed to be underlain by a hard bottom. This has the effect of limiting the lateral extent of the computed deflection bowls and approximates the response of a more realistic subgrade with a modulus of elasticity that increases with depth.

Hogg Model

The authors have been using the Hogg model (1,2) of a thin plate on an elastic foundation for interpreting deflection measurements on road and airfield pavements for 10 years. Extensive use of the Hogg model has shown it to yield satisfactory results for the modulus of elasticity of the subgrade (E_o) compared with values obtained from in situ testing. In addition to its simplicity, one of the advantages of thin plate theory is that E_o can be computed from the deflection bowl measurements without prior knowledge of the thickness or other characteristics of the pavement layers above the subgrade. Others have also found the Hogg model to be useful in pavement evaluation studies (3).

The background and computational routines for the use of the Hogg model in pavement evaluation have been described elsewhere (4-6) and will not be repeated here.

Burmister Model (two layer)

When the Hogg model, which is that of a thin plate on an elastic subgrade, is used for interpreting surface deflection measurements, it is assumed that vertical strains within the pavement structure are small and can be ignored. For conventional flexible pavements the measured value of Δ_o, which is measured at the center of load application at the surface of the pavement, obviously includes vertical strains in the pavement. Thus the measured Δ_o is greater than that assumed for the mathematical model and Δ_r/Δ_o is therefore smaller than assumed. This leads to an underestimate of the characteristic length of the deflection bowl (ℓ). It can be shown that if Δ_r is measured at a distance (r) where Δ_r/Δ_o is about 0.5, these errors are compensatory and therefore have a negligible influence on the computed value of E_o.

When E_o and the characteristic length of the deflection bowl (ℓ) have been computed, the flexural rigidity (D) of the pavement structure is easily computed. If the combined thickness (h*) of the pavement structure is known, the combined modulus (E*) of the pavement can be computed. This procedure can be used for rigid pavements and sometimes gives reasonable results for flexible pavements (3).

The use of Burmister two-layer theory appears to be a more promising approach for determining the combined modulus (E*) of the pavement structure (5). Assume that the subgrade modulus (E_o), the combined thickness of the pavement (h*), and the radius of the loaded area (a) are known. Using only the measured center deflection (Δ_o), the computation of E^*/E_o and hence of E* is easily performed using Odemark's approximation to the Burmister solution (6,7).

Computations have been performed for E^*/E_o for various values of F (i.e., the ratio of the center deflection for the two-layer system to the computed deflection for the Boussinesq case) and for h*/a using both the Hogg model and the Burmister model. The results are shown in Figure 5. It may be observed that only for strong thin pavements do the two models give similar results. It should also be noted that the Burmister model, which accounts correctly for the vertical strain in the pavement structure, is not sensitive to inaccuracy in the total pavement thickness (h*) for thicker flexible pavements.

Three-Layer Elastic Model

Several computer codes are available for obtaining an exact solution for surface deflections for layered linear elastic media of given elastic material parameters and layer thicknesses. The computer code used here is called CRANLAY (8,p.131). The analytical solutions for displacement are found by integral transform methods and are evaluated by numerical integration. To obtain the three unknown elastic moduli from measured deflection bowls, the following procedure was developed.

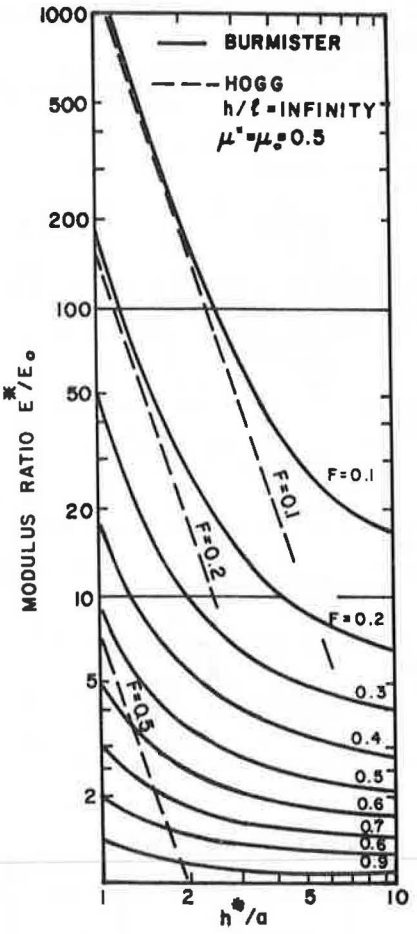

FIGURE 5 Comparison of E^*/E_o computed by the Hogg and Burmister models.

For each test area with known pavement thicknesses the CRANLAY computer code was used to compute surface deflections at the required offset distances for a range of modular ratios. The moduli of elasticity of the three pavement layers were then computed by solving a system of three equations that relate the surface deflections at the given offset distances to the moduli of elasticity. In this procedure the number of measured deflections used must equal the number of unknown moduli. The method is not iterative and the three equations are solved by direct numerical methods.

As a check on the method several computations were done using the evaluated elastic moduli obtained as input in the CRANLAY program. The computed surface deflections were then compared to the measured deflections used for computing the elastic moduli. In all cases the difference between the measured and and the computed deflections was found to be less than 0.5 percent.

Simplified Multilayer Model

This model is based on Odemark's method of "equivalent thicknesses" (6,7) and has been further devel-

oped and described in detail by Ullidtz and Peattie (9,10). The computations for surface deflection are performed for a transformed section using the Boussinesq equation for circular loading for the center deflection (Δ_o) and the equations for point loading for offset deflections (Δ_r). The pavement is assumed to be made up of layers of known thickness and Poisson's ratio is assumed to be known; however, the moduli of elasticity are unknown. It is further assumed that the center deflection (Δ_o) and the deflection (Δ_r) at several offset distances (r) have been measured with an NDT device applying a known load (P) on a circular plate of radius a.

The procedure followed is iterative. First, the unknown moduli of elasticity are "guessed" for the various pavement layers and then the resulting deflections at the center of load application and at offset distances (r) at which measurements were made are computed. The modulus of elasticity values are then modified until an "acceptable" match is obtained between the computed and the measured deflections.

The method can be used for two or more pavement layers and is known to give computed surface deflections quite close to those computed by the most exact methods. It will be demonstrated that, when used in the reverse mode as described earlier, it also yields evaluated layer elastic parameters similar to those obtained with the most exact methods.

The computations were done using a personal computer in the interactive mode. The match between measured and computed deflections was considered to be acceptable when the center deflections matched within 3 percent and the remaining deflections matched within 10 percent. For the two concrete pavements the center deflection and the furthest measured deflection matched to less than 0.5 percent.

COMPUTED ELASTIC PARAMETERS--A COMPARISON OF MODELS

The various pavement models and computational routines that have been presented have been used to analyze the 15 average deflection bowls. For a known pavement section and elastic moduli, each of the pavement models would produce slightly different deflection bowls. However, it was of considerably more interest to compare the evaluated elastic parameters.

The subgrade modulus values for all three pavement types computed with the Odemark-Ullidtz simplified multilayer elastic model showed excellent agreement with those values computed with the "exact" CRANLAY computer program (Figure 6). The simpler Hogg model also showed good agreement with the CRANLAY computations for the subgrade modulus (Figure 7).

Figure 8 shows the combined modulus (E*) for a two-layer system for all pavements tested using Odemark-Ullidtz compared with the Hogg model for determining the subgrade modulus (E_o) and Odemark's approximation for the Burmister solution, for center deflection only, for determining E^*/E_o and hence E*. For the rigid pavement, h* is the thickness of concrete, for the flexible pavements the combined thickness of asphaltic concrete and base, and for the composite pavement the combined thickness of asphalt concrete overlay and the old concrete pavement. The agreement is excellent.

Shown in Figure 9 are the subgrade, base course, asphalt concrete, and portland cement concrete moduli for the rigid and flexible pavements. The values were computed using the same deflection bowls with the Odemark-Ullidtz simplified method of computation and the CRANLAY computer program. It should be noted that the scales in Figure 9 are log-log. The agree-

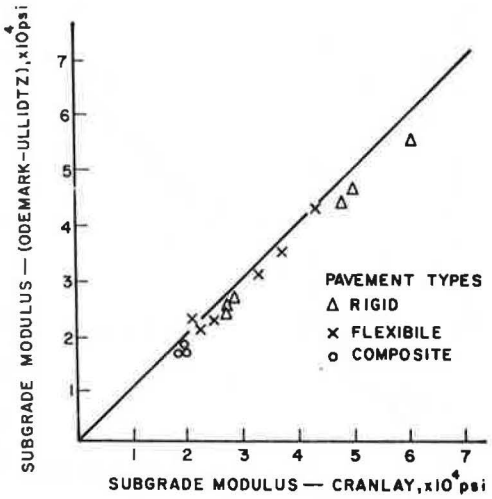

FIGURE 6 Comparison of subgrade modulus computed using Hogg and CRANLAY.

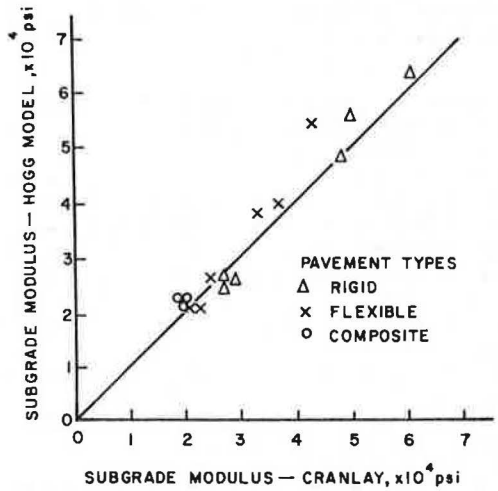

FIGURE 7 Comparison of subgrade modulus using Odemark-Ullidtz and CRANLAY.

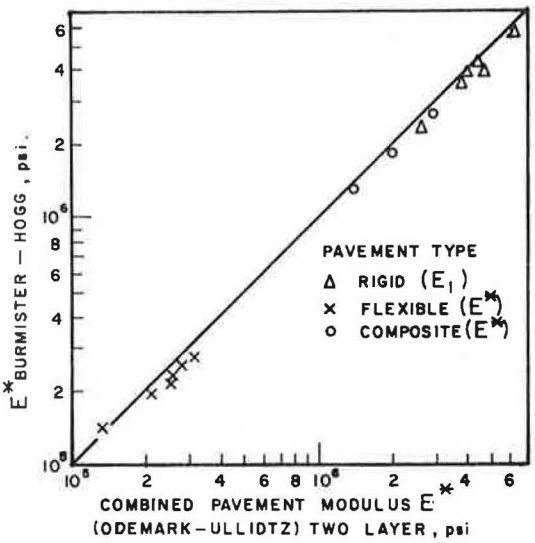

FIGURE 8 Comparison of combined modulus (E*) computed using Burmister-Hogg and Odemark-Ullidtz.

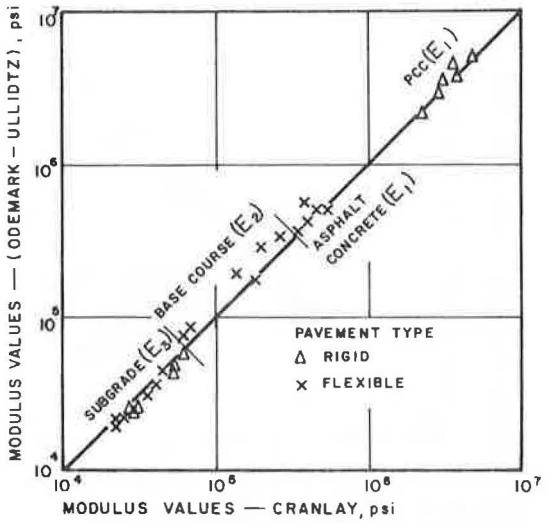

FIGURE 9 Comparison of E_1, E_2, and E_3 using Odemark-Ullidtz and CRANLAY.

ment between the two methods of computation is again remarkably good.

COMPARISON OF LAYER MODULI COMPUTED FOR AVERAGE DEFLECTION BOWLS OBTAINED WITH THE VARIOUS NDT DEVICES

For the purposes of this comparison, the discussion will be limited to the layer modulus values computed by the approximation to the layered elastic model used in the method of equivalent thicknesses. These moduli for the five test areas and the three NDT devices are shown graphically on a logarithmic scale in Figure 10.

The first and most striking observation is that, on the basis of knowledge of materials in the pavement sections at the five test areas, almost all of the layer modulus values obtained with the three NDT devices are reasonable. The two exceptions (out of a total of 39 determinations of layer moduli) were 6.6 million psi for the 20-in. concrete determined in Test Area 1 and the 8 million psi for the 6-in. overlaid concrete determined in Test Area 4, both with the Pavement Profiler.

The modulus values for the subgrade ranged from 20,000 to 26,000 psi for Areas 3, 4, and 5 and from 34,000 to 54,000 psi for Areas 1 and 2, for all three NDT devices. There was a consistent pattern for all areas (except Test Area 4) with the heavier load device giving the lower evaluated subgrade modulus. It should be pointed out, however, that the maximum difference between NDT devices for the subgrade modulus is about 25 percent.

In general, the modular values for portland cement concrete and for asphalt concrete are reasonable and do not differ significantly with the various NDT devices. The one exception as mentioned previously is the Pavement Profiler on the 20-in. concrete pavement.

The modulus values for the base course ranged for the Pavement Profiler and the 16-kip vibrator from 135,000 to 270,000 psi and were about 65,000 psi for the FWD. The 16-kip vibrator gave higher values for Test Area 3 and lower values for Test Area 2 than did the Pavement Profiler.

The lower evaluated moduli for the base course in Test Areas 2 and 3, based on an interpretation of the deflection bowls measured with the FWD, require further study that is beyond the scope of this

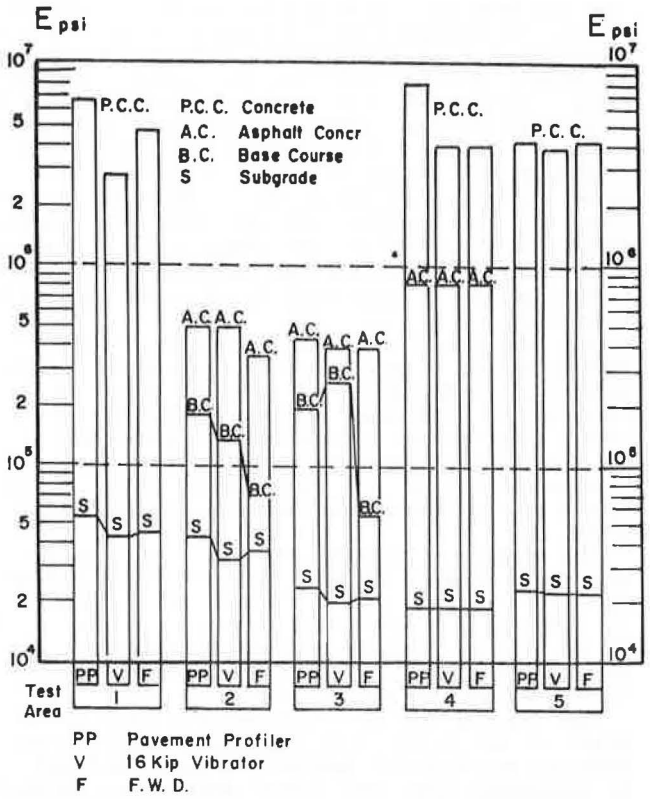

FIGURE 10 Comparison of layer moduli for Test Areas 1-5 for three NDT devices.

paper. Refer to Figure 1 and the overall stiffnesses based on center deflection alone. It is now evident that the lower stiffnesses measured in Test Areas 2 and 3 with the FWD are due to the response of the base course to impulse loading and not just to the smaller diameter plate.

MATERIAL VARIABILITY

Material variability and its effect on design have been and will continue to be of prime importance in all geotechnical problems (11). Pavement design, evaluation, and rehabilitation involve the determination of parameters that possess natural variability. For each problem the appropriate percentile level of the distribution can be selected on the basis of reliability considerations. For example, in overlay design based on center deflection measurements, the 80th and 97th percentiles are sometimes used (12,13). When the deflection bowl is measured at several offset distances from the load, and its interpretation is expressed in terms of moduli of elasticity of the pavement layers, the statistical analysis of the results and its implications are not yet clear. It is the purpose of this section to discuss the problem. The test sections are those reported previously, and the results of analysis refer to the deflection bowl interpretation using multilayer elastic theory.

Table 1 gives the coefficients of variation (CV) of the deflections measured at four distances with three different NDT devices. It is seen that the coefficient of variation lies between 8 and 19 percent, with the higher values obtained using the Pavement Profiler.

Table 2 gives the coefficients of variation of the moduli derived for all tests. It is seen that

TABLE 2 Coefficients of Variation of Elastic Moduli of Pavement Layers—CRANLAY

No. of Test Points	Equipment	Coefficient of Variation (percentage) E1	E2	E3
Test Area 1				
28	WES vibrator	16		10
27	FWD	23		13
8	PP	14		21
Test Area 2				
7	WES vibrator	21	22	14
8	FWD	41	29	15
8	PP	35	50	18
Test Area 3				
9	WES vibrator	50	52	7
11	FWD	38	38	8
10	PP	85	77	15
Test Area 5				
35	WES vibrator	17		11
34	FWD	22		10
22	PP	19		13

the coefficients of variation of the subgrade (E3) are of the order of 7 to 21 percent. The values are similar to those obtained in deflection analyses of Sensor 4 (Table 1). Therefore, it appears that the deflections of the sensor far from the load and their coefficients of variation are mainly related to the subgrade modulus and its coefficient of variation. The coefficients of variation of the concrete modulus (E1 in Test Areas 1 and 5) are of the order of 14 to 23 percent and are similar for all NDT devices. An examination of Tables 1 and 2 shows that the coefficients of variation of the moduli of the asphaltic concrete and the base course are 2 to 7 times those of the deflections.

Therefore, it appears that statistical analysis of the deflections can provide an estimate of the variability of the subgrade. However, it does not represent the variability of the pavement layers. It is not clear at this stage which part of the variability is due to the equipment. It is worth mentioning that determining the moduli using an average deflection bowl and averaging the moduli obtained from deflection interpretation give about the same result.

It can be seen, however, that analyzing all deflection bowls instead of an average deflection bowl gives additional information on the pavement condition and is therefore useful in pavement evaluation. The use of an iterative procedure with a multilayer computer program like CRANLAY is in most cases prohibitively expensive. Therefore, development and use of simplified methods for analyzing a large amount of data are of considerable importance.

CONCLUSIONS

The Pavement Profiler, the 16-kip vibrator, and the falling weight deflectometer all have instrumentation satisfactory for measuring both applied force and resulting deflections. This is evidenced by the almost identical deflection bowls for the 10.5-in. concrete pavement of Test Area 5 when normalized with respect to applied load.

Deflection bowls normalized with respect to load (i.e., plotted as deflection per unit load) are especially useful in comparing NDT devices that apply different loads to the pavement. Deflection bowls normalized with respect to center deflection are particularly useful in comparing different pavements. For example, the flexible pavement in Test Area 2 and the composite pavement of Test Area 4 have almost identical center deflection per unit load, but the characteristics of the bowl of deflection ratios are entirely different.

The shapes of the deflection bowls produced by all three NDT devices are sufficiently close to those predicted by the Hogg model to allow it to be used with confidence in pavement evaluation, particularly for evaluating the modulus of the subgrade.

The combined Burmister-Hogg computational routine using the Odemark approximation is useful and efficient for obtaining a combined modulus (E*) for the pavement (Figure 8).

The Odemark-Ullidtz simplified multilayer elastic method gave evaluated elastic moduli almost identical to those computed with the most exact methods, except for the base course (Figure 9).

All three NDT devices gave similar layer moduli for concrete, asphaltic concrete, and the subgrade. The moduli for the base course determined from the deflection bowls produced by the falling weight deflectometer were significantly lower than those obtained from analyzing the deflection bowls produced by either the Pavement Profiler or the 16-kip vibrator (Figure 10).

Variability in measured pavement deflections can be a reasonable measure of variability in subgrade modulus. However, to obtain a measure of material variability for the various layers of the pavement it is necessary to analyze a large number of deflection bowls. The simplified models presented in this paper have been found useful in this context.

REFERENCES

1. A.H.A. Hogg. Equilibrium of a Thin Plate Symmetrically Loaded Resting on an Elastic Foundation of Infinite Depth. Philosophic Magazine, Vol. 25, No. 168, 1938.
2. A.H.A. Hogg. Equilibrium of a Thin Slab on an Elastic Foundation of Finite Depth. Philosophic Magazine, Vol. 35, No. 243, 1944.
3. W.T. Hoyinck, R. Van Den Ban, and W. Gerritsen. Lacroix Overlay Design by Three-Layer Analysis. Proc., Fifth International Conference on the Structural Design of Asphalt Pavements, Delft, The Netherlands, Vol. 1, 1982, pp. 410-420.
4. G. Wiseman. The Deflection of an Elastic Plate on an Elastic Foundation. Proc., Fifth Asian Regional Conference on Soil Mechanics and Foundation Engineering, Bangalore, India, Vol. 1, 1975, pp. 341-346.
5. G. Wiseman, J. Uzan, M.S. Hoffman, I. Ishai, and M. Livneh. Simple Elastic Models for Pavement Evaluation Using Measured Surface Deflection Bowls. Proc., Fourth International Conference on Structural Design of Asphalt Pavements, Ann Arbor, Mich., Vol. 2, 1977, pp. 416-426.
6. G. Wiseman and J. Greenstein. Comparison of Methods of Determining Pavement Parameters from Deflection Bowl Measurements. Proc., Seventh Asian Regional Conference on Soil Mechanics and Foundation Engineering, Haifa, Israel, Vol. 1, 1983, pp. 158-165.
7. N. Odemark. Investigation as to the Elastic Properties of Soils and the Design of Pavements According to the Theory of Elasticity. Report 77. National Swedish Road and Traffic Research Institute, Linkoping, Sweden, 1949.
8. W.J. Harrison, L.J. Wardle, and C.M. Gerrard.

Computer Programmes for Circle and Strip Loads on Layered Anisotropic Media. Division of Applied Geomechanics, Commonwealth Scientific and Industrial Research Organisation (Australia), 1972.
9. P. Ullidtz and K.R. Peattie. Pavement Analysis by Programmable Calculators. Journal of the Transportation Engineering Division, ASCE, Vol. 106, No. TE5, 1980, pp. 581-597.
10. K.R. Peattie and P. Ullidtz. Simplified Computing Techniques for Analysing Flexible Pavements. Proc., Institute of Civil Engineers, Part 2, Vol. 71, London, England, March 1981, pp. 185-196.
11. E.J. Yoder and M.W. Witczak. Principles of Pavement Design, 2nd ed. John Wiley and Sons, Inc., New York, N.Y., 1975, Chapter 13, Material Variability, pp. 413-442.
12. J.A. Mattew. Pavement Evaluation Using Nondestructive Testing. Proc., Twenty-Ninth California Transportation and Public Works Conference, San Diego, Calif., 1977, pp. 278-295.
13. Asphalt Overlays and Pavement Rehabilitation. MS-17. The Asphalt Institute, College Park, Md., 1977.

Publication of this paper sponsored by Committee on Mechanics of Earth Masses and Layered Systems.

Analytical-Empirical Pavement Evaluation Using the Falling Weight Deflectometer

P. ULLIDTZ and R. N. STUBSTAD

ABSTRACT

Because of the rapid development of hardware and software during the past 10 years, it is now possible to use an analytical-empirical (or mechanistic) method of structural pavement evaluation on a routine basis. The Dynatest 8000 falling weight deflectometer that, when used with the ELMOD program, determines the modulus of each structural layer in a pavement system is described. The moduli are determined nondestructively and in situ under conditions that closely resemble those under the influence of heavy traffic. Some practical examples illustrating the use of the method are presented, and its empirical components are discussed. These empirical components are also programmed into the ELMOD program so an overlay design may be carried out concurrently with the analytical determination of layered elastic moduli. The method may be used for both flexible and rigid pavements, where joint evaluation is not needed. The evaluation of joint or corner conditions in jointed portland cement concrete pavements is not addressed in this paper.

Structural design of pavement systems should be based on an "analytical-empirical" approach. Often, such an approach is referred to as an "analytical method" or a "mechanistic method," but because it still contains an important empirical component (see the fourth section), the term "analytical-empirical" is more correct. The desirability of an analytical-empirical approach appears to be a universally agreed-on precept among pavement engineers, particularly as a result of the Fifth International Conference on the Structural Design of Asphalt Pavements held in Delft, The Netherlands, in 1982.

The analytical-empirical method presented here makes use of the same approach that is used in most other structural engineering design, that is:

1. The loadings and environmental conditions are determined;
2. The elastic modulus (Young's modulus) is determined for each material in the structure;
3. The critical stresses or strains, as a result of loadings, are calculated in each material; and
4. The thicknesses (or the materials) are modified until the critical stresses or strains do not exceed permissible values.

One reason (of many) for using this approach is the increased need for pavement maintenance and rehabilitation. To make the right choice from many potentially feasible maintenance and rehabilitation measures, the engineer must base his decision on a rational evaluation of the mechanical properties of the materials in the existing pavement structure. To accomplish this, existing empirical methods of pavement design are inadequate. Instead, a combined analytical-empirical evaluation procedure should be followed.

One serious obstacle, however, has been the difficulty of determining the in situ elastic moduli of pavement materials. Three- or four-point bending tests or dynamic triaxial tests are both cumbersome and costly, and the results are not necessarily representative of in situ conditions. Estimating moduli from empirical relationships based on California bearing ratios (CBRs), R-values, or other parameters is hardly satisfactory.

Now, however, the recent rapid development of appropriate hardware and software has made it possible to determine the elastic modulus of each structural layer in a pavement structure. This can be accomplished in situ, nondestructively, and rapidly. With a proper falling weight deflectometer (FWD) and suitably associated software, it is possible to carry out analytical-empirical pavement evaluation on a routine basis. The following is a brief description of one such system, namely the Dynatest 8000 FWD (Figure 1) and the Evaluation of Layer Moduli and Overlay Design (ELMOD) program.

FIGURE 1 Dynatest Model 8000 FWD.

DYNATEST 8000 FALLING WEIGHT DEFLECTOMETER

For a deflection testing device to be used to determine in situ moduli of pavement materials, the following requirements should be met:

1. The load must resemble that of a heavy wheel passage in terms of both load magnitude and duration.
2. Deflections must be measured extremely accurately, especially at distances from 0.6 m (2 ft) to 1.5 m (5 ft) from the center of the loaded area. These deflections are used to determine the modulus of the subgrade and must therefore be accurate because the subgrade generally contributes 60 to 80 percent of the total center deflection. A small error in the determination of the subgrade modulus could, therefore, lead to extremely large errors in the moduli of the other pavement layers. (For the same reason, it is also essential to consider any existing nonlinearity of the subgrade.)

With respect to load magnitude, any appropriate "design" half-axle load (e.g., 9,000 lbf, 50 kN) may be simulated by the Dynatest FWD. A load of more than 10 metric tons (approximately 24,000 lbf) may also be obtained if desired (e.g., for evaluating airfield pavements). The duration of the load is generally fixed at 25 to 30 msec, roughly corresponding to a wheel velocity of 40 to 50 MPH (60 to 80 km/hr). The deflections are measured with geophones at seven different distances from the loading plate, and, because no reference point or support is needed (the reference point is the center of gravity of the earth), the deflections may be determined quite accurately. A typical accuracy is 0.5 percent ± 1 μm (1 μm = 1/1000 mm = 0.04 mil).

On many occasions, pavement response in terms of stresses, strains, and deflections from an FWD-imposed load has been compared to the response to a moving wheel load. Details of some of these comparisons may be found elsewhere (1-3). All these comparisons have shown that the response to an FWD test is quite close to the response to a moving wheel load of the same magnitude, even though the impulse load of the FWD, in some respects, differs from a moving wheel load.

If, therefore, an accurate deflection basin is measured under an FWD test and then the theory of elasticity is used to determine the elastic moduli of the individual layers such that the same deflection basin is produced, the engineer can be reasonably certain that the layer moduli thus obtained will be representative of the response of the pavement materials under heavy traffic loading, even though, strictly speaking, the analysis technique is quasi-static whereas the loading is dynamic.

Details of the Dynatest FWD test system may be found elsewhere (4), but it may be added here that the production capacity is some 200 to 300 test points per day, depending on the distance between points, and that more than 30 of these test systems are now in operation (mostly in North America and Europe).

CALCULATION OF ELASTIC MODULI

Pavement sections are not composed of ideal elastic materials. In addition to elastic deformations, most pavement materials exhibit plastic, viscous, viscoelastic and/or viscoplastic deformations under load, and in most cases the relationships between load and deformation are nonlinear. Many materials are anisotropic, often as a function of the state of stress, and few materials are homogeneous--some are even "particulate," consisting of significantly large, discrete particles. Adding to this the variability of the materials with time and place and the dynamic loading conditions, it should be clear that layered elastic theory is just an approximation of "real-life" conditions.

Nevertheless, this approximation of reality offers, at the present time, the most promising approach to reaching a more fundamental understanding of the performance of pavements. For this reason, elastic theory has been incorporated into a number of current design methods, such as those by Shell, Chevron, and the Asphalt Institute as well as those implemented by several countries. "Elastic modulus" in this paper should be understood to be an apparent modulus or effective stiffness.

To determine moduli, programs developed by Chevron, Shell, and the Laboratoire Central des Chaussées as well as several other institutions may be used. However, the method of equivalent thicknesses (MET) (5,6) used in the ELMOD program is at least as reliable and effective as the other, more sophisticated programs for use on FWD-generated test data. There are two primary reasons for this:

1. First, a mainframe computer is not needed. The calculations can be rapidly carried out on a microcomputer. This means that each FWD deflection basin, instead of just a few "representative" or average basins, may be analyzed. Even more important, the MET may be easily incorporated in a pavement management system, under which critical stresses or strains may have to be evaluated literally millions of times.

2. Second, and most important, it is quite easy to incorporate a nonlinear, elastic subgrade into the MET procedure, and this is essential for determining even reasonably accurate layer moduli from measured FWD deflections, because of the lateral variation of subgrade modulus under load. This procedure is discussed in detail elsewhere (7).

The basic assumption in the MET is that the stresses, strains, and deflections below a given layer interface depend on the stiffness and thickness of the layers above that interface. This concept is used to transform a layered structure into an equivalent uniform, semi-infinite material, to which Boussinesq's simple equations may be applied.

There is a certain resistance against using this relatively "simple" method today because a number of "exact" elastic layered programs are readily available. It should not be overlooked, however, that the assumptions on which these "exact" programs are based are not really indicative of the actual conditions existing in a pavement structure.

As mentioned previously, deformations under load are not only elastic but also plastic, viscous, and/or viscoelastic. The materials are often nonlinear (stress dependent), anisotropic, and inhomogeneous; some even consist of large, discrete particles (e.g., coarse granular materials). These differences between the idealized assumptions on which layered elastic programs are based, coupled with the complex nature of actual pavement materials, are not mitigated by the use of complex mathematics.

Even though the elastic layer programs cannot be considered more exact than the MET when it comes to the behavior of real pavements, the MET has, on a number of occasions, been compared to different elastic layer programs (6). In general, the results have indicated a reasonably good agreement for deflections and stresses, and somewhat less satisfactory agreement for strains.

ELMOD Program

Using FWD-derived load deflection data, the structural evaluation may be carried out with the ELMOD program, which is based on the MET. This program operates on the same microcomputer that controls the FWD field operation. An IBM personal computer version of the program is also available.

The FWD measures the force applied to the pavement plus the deflections at seven different distances from the loading plate. During testing, these values are stored on magnetic tape and later are read by the ELMOD program. In addition, the thicknesses of the structural layers in the pavement must be input (Figure 2). A two-, three-, or four-layer system may be specified.

The ELMOD program will then automatically determine the layer moduli that will produce the same deflection basin as measured. During this iteration, the program also determines any actual or apparent nonlinearity of the subgrade. The lateral variation of subgrade stress is considered and, therefore, the subgrade may be treated as a single, nonlinear elastic layer. This nonlinearity is extremely important in facilitating a reasonably accurate determination of both the subgrade and the remaining, overlying structural layer moduli.

A series of checks was made to compare the ELMOD program with the CIRCLY computer program (8). For 42 different three-layer structures, the surface deflections corresponding to a standard FWD load were calculated with CIRCLY at distances 0, 1.5a, 2a, 3a, 4a, 6a, 8a, and 10a, where "a" is the radius of the loaded area. The range of employed layer moduli and thicknesses was as follows:

E_1/E_3 = 10, 20, 50, 100, 200, 400
h_1/a = 0.5, 0.67, 1, 1.33, 2, 2.67, 3.33
E_2/E_3 = 3
h_2/a = 2

where

E_1 = modulus of Layer 1,
h_1 = thickness of Layer 1,
E_2 = modulus of Layer 2,
h_2 = thickness of Layer 2, and
E_3 = modulus of the (semi-infinite) subgrade.

In all calculations it was assumed that the FWD load was uniformly distributed over a circular area; that all materials (layers) were homogeneous, isotropic, and linear elastic; and that all had a Poisson's ratio of 0.35. All interfaces were considered "rough" (no slip between layers).

The calculated deflections were then used as input to the ELMOD program and the moduli of the three layers were calculated. The thickest and stiffest structures, for which both $E_1/E_3 \geq 100$ and $h_1/a \geq 2$, were treated as two-layer structures.

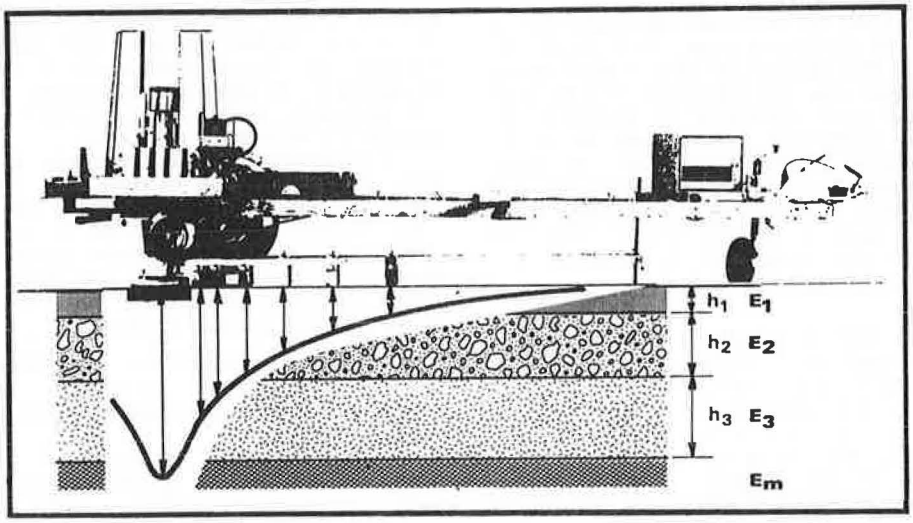

FIGURE 2 Principle of Moduli Determination.

Denoting the moduli obtained with the ELMOD program E'_i and those used as CIRCLY input values E_i, and assuming a log-normal distribution of moduli ratios, the following ratios between ELMOD-calculated and CIRCLY input values were obtained:

	Mean Value	90 Percent Certainty Range
E'_1/E_1	1.01	0.77 - 1.34
E'_2/E_2	1.03	0.70 - 1.52
E'_3/E_3	1.00	0.95 - 1.06

Although the mean values were close to unity, a fairly wide scatter is noted for E_1 and E_2, whereas the agreement for the subgrade modulus (E_3) is extremely good. But even for Layers 1 and 2, the agreement is quite good given that many of the structures were outside the recommended range for use in the ELMOD program and that a coefficient of variation in layer thickness of only 6 percent for Layer 1 and 9 percent for Layer 2 would result in the same scatter. Inaccuracies in assumed layer thicknesses may be quite important for the calculated moduli, but fortunately the layer stiffnesses will still be approximately correct, and therefore the critical stresses and strains calculated subsequently will also be equally correct.

Comparing Theoretical and Measured Values

More important than comparing "exact" layered elastic theory and the MET, is keeping in mind that large differences exist between theoretical models and actual pavement structures. Only by comparing theoretical values to measured stresses, strains, and deflections in situ is it possible to determine whether a given model or approach is satisfactory.

Although deflections may be measured quite accurately in situ, it is much more difficult to measure in situ stresses and strains in a pavement structure. If there is a difference between a measured and a calculated value, there is, at the present time, no way of telling which one is really "correct."

Nevertheless, two comparisons are presented here because they illustrate the type of variations that can be expected between the various theoretical models and measured values of stresses, strains, and deflections:

Example 1

In Figure 3, a comparison of measured and calculated values from two instrumented, full-scale pavements is shown (2). Section 1 was a full-depth asphalt

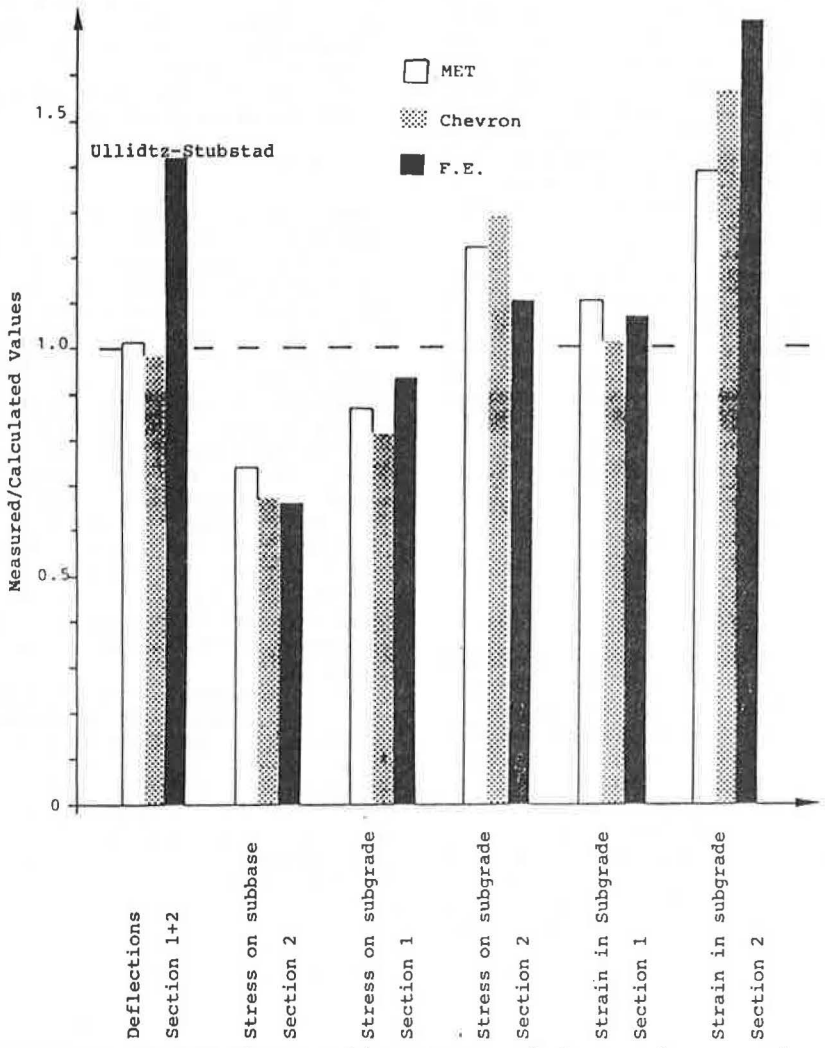

FIGURE 3 The MET, Chevron, and finite element method compared to measured deflections, stresses, and strains.

placed directly on a cohesive (moraine clay) subgrade. Section 2 had, in addition, a granular subbase. Three methods were used to calculate the response: the Chevron program, a finite element (FE) program developed at the University of California, Berkeley (9), and the MET. The input moduli were determined from backcalculations of deflection data using the MET and Chevron approaches and from three-point bending tests on the asphalt materials and triaxial tests on the unbound materials for the FE program input.

Four test series were carried out under different climatic conditions. The results shown in Figure 3 are the mean values of the ratio of measured versus calculated values from all tests conducted. There is a considerable scatter between measured and calculated values and the various methods of calculation, but there is clearly no indication that the MET is any less "correct" than any of the other methods.

Example 2

Comparisons of measured and calculated strains were made by the Organization for Economic Co-operation and Development (OECD) Common Measurement Program Group at Nardo. As a part of the OECD Road Transport Research Program, a Scientific Expert Group on Full-Scale Pavement Tests was formed. The main purpose of this group is to investigate possibilities for coordinating the extremely costly, full-scale pavement testing presently being carried out, or planned for the near future, by member countries of the OECD.

The Common Measurements Program Group, consisting of nine teams from eight member countries, conducted measurements of horizontal strains in the asphalt layer of a test road under heavy truck traffic. More than 200 strain gauges were installed. Details of the experiments and results thereof are to be published by the OECD.

FWD measurements were also carried out at one of these OECD test sites on April 11 and 12, 1984. Using the results of these tests, strains at the bottom of the asphalt layer were calculated with the MET and compared to the values measured under truck traffic. The team from the Technical University of Denmark found the following ratios between measured and calculated strains:

Date	Measured/Calculated Strains
April 11	1.10
April 12	0.93 to 1.07

Conclusion on Calculation of Moduli

On the basis of approximately 20 years' experience with FWD testing, it can be concluded that the layer moduli of a pavement structure can be determined reasonably accurately from FWD test results and that these moduli may be used to calculate the critical stresses and strains in a structure under heavy traffic.

The complex nature of pavement structures and the inadequacy of existing theoretical models, however well computerized, should be realized. More realistic models, like the distinct element method (10), should be developed, but at the present time it does not appear that the mathematically more complex methods offer any important advantages over the more simple method of equivalent thicknesses (except, perhaps, in special cases).

The analytical part of the analytical-empirical method may, therefore, be used with a reasonable degree of confidence, and because it is based on fundamental physical principles it may be used with all types of materials, environments, loadings, and so forth. Of course, the approximations made in the theoretical approach discussed previously should be kept in mind.

RESIDUAL LIFE AND NEEDED OVERLAY

Theoretical models like VESYS (11) and MMOPP (12) may be used to predict future pavement performance in terms of roughness, rutting, and cracking. Because of the large number of input parameters required, however, these models are not well suited for routine purposes. Instead, it appears to be necessary at the present time to rely on empirical relationships between pavement response (i.e., to load) and pavement performance.

Two relationships are generally used, one for predicting cracking of bound layers and one for predicting permanent deformations (roughness or rutting). Preferably, the two predictions should be interrelated so that the predicted structural deterioration (cracking) is considered in the model for predicting functional deterioration (roughness and rutting), but this is seldom attempted or even suggested. It should be noted that the words functional and structural are used to describe two distinct types of pavement condition. Thus, functional condition relates to ride quality and structural condition to bearing capacity. The words are not used to indicate the reason for a specific kind of deterioration, as is sometimes suggested.

Most of the empirical relationships used today are of the exponential form:

$$N = K \times S^a \quad (1)$$

where N is the number of loads to cause a certain deterioration at a stress or strain level (S) at the critically loaded position in the layer and K and a are constants, depending on the type of material and the environmental conditions. In the ELMOD program, equations of this type are used with K and a as user-controlled input parameters. Seasonal variations of the critical stresses and strains are also considered. As many as 12 "seasons" may be specified in the program, and the moduli of all layers (including the subgrade) may be varied with season. The damage caused in each season is calculated and summed using Miner's law. The design wheel load may be a single wheel, a dual wheel, or two dual wheels in tandem (useful for airfield pavement design). The effect of previous loads may or may not be subtracted, as specified by the program user. The positions at which the critical stresses or strains are evaluated by ELMOD under a dual wheel are shown in Figure 4.

If the residual life of a pavement is insufficient, the program will determine the needed overlay thickness of a given material to satisfy Equation 1, as specified for each layer in the structure. The needed overlay thicknesses along the length of the roadway may be plotted or a special routine may be used to automatically divide the roadway into uniform subsections, each with its unique design life and most representative FWD test point. An example ELMOD output is shown in Figure 5.

Structural Deterioration

A vast amount of literature exists on fatigue cracking of bituminous- and cement-bound materials. Usually, the horizontal tensile stress or strain at the bottom of the layer is assumed critical. In prac-

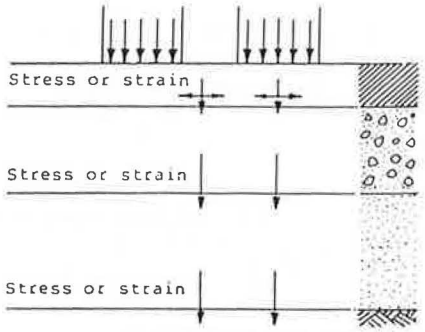

FIGURE 4 Possible location of critical stresses or strains under a dual wheel load.

tice, however, cracking of an asphalt layer has often been found to originate at the top of the layer not at the bottom. A few theoretical studies have been made of this phenomenon (13,14), but no method suitable for routine purposes appears to have been developed yet.

When the maximum tensile stress or strain at the bottom of a bound layer is used, the relationship with performance should be based on empirical evidence (i.e., actual experience) with existing pavements because correlations between the results of laboratory fatigue tests and performance of existing pavements have been rather unsatisfactory. Brown et al. suggest a factor of 100 (15) or 440 (16,p.38) to get from laboratory to in situ fatigue life of asphalt-bound layers, and Thrower (17) has calculated

```
**********************************

FILE ST 1 3 TO 3.9 ON 85-1-9

ROAD No  128  /OUTERWHEEL

LAYER NO. 1 CONSISTS OF
 4 IN ASPHALT
LAYER NO. 2 IS  6 IN THICK
LAYER NO. 3 IS  12 IN THICK

ΔPSR=  5

EQUIVALENT GEARS/LANE/SEASON

SEASON      ESGL
   1       75000
   2       75000
   3       75000
   4       75000

**********************************

E-VALUES, ksi 85/1/9

  ST      E1   E2   E3   EM

 3.10   391   38   23   11
 3.30   214   29   17    8
 3.50   271   25   15    7
 3.70   325   20   12    8
 3.90   148   33   20   10

**********************************

NON-LINEAR PARAMETRES
85/1/9

  ST    C0     N

 3.10    8 -0.15
 3.30    6 -0.14
 3.50    6 -0.15
 3.70    7 -0.08
 3.90    9 -0.09

**********************************

REMAINING LIFE ΔPSR=  5

  ST     LIFE  CRITICAL  FAILURE
         YEARS  LAYER      MODE

 3.10     1.5     2     FUNCTIONAL
 3.30     0.2     1     STRUCTURAL
 3.50     0.2     1     STRUCTURAL
 3.70     0.2     1     STRUCTURAL
 3.90     0.2     1     STRUCTURAL
```

```
**********************************

MODULI FOR EACH SEASON, ksi

 S   ST      E1   E2   E3   EM
 1   3.10   438   38   22   10
 2   3.10   317   52   31   14
 3   3.10   184   62   37   17
 4   3.10   257   49   29   14

 S   ST      E1   E2   E3   EM
 1   3.30   240   29   17    8
 2   3.30   173   40   24   10
 3   3.30   101   48   29   13
 4   3.30   141   37   22   10

 S   ST      E1   E2   E3   EM
 1   3.50   304   24   15    7
 2   3.50   220   34   20    9
 3   3.50   128   41   24   11
 4   3.50   179  -32   19    9

 S   ST      E1   E2   E3   EM
 1   3.70   365   20   12    8
 2   3.70   264   27   16   10
 3   3.70   153   33   20   12
 4   3.70   214   26   15   10

 S   ST      E1   E2   E3   EM
 1   3.90   166   33   20    9
 2   3.90   120   45   27   13
 3   3.90    70   55   33   16
 4   3.90    98   43   25   12

**********************************

NEEDED OVERLAY THICKNESS  IN

  ST      OVERLAY
           IN

 3.10      1.22
 3.30      3.07
 3.50      2.99
 3.70      3.15
 3.90      3.35
```

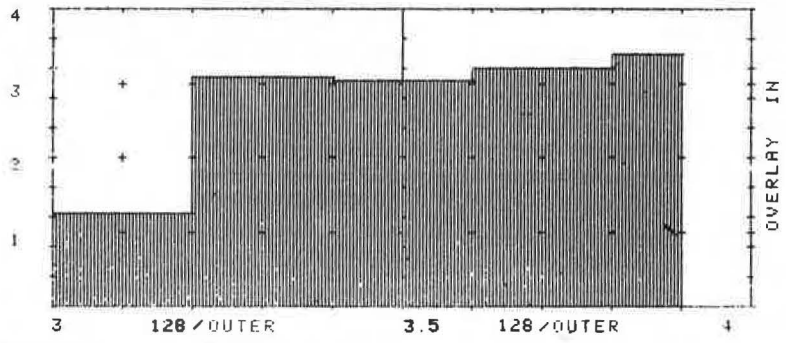

FIGURE 5 Sample ELMOD output.

factors of up to 5000. Full-scale testing with the Danish Road Testing Machine (3) and at the University of Nottingham (18) has shown similar differences between the results obtained on laboratory specimens and on full-scale asphalt pavements.

For cement-bound materials, the power a in Equation 1 is usually reported to be between -20 and -30 based on laboratory tests, whereas the AASHO Road Test showed a power of -4 and Road Note 29 indicates a power of about -3.

Great care, therefore, should be exercised when selecting the constants K and a in Equation 1. With the ELMOD program, these values are user controlled, and it is therefore possible to "calibrate" the program to suit any specific conditions of materials and climate. Some structural deterioration may also take place in the unbound materials. However, this deterioration does not appear to be quantifiable at the present time.

Functional Deterioration

The purpose of the structural layers in a pavement system is to provide a smooth ride. If the pavement remains smooth, its structural condition is, by definition, satisfactory even if structural deterioration is taking place. Most pavements, however, do not remain smooth. Roughness, or rutting, or both develop as a function of loading and climatic conditions and may or may not be accompanied by true structural deterioration (e.g., fatigue cracking).

Functional deterioration may also be associated with degradation of the wearing course, which is unrelated to structural condition. Such surface deterioration will be in addition to that predicted from the structural condition and must, in most cases, be evaluated subjectively.

Thus, the primary purpose of analyzing a pavement structure using the FWD is to predict the development of the future functional condition. Most of the relationships used today are of the form:

$$N = K \times S^a \times E^b \times (P_I - P_T)^c \quad (2)$$

where

- N = the number of load repetitions to cause the performance measure to change from:
- P_I = the initial level to
- P_T = the terminal level, and
- S = the critical stress or strain,
- E = the modulus of the material, and
- K, a, b, and c are constants.

Again, it is strongly recommended that this "response-versus-performance" relationship be based on experience with the actual pavement structures in the region where it is being applied.

In the ELMOD program, the power c in Equation 2 is assumed to equal 1. The AASHO Road Test results indicated that c is initially close to 1, later becoming rather large. A sudden failure, caused for example by unfavorable conditions during a single season, will result in a large value of c (rapidly increasing rate of deterioration). At the AASHO Road Test, most of the flexible pavements failed during spring thaw. Because the seasons are considered separately in the ELMOD program, it is reasonable to assume that c = 1.

For the remaining constants in Equation 2, Kirk (19) has determined values through an analysis of the AASHO Road Test, resulting in the following equation:

$$N = 440/R \times (\sigma_z/1MPa)^{-3.26} \times (E/160MPa)^b \quad (3)$$

where

- N = number of loads to decrease the present serviceability rating (PSR) by 1,
- R = regional factor,
- σ_z = critical vertical stress on the layer considered,
- E = modulus of the material, and
- b = 3.78 for E < 160 MPa or 3.26 for E > 160 MPa.

Equation 3 has been found to agree reasonably well with the actual performance of road pavements in many parts of the world and may be used as a first estimate when calibrating the method to new conditions of materials and environment.

CONCLUSION

The analytical-empirical (or mechanistic) method of evaluating pavement structures may now be routinely used. Through the use of a sufficiently accurate falling weight deflectometer and appropriate software, the modulus of each structural layer in an existing pavement may be determined. The moduli are determined nondestructively and in situ under conditions that closely resemble the conditions under heavy traffic loading.

The critical stresses or strains in the structure may then be calculated by analytical methods. Changes in moduli due to seasonal changes in temperature or moisture content may be easily incorporated, and any design load or combination of design loads may be used.

The analytical part of the evaluation (i.e., calculating the moduli and determining the critical stresses and strains for design conditions) may be carried out on a microcomputer using the method of equivalent thicknesses. Except for some special cases, this may be done without any loss of accuracy compared with the mathematically more complex methods. The MET has the additional advantage that it may be incorporated in a pavement management system so that prediction of future performance may be based on the actual existing (as measured) structural condition of the pavements.

The analytical part of the method is based on fundamental physical principles and may therefore be used for any conditions of materials, environment, loadings, and so forth.

The weakest parts of the method are the empirical relationships between pavement performance (roughness, rutting, and cracking) and pavement response (stresses and strains). In many parts of the world, a considerable amount of research has been carried out in this field, and reasonably good relationships have been developed. When using the method for new materials or environmental conditions, however, the empirical relationships must be locally calibrated. Through routine use of the suggested analytical-empirical method, a considerable fund of knowledge has already been collected. At present, more than 35 FWD test systems are in service in North America and Europe (and a few in the Near East and Australia), primarily operated by public highway agencies and research institutions. The increased insight gained through actual use of the analytical-empirical method will undoubtedly facilitate its future development, dependability, and accuracy.

Discussion

Waheed Uddin*

The falling weight deflectometer (FWD) is becoming an increasingly popular device for nondestructive testing of pavements because of its capability of applying variable and overload ranges. Several versions of this impulse-generating device are currently in use (20) (see also the paper by Bush and Alexander in this Record). A simplified approach to analyzing FWD deflection basins for pavement evaluation is favored by many engineers. The ELMOD program, which has been described in several publications, is such an approach. However, the desire for simplification should not overshadow research efforts to determine a precise and exact interpretation of dynamic deflection data. The conclusions in this paper imply that the oversimplified approach of ELMOD is more accurate than the results of the multimillion dollar and statistically designed AASHO Road Test. A comparison of ELMOD results with layered theory analysis for some isolated test sections is described. No details about the test sections are given. The authors admit that there is a wide scatter in the results but do not apply or recommend proper limits to their inferences.

The development of computer programs for multilayered elastic theory and finite element programs has taken place in the last two decades. Furthermore, mechanistic interpretation of NDT data for pavement evaluation is still an area of active research. These research efforts should not be discredited just because the behavior of pavement materials is not truly linearly elastic. The inherent weakness in these conventional procedures is the assumption of a static load instead of the peak force of a falling weight deflectometer. Moreover, ELMOD probably works under the assumption of a semi-infinite subgrade. If a rock layer exists at a shallow depth, considerable error in backcalculated moduli can be expected.

The authors have ignored the dynamic effects of FWD tests. Generally, field evidence shows that the dynamic deflection data from a falling weight deflectometer exhibit considerable variability and device dependency (20) (see also the paper by Bush and Alexander in this Record). Like a moving wheel load, an FWD generates a transient load signal, but loading-mode effects still prevail because of the differences in shape and duration (21) of dynamic signals under the two types of excitation forces. Dynamic loading on a pavement surface causes disturbance in the pavement-subgrade system. If the pavement-subgrade system is assumed to be linearly elastic, a true dynamic analysis of this problem is possible by the application of the theory of stress wave propagation in layered elastic media. For a falling weight deflectometer, a true dynamic analysis will require an examination of the spectrum of frequencies excited by its transient impulse.

Authors' Closure

The authors wish to thank Waheed Uddin for his suggestions and comments on our paper. We certainly agree that the ELMOD program, or any other existing "layered elastic" software for that matter, should not preclude continuing research on the behavior and modeling of layered elastic systems under the influence of (transient) moving wheel and vibratory loads.

Indeed, much work still needs to be accomplished in this area. Many American universities, such as the University of Texas, as well as foreign universities, are presently engaged in such research. It was definitely not the intention of the authors to demean any present or future research in any way. Indeed, it was somewhat discouraging to discover that anyone would read such an intention into this paper.

We would, however, like to take this opportunity to briefly summarize our views on the subject matter addressed by Uddin from a more general point of view in order to put matters somewhat into perspective.

Although the FWD and ELMOD programs certainly have their limitations, some of which Uddin outlined in his comments, we believe we have addressed the primary problems associated with the analytical portion of NDT pavement evaluation and analysis, as follows:

1. Although the FWD does not perfectly simulate the effect of a moving wheel load, it has been shown through a number of research projects (7,22) that the deflections generated by the FWD do indeed correspond well to the deflections generated by an equally loaded moving wheel load. We believe that this renders an ensuing layered elastic analysis quite relevant for the purposes at hand, except in the few cases where the so-called "dynamic" effect becomes predominant due, for example, to the presence of a layer of bedrock relatively close to the pavement surface. Further research and development work on the dynamic effects of FWD loadings is thus indeed relevant--but certainly not critical--because the FWD design minimizes such effects by not exciting the pavement at a single, vibratory frequency.

2. The major drawback of most other iterative, reverse layered elastic procedures is that the typically nonlinear subgrade stress-strain properties are not considered in a horizontal direction, which is the way deflection basins are measured. Because the subgrade generally contributes to more than 50 percent of all deflection readings, this nonlinearity should be considered in most instances in order to arrive at reasonably correct E-values, as explained in our paper. The ELMOD program accomplishes this goal quite effectively.

3. If other pavement layers are also sufficiently nonlinear, the ISSEM4 (23) and MODCOMP2 (24) programs are also available. For bedrock or frozen layers close to the surface, the ELMOD program also contains a subprogram called "ELROC," which calculates the (equivalent) depth to any hard layer, along with the requisite E-values of the materials above this layer.

4. In spite of the inherent drawbacks in this approach, as Uddin has delineated, we are quite sure that the weakest link in the whole process of pavement evaluation in general is the link between mechanistic pavement properties (i.e., E-values, stresses, and strains) and performance. We would recommend, therefore, that the major thrust of research should be directed toward improving the distress models used for this purpose, through both continuing theoretical and applied research, as well as through empirical observations of existing pavements. This problem is, in our view, considerably more important than a "fine tuning" of the analytical procedures involved in FWD testing and interpretation through layered elastic analysis procedures.

*ARE, Inc., 2600 Dellana Lane, Austin, Tex. 78746

REFERENCES

1. H.J. Ertman Larsen and R.N. Stubstad. The Use of Non Destructive Testing in Flexible Pavement Rehabilitation Design. International Symposium on Bearing Capacity of Roads and Airfields, Trondheim, Norway, June 1982.
2. P. Ullidtz. En Studie af to Dybdeasfaltbefæstelser. Ph.D. dissertation. Technical University of Denmark, Lyngby, 1973.
3. Busch et al. Accelereret Afprøvning af Resourcebesparende Vejbefæstelser: Sammenligning af en Fuld-dybdeasfalt og en Traditionel Bafæstelse. Laboratory Report 47. Statens Vejlaboratorium (Danish National Roadbuilding Laboratory), Roskilde, Denmark, 1980 (English summary).
4. A. Sorensen and M. Hayven. The Dynatest 8000 Falling Weight Deflectometer Test System. International Symposium on Bearing Capacity of Roads and Airfields, Trondheim, Norway, June 1982.
5. N. Odemark. Undersökning av elasticitets egenskaparne hos olika jordarter samt teori för berakning av belagningar enligt elasticitets teorien. Report 77. National Swedish Road and Traffic Research Institute, Linkoping, Sweden, 1949.
6. P. Ullidtz and K.R. Peattie. Pavement Analysis by Programmable Calculators. Journal of the Transportation Engineering Division, ASCE, Vol. 106, No. TE5, Sept. 1980, pp. 581-597.
7. P. Ullidtz. Overlay and Stage by Stage Design. Proc., Fourth International Conference on the Structural Design of Asphalt Pavements, Ann Arbor, Mich., Vol. 1, 1977.
8. L.J. Wardle. Program CIRCLY--User's manual. Geomechanics Computer Program 2. Division of Applied Geomechanics, Commonwealth Scientific and Industrial Research Organization, 1977.
9. J.M. Duncan, C.L. Monismith, and E.L. Wilson. Finite Element Analysis of Pavements. In Highway Research Record 228, HRB, National Research Council, Washington, D.C., 1968, pp. 18-33.
10. P.A. Cundall. BALL--A Program to Model Granular Media Using the Distinct Element Method. Technical Note TN-Lk-13. Advanced Technology Group, Dames & Moore, Los Angeles, Calif., 1978.
11. W.J. Kenis, J.A. Sherwood, and T.F. McMahon. Verification and Application of the VESYS Structural Subsystem. Fifth International Conference on the Structural Design of Asphalt Pavements, Delft, The Netherlands, Aug. 1982.
12. P. Ullidtz and B.K. Larsen. Predicting Design of Flexible Pavements--Verified through Computer Simulation of the AASHTO Road Test. Report 35. Institute of Roads, Transport and Town Planning, The Technical University of Denmark, Lyngby, 1982.
13. C.M. Gerrard and L.I. Wardle. Rational Design of Surface Pavement Layers. Journal of the Australian Road Research Board, Numawading, Victoria, Australia, Vol. 10, No. 2, June 1980.
14. J.M. Kirk. Udmattelsesbrud i Slidlag. Internal Report 66. Danish Asphalt Industries Road Research Institute, Hvidovre, Denmark, Sept. 1983.
15. S.F. Brown, P.S. Pell, and A.F. Stock. The Application of Simplified, Fundamental Design Procedures for Flexible Pavements. Proc., Fourth International Conference on the Structural Design of Asphalt Pavements, Ann Arbor, Mich., 1977.
16. S.F. Brown, J.M. Brunton, and P.S. Pell. The Development and Implementation of Analytical Pavement Design for British Conditions. Proc., Fifth International Conference on the Structural Design of Asphalt Pavements, Delft, The Netherlands, Vol. 2, Aug. 1982.
17. E.N. Thrower. A Parametric Study of a Fatigue Prediction Model for Bituminous Road Pavements. Report 892. Transport and Road Research Laboratory, Crowthorne, Berkshire, England, 1979.
18. S.F. Brown, B.V. Brodrick, and I.W. Pappin. Permanent Deformation of Flexible Pavements. University of Nottingham, England, 1980.
19. J.M. Kirk. Revideret Metode til Dimensionering af Bituminose Befæstelser. Asfalt No. 42, 1973.
20. O. Tholen, J. Sharma, and R.L. Terrel. Comparison of Falling Weight Deflectometer with Other Deflection Testing Devices. In Transportation Research Record 1007, TRB, National Research Council, Washington, D.C., 1985, pp. 20-26.
21. A. Bohn, P. Ullidtz, R. Stubstad, and A. Sorensen. Danish Experiments with the French Falling Weight Deflectometer. Proc., Third International Conference on Structural Design of Asphalt Pavements, Ann Arbor, Mich., Vol. I, Sept. 1972, pp. 1119-1128.
22. M.S. Hoffman. Mechanistic Interpretation of Nondestructive Pavement Testing Deflections. Ph.D. thesis. University of Illinois at Champaign-Urbana, 1980.
23. R.N. Stubstad and J. Sharma. Deriving Mechanistic Properties of Pavements from Surface Deflections. The International Conference on Computer Applications in Civil Engineering, Roorkee, India, 1979.
24. L.H. Irwin. User's Guide to MODCOMP2, Version 2.0. Local Roads Program, Cornell University, Ithaca, N.Y., 1983.

Publication of this paper sponsored by Committee on Mechanics of Earth Masses and Layered Systems.

Modeling of Granular Materials in Pavements

S. F. BROWN and J. W. PAPPIN

ABSTRACT

The problem of theoretical modeling of granular materials in pavements is considered; a previously published technique and associated materials data are used. A detailed stress-resilient strain model was used in a finite element configuration that is based on a secant modulus approach. A parametric theoretical study involving 56 different pavement structures with two granular materials provided extensive data on the in situ stress conditions in unbound layers and their equivalent stiffnesses. The incidence of failure elements is discussed and the conclusion is drawn that the simple K-θ nonlinear model and linear elastic layered systems are inadequate for computing stresses within the granular layer. Arbitrary adjustments to computed stresses that indicate apparent failure or tensile conditions are unnecessary when an accurate material model and associated computational techniques are used. The concept of a fixed modular ratio between a granular layer and a subgrade was found to be inappropriate because a particular granular material has an essentially constant equivalent stiffness. Linear elastic layered system computer programs can be used to determine critical design parameters when the granular layer stiffness is chosen on the basis of results from detailed nonlinear analysis.

In the design of new roads and in the expanding field of pavement structural evaluation, there is a continuing need for an adequate means of modeling unbound granular layers. The problem is not new; the nonlinear elastic properties of granular materials have long been appreciated and a number of techniques have been used to take these into account in structural analysis. These methods have included an iterative approach using linear elastic layered systems, first outlined by Monismith et al. (1) and application of the finite element method (2). This latter technique has been used as a basis for developing nomographic procedures for pavement design (3).

The majority of the work done in this field has used the so-called K-θ model to describe the nonlinear elastic characteristics of granular materials. This model was developed from repeated load triaxial test results and is of the form:

$$M_r = K_1\theta^{K_2} \quad (1)$$

where

M_r = resilient modulus, which is the repeated deviator stress divided by the axial resilient strain;
θ = peak value of the sum of the principal stresses; and
K_1, K_2 = material constants.

Brown and Pappin (4) have described a more detailed model for granular materials, which has wider applicability, and have discussed the limitations of the K-θ model. They also presented a computational procedure to incorporate their model in a finite element package, known as SENOL, to analyze pavement structures. The use of their procedure has also been illustrated (5).

The SENOL computer program has since been used to analyze a wide range of pavements and the results have thrown some additional light on the in situ behavior of granular materials. Use of the K-θ model has also been further investigated to establish its limitations. Because finite element analysis is still regarded as essentially a research tool in pavement engineering, SENOL has also been used to calibrate simpler analysis techniques based on linear elastic layered systems. The limitations of these have also been established.

GRANULAR MATERIAL MODELS

The resilient strain model described by Brown and Pappin (4,6) was developed from a comprehensive set of repeated load triaxial test data. The strains were expressed in terms of resilient shear and volumetric components leading to stress-dependent shear and bulk moduli. Stresses were expressed in terms of the invariants, mean normal effective stress ($p' = \theta/3$) and deviator stress (q). This model is referred to as the "Contour Model" because it is best illustrated, as in Figure 1, by use of strain contours in p'-q stress space.

Two materials are considered in this paper. The first, Model A, is a well-graded crushed limestone, and the second, Model B, is a uniformly graded material from the same source. They were selected to represent good- and poor-quality material in terms of stiffness. Details of both models have been presented by Brown and Pappin (4).

Coefficients in the corresponding K-θ relationships for these two materials are as follows:

Model A: $K_1 = 8634$ kPa, $K_2 = 0.69$

Model B: $K_1 = 19\,454$ kPa, $K_2 = 0.5$

The contour models cannot be expressed as succinctly as this, so reference should be made to Brown and Pappin (4,5) for full details. Figure 2 shows a typical stress pulse in p'-q space for an element of granular material in a pavement. Point A represents overburden pressure and Point B is the peak stress that occurs when the wheel load is immediately above the element. The contour model was developed from a large number of stress paths such as AB covering the stress space of Figure 2 but limited to peak values of $q/p = 1.67$. This was done to avoid the development of significant permanent

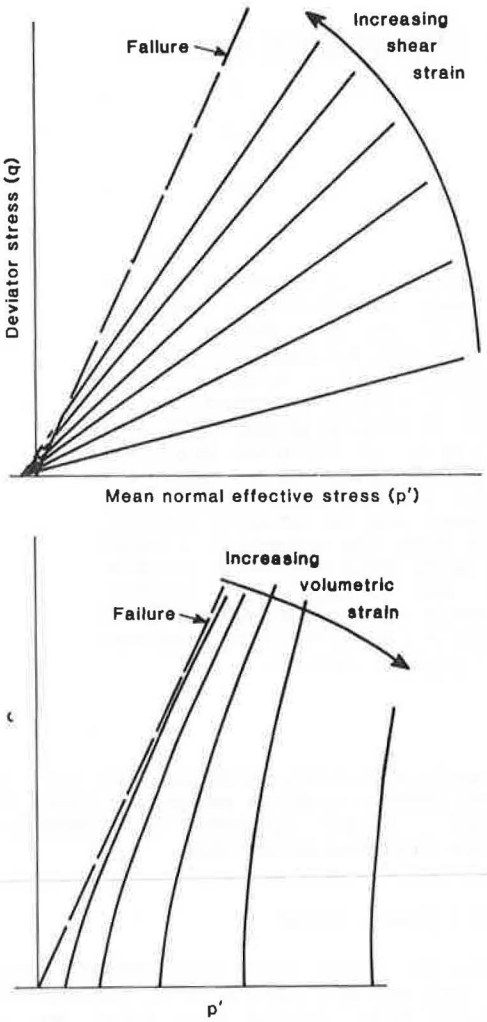

FIGURE 1 Contour model in p'-q stress space.

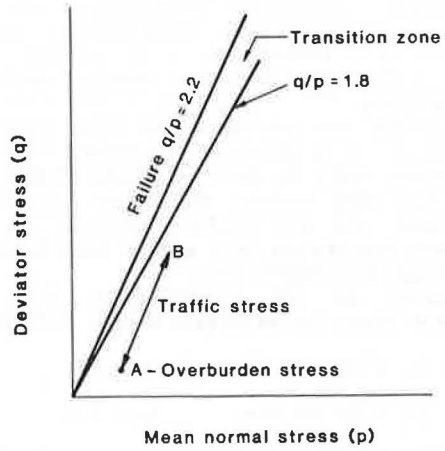

FIGURE 2 Typical in situ stress path due to wheel loading.

strains that occur when peak stresses probe close to the failure line; q/p = 2.2 for this material (both well graded and single sized). Some tests involving these high stress ratios showed that the basic resilient strain model was capable of extrapolation into this zone.

The K-θ model was developed from tests involving constant confining stress and deviator stress pulsed from zero to a peak value. The stress paths in Figure 2 for such tests would involve Point A being on the p' axis (equal to the confining stress at that point) and the slope of AB being 3. The parameter θ in Equation 1 is the value corresponding to Point B in Figure 2.

Hence the contour model is a more exact representation of the material behavior and is better able to predict stress conditions in a pavement in which a wide range of stress paths is possible.

In the computations that were performed during this investigation, both the asphalt and the subgrade layers in each pavement were assumed to be linearly elastic. When linear elasticity is applied to materials the basic characteristics of which are either nonlinear or viscoelastic, the term "elastic stiffness" is used in place of Young's modulus in this paper.

COMPUTATIONAL PROCEDURES

The finite element program SENOL was designed specifically to apply the contour model for granular materials to pavement analysis. Details of the computational procedure have been published by Brown and Pappin (4,5) but will be summarized here.

The starting point for analysis in a particular element is the overburden stress. This is used to establish the initial values of bulk and shear modulus. The effects of wheel load are then computed by applying it in 10 equal steps and, finally, iterating until satisfactory convergence is obtained. A significant feature of the procedure is that it is based on the secant modulus at each step (i.e., both stress and strain values are relative to zero).

When a convergent solution has been obtained, the program computes an equivalent Young's modulus and Poisson's ratio on the basis of the application of traffic loading alone. This is essentially a chord modulus and is of interest in calibrating simpler linear elastic procedures such as BISTRO (7,pp. 34-35) or the Chevron (H. Warren and W.L. Dieckman, Numerical Computation of Stresses and Strains in a Multiple-Layer Asphalt System, unpublished internal report, Chevron Research Corporation, 1963) layered system programs. These deal only with stresses induced by wheel loading and, because all layers are assumed to be linearly elastic, require an equivalent single value of Young's modulus for the granular layer. The SENOL program was used to determine appropriate values.

In applying the K-θ model to pavement analysis using the finite element method, the peak stress (overburden plus traffic) is calculated using an assumed initial value. The value of θ at this peak stress is then computed and the corresponding resilient modulus is determined from Equation 1. This is regarded as Young's modulus and is combined with an appropriate value of Poisson's ratio, usually a constant value, for proceeding with the calculation. The inadequacies of the K-θ model lead to some elements exceeding failure conditions and these are arbitrarily adjusted to bring the stress condition down to an acceptable level (2). Arbitrary adjustments of this kind are also used in those approaches that adopt a "tension correction" for elements in a granular layer.

These adjustments are not necessary when using SENOL with the contour model because elements approaching failure are automatically assigned low stiffnesses in accordance with the greater detail of this model. Nonetheless, some elements do have final stress conditions just above failure. This is a con-

sequence of the slight shortcomings of the contour model for stress conditions close to failure.

Computations were performed using the K-θ model as well as the contour model for the two materials noted previously. In applying the K-θ model, the same basic computational procedure was followed as for the contour model; that is, a secant modulus approach with the load applied in stages as described previously. In this case, secant values of E were determined at each stage of loading and a constant value of Poisson's ratio (0.3) was adopted throughout. In addition, linear elastic solutions were obtained for several structures using the BISTRO (7) computer program.

The results from these various computations were used to study the following points:

1. Stress conditions in the granular layer and the incidence of failure in particular elements,
2. Comparison of Models A and B for the granular layer,
3. Equivalent values of Young's modulus,
4. Comparison of critical parameters computed using SENOL and BISTRO, and
5. Assessment of the K-θ model.

DETAILS OF PAVEMENT STRUCTURES

A parameter study was conducted using the SENOL computer program and it involved computations on 56 pavement structures definitions of which are given in Table 1. Each structure consisted of a linear elastic asphalt layer, a nonlinear granular layer, and a linear elastic subgrade. Table 1 gives the combinations of stiffnesses and thicknesses that were used. Granular material Model A was adopted for all 56 cases. In addition, six cases, numbered 3 to 8 in Table 1, were analyzed using Model B and eight cases (1 to 8 in the table) were also analyzed using the BISTRO linear elastic procedure. Comparisons of the contour and K-θ models were made using structures numbered 3 to 8. A summary of the eight structures that were examined in detail is given in Table 2. In each case a 40-kN wheel load having a contact pressure of 500 kPa was used.

For the 56 structures that were analyzed, five solutions did not converge, some indicated elements at or slightly above failure ($q/p' > 2.2$), others included elements in the zone just below failure ($2.2 < q/p' < 1.8$), and all elements in the remainder were in the region of lower stress levels within which the contour model has greatest validity. These various categories are identified in Table 1, which shows a trend from the weakest (nonconvergent) structures, through the intermediate areas, to those strong pavements with the lowest peak stress ratios.

The significance of a nonconvergent solution is that a large number of elements within the granular layer are at failure. The general implication of this is that significant permanent deformations are likely to develop in such a structure. Shaw (8) has shown that the parameter that determines the tendency for permanent strain to accumulate under repeated loading is the minimum horizontal distance (value of p') between the end of the stress path and the failure line (see Figure 2).

Figure 3 shows, in more detail, the incidence of failure elements in Structures 1 and 2 of those investigated in detail. The elements with stress ratios in the transition zone just below failure are also shown. In both these cases the stress conditions in the granular layer are generally high and such pavements are unlikely to have long lives.

Structures 3 and 4 (Table 2) had some elements in the transition zone, and the remaining structures had all elements at stress ratios less than 1.8. The relative potential performance of the granular layer in six cases is reflected by the pavement lives given in Table 2. These were calculated using the pavement evaluation techniques developed by Brunton and Brown (9) and relate to British conditions. In all cases, except Pavement 4, the potential failure mechanism was fatigue cracking of the asphalt. In Pavement 4 it was excessive rutting. The elastic stiffness of the granular material used in this evaluation, which is based on linear elastic analysis, was derived from the SENOL computations. This point is dealt with in the next section.

TABLE 1 Modular Ratios Between Granular Layer and Subgrade

		h_1 (mm)		
h_2 (mm)	E_3 (MPa)	50	100	200
Asphalt Stiffness = 4 GPa				
200	20			
	30			2.5+
	50			1.5[6]
	70			1.5
450	20			4.0
	30			3.5
	50		2.5[2]*	2.0
	70		2.0*	1.5
700	20			6.0
	30		5.0*	4.0[5]
	50		3.0*	2.5
	70			
Asphalt Stiffness = 7 GPa				
200	20			3.5
	30			2.5
	50		2.0+	1.5
	70	2.5*	1.5+[4]	1.5
450	20		5.5*	5.0
	30		3.5+	3.0
	50	2.0*	2.0+	2.0
	70	2.5*	1.5+	
700	20		5.5+[3]	5.0
	30	6.0*	3.5+	4.0
	50	3.5*	2.5+	
	70			
Asphalt Stiffness = 12 GPa				
200	20		3.5*	3.0
	30	NC	2.5+	
	50	NC	2.0	
	70	NC	1.5[8]	
450	20	NC	4.5[7]*	
	30	5.5*	3.5+	
	50	3.5*	2.0	
	70	2.5*		
700	20	NC	7.5+	
	30	6.0[1]*		
	50	4.0*		
	70			

Note: h_1 = asphalt thickness, h_2 = granular thickness, E_3 = subgrade stiffness, * = some failure elements, NC = noncovergence—general failure, and + = elements close to failure; superscripts 1 to 8 refer to pavement numbers in Table 2.

EQUIVALENT STIFFNESSES FOR THE GRANULAR LAYER

Values of Young's modulus and Poisson's ratio are computed in the SENOL program on the basis of the stresses and resilient strains resulting from traffic loading alone. This "chord modulus" is printed out for each element together with the corresponding Poisson's ratio.

The variation of these parameters through each of the 56 structures that were analyzed allows conclusions to be drawn about the equivalent Young's mod-

TABLE 2 Details of Pavement Structures Investigated in Detail

Pavement No.	Life (msa)[a]	Asphalt Stiffness (GPa)	Asphalt Thickness (mm)	Granular Thickness (mm)	Granular Nonlinear Model	Subgrade Stiffness (MPa)	BISTRO Calculation
1	0.5	12	50	700	A	30	No
2	0.1	4	100	450	A	50	No
3	0.5	7	100	700	A,B, K-θ	20	Yes
4	0.3	7	100	200	A,B, K-θ	70	Yes
5	2.3	4	200	700	A,B, K-θ	30	Yes
6	1.3	4	200	200	A,B, K-θ	50	Yes
7		12	100	450	A,B, K-θ	20	Yes
8		12	100	200	A,B, K-θ	70	Yes

[a]msa = millions of standard (80 kN) axles.

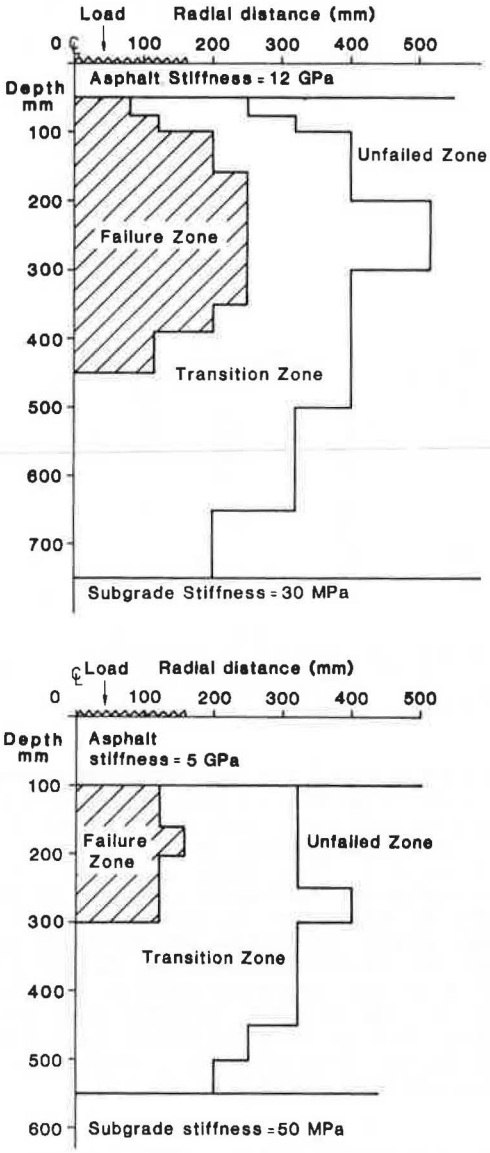

FIGURE 3 Incidence of failure elements in Pavements 1 and 2.

ulus, or stiffness, that the granular material mobilizes in situ. This information is particularly useful for allowing selection of the appropriate single value of granular material stiffness for use with linear elastic layered system programs such as BISTRO (7) and the Chevron program. Alternatively, it could form a basis for subdividing the granular layer if this were more appropriate.

In the past the approach to defining stiffness for a granular layer has been to use a certain value of modular ratio between this layer and the subgrade. Values in the range 1.5 to 5 have been generally adopted with 2 the most common. This approach implies that the stiffness of a particular granular material adjusts itself in situ in response to the stiffness of the support and the consequent stress conditions.

The SENOL data for all 51 of the structures, for which solutions were obtained, were studied and mean values of modular ratio, based on the computed chord moduli, were extracted. These are given in Table 1 from which it will be seen that they range from 1.5 to 7.5, a spread similar to that reported from in situ vibration testing (10). However, it will be noted that the high ratios were for the soft subgrade and vice versa, implying that the actual stiffness of the granular layer does not vary greatly.

To produce reliable values of these deduced equivalent stiffnesses for the granular layer, only those structures with peak stress ratios below 1.8 (well below failure) were considered. This reduced the number of relevant solutions to 22 as can be seen from Table 1.

Because a value of chord modulus is computed for each element, variations within the structure were studied. Within a radius of 350 mm from the load centerline the variation of this parameter and the associated Poisson's ratio were quite small. Figure 4 illustrates this point for Pavements 5 and 6 of those analyzed in detail (Table 2). The shaded zones cover the range of values up to a radius of 350 mm and results are shown for both granular material Models A and B. There is a general trend for stiffness to increase slightly with depth in each case. However, this variation is sufficiently modest to consider a single equivalent value of stiffness for the layer as a whole, when contemplating linear elastic layered system calculations.

For Model A, the mean equivalent stiffness for the 22 structures under consideration varied from 60 to 125 MPa. These values are small in relation to the stiffnesses of the asphalt layers (4 to 12 GPa). It was, therefore, considered appropriate to use a single value of 100 MPa in pavement design calculations based on linear elasticity and involving good quality granular subbases. This was adopted for the Nottingham analytical design procedure (9).

For Model B, representing poorer quality material, only six pavements were studied (3 to 8 in Table 2) with stress levels well below failure. The range of mean stiffnesses was 35 to 50 MPa and a mean value of 40 MPa is suggested for routine design. For both models, Poisson's ratio was 0.3 to 0.4, the former value having been adopted for design.

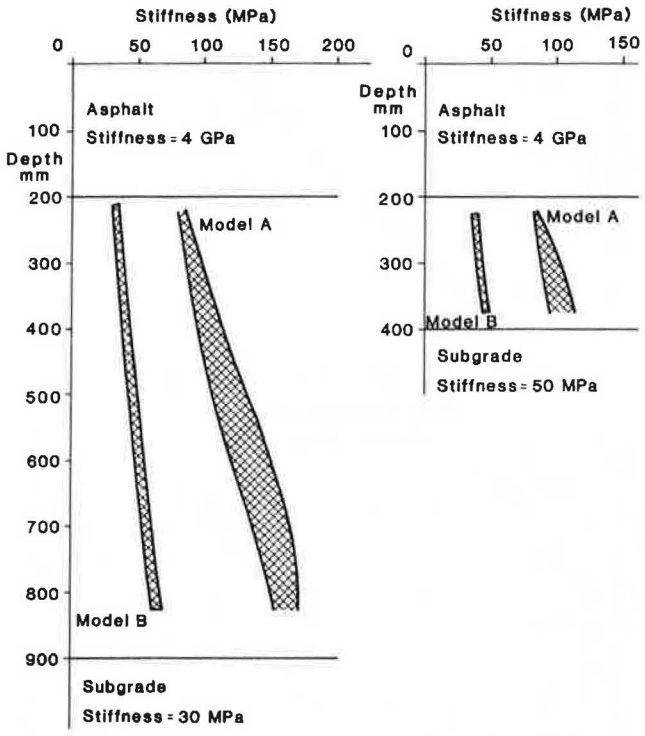

FIGURE 4 Variation of chord modulus (stiffness) through the granular layer.

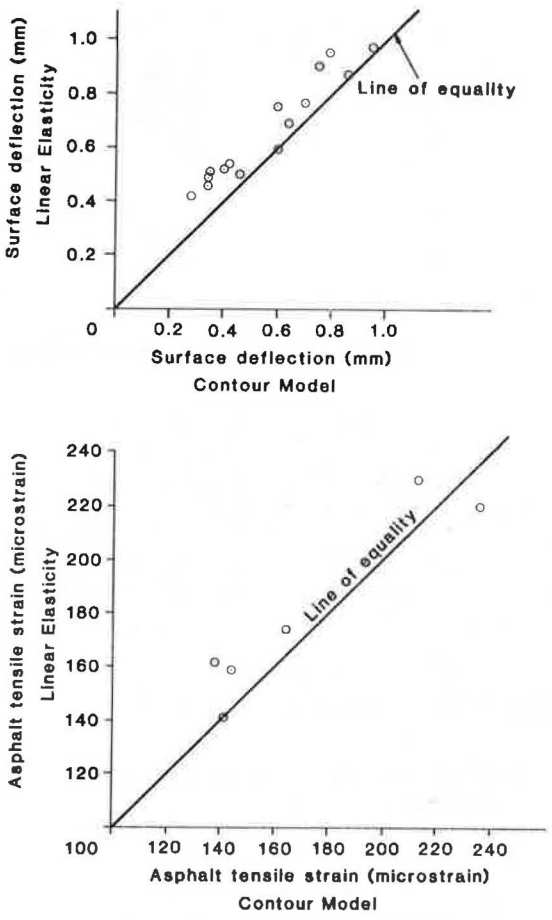

FIGURE 5 Comparison of results from SENOL and BISTRO computations.

EVALUATION OF LINEAR ELASTIC SOLUTION

Against the foregoing background, a number of calculations were carried out using the BISTRO computer program so that comparisons could be made with SENOL results for certain critical parameters. The parameters selected were tensile strain at the bottom of the asphalt layer (the fatigue cracking design criterion) and surface deflections at radii up to 350 mm as an indication of overall pavement response. Model A material was used and a mean stiffness of 100 MPa was adopted for the granular material in the BISTRO computations.

Figure 5 shows comparisons that generally indicate that the linear elastic layered system approach produces quite reasonable values for these two parameters, although surface deflections computed using BISTRO are somewhat high. There was no significant difference in the deflection comparisons at different radial positions.

In reality, not only is the granular layer nonlinear, so is the subgrade. A few calculations were conducted with a nonlinear elastic model for the subgrade (5) derived from work by Brown et al. (11). The results, based on a linear elastic subgrade, were compatible with those discussed in this paper.

STRESS CONDITIONS IN GRANULAR LAYERS

The foregoing section has shown that linear elastic layered system computations can determine critical design parameters when an appropriate equivalent stiffness is assigned to the granular layer. They are unlikely, however, to be able to reliably calculate stress conditions within the granular layer itself.

One of the particular problems in this connection is the tendency for tensile stresses to be apparent in granular layers when linear elastic assumptions are used. This point is illustrated in Figure 6 for Pavements 3 and 4 (see Table 2), and the results from BISTRO calculations are compared with those from SENOL using Model A material. The left line of each pair represents the traffic-induced horizontal stress in the granular layer, and the right line shows the influence of the compressive overburden pressure. For linear elasticity, even when overburden is included, tensile stresses still result in the lower half of the layer. Similar analysis for Pavements 5 and 6, which were stronger, showed that these combined stresses can become compressive in favorable circumstances. However, by contrast, the SENOL results show compressive stresses in all these cases and in most others as well.

The incidence of tensile stress in a granular layer does generally imply a failure condition. However, failure is defined by the stress ratio (q/p'), which is influenced by vertical stresses as well as horizontal ones.

Tensile total stresses, in soil mechanics terms, may correspond to compressive effective stresses if the granular material is subject to negative pore pressure, which in general it will be. However, quantification of this pore pressure may not be easy.

Table 3 gives the peak q/p' ratios determined at the top and bottom of the granular layer for Pavements 3 to 6. The SENOL values range from 0.8 to 2.1, all below the failure condition of 2.2, and in only two cases are the BISTRO values below failure. These data, therefore, confirm the point that detailed study of stress conditions within granular layers cannot be undertaken using linear elastic theory.

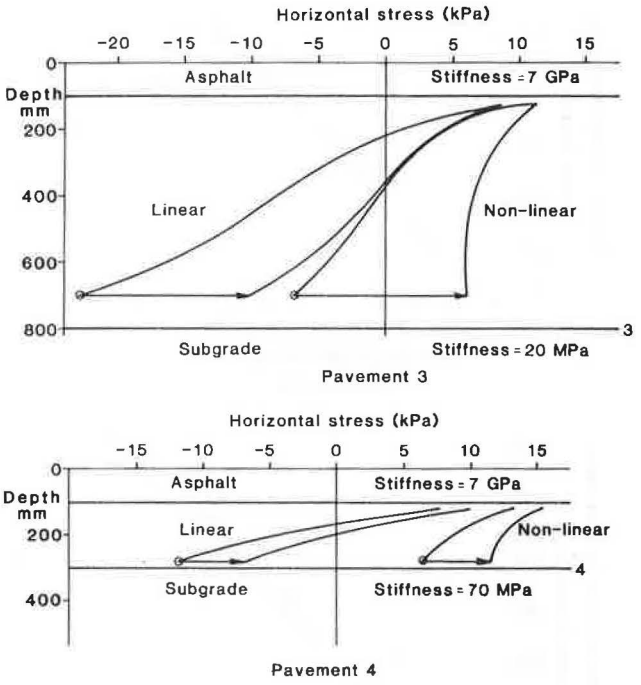

FIGURE 6 Horizontal stresses in granular layer.

TABLE 3 Stress Ratios at Top and Bottom of Granular Layer

Pavement No.	q/p			
	SENOL/Contour		BISTRO	
	Top	Bottom	Top	Bottom
3	2.10	1.77	2.15	17.5
4	1.92	1.81	2.27	4.34
5	1.73	0.80	2.53	2.23
6	1.71	1.40	1.14	2.47

EVALUATION OF K-θ MODEL

The K-θ equation for the well-graded crushed limestone was used in the SENOL program with a secant modulus approach for Pavements 3 to 8 (Table 2). The maximum tensile strain in the asphalt and surface deflections up to a radius of 350 mm were extracted from the output for comparison with the contour model results. Figure 7 shows that the deflections compare favorably. However, the K-θ approach underpredicts the tensile strain and is less satisfactory than the linear elastic layered system solutions (Figure 5), which used a single value of stiffness for the granular layer.

Although the K-θ model may be of use in evaluating effects in other layers, the results showed that stress conditions in the granular layer are not correctly determined. This point is illustrated by Figure 8, which shows substantial numbers of failure elements in Pavements 5 and 6 that were analyzed using the K-θ approach, whereas no failure elements were predicted using the contour model.

CONCLUSIONS

1. A detailed study of the structural behavior of unbound granular materials in pavements requires an accurate stress-strain model to define nonlinear elastic response.

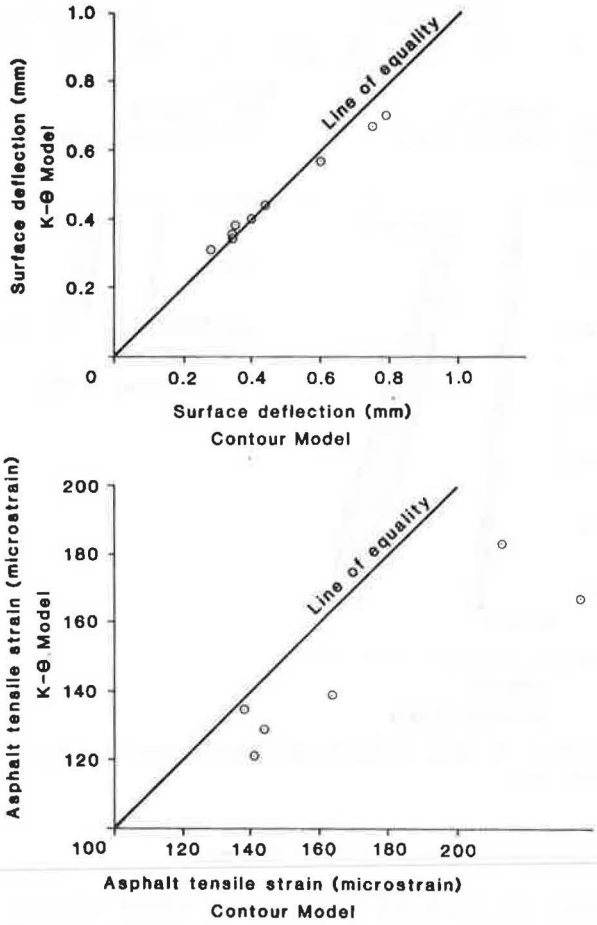

FIGURE 7 Comparison of results from contour and K-θ models.

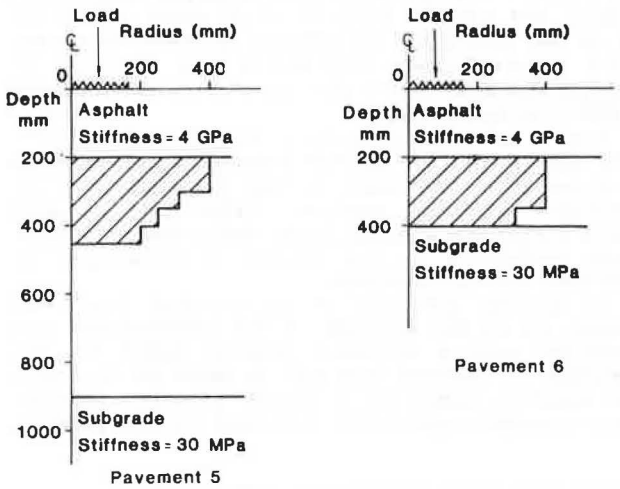

FIGURE 8 Incidence of failure elements in Pavements 5 and 6 using the K-θ model.

2. The contour model published by Brown and Pappin and the associated SENOL finite element computer program allow this to be done, but improved modeling is still desirable.

3. The SENOL program and the contour model allow equivalent elastic stiffnesses for granular layers to be determined for use in layered system analysis.

4. The concept of a fixed modular ratio between

a granular layer and the subgrade appears inappropriate because a single value of stiffness, dependent on the granular material, may be used in linear elastic analysis to determine effects in other layers of the structure for pavement design and evaluation purposes.

5. A well-graded crushed limestone base has an equivalent stiffness of 100 MPa, whereas a poorly graded material has a stiffness of only 40 MPa for the range of conditions investigated.

6. Linear elastic layered system programs can determine surface deflections and maximum asphalt tensile strains to an acceptable accuracy for design when the correct equivalent stiffness is assigned to the granular layer.

7. The finite element method incorporating the K-θ model can be used to determine surface deflections and asphalt tensile strains but is unable to determine the stress conditions within the granular layer.

8. Conclusions 6 and 7 suggest that the simplest approach to design calculations for surface deflection or asphalt tensile strain involves the use of linear elastic layered systems, provided the correct equivalent stiffness is defined from detailed nonlinear finite element analysis.

9. Design computations involving deformation or failure within the granular layer require a detailed model and finite element analysis.

ACKNOWLEDGMENTS

This study formed part of a project sponsored by the European Research Office of the U.S. Army and ICI Fibres. Related work under contract to the Transport and Road Research Laboratory and British Rail made the computations possible. The authors are grateful for this support and the assistance of their colleagues, P. Shaw and Janet Brunton, who performed some of the calculations. The facilities of the Department of Civil Engineering under R.C. Coates and, subsequently, P.S. Pell, were made readily available, and the service of the Cripps Computing Centre at the University of Nottingham is also acknowledged.

REFERENCES

1. C.L. Monismith, H.B. Seed, F.G. Mitry, and C.K. Chan. Prediction of Pavement Deflections from Laboratory Repeated Load Tests. Proc., Second International Conference on the Structural Design of Asphalt Pavements, 1967, pp. 109-140.
2. L. Raad and J.L. Figueroa. Load Response of Transportation Support Systems. Journal of the Transportation Engineering Division, ASCE, Vol. 106, No. TE1, 1980, pp. 111-128.
3. J.L. Figueroa and M.R. Thompson. Simplified Structural Analysis of Flexible Pavements for Secondary Roads Based on ILLI-PAVE. In Transportation Research Record 766, TRB, National Research Council, Washington, D.C., 1980, pp. 5-10.
4. S.F. Brown and J.W. Pappin. Analysis of Pavements with Granular Bases. In Transportation Research Record 810, TRB, National Research Council, Washington, D.C., 1981, pp. 17-23.
5. S.F. Brown and J.W. Pappin. Use of Pavement Test Facility for the Validation of Analytical Design Methods. Proc., Fifth International Conference on the Structural Design of Asphalt Pavements, Delft, The Netherlands, Vol. 1, 1982, pp. 209-220.
6. J.W. Pappin and S.F. Brown. Resilient Stress-Strain Behaviour of a Crushed Rock. Proc., International Symposium on Soils under Cyclic and Transient Loading, Swansea, England, Vol. 1, 1980, pp. 169-177.
7. M.G.F. Peutz, H.M.P. Van Kempen, and A. Jones. Layered Systems under Normal Surface Loads. In Highway Research Record 228, HRB, National Research Council, Washington, D.C., 1968, pp. 34-45.
8. P. Shaw. Stress-Strain Relationships for Granular Materials under Repeated Loading. Ph.D. dissertation. University of Nottingham, England, 1980.
9. J.M. Brunton and S.F. Brown. Computer Programs for the Analytical Design of Asphalt Pavements. Highways and Transportation, Vol. 31, No. 8/9, 1984, pp. 18-27.
10. W. Heukelom and A.J.G. Klomp. Dynamic Testing as a Means of Controlling Pavements During and After Construction. Proc., International Conference on the Structural Design of Asphalt Pavements, Ann Arbor, Mich., 1962, pp. 627-679.
11. S.F. Brown, A.K.F. Lashine, and A.F.L. Hyde. Repeated Load Triaxial Testing of Silty Clay. Geotechnique, Vol. 25, No. 1, 1975, pp. 95-114.

Publication of this paper sponsored by Committee on Mechanics of Earth Masses and Layered Systems.

Characterization of Granular Material

JACOB UZAN

ABSTRACT

Evaluation of the resilient modulus of granular material as used in design and structural evaluation of flexible pavements is addressed. It is shown that the well-known equation relating the modulus to the sum of principal stresses does not properly describe granular material behavior: the predicted response is not compatible with laboratory test results that show a strong dependence of the modulus on the stress ratio from which the equation is derived. A general law that includes the effect of shear strains is shown to be in good agreement with test results. The response of nonlinear materials is sensitive to their state of stress during loading. A literature review covers case histories of full-scale retaining wall models with compacted backfill, where residual stresses induced by compaction were measured. A proposed theory based on limit equilibrium is reported to give good estimates of residual stresses. It is found that granular base and subbase materials, compacted with heavy rollers, may develop relatively high residual horizontal stresses. The general law for characterizing granular materials is used with different postulated residual stresses in pavement analyses. The results obtained appear to be in good agreement with all aspects of granular material behavior, provided that a residual stress of the order of 1 to 2 psi is assumed to be induced by compaction.

Design and structural evaluation of flexible pavements are currently based on the layered elastic theory. This approach offers the possibility of a rational solution of the problem. The success of this approach depends on the accuracy with and manner in which material properties are evaluated and used in the analysis. The existence of nonlinear stress-strain characteristics in granular materials and soils has been well known for many years. Experimental data show that the response of these materials and especially that of the granular materials depends strongly on the prevailing state of stress. Therefore knowledge of the correct in situ stress conditions is vital for the rational approach to design and structural evaluation of flexible pavements.

In the last decade most research in the field of characterization of granular subbase and base layers has involved repetitive loading tests and has concentrated on developing nonlinear stress-strain models. The simple model, which is widely used and relates the resilient modulus to the sum of principal stresses, appears to have serious limitations. More complex and sophisticated models expressed in terms of shear and volumetric stress-strain relationships lead to quite low and unrealistic moduli when used in pavement analyses. Neither the material model nor the analysis is at fault: it appears that the state of stress prevailing in the field is not reproduced in the analysis.

This discussion suggests that residual compressive stresses induced by compaction during construction of the pavement or during repeated traffic loadings, or both, may be the cause of the incompatibility between common engineering values and the results of analyses of the sophisticated model. The existence of residual stresses in compacted materials is well supported in the literature by laboratory tests and full-scale retaining wall model tests with backfill compacted with equipment similar to that used in highway construction. If these residual stresses are taken into account in analysis as initial conditions, the state of stress that prevails in the field is reproduced and the granular material moduli are realistically evaluated.

A literature review of the characterization of granular material and an estimation of residual stresses induced by compaction are presented. An analysis of a layered system is included to illustrate the effect of residual stresses on the moduli of granular material and to compare the results with values used in existing pavement design procedures.

LITERATURE REVIEW OF CHARACTERIZATION OF GRANULAR MATERIAL

Two different approaches exist for estimating the granular material properties used in the analysis of pavement systems. In the empirical or semiempirical one, the resilient modulus is related to layer thickness and underlying subgrade modulus (1) as well as to material type (2) or asphalt concrete modulus of elasticity (3). The values obtained from these procedures are similar and appear realistic from an engineering and phenomenological point of view. In the last decade research has concentrated on the rational approach in which the behavior of granular material is described by nonlinear stress-strain characteristics. Three different relationships are currently implemented: (a) the well-established one, relating the resilient modulus to the bulk stress (4-6); (b) the hyperbolic law proposed by Kondner (7) for static loading and extended by several researchers (8,9); and (c) the fundamental one (10-12) relating the bulk and shear moduli to octahedral stresses and stress path.

The first model is expressed as

$$MR = k_1\theta^{k_2} \quad (1)$$

where MR is the resilient modulus, $\theta = \sigma_1 + \sigma_2 + \sigma_3$ is the sum of principal stresses, and k_1 and k_2 are regression coefficients derived from laboratory test results. Equation 1 has been implemented in

various computer programs (5,6) using iterative computation schemes.

Figure 1a presents the results of tests conducted on a dense graded aggregate (13,14). Lines of equal confining pressures (σ_3) have been added to indicate the tendency of variation of MR as a function of σ_3. The relationship given by Equation 1 is also drawn.

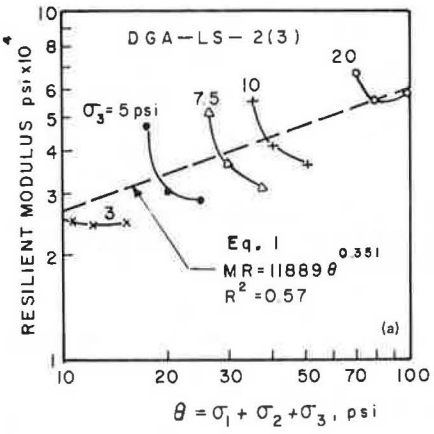

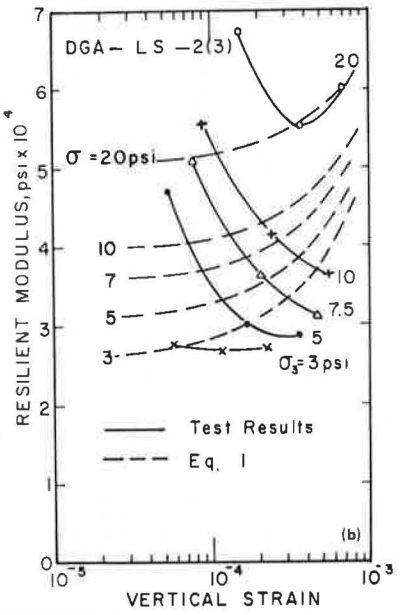

FIGURE 1 Test results and predicted behavior using Equation 1 for a dense graded aggregate *(13, 14)*.

It is seen that Equation 1 fits the results quite well. However, reversed trends of resilient modulus at constant confining pressures are noticed. Figure 1b shows the same test results of the resilient modulus as a function of the resilient vertical strain (ε_a). Included, for comparison, is the following predicted relation derived from Equation 1:

$$\varepsilon_a = (\sigma_d/MR) = [(\theta - 3\sigma_3)/MR]$$
$$= \{[(MR/k_1)^{1/k_2} - 3\sigma_3]/MR\} \quad (2)$$

where $\sigma_d = \sigma_1 - \sigma_3$ is the repeated vertical stress. It is seen from Figure 1b that the predicted resilient modulus at constant confining pressure increases monotonically as the vertical strain increases.

The general form of the hyperbolic law is

$$1/E = (\varepsilon_a/\sigma_d) = a + b\varepsilon_a \quad (3)$$

where E is the elastic modulus, ε_a is the axial strain, and a and b are regression coefficients that correspond to the inverse of the initial tangent modulus of elasticity (at $\sigma_d = 0$) and stress at ultimate failure, respectively. Equation 3 corresponds to a nonlinear stress-strain relationship with E decreasing gradually as ε_a and σ_d increase. The initial modulus function resembles Equation 1 in which the sum of principal stresses is replaced by the confining pressure. Equation 3 has been widely used for characterizing subgrade soils in the static loading mode and for permanent deformation under repeated loads (8,9). It has also been suggested for resilient deformation of granular material, using only the initial modulus term (15, p.57). That is,

$$MR = k_5 p_a (\sigma_3/p_a)^{k_6} \quad (4)$$

where p_a is atmospheric pressure and k_5 and k_6 are regression coefficients. In Equation 3 the modulus decreases as the vertical strain increases, in contradiction with the trend predicted by Equation 1.

Brown and Pappin (10,12) developed a nonlinear stress-strain relationship that is capable of taking into account effective, mean, and deviatoric stress and stress path dependence. The material properties are expressed in terms of bulk and shear moduli. The expressions derived are quite complex and may be used only in finite element analysis. It is interesting to study the predicted resilient modulus-vertical strain relationship at constant confining pressures, corresponding to the conventional triaxial test. Figure 2 shows the computed relations for the crushed limestone tested and those obtained using the Brown and Pappin model. It is seen that as the vertical strain increases, the modulus decreases first and increases afterwards at vertical strains greater than 2×10^{-4}. For comparison, the predicted modulus calculated using Equation 1 is also shown in

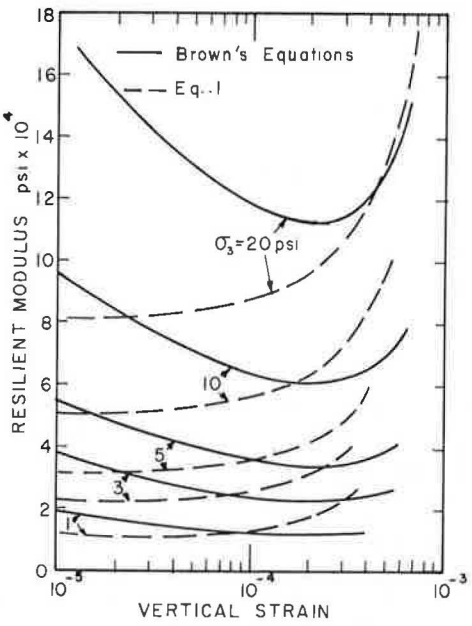

FIGURE 2 Comparison of predicted behavior of crushed stone using Brown's equations and Equation 1.

Figure 2. It is seen that the two predicted relations are quite different.

Discussion

These results summarize the state of the art in the field of granular material characterization for pavement design. The model developed by Brown and his colleagues appears to be the most promising. Its application to realistic conditions in pavements has been criticized for being based on triaxial tests where two principal stresses are equal. It is this author's opinion that its refinement in the full three-dimensional state of stress and strain will not lead to drastic changes in the values of the predicted modulus.

Figure 2 shows clearly that, for low vertical strain values, the modulus decreases as the vertical strain increases. The increase in the modulus values occurs at maximum to minimum principal stress ratios (σ_1/σ_3) of more than 2 to 3. In the model, the bulk modulus increases monotonically as the ratio of deviatoric to mean stress (q/p) increases. This behavior is well known in dense granular material as dilation. Therefore the increase of the resilient modulus in repetitive loading could be attributed to dilation effects and to the accumulation of permanent shear strain.

According to Figure 2, Equation 1 fails to describe the descending branch of the relationship and predicts a quite sharp ascending branch. It should be noted that, according to May and Witczak (16), Equation 1 neglects the effect of shear strain and is therefore applicable only in the range of low strain values. The complete expression for Equation 1 should read:

$$MR = k_1\theta^{k_2} f(\varepsilon_a) \quad (5)$$

where $f(\varepsilon_a)$ is the correction function that decreases as ε_a increases. Equation 5 is similar to that used in earthquake analyses: the function is given at discrete values of the shear strain, and the computer program performs the required interpolation.

It has been suggested that this function be approximated as follows:

$$MR = k_1\theta^{k_2}\varepsilon_a^{k_3} \quad (6a)$$

or

$$MR = k_1\theta^{k_2}\sigma_d^{k_4} \quad (6b)$$

with

$$\varepsilon_a > 10^{-5}$$

$$\sigma_d > 0.1\sigma_3$$

Test results (13,14) are used with multiple regression analyses to derive k_1, k_2, and k_4 material parameters. Figures 3-5 show comparisons of measured and predicted moduli using Equation 6b. (For the crushed limestone in Figure 3, the "measured" values were computed using the Brown and Pappin model.) It is seen that the prediction is quite good.

It is worth mentioning that the hyperbolic law (Equation 3) fails to describe the effect of dilation and accumulation of permanent shear strains. However, under the load where the vertical strain is between 1 to 5 x 10^{-4}, the modulus could be approximated by Equation 4, which states that the modulus depends on the confining pressure only.

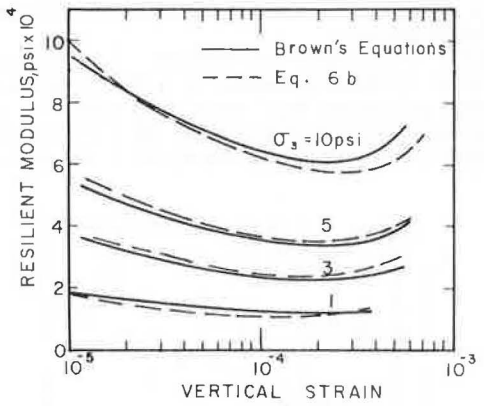

FIGURE 3 Comparison of predicted behavior of crushed stone using Brown's equations and Equation 6b.

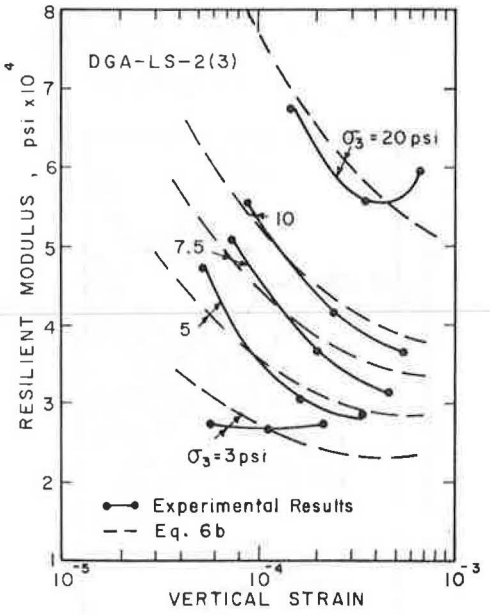

FIGURE 4 Comparison of test results and predicted behavior using Equation 6b for a dense graded aggregate *(13,14)*.

Application to Pavement Analyses

The three models presented have all been used to predict deflections, stresses, and strains in pavements. The first model is currently included in a pavement design method (6). Chou (15) conducted a comparative study with different stress-strain relations for granular materials and subgrade soils. He included Equations 1 and 4 for the granular materials and used finite element analyses.

The computed deflection at the pavement surface using Equation 4 was greater than that obtained using Equation 1. Chou (15,p.57) stated that "when tensile stresses were developed at the bottom of granular layers, the elastic modulus reduced drastically as the load increment increased," while "the use of Equation 1 can greatly increase the elastic moduli of granular materials." Because Equation 4 is inapplicable when tensile minimum principal stress develops, it has been abandoned, and Equation 1 has become well established. Its use has been improved by the addition of the Mohr-Coulomb failure law in

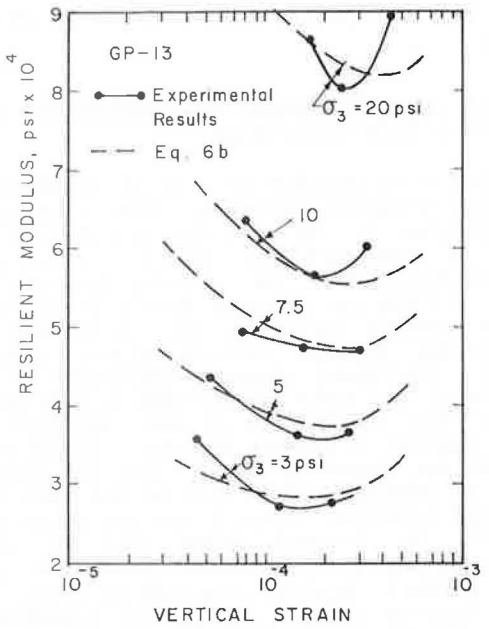

FIGURE 5 Comparison of test results and predicted behavior using Equation 6b for a bank gravel *(13,14)*.

order to keep the stress values inside the space delimited by the failure law envelope.

Recently Witczak (Use of NDT Deflection Data to Estimate In-Situ Material Moduli, working paper presented to TRB Task Force A2T56--Nondestructive Evaluation of Airfield Pavements, Fredericksburg, Virginia, 1981) compared the computed pavement response using Equation 1 and surface deflection measurements. He found that "an adjustment must be made to the values of any unbound granular material." May and Witczak (16) suggested that the adjustment factor for getting an effective resilient modulus is a function of the shear strain induced by the surface loading. Smith and Witczak (14) compared the computation results using Equation 1 and those of the empirical approach (1-3). They found that (a) for high-quality base materials, the results are in quite good agreement, especially for k_1 = 8000, and (b) for poorer quality materials, the comparison is not as good. It should be noted that these analyses indicate that the elastic modulus of the granular material is essentially independent of its thickness. Moreover, the computation results presented later in this paper show that the modulus increases slightly with increasing applied load.

Brown and Pappin (11,12) presented measured and predicted stresses and strains in an experimental section. Large discrepancies were reported. For example, the measured vertical strain near the bottom of the crushed stone layer was about 500 microstrains whereas the predicted one was about three times larger. The measured radial and tangential strains were lower than the predicted ones by a factor of two.

The results of analyses conducted using the accurate model for characterizing granular material and the finite element method have led Brown (17, p.56) to assign quite low moduli to the subbase and base layers. Suggested design values are about 100 MPa (15 ksi) and 40 MPa (6 ksi) for well-graded crushed rock and poorer material, respectively. These values are not realistic.

In the light of these results, it seems that the characterization of granular material is incomplete at present. The lack of agreement is frequently attributed to the axisymmetric stressing conditions of the triaxial test that do not correspond to the actual conditions in pavements. This criticism is basically correct; however, it is believed that improvement of the model cannot lead to drastic changes in the values of the moduli. Therefore it is suggested that residual stresses induced during compaction of the material be taken into account in order to be closer to the real conditions existing in pavements.

It should be noted that Stock and Brown (18) recognized the effect of compaction equipment on the granular material. They adopted coefficients of earth pressure at rest from the overconsolidation theory, which give relatively high horizontal stresses. The existence of the residual stresses and their magnitude are discussed hereafter.

RESIDUAL STRESSES INDUCED BY COMPACTION

Compaction of granular materials in pavements is required to provide sufficient strength and stability (i.e., to resist shear failure and permanent deformation under applied repetitive loads). The effect of compaction on material characterization has in the past been taken into account in analyses only through the effect of density and degree of saturation on the material property. However, because the material is highly nonlinear and undergoes large shear deformation, compaction creates a stress history for the finished material. In other words, even in a newly constructed pavement, the initial stress condition is not stress free, as is generally assumed.

Compaction produces a stable layer that will not deform under further rolling of the compaction equipment. This condition suggests that the finished material is confined. The hypothesis that residual compressive stresses are induced by compaction is well supported by laboratory test results (19) and full-scale retaining wall models with compacted backfill (20,p.18; 21,p.21). The analysis evaluating the induced lateral pressures can be only approximate because large deformations are involved and the stress path in each material element is quite complex. The simple method proposed by Broms (22) and Ingold (23,24) appears to predict quite well the compaction-induced lateral earth pressure. This method is based on

1. Classical earth pressure theory that defines the extreme limits for the lateral pressures that can be developed in a soil mass.
2. The assumption that, under loading, the vertical stress increases and the horizontal stress remains unchanged until limit equilibrium is reached; then both the vertical and the horizontal stresses increase according to the limit corresponding to the active state case. That is,

$$\sigma_h = K_a \sigma_v \tag{7}$$

where σ_v and σ_h are the vertical and horizontal stresses, respectively, and K_a is the coefficient of active lateral earth pressure. Therefore, horizontal compression develops in the soil mass.

3. The assumption that, under unloading, the vertical stress decreases and the horizontal stress remains unchanged until limit equilibrium is reached; then both vertical and horizontal stresses decrease, according to the limit corresponding to the passive state case. That is,

$$\sigma_h = K_p \sigma_v \tag{8}$$

where K_p is the coefficient of passive lateral earth pressure. The final state of stress is reached when the vertical stress is equal to the overburden.

4. Vertical stress under the roller is determined using line loading condition and semi-infinite elastic mass (Boussinesq case).

Figure 6 shows the method of analysis for a vibratory compactor applying 3 ton/ft (100 kN/m) and for a well-graded subbase or base material with c = 0.7 psi (5 kN/m²) and ϕ = 45 degrees. The vertical stress of 61 psi (420 kN/m²) is determined at a 6-in. (0.15-m) depth corresponding to the bottom of the layer being compacted. It is seen that, under 0.44 psi (3 kN/m²) overburden pressure, a maximum residual horizontal stress of about 6 psi (40 kN/m²) is expected to be induced. This example may be viewed as representative of granular materials in pavement because the cohesion, the angle of internal friction, and the load magnitude are typical of present pavement construction technology.

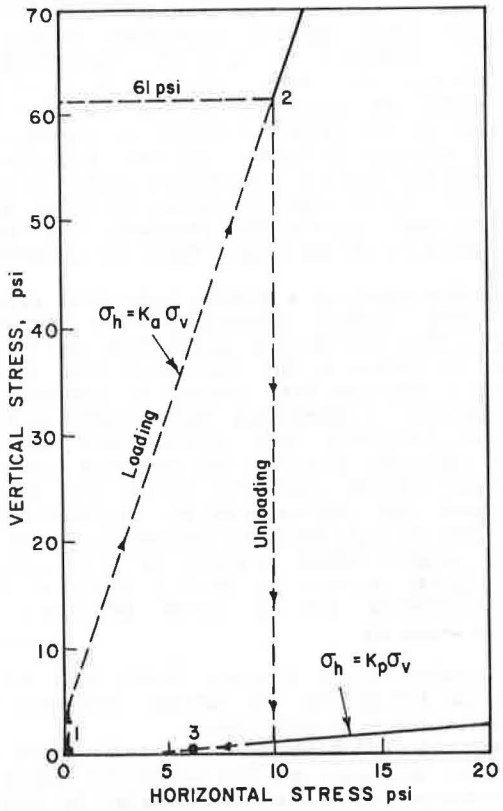

FIGURE 6 Schematic representation of stress path during compaction.

It is worth mentioning that, according to the method of analysis, the residual stress depends on the material properties and on the compacting load. For a cohesionless material, the envelope for the passive case (lower envelope in Figure 3) intersects the overburden line at quite low horizontal stress compared to cohesive material. Furthermore, to develop residual stresses, sufficient load must be applied to reach the active state condition.

Lateral earth pressures of 2 psi (15 kN/m²) and 6 psi (40 kN/m²) have been measured for cohesionless and cohesive materials, respectively, compacted behind retaining walls and bridge abutments (23,24). The values of the measured residual stresses were found to be in good agreement with this method of analysis.

ANALYSIS OF LAYERED SYSTEMS AND INVESTIGATION OF BEHAVIOR OF GRANULAR MATERIAL

The behavior of granular material is investigated by analyzing different pavements, using a finite element program for axisymmetric problems. Constant moduli of elasticity are assigned to the asphalt concrete layer and to the subgrade. Equations 1 and 6b are used for the resilient moduli of the base and subbase granular materials. With Equation 1, only the geostatic stresses (vertical stress = overburden pressure; horizontal stress = coefficient of earth pressure at rest times the vertical stress) are considered. When Equation 6b is used, different additional residual horizontal stresses (induced by compaction) are assumed to exist in granular layers. It should be mentioned that, because the intermediate and minor principal stresses are not equal in the pavement, the deviator stress (σ_d) in Equation 6b was replaced by the octahedral shear stress.

The pavements analyzed are made of 4 in. of asphalt concrete with a modulus of elasticity of 500,000 psi, 6 in. of dense graded aggregate base (see Figure 4), 8 or 14 in. of gravel subbase (see Figure 5) in Pavements I and II, respectively. Two subgrade moduli were included in the analysis, 4,500 and 15,000 psi. Poisson's ratios of 0.4 were assumed for all materials. Because granular material behavior is described by a nonlinear law and the finite element program used treats the two dimensional (axisymmetric) case, only a single wheel load is applied at the pavement surface. A contact area with a constant radius of 6 in. and uniformly distributed contact pressures were assumed.

Figure 7 shows the distribution with depth of the computed moduli close to the axis of the wheel load when applying a contact pressure of 70 psi. The results shown correspond to Pavement I, and, using Equation 6b with different residual stresses and Equation 1, it is seen that (a) as the residual stress increases, the computed modulus increases and (b) the modulus computed using Equation 1 (without the additional residual stresses) appears to correspond to a residual stress of about 2 psi in the

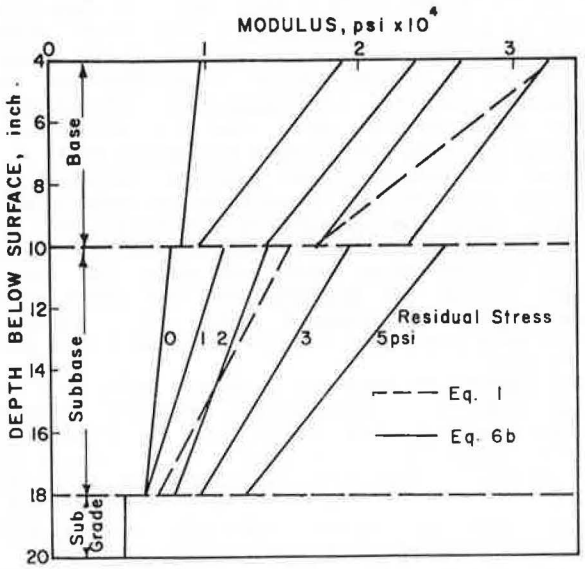

FIGURE 7 Distribution with depth of base and subbase moduli under the load.

subbase and of more than 3 psi in the base (with Equation 6b).

Figures 8 and 9 show the distribution along the radial distance of the computed moduli at middepth of the base and subbase layers for subgrade moduli of 4,500 and 15,000 psi, respectively. It is seen that: (a) The distributions obtained using Equations 1 and 6b are different. With Equation 1, the modulus is higher under the load than far from it. With Equation 6b, the modulus is in some cases higher and in other cases lower under the load than far from it. The distribution depends on the subgrade modulus that controls the sum of principal stresses and deviatoric stresses, especially under the load. (b) The modulus varies with the radial distance. Therefore the commonly used layered analyses with constant moduli for the granular layers must be viewed as approximate.

To compare the results of analyses with the empirical approach, an equivalent modulus of the granular material (base and subbase) was computed. It was derived on the basis of equal deflections at the center of the circular wheel load.

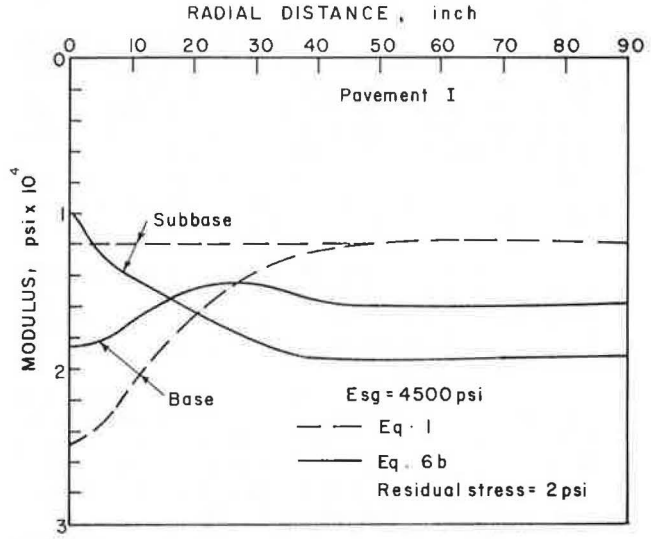

FIGURE 8 Distribution of base and subbase moduli versus radial distance (subgrade modulus 4,500 psi).

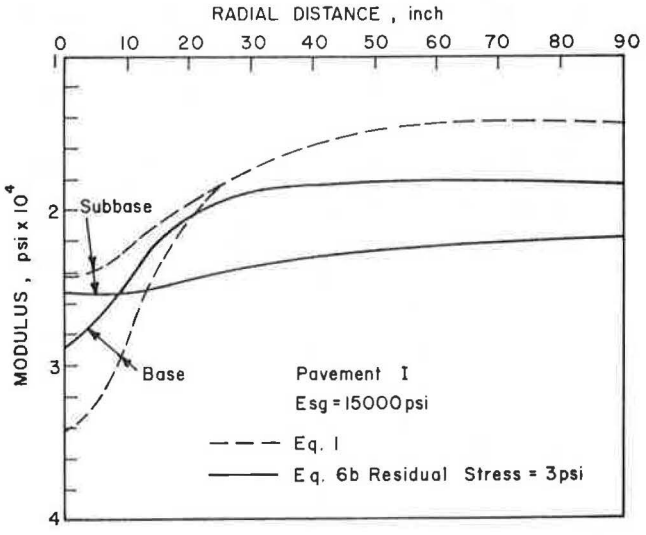

FIGURE 9 Distribution of base and subbase moduli versus radial distance (subgrade modulus 15,000 psi).

Figure 10 shows the results of computations for Pavement I and a subgrade modulus of 4,500 psi. Three load levels are included. It is seen that (a) the modulus according to Equation 6b increases with increasing residual stresses and with decreasing load level, (b) the modulus according to Equation 1 increases slightly with increasing load level, and (c) the range of empirical moduli of granular material corresponds to residual stresses of up to 3 psi.

Similar results are shown in Figure 11 for Pavement II. From Figures 10 and 11, it can be clearly seen that the equivalent modulus increases with increasing thickness of the granular material. The increase in the modulus is slightly more pronounced

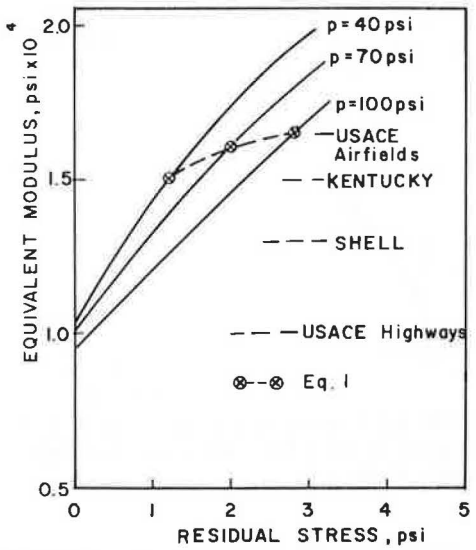

FIGURE 10 Equivalent modulus of granular material for Pavement I and subgrade modulus of 4,500 psi.

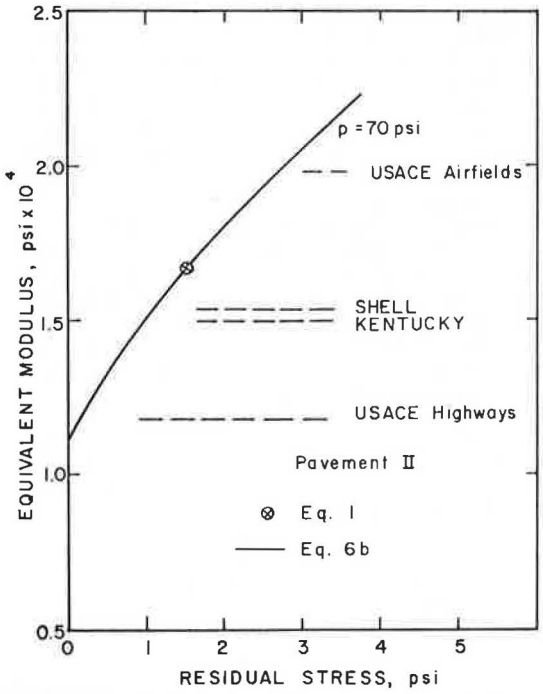

FIGURE 11 Equivalent modulus of granular material for Pavement II and subgrade modulus of 4,500 psi.

with Equation 1. Figure 12 shows results of computations for a subgrade modulus of 15,000 psi and a contact pressure of 70 psi. It should be noted that, in this case of a strong subgrade, the empirical procedure predicts a modulus of the order of 40,000 psi, a value that is not reached even with 5 psi residual stresses.

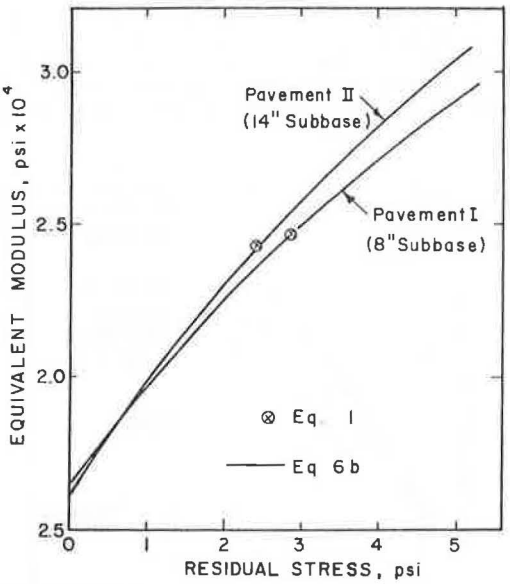

FIGURE 12 Comparison of equivalent moduli of granular material for Pavements I and II (subgrade modulus 15,000 psi).

SUMMARY AND CONCLUSIONS

It has been demonstrated that Equation 1 is not sufficient to describe the behavior of granular material in the test results from which it is derived. Although the modulus values obtained in pavement analyses are in the proper range, their variation with respect to load level and position (under and far from the load) does not appear to fit experimental results. Analyses with Equation 1 show that the granular modulus increases as the load level increases, a trend that is not, to the knowledge of this author, supported by field test results. It should be remembered that Equation 1 neglects the effect of shear strains.

The results of analyses using Equation 6b appear to be in good agreement with all aspects of granular material behavior, provided that a residual stress induced by compaction is postulated. The modulus increases with decreasing load level and increasing granular layer thickness. The residual stress required to develop values in the proper range, compared to empirical values, appears to be 1 to 2 psi. On full-scale retaining wall models, such values have been measured even with sandy backfill. It will therefore be not unrealistic to assume that dense subbase and base materials that comply to specifications will develop residual stresses of this order of magnitude.

Further research is required to better understand the material properties and construction techniques that govern the induction of residual stresses.

REFERENCES

1. A.I.M. Claessen, J.M. Edwards, P. Sommer, and P. Uge. Asphalt Pavement Design--The Shell Method. Proc., Fourth International Conference on the Structural Design of Asphalt Pavements, Ann Arbor, Mich., Vol. I, 1977, pp. 39-74.
2. W.N. Brabston, W.R. Barker, and G.G. Harvey. Development of a Structural Design Procedure for All Bituminous Concrete Pavements for Military Roads. Technical Report S-75-10. U.S. Army Engineer Waterways Experiment Station, Vicksburg, Miss., July 1975.
3. R.C. Deen, H.F. Southgate, and J.H. Havens. Structural Analysis of Bituminous Concrete Pavements. Research Report 405. Division of Research, Kentucky Department of Highways, Frankfort, May 1971.
4. R.G. Hicks and C.L. Monismith. Factors Influencing the Resilient Response of Granular Materials. In Highway Research Record 345, HRB, National Research Council, Washington, D.C., 1971, pp. 15-31.
5. F. Finn, C. Saraf, R. Kalkarni, K. Nair, W. Smith, and A. Abdullah. The Use of Distress Prediction Subsystems for the Design of Pavement Structures. Proc., Fourth International Conference on the Structural Design of Asphalt Pavements, Ann Arbor, Mich., Vol. 1, 1977, pp. 1-38.
6. J.F. Shook, F.N. Finn, M.W. Witczak, and C.L. Monismith. Thickness Design of Asphalt Pavements--The Asphalt Institute Method. Proc., Fifth International Conference on the Structural Design of Asphalt Pavements, Delft, The Netherlands, Vol. 1, 1982, pp. 17-44.
7. R.L. Kondner. Hyperbolic Stress-Strain Response: Cohesive Soils. Proc., American Society of Civil Engineers, Vol. 89, No. SM1, 1963, pp. 115-143.
8. R.D. Barksdale. Laboratory Evaluation of Rutting in Base Course Materials. Proc., Third International Conference on the Structural Design of Asphalt Pavements, London, England, Vol. 1, 1972, pp. 161-174.
9. C.L. Monismith, K. Inkabi, C.F. Freeme, and D.B. McLean. A Subsystem to Predict Rutting in Asphalt Concrete Pavement Structures. Proc., Fourth International Conference on the Structural Design of Asphalt Pavements, Ann Arbor, Mich., Vol. 1, 1977, pp. 529-539.
10. J.W. Pappin and S.F. Brown. Resilient Stress-Strain Behaviour of a Crushed Rock. Proc., International Symposium on Soils Under Cyclic and Transient Loading, Swansea, England, Vol. 1, 1980, pp. 169-177.
11. S.F. Brown and J.W. Pappin. Use of a Pavement Test Facility for the Validation of Analytical Design Methods. Proc., Fifth International Conference on the Structural Design of Asphalt Pavements, Delft, The Netherlands, Vol. 1, 1982, pp. 209-220.
12. S.F. Brown and J.W. Pappin. Analysis of Pavements with Granular Bases. In Transportation Research Record 810, TRB, National Research Council, Washington, D.C., 1981, pp. 17-23.
13. G. Rada and M.W. Witczak. Comprehensive Evaluation of Laboratory Resilient Moduli Results for Granular Materials. In Transportation Research Record 810, TRB, National Research Council, Washington, D.C., 1981, pp. 23-33.
14. B.E. Smith and M.W. Witczak. Equivalent Granular Base Moduli: Prediction. Journal of the Transportation Engineering Division, ASCE, Vol. 107, No. TE6, 1981, pp. 635-652.
15. Y.T. Chou. Evaluation of Nonlinear Resilient Moduli of Unbound Granular Materials from Accelerated Traffic Test Data. Report FAA-RD-76-65. U.S. Army Engineer Waterways Experiment Station, Vicksburg, Miss., 1976.
16. R.W. May and M.W. Witczak. Effective Granular

Modulus to Model Pavement Responses. In Transportation Research Record 810, TRB, National Research Council, Washington, D.C., 1981, pp. 1-9.
17. S.F. Brown. Discussion. Proc., Fifth International Conference on the Structural Design of Asphalt Pavements, Delft, The Netherlands, 1982, Vol. 2.
18. A.F. Stock and S.F. Brown. Nonlinear Characterization of Granular Materials for Asphalt Pavement Design. In Transportation Research Record 755, TRB, National Research Council, Washington, D.C., 1980, pp. 14-20.
19. G.F. Sowers, A.D. Robb, C.H. Mullis, and A.J. Glen. The Residual Lateral Pressures Produced by Compacting Soils. Proc., 4th International Conference on Soil Mechanics and Foundation Engineering, 1957, pp. 243-247.
20. D.R. Carder, R.G. Pocock, and R.T. Murray. Experimental Retaining Wall Facility--Lateral Stress Measurements with Sand Backfill. TRRL Laboratory Report 766. Transport and Road Research Laboratory, Crowthorne, Berkshire, England, 1977.
21. D.R. Carder, R.T. Murray, and J.V. Krawczyk. Earth Pressures Against an Experimental Retaining Wall Backfilled with Silty Clay. TRRL Laboratory Report 946. Transport and Road Research Laboratory, Crowthorne, Berkshire, England, 1980.
22. B. Broms. Lateral Earth Pressures Due to Compaction of Cohesionless Soils. Proc., 4th Budapest Conference on Soil Mechanics and Foundation Engineering, 1971, pp. 373-383.
23. T.S. Ingold. The Effects of Compaction on Retaining Walls. Geotechnique, Vol. 4, 1979, pp. 265-283.
24. T.S. Ingold. Lateral Earth Pressures--A Reconsideration. Ground Engineering Journal, May 1980, pp. 39-43.

Publication of this paper sponsored by Committee on Mechanics of Earth Masses and Layered Systems.

Failure Criteria and Lateral Stresses in Track Foundations

HARRY E. STEWART, ERNEST T. SELIG, and GILLIAN M. NORMAN-GREGORY

ABSTRACT

In conventional track systems the ties are supported by an unbound ballast layer underlain by subballast or the subgrade, or both. Analytical models used to estimate stresses and deflections of these multilayer systems predict that the lower portions of the unbound layer will develop significant incremental tensile stresses. Their magnitude is such that, when combined with the normally expected geostatic stresses, failure of the ballast is predicted. Some analytical models have incorporated failure criteria for the unbound layer as a means of limiting these stresses to permissible values. A discussion of these approaches is presented along with the implications that predicted failure would have for permanent deformation prediction methodologies. An alternative method based on residual lateral stresses in the ballast is presented. A description is given of a laboratory box testing device used to measure residual lateral stresses. Experimental results are shown that indicate that relatively large residual stresses, due to repeated applications of loading, can develop in ballast. The effects of combining the initial lateral stresses in the unbound layer with the incremental tensile stresses predicted by continuum or finite element models are discussed. Particular attention is given to the effects that these residual stresses have on prediction of permanent deformation.

The deformation analysis of conventional track structures requires characterization of the overall track system. This system includes the rails and ties that are supported by a foundation. The foundation consists of a ballast layer that is underlain by a subballast layer, in some cases, followed by a subgrade. This foundation is a multilayer system wherein a relatively stiff ballast layer lies above a softer subballast or subgrade. The stiffness of each layer is generally represented by its resilient Young's modulus (E_Y).

There is a need to improve the modeling of these

systems with emphasis on the geotechnical properties of the foundation layers. Methods of practice may make use of simplified approaches for estimating vertical stresses on the subgrade. Although the American Railway Engineering Association (AREA) Manual of Practice does not contain a method for predicting foundation stresses, a procedure such as that described by Talbot in the 1920s may be used. These simplified procedures do not address the multilayer nature of the foundation, nor do they address the internal stresses in the ballast that would be needed to predict permanent deformations of that layer.

Analytical models (1,2) are used to obtain estimates of the stresses and deflections in these multilayer systems under specified loading conditions. These results are then used for design applications by predicting either allowable resilient deflections or permanent deformation. These models, based on either multilayer elastic theory or finite element methods, predict that loading will cause significant incremental horizontal tensile stresses to develop in the lower portions of the ballast layer. When these stress states at the base of the ballast layer are combined with the normally expected geostatic stresses, the resulting total horizontal stresses are usually still tensile and thus a failure condition is predicted.

Methods have been used to limit these stresses to allowable values by incorporating either special conditions for the failed zones or specific failure criteria for the unbound ballast layer. A discussion of these methods will be presented, along with the implications that predicted failure would have for permanent deformation prediction methodologies.

An alternative method is based on residual lateral stresses in ballast. These residual lateral stresses affect the unloaded or geostatic stress state and thus influence the total stress states in the loaded condition. A description will be given of a laboratory testing device used to observe residual lateral stresses, along with experimental results that indicate that relatively large residual lateral stresses can develop in ballast as a result of repeated loadings.

The effects of combining these unloaded stresses with the predicted incremental tensile stresses will be discussed. Attention will be directed toward the implications that these residual stresses have for predictions of permanent deformation.

STRESS STATES

The unloaded vertical stresses (σ_{vo}) at depths within the ballast layer are determined by the weight of the overlying track structure (rails and ties) and the unit weight of the ballast. The unloaded lateral stresses (σ_{ho}) are typically defined as $\sigma_{ho} = K_o\sigma_{vo}$, where K_o is the coefficient of lateral earth pressure at rest. For the purposes of this paper it is assumed that the ballast is clean and free draining so that any effects of pore pressure can be neglected. The unloaded stress state at the base of the ballast is entirely compressive, as shown in Figure 1a. When surface loads are applied to the multilayer system wherein the modulus of the ballast layer is greater than that of the underlying subballast or subgrade layer, incremental compressive vertical and tensile lateral stresses will be analytically predicted near the base of the ballast layer, as shown in Figure 1b.

The stress states in the loaded condition are determined by adding the initial to the incremental stress states such that $\sigma_v = \sigma_{vo} + \Delta\sigma_v$ and $\sigma_h = \sigma_{ho} + \Delta\sigma_h$. Beneath the loaded area, at all depths, the vertical stresses are always compressive. The incremental horizontal stresses are compressive near the top of the stiff upper layer and become tensile in the lower regions. The transition depth from incremental compressive to incremental tensile horizontal stresses is affected by the depth of the ballast layer and the relative stiffness of the ballast compared to the underlying layer.

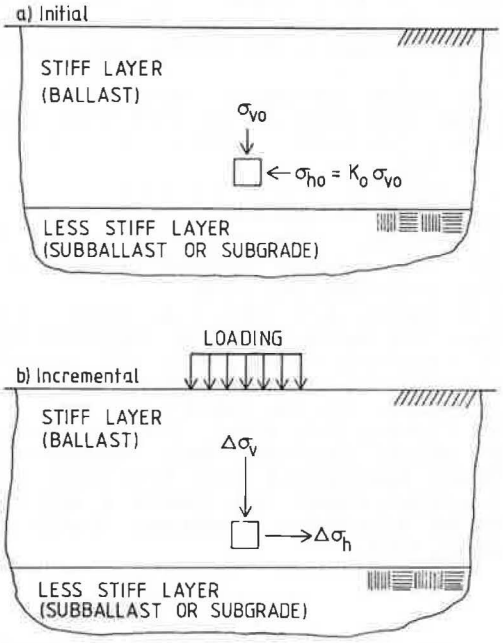

FIGURE 1 Initial and incremental stresses at the base of a layered system.

Many analyses in geotechnical engineering require assuming a value of K_o because of a lack of either laboratory or field data. Typical values of K_o might be in the range of 0.5 to 1.0 for granular materials such as ballast. The loaded stress states at the bottom of the ballast layer, for a K_o value of 1.0 and the incremental tensile stresses shown in Figure 1, are shown in Figure 2. This Mohr circle stress state is not allowable because it exceeds the Mohr-Coulomb failure envelope. Thus, near the base

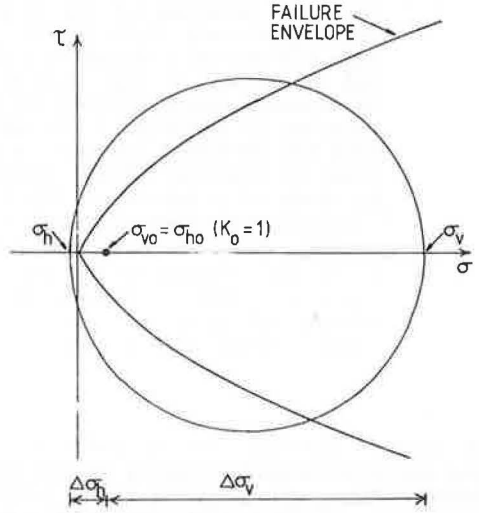

FIGURE 2 Loaded stress state in the tension zone for low K_o conditions.

of the ballast layer, the incremental tensile stresses combined with the geostatic conditions described previously would indicate a condition of static failure. Because the loaded stress state shown in Figure 2 cannot occur, differences must exist between the predicted and the actual stress states in the "tension" zone.

PREVIOUS APPROACHES

Various methods have been proposed to circumvent the problem of predicted failure. One method is to subdivide the upper granular layer into many small sublayers about 1 in. thick (3). However, tensile stresses will still develop in the lower portions of at least some of the sublayers, or possibly in an entire sublayer. To determine the stress state for the stress-dependent resilient modulus for each of the sublayers, a middepth location is often used. This location may be above the predicted tension zones for some sublayers, but the predicted tensile stresses still may exist at middepth for lower sublayers. In such cases a lower modulus is arbitrarily assumed for the sublayer. This approach will cause the newly computed resilient moduli to decrease with depth and cause more gradual transitions in modular ratios, which reduces the tendency for tensile stresses. However, this method still does not address the actual material behavior and may increase the computer time necessary to obtain the solutions.

Another approach is to lower the modulus of the granular material in those areas where predicted failure occurs (1). This provides for a more gradual transition between the stiffer ballast layer and the softer underlying subballast or subgrade, but it is a compensating scheme that is not consistent with the material response.

Figure 3 is a representation of a triaxial test result in which the sample is loaded to a failure or near-failure state and then unloaded and reloaded several times. During the primary loading, the tangent modulus decreases as the sample approaches failure. When the material is unloaded the resilient portion of the strain is recovered and some permanent strain remains. On reloading, the soil is stiffer than during primary loading. As the soil stresses approach the failure level, followed by another unloading, additional permanent strain develops while the resilient strain is recovered. Even though the tangent modulus may be low near the failure state, the resilient modulus remains high.

The appropriate soil modulus for the ballast layer in a track system, or for any layer in a system subjected to repeated loadings, is the resilient modulus, shown in Figure 3, that remains high even

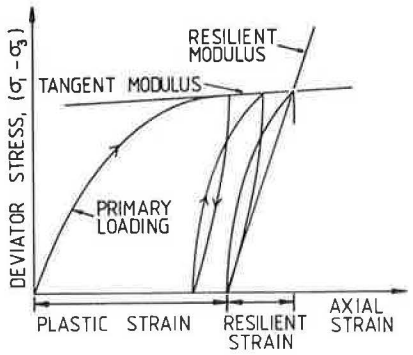

FIGURE 3 Representation of a stress-strain curve from a repeated load triaxial test to near-failure conditions.

when the material is repeatedly stressed to levels at or near static failure. Imposing an arbitrarily low modulus in those zones predicted to be in a state of static failure is equivalent to using a near-failure tangent modulus. This is not representative of the material's resilient response under the predicted stress state. The resilient modulus should remain high. The use of low moduli may eliminate the tension zone predictions, but such moduli are uncharacteristic of actual material behavior and will overpredict elastic deformation.

The Mohr-Coulomb failure criterion has been used directly to modify the stresses predicted at the base of the granular layers in a multilayer system (4). To do this, Mohr-Coulomb parameters c and ϕ are first assigned to the granular materials. Presumably, the parameters c and ϕ may be taken as the effective stress parameters for a granular material, and the inclusion of the cohesion term (c) is to account for the curvature of the Mohr-Coulomb failure envelope and not to be interpreted as true material cohesion.

The procedure given by Raad and Figueroa (4) sets numerical limits on the major and minor principal stresses that can be developed at depths within the granular layer. These limiting stress states are based on principal stress ratios for active and passive failure, using the calculated values of vertical stress (σ_v) in each soil element as one of the principal stresses. These limiting principal stress states, for a given σ_v, are shown in Figure 4 as $(\sigma_1)_{max}$ and $(\sigma_3)_{min}$. The computed minor principal stress (σ_3) within a soil element is then compared with these limiting values and adjustments are made to the element stresses so that the modified

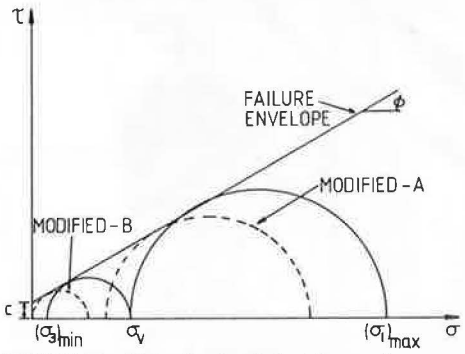

FIGURE 4 Mohr-Coulomb limiting and modified failure stress conditions.

stresses result in a Mohr circle, tangent to the failure envelope but having principal stresses between the $(\sigma_1)_{max}$ and $(\sigma_3)_{min}$ limits. This modified stress circle is shown as dashed line A in Figure 4. Alternatively, if σ_3 is negative, the element stress state is set at that represented by dashed line B in Figure 4. The modified stresses are then used in a stress-dependent resilient modulus formulation, generally one based on bulk stress, and the foundation stresses are reanalyzed. This method is said (4) to converge and satisfy equilibrium and boundary conditions. The result of this procedure is that any predicted tensile stresses are adjusted to nontensile values and a high resilient modulus is maintained. However, conditions of static failure still exist, which makes the method unreasonable for use in permanent deformation predictions.

Brown and Pappin (see their paper in this Record) have reviewed the results of the University of Nottingham research on layered system response. They

use the program SENOL to evaluate layer behavior including the stresses developed in the unbound granular layer. Their soil model, termed "contour" model, is represented by families of strain contours on a deviator stress-mean normal stress plot. These plots were developed from extensive repeated load triaxial tests. This soil model is thus nonlinear and stress state dependent. The results show that the incremental horizontal stresses from the load given by SENOL in the lower part of the granular layer are tensile. However, when the geostatic stresses are added, assuming $K_o = 1$, the combined loaded stress states are compressive. Furthermore, the stress state in the lower part of the granular layer is below failure.

The elimination of the failure state in the approach by Brown and Pappin is believed to be a result of a more accurate soil model than that used in any other approaches.

RESIDUAL STRESSES

An examination of the horizontal stresses predicted from elastic multilayer theory led to the hypothesis that residual horizontal stresses are induced in ballast by repeated wheel loads. A laboratory study was undertaken to examine the nature and extent of these horizontal stresses. To do this a ballast box was constructed (Figure 5) with instrumented side and end panels to measure horizontal stress and a flexible bottom to represent the effect of subgrade conditions. The box was intended to simulate conditions in track near the rail seat and adjacent crib areas. The ballast box was 12 in. wide, 24 in. long, and 19 in. deep. Further details on construction of the box are given elsewhere (5).

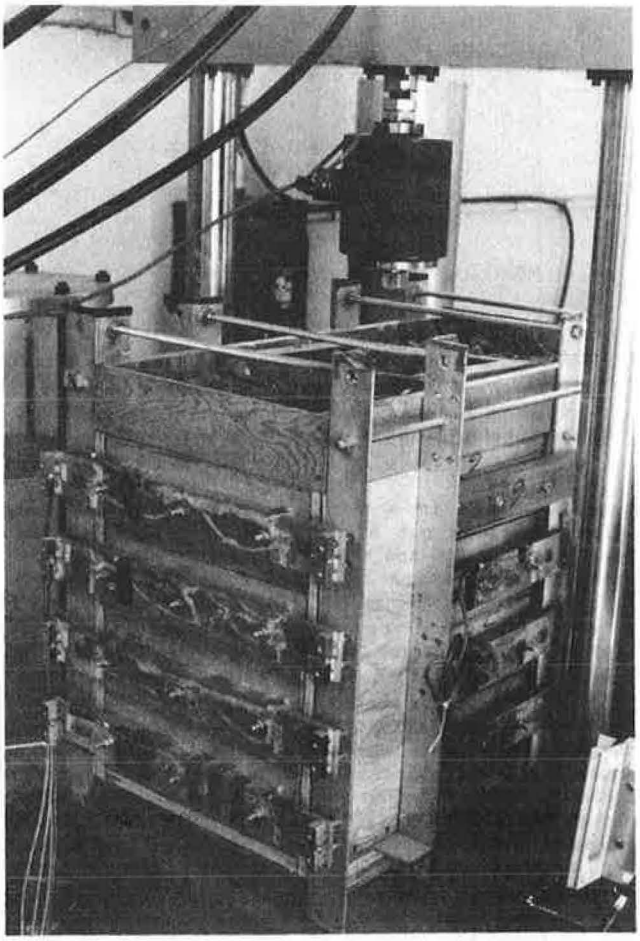

FIGURE 5 Ballast box apparatus.

The ballast material used in these tests was an angular traprock with an AREA No. 4 gradation. The loads were applied through a tie segment 9 in. wide by 11.5 in. long. The ballast depth below the tie segment was about 12 in. The maximum cyclic load was 4,000 lb, producing a tie contact pressure equivalent to that of a 32-kip wheel load from a train.

Typical measurements from the side panels of the box are shown in Figure 6. The results indicated that there was a rapid buildup of horizontal stresses during the first loading and that high residual stresses develop after the first unloading. Furthermore, the horizontal stresses in the loaded state decreased and the residual stresses increased up to about 100 cycles. After 100 cycles, the horizontal stresses tended to stabilize and the unloaded value tended to converge to the loaded value. This means that the horizontal stresses tended to become constant during the load cycle. The maximum horizontal stresses acting on the side panels occurred at about middepth of the ballast. The minimum horizontal stresses on the side panels occurred near the base of the ballast layer.

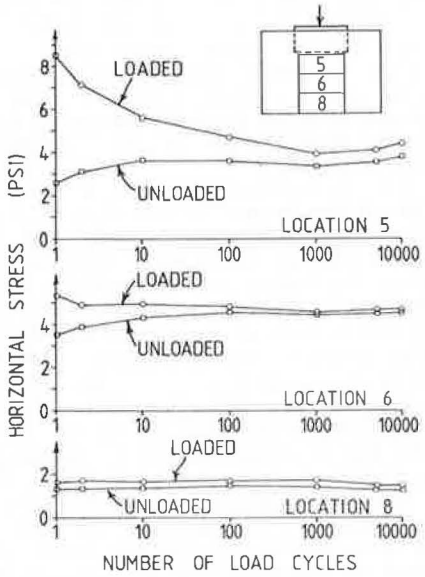

FIGURE 6 Horizontal stresses on side panels.

The measured horizontal stresses at the end panels are shown in Figure 7. Similar rapid buildup of the lateral residual stresses was observed at the ends of the box. The maximum lateral stresses again occurred about 6 in. above the base of the ballast layer.

Although the magnitude of the effects may be a function of the box boundary conditions, these tests clearly show that substantial horizontal residual stresses can develop in ballast. The measured residual stresses in the unloaded state were used to calculate values of K_o. Theoretically, the maximum residual horizontal stress must be limited to stresses at the passive failure condition. The ratio of the major principal stress at failure ($\bar{\sigma}_{1f}$) to the minor principal stress at failure ($\bar{\sigma}_{3f}$) at the passive

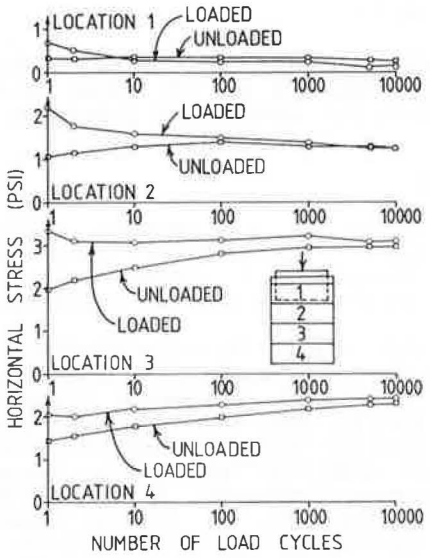

FIGURE 7 Horizontal stresses on end panels.

failure condition, for a strictly cohesionless material such as ballast, is defined as

$$\bar{\sigma}_{1f}/\bar{\sigma}_{3f} = (K_o)_{max} = K_p = [(1 + \sin \bar{\phi}) \div (1 - \sin \bar{\phi})] \quad (1)$$

The calculated K_o values, based on the unit weight of the ballast, the static surcharge of the tie segment, and the box test side and end panel measurements, are shown in Figure 8. All are greater than unity except in the crib above the base of the tie segment. The extremely large values of K_o for the upper portion of the side zone would require a friction angle ($\bar{\phi}$) of about 56.5 degrees, which is unusually high. However, if the curved failure envelopes, the possible interlock of the large particles, and the low vertical stresses in this zone are considered, a friction angle of this magnitude is possible. Certainly, values of $K_o = 6$ would be possible because the required friction angle would be only about 45.5 degrees. Triaxial tests, run on a variety of ballast materials, have shown that friction angles within this range are possible for low effective confining pressures.

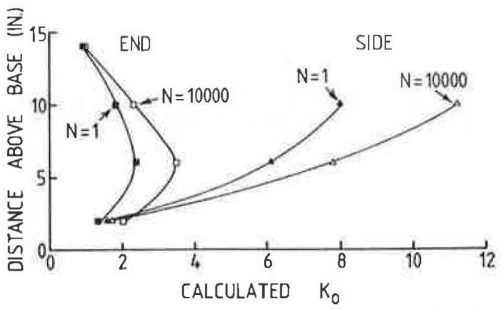

FIGURE 8 Variation of K_o as a function of depth from box experiments.

These experimental observations of the high residual lateral stresses and correspondingly high K_o values may be one of the main considerations necessary to account for what actually occurs in the lower portions of the granular base in a multilayer system.

IMPLICATIONS FOR PERMANENT DEFORMATIONS

Methods of analysis that make use of significantly reduced moduli and static failure criteria contain inconsistencies or make assumptions that are not compatible with observed material response. One main disagreement is that a condition of static failure cannot exist at the base of a granular layer such as the ballast in track. Static failure, in terms of the Mohr-Coulomb criterion, represents a limiting stress condition where the full strength of the material has been developed. Unlimited strains would result if such a stress state were developed. In track systems, such a failure condition near the base of the ballast would mean that excessive deformations would occur under a single load cycle. However, because the layered systems used in track and pavements do not fail under even one load cycle, let alone continuously fail under repeated load as would be evidenced by large, rapid surface deterioration, the use of failure criteria contains fundamental inconsistencies.

The loaded stress states in track are dependent on both the geostatic stresses and the incremental stresses imposed by the applied loading. The existence of high residual compressive stresses in the unloaded state could offset the predicted incremental tensile stresses. If these residual stresses are large enough, a nonfailure final stress state would result. This is shown in Figure 9 for the same magnitude of initial vertical stress (σ_{vo}) and incremental stresses ($\Delta\sigma_v$ and $\Delta\sigma_h$) as shown in Figure 2. The initial residual horizontal stress (σ_{ho}) is larger than σ_{vo} because the K_o value is greater than unity. The final vertical stress (σ_v) in Figure 9 is the same as that given in Figure 2, but the final horizontal stress (σ_h) is sufficient to reduce the maximum stress difference and thus maintain a nonfailure loaded stress state.

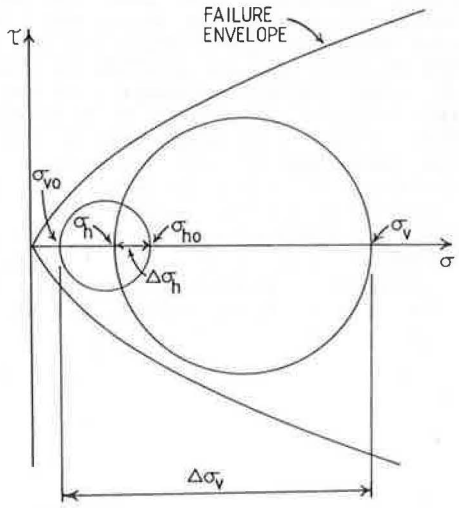

FIGURE 9 Loaded stress state in the tension zone for high K_o conditions.

Considerable effort has been devoted, both in the United States and abroad, to predicting the permanent deformations that accumulate in track due to

repeated loadings (6-8). The approaches taken in the United States make use of the stress path method by combining estimates of stresses in a layered track system with laboratory measurements of the inelastic soil response under representative stress conditions in a triaxial test. When zones in the track foundation are predicted to be in a state of failure, there is no way to predict the amount of permanent strain that can be expected to develop. When residual stresses are used to eliminate the nonallowable tensile lateral stresses such that the final stresses are permissible, as conceptually shown in Figure 9, the stress path approach can be used. The approach taken by Brown and Pappin (see their paper in this Record) showed that $K_o = 1$ was sufficient to eliminate the tensile stresses. Use of even higher K_o values such as observed in the ballast box will result in lower permanent strain predictions that could well prove to be even more realistic when combined with their estimated stress paths.

SUMMARY

The purpose of this paper has been to discuss methods of dealing with predicted failure zones in a layered system. An approach based on experimental measurements of residual lateral stresses is recommended.

The use of many sublayers and the selection of depth points above the predicted tension zone may, in some cases, give reasonable results, but this bypasses and does not fully address the problem. Adjustment of the soil modulus to a low value may reduce the tendency for incremental tensile lateral stresses to develop but does not represent the actual resilient modulus of the granular material even at a failure condition. Thus even the predicted elastic deformations should be unrealistic. The application of static failure criteria and the adjustment of the stresses to limit equilibrium conditions may result in satisfactory predictions of the resilient surface vertical deformation of a layered system. However, failed soil zones beneath the loaded areas would imply large plastic deformations, which is inconsistent with actual responses. The use of residual horizontal stresses, as observed in the ballast box experiments, does not eliminate the predicted incremental tensile stresses. Instead, these residual stresses compensate for the tensile stresses and result in nonfailure loaded stress states.

ACKNOWLEDGMENTS

This study was partly supported by the Association of American Railroads and the Federal Railroad Administration, U.S. Department of Transportation.

REFERENCES

1. S.D. Tayabji and M.R. Thompson. Finite Element Analysis of a Railway Track Support System. Report FRA-OR&D-76-257. Federal Railroad Administration, U.S. Department of Transportation, May 1976.
2. H.E. Stewart and E.T. Selig. Predicted and Measured Resilient Response of Track. Journal of the Geotechnical Engineering Division, ASCE, Vol. 108, No. GT11, Nov. 1982, pp. 1423-1442.
3. D.R. Luhr and B.F. McCullough. Structural Analysis of AASHO Road Test Flexible Pavements for Performance Evaluation. In Transportation Research Record 888, TRB, National Research Council, Washington, D.C., 1982, pp. 63-69.
4. L. Raad and J.L. Figueroa. Load Response of Transportation Support Systems. Journal of the Transportation Engineering Division, ASCE, Vol. 106, No. TE1, Jan. 1980, pp. 111-128.
5. G.M. Norman and E.T. Selig. Ballast Performance Evaluation with Box Tests. AREA Bulletin 692, Vol. 84, May 1983, pp. 207-239.
6. J.E.D. Alva-Hurtado. A Methodology to Predict the Elastic and Inelastic Behavior of Railroad Ballast. Ph.D. dissertation, Report OUR80-245D. Department of Civil Engineering, University of Massachusetts at Amherst, May 1980.
7. H.E. Stewart. The Prediction of Track Performance Under Dynamic Traffic Loading. Ph.D. dissertation, Report FRA82-292D. Department of Civil Engineering, University of Massachusetts at Amherst, May 1982.
8. M.J. Shenton. Ballast Deformation and Track Deterioration. Proc., Track Technology for the Next Decade, Institute of Civil Engineers, University of Nottingham, England, July 1984, pp. 175-187.

Publication of this paper sponsored by Committee on Mechanics of Earth Masses and Layered Systems.

Measurement and Prediction of Vertical Track Modulus

HARRY E. STEWART

ABSTRACT

Field measurements of vertical deflections and track modulus under static loading conditions were obtained at four revenue service track locations. The track sections contained both concrete and wood ties. The measurements were made before a scheduled track maintenance operation and were repeated after the surfacing to determine the effects of maintenance on the vertical track response. Differences between the pre- and postmaintenance results were found and are discussed in terms of physical state of the ballast and the characteristics of the layered track systems. The resilient foundation properties of the field sites were obtained from both field and laboratory measurements. Predictions of vertical track response at the sites were then made using a three-dimensional, nonlinear, elastic, multilayer track analysis program. The predicted values of vertical track response were in general agreement with the measured values, although some differences were evident. The major variables affecting track modulus are identified and conclusions are presented on the usefulness of vertical track modulus as a measure of track performance.

The supporting capacity of conventional track is frequently characterized by the track modulus. An understanding of the factors influencing track modulus and of the effects of maintenance on the track support values is important. This is particularly evident when track modulus values are used for design purposes or in assessing track performance.

The results of field measurements of vertical track response, under static loading conditions, from four revenue service track locations are presented. The measurements were made before a scheduled track maintenance operation and were repeated after the surfacing. In addition, field and laboratory measurements of the resilient foundation properties were made. These properties were used to predict the track responses at each of the sites so that a further understanding of the factors influencing vertical track response could be developed by comparing measured and predicted track moduli.

DESCRIPTION OF SITES

Four revenue service track locations were selected as test areas for this project. The revenue service sites included three locations that contained concrete cross ties and a control section with wood cross ties. The wood tie control section and one concrete tie section are located in Leeds near Streator, Illinois, in the north-central section of the state. The remaining two concrete tie test sections are located at Aberdeen, Maryland, and Lorraine, Virginia. A detailed description of each of these four sites is given elsewhere (1).

The wood tie test section at Leeds is an 800-ft-long portion of tangent track owned by the Atchison, Topeka, and Santa Fe (ATSF) Railroad. It is built on a fill embankment approximately 12 ft high. The ballast in this section is slag, and the ties are hardwood at 19.5-in. nominal center-to-center spacing.

The Leeds concrete tie test section is contiguous to the wood tie section on the same track. This concrete tie section contains granite ballast, and both RT-7S and Costain Conforce CC244C ties at 24-in. center-to-center spacing. The total test section length is 800 ft, but the tests and measurements were confined to the track section having the Costain ties. Pandrol spring-clip fasteners are used on the Costain-type ties.

The Lorraine, Virginia, concrete tie test installation is owned by the Chessie system and is located in the western Richmond suburb of Lorraine, on the north bank floodplain of the James River. The test section is on a single main-line track built on an embankment about 7 ft high on the south side. This Lorraine concrete tie test section contains both CC224 ties and RT-7S ties. The test section is in the middle of a 3-degree curve, with a 3-in. superelevation on the outside rail. The ballast is predominantly gneiss and limestone. The ties are located at 25-in. center-to-center spacings.

The Aberdeen, Maryland, site is on one of three parallel main-line electrified tracks, owned by Consolidated Rail Corporation (Conrail), that carry traffic between Baltimore and New York. The ballast in the test section is a traprock. The track is tangent with RT7-SS2 concrete cross ties at 24-in. center-to-center spacings.

TRACK MODULUS FORMULATION

The use of track modulus for assessing track performance is common in the railroad industry. The theoretical formulation of track modulus is based on the assumption that the rail acts like a beam continuously supported on an elastic foundation. Track modulus (u) is defined as the supporting force per unit length of rail per unit deflection in the track system. A diagram of the assumed conditions for the formulation of track modulus is shown in Figure 1.

The differential equation describing the deflection, due to an applied vertical load, of a uniformly supported rail on a linear elastic foundation is given by

$$EI(d^4\delta/dx^4) = q = -u\delta \quad (1)$$

where

EI = rail bending stiffness (units = FL^2);
δ = vertical rail deflection (units = L);

x = horizontal distance along the rail, measured from the applied load point (units = L);
u = track modulus (units = F/L/L); and
q = vertical foundation supporting force (units = F/L).

The solution to Equation 1 is given by

$$\delta = [(\beta P/2u)e]^{-\beta x}(\cos \beta x + \sin \beta x) \quad (2)$$

where P is the applied load and

$$\beta = (u/4EI)^{1/4} \qquad (\text{units} = 1/L) \quad (3)$$

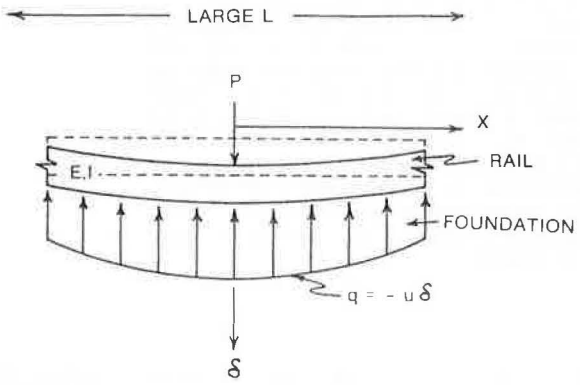

FIGURE 1 Assumed conditions for beam theory formulation of track modulus.

The maximum rail deflection occurs at x = 0, and is given by

$$\delta_{x=0} = \beta P/2u \quad (4)$$

The equation for maximum rail deflection can be rearranged by substituting β from Equation 1 and solving for u. The resulting equation for track modulus is

$$u = 1/4[(P/\delta)^4 \cdot 1/EI]^{1/3} \quad (5)$$

An important difference between the actual track support and the idealized formulation of a rail on an elastic support is that the rail load is actually applied to the foundation through discrete supports, which are the ties, not through support distributed along the track foundation. Another difference, for concrete tie track systems, is the inclusion of flexible tie pads between the rails and the tie rail seats. Even though these differences exist between the actual track structure and the theoretical formulation, the track modulus has historically been used as a measure of track quality. Further details on the historical development and interpretation of track modulus can be found elsewhere (2,3).

SELECTION OF PARAMETERS FOR PREDICTIONS

The GEOTRACK model (4,5) was used to determine track deflections for predicting values of track modulus for the revenue field sites. To do this, the track structural properties and foundation characteristics of each site had to be chosen. Table 1 gives the structural properties representing each of the sites.

The subgrade layer properties used for the GEOTRACK analyses were chosen on the basis of the results shown in Figures 2 and 3. The subgrade values shown in Figures 2 and 3 were derived from repeated load triaxial tests (6) and additional correlations made between cone and standard penetration data (7). Layer divisions for the subgrades were made where there appeared to be significant changes in the measured resilient properties. The average resilient modulus for each layer was used as the representative value for the layer. The moduli for the subgrade layers were held constant because stress-state-dependent relationships were not available for the subgrade.

A shear stress-resilient strain formulation (8) was used to characterize the stress-dependent ballast properties for these sites. The moduli (E_r) of the ballast from the final iteration of the

TABLE 1 Track Structural Properties for Field Sites

Parameter	Leeds		Aberdeen	Lorraine
	Wood	Concrete		
Tie type	Hardwood	CC244C	RT7-SS2	CC244
Tie spacing (in.)	19.5	24.0	24.0	25.0
Tie length (in.)	102	102	102	102
Tie bottom width (in.)	9.00	10.75	10.75	10.75
Tie bending stiffness [EI(lb/in.^{2} x 10^6)]	386	1740	1740	1740
Rail section	136RE	136RE	140RE	122RE
Rail bending stiffness [EI(lb/in.^{2} x 10^6)]	2742.6	2742.6	2797.5	2138.6
Rail fastener type	Cut spikes	Pandrol	Pandrol	Pandrol
Rail fastener or pad stiffness (lb/in.^{2} x 10^6)	6	4	4	4

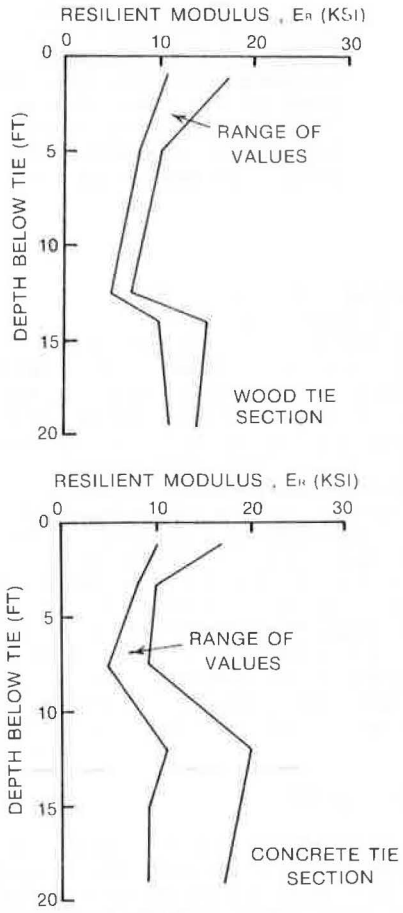

FIGURE 2 Resilient modulus versus depth for Leeds wood and concrete tie sections.

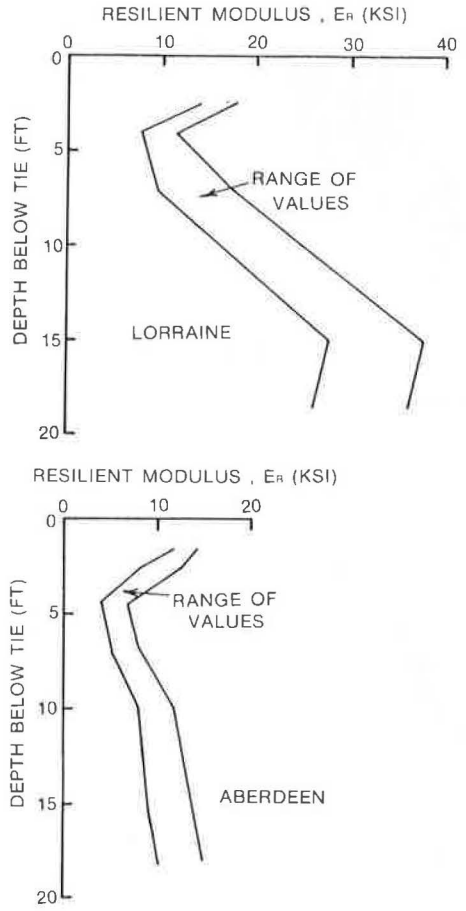

FIGURE 3 Resilient modulus versus depth for Lorraine and Aberdeen.

GEOTRACK program for the track modulus predictions are given in Table 2. The dependency of the ballast resilient modulus (E_r) on stress state is evident from the change in modulus with wheel load.

COMPARISON WITH FIELD MEASUREMENTS

Measurements of track vertical load-deflection response were made at each of the revenue field sites by Battelle-Columbus Laboratories (BCL). For the test, a point load of known magnitude was simultaneously applied to both rails using vertical hydraulic jacks reacting against a loaded freight car. Rail deflections were measured by sighting a steel scale with a surveyor's theodolite. The scale was attached to the rail. Seven to ten measurements at random tie locations were made to assess the variability in the load-deformation responses within the track sections. These measurements were made both before and after the maintenance operations to determine what differences in track support resulted from the surfacing operation.

TABLE 2 Ballast Moduli Determined for Track Modulus Predictions

Site	Thickness of Ballast Layer (in.)	Resilient Modulus (E_r) in psi	
		Wheel Load = 6 Kips	Wheel Load = 30 Kips
Leeds			
Wood	9	5,300	25,500
Concrete	7	10,000	35,000
	7	7,800	15,500
Lorraine	14	8,700	29,000
	14	6,500	17,200
Aberdeen	10	10,800	34,500
	10	9,500	15,000

The measured averages and standard deviations for the pre- and postmaintenance load-deflection curves are shown in Figures 4-7 for the Leeds wood, Leeds concrete, Lorraine, and Aberdeen sites, respectively. The premaintenance curve for the Leeds concrete section (Figure 5) was based on measurements taken after about 1 month of traffic had passed instead of immediately before maintenance because a surfacing operation had taken place just before the initial site visit. Although both pre- and postmaintenance values for the Aberdeen site were recorded, only the postmaintenance results were reported by BCL.

A small amount of slack may have been present in the track structure as indicated by an initial break in the curves as shown in Figures 4-7. This initial slack was assumed to have been eliminated after about a 6-kip load was applied. To remove this effect, the track modulus values were calculated for the 6- to 30-kip load range.

The variabilities of the track modulus measurements were estimated using the mean track deflections from the averaged load-deflection curves, and the deflections at ±1 standard deviation at the 6- and 30-kip load levels shown in Figures 4-7. However, the actual variabilities of the track modulus measurements were probably greater than the estimates determined in this manner. For the purposes of this paper, the standard deviations of the track modulus values will refer to the limits calculated on the basis of the standard deviations of the rail deflections. It must be noted that these are not the true standard deviations, and these values of standard deviation are not symmetrical about the mean values.

To determine track modulus with GEOTRACK, deflections were calculated for the single-axle solution with loads of 6 and 30 kips. The difference in loads and the difference in deflections were substituted into Equation 5 to obtain track modulus.

The measured values of track modulus and the estimated standard deviations for all of the revenue field sites are given in Tables 3 and 4 and shown in Figure 8, along with the predicted values based on the GEOTRACK analyses. Several items on Figure 8 deserve attention. First, there were no significant changes in the track modulus values as a result of the surfacing operations. However, the premaintenance values did appear to be less variable than the postmaintenance values. This variation is also apparent in the average load-deflection curves (Figures 4-7) where the scatter about the mean is visibly larger for the postmaintenance values. That the average measured values were greater in the Leeds wood and Lorraine sections after maintenance is probably not statistically significant because the estimated standard deviations all overlap.

Another observation from Figure 8 is that there did not appear to be a correlation between height of raise and postmaintenance track modulus. Raises of 1.5 to 2 in. were given to the Leeds and Lorraine sections and only about 0.1 in. to the Aberdeen section. In spite of this, the pre- and postmaintenance values for any one test section were approximately equal, and the Aberdeen value was between the Lorraine and Leeds values.

An explanation of the increased variability of the postmaintenance modulus values compared to the premaintenance values could be that the surfacing decreased the uniformity of track support conditions

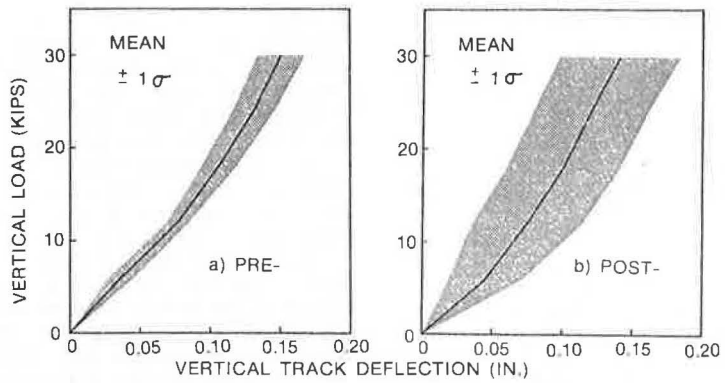

FIGURE 4 Track load-deflection curves for Leeds wood.

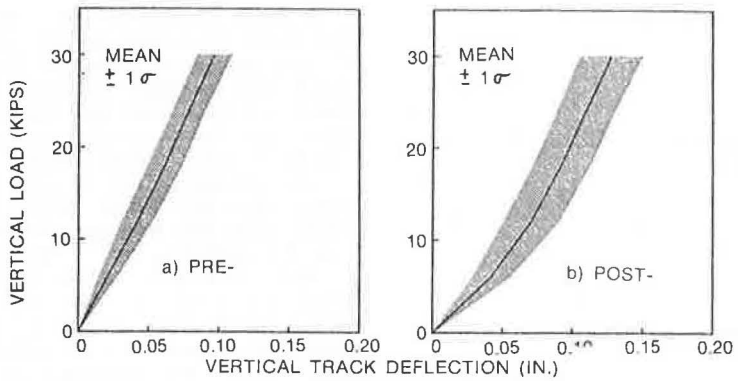

FIGURE 5 Track load-deflection curves for Leeds concrete.

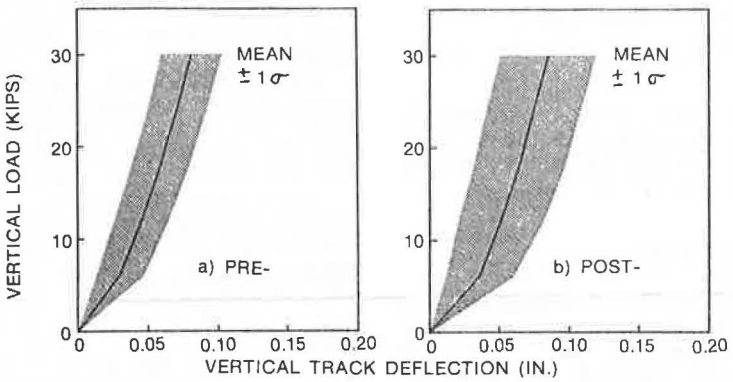

FIGURE 6 Track load-deflection curves for Lorraine.

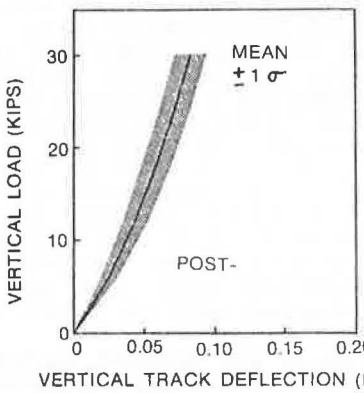

FIGURE 7 Track load-deflection curve for Aberdeen.

between the locations. One purpose of track maintenance is to improve the overall track surface by smoothing out longitudinal differential track deformations. Varying amounts of raise must be applied beneath the ties to achieve a uniform surface. Variations in the actual raises applied beneath the individual ties could cause local differences in the amount of ballast disturbance, hence variations in physical state of the ballast from one tie to another.

Part of the difference in absolute magnitude of the average field track modulus measurements can be explained in terms of the differences in the track substructures. A parametric study using the GEOTRACK model (5) indicated that track modulus increased as ballast depth increased. The Leeds wood section had only about 9 in. of ballast beneath the tie, whereas the Leeds concrete section contained about 14 in. The Aberdeen site had 20 in. of ballast, and the

TABLE 3 Measured Averages and Estimated Standard Deviations for Revenue Field Sites

	Track Modulus for 6- to 30-Kips Load Range					
	Premaintenance			Postmaintenance		
Field Site	$-\sigma$	Average	$+\sigma$	$-\sigma$	Average	$+\sigma$
Leeds						
Wood	2.1	2.2	2.5	2.3	2.9	3.7
Concrete	3.5	3.9	4.3	2.9	3.3	3.8
Lorraine	6.4	7.0	7.9	6.0	7.6	10.6
Aberdeen				4.9	5.5	6.5

TABLE 4 Predicted Values for Revenue Field Sites

Field Site	Track Modulus (u)
Leeds	
Wood	5.2
Concrete	5.5
Lorraine	8.9
Aberdeen	5.6

Note: Units of u = kips/in.^{2}

ballast depth at Lorraine was estimated to be 28 in. below the tie. Although the influence of site location cannot be separated from the results, this trend of increasing track modulus with increasing ballast depth for the field sites was confirmed by the field measurements as shown in Figure 9.

SUBGRADE EFFECTS

The track modulus is also influenced by the subgrade characteristics. The GEOTRACK model indicates that the compression of the ballast layer accounts for about 10 to 20 percent of the total vertical deflection of the track structure. The remainder of the total deflection is due to the compression of the subgrade materials. Furthermore, 25 to 40 percent of the subgrade deformation indicated by GEOTRACK occurs below a depth of about 10 ft, even though the stresses below this depth are low (5).

The Lorraine test section was found to have the greatest depth of ballast-type material and the stiffest subgrade. Correspondingly, the Lorraine section had the highest values of measured and predicted track modulus. As can be seen in Figure 9, the predicted value of track modulus was higher than the average measured values but well within the estimated standard deviations.

The Aberdeen postmaintenance value was lower than the Lorraine value because of a combination of reduced ballast thickness and lower overall subgrade stiffness. The predicted track modulus for the Aberdeen site was in close agreement with the measured values.

For the Leeds sites, the predicted values of track modulus were higher than the field values. However, the field values appear to be unusually low. The lower ballast thickness at the Leeds sites can account for some of the differences between the Leeds sites and the other two field sites, but these differences in ballast layer thicknesses were not enough to cause the low values measured at both Leeds sites.

Given the similarity between the subgrade stiffnesses at the Leeds sites and the Aberdeen site, closer agreement between the field measurements from these sites would be expected. It is possible that the embankment in the Leeds wood section resulted in reduced subgrade confinement and hence increased vertical deflections. This would result in lower values of track modulus. However, the concrete section at Leeds, which was built at grade, had comparably low track modulus values. Thus the embankment condition must not have been a major factor.

It would be necessary to reduce the subgrade stiffnesses that were used in the GEOTRACK analyses by at least 50 percent to match the field track modulus measurements at the Leeds test sections. However, no rational justification for making adjustments of these magnitudes could be found. If the soil moduli were overestimated at the Leeds sites, a similar systematic error should have occurred with the Lorraine and Aberdeen subgrades. Because the predicted Lorraine and Aberdeen values were in good agreement with the measurements, a similar adjustment to the subgrade moduli at those sites would shift the predicted values away from the measurements.

SUPPORT CONDITIONS AND MAINTENANCE EFFECTS

The measured and predicted values of track modulus are dependent on several factors, one of which is the support condition of the tie. Support conditions are a function of track settlement and maintenance

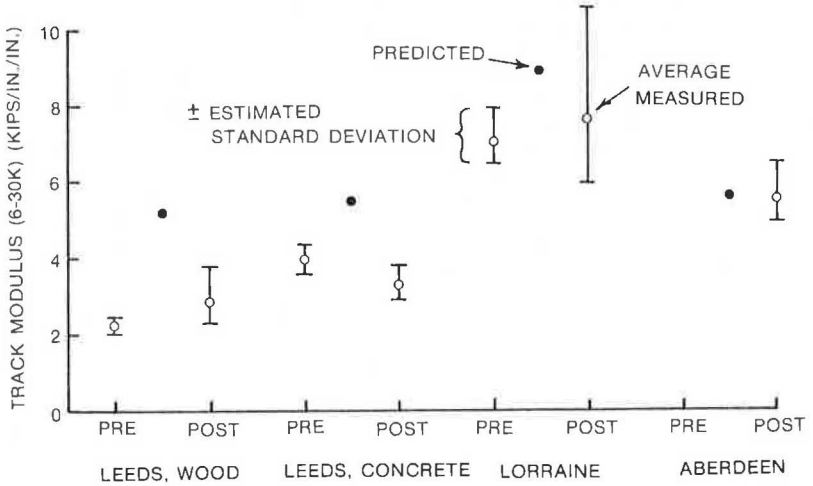

FIGURE 8 Measured and predicted track moduli for field sites, 6- to 30-kip load range.

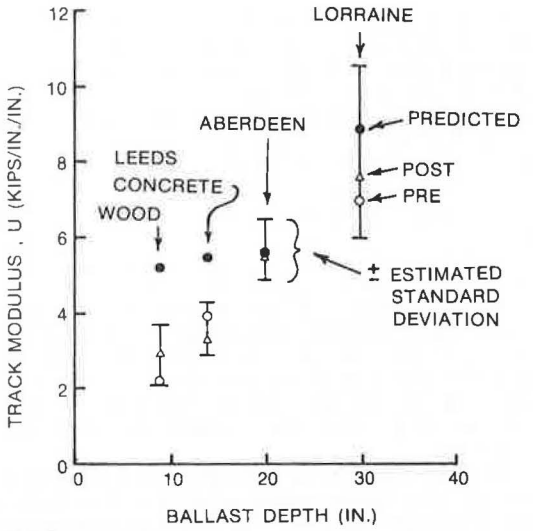

FIGURE 9 Ballast depth versus track modulus for field sites.

effects. The support conditions would affect concrete and wood ties in different fashions.

The GEOTRACK model uses uniform properties throughout each layer, including under all ties. Field plate load tests (9) showed that the ballast stiffness was not uniform under the ties: it was greater near the rail seat areas than under the tie centers. Furthermore, after maintenance the physical state of the ballast was more uniform than before maintenance. However, even uniform physical state or modulus does not result in uniform support conditions along the tie.

After a maintenance operation in which a high raise was given to the track, the physical properties of the ballast would be more uniform. However, the tamping and raise during the maintenance is done only near the rail seats, which would cause a gap near the center of the ties. This causes the actual load-bearing areas to be near the rail seats because of the lack of contact near the tie centers. This increased load bearing near the rail seats would cause higher rail deflections directly under the applied load than would result from a continuously supported condition. The GEOTRACK model uses continuous contact between the tie directly under the applied vertical load and the ballast surface, leading to a lower rail deflection and a higher track modulus than measured in the field after maintenance.

As traffic accumulates over the track, the ballast beneath the rail seats is recompacted and becomes stiffer, but the tie contact becomes continuous. The more uniform support across the tie leads to a lower rail deflection and hence a higher track modulus. In the case of a small maintenance raise, the initial physical state of the ballast may be less uniform under the tie than after a large raise. However, the contact may be more continuous. This would result in a higher track modulus after a small raise than after a large raise, or at least not much change in the pre- and postmaintenance values.

In the case of centerbound track, for example, a greater portion of the rail loads would be carried by the central portion of the ties. In this situation, as the applied loads increased, the wood ties would begin to conform more to the ballast surface and this would probably lead to a more uniformly distributed surface load than the concrete ties because the bending stiffness of concrete ties is about 4.5 to 6 times greater than that of wood ties. Load transfer to the tie center would cause lower rail deflections under a particular applied load and, therefore, comparatively higher values of track modulus.

The interactions among variable physical states of ballast, tie support conditions, and structural factors such as tie stiffness and rail size make generalizations about track modulus uncertain. This is particularly true because the degree and type of maintenance disturbance and traffic history of a site can change the physical state of ballast in varying amounts. The scatter of the field measurements was such that there were no clear trends distinguishing the premaintenance track modulus values from the postmaintenance values. The predictions of track modulus using the GEOTRACK program are somewhat limited by the uniform layer property, the full contact representations, and the inability to represent the maintenance factors for the field sites. For these reasons variations between the measured and the predicted track modulus values for the sites can be expected because of the variations in ballast properties and support conditions that were affected by the maintenance operations.

The possible centerbinding and uniformity of support conditions beneath the tie bottom may not, however, be a significant factor contributing to the track modulus values, although the effects are physically rational. Differences between the bending stiffnesses of wood and concrete ties would also not result in large differences in track moduli. Because only 10 to 20 percent of the total track deformation is due to ballast compression, the subgrade deflections appear to be much more important. It has been shown that variations in tie stiffnesses (8) do not have a major effect on the vertical subgrade stresses beneath the rail seats. Thus the subgrade contribution to track modulus should be about the same for wood and concrete ties. Also, dynamic measurements of resilient subgrade deflection (5) showed no significant difference between the deflections in wood and in concrete sections. This would indicate that, although the stress distributions and deformations in the ballast layer were affected by tie stiffness and possibly centerbinding, the subgrade responses were controlled mainly by the subgrade properties, with some effects of ballast layer thickness.

SUMMARY

The main purpose of this paper was to make available the experimental results of maintenance effects on track modulus and, by comparing the field measurements with predictions of track modulus for the revenue sites, to develop a further understanding of the factors affecting vertical track response.

Several observations were made on the basis of the results presented. The field measurements did not indicate that significant changes in the magnitude of track modulus could be attributed to maintenance. Also, the longitudinal variability of the track support was not improved as a result of the surfacing, as shown by the increased variability of the postmaintenance load-deflection curves.

The uniformity of ballast properties under individual ties was improved by the raise and tamping operations, as was indicated by the plate load tests (9). The uniformity of contact between the ties and ballast surface, however, may not be improved. Uniformity of ballast properties and contact should lead to a lower track modulus, but because the ballast is always relatively stiff compared to the subgrade and the relative contribution of the ballast deformation to the overall track deflection is small, maintenance does not have a great effect on track modulus.

The major factors contributing to the magnitude of vertical track modulus were ballast depth and subgrade stiffness. Variations due to tie spacing or tie stiffness were not significant factors. Predictions of track vertical deflections made with GEOTRACK were generally in reasonable agreement with the field measurements. The use of track modulus alone for assessment of the quality of track may not be too helpful, especially if the assessment is based only on the average magnitude of track modulus. The variability of track modulus between tie locations is a direct measure of the longitudinal uniformity of the track, which is extremely important.

ACKNOWLEDGMENTS

This study was partly sponsored by the Federal Railroad Administration, U.S. Department of Transportation, under the Improved Track Structures Research Program and Office of Rail Safety Research. This work was conducted through the University of Massachusetts under the direction of E.T. Selig, and through Battelle-Columbus Laboratories. The author appreciates the assistance given by Howard G. Moody of the FRA, who served as program manager for portions of this study, and the contributions of Harold D. Harrison, who served as project engineer for BCL.

REFERENCES

1. H.D. Harrison, F.E. Dean, E.T. Selig, and H.E. Stewart. Correlation of Concrete Tie Track Performance in Revenue Service and at the Facility for Accelerated Service Testing. Vol. 1 of Final Report FRA/ORD-82/44.1. Office of Research and Development, FRA, U.S. Department of Transportation, Sept. 1982.
2. ASCE-American Railway Engineering Association Special Committee on Stresses in Railroad Track. First and Second Progress Reports. AREA Bulletin, Vol. 19, 1918, and Vol. 20, 1920.
3. A.M. Zarembski and J. Choros. On the Measurement and Calculation of Vertical Track Modulus. AREA Bulletin 675, Nov.-Dec. 1979, pp. 156-173.
4. C.S. Chang, C.W. Adegoke, and E.T. Selig. The GEOTRACK Model for Railroad Track Performance. Journal of the Geotechnical Engineering Division, ASCE, Vol. 106, No. GT11, Nov. 1980, pp. 1201-1218.
5. H.E. Stewart and E.T. Selig. Predicted and Measured Resilient Response of Track. Journal of the Geotechnical Engineering Division, ASCE, Vol. 108, No. GT11, Nov. 1982, pp. 1423-1442.
6. R.F. Bukoski. Railroad Subgrade Soil Characterization for Track Performance. M.S. project report, Report FRA81-263P. University of Massachusetts at Amherst, 1981.
7. R.F. Bukoski and E.T. Selig. Investigation of Railroad Subgrade Properties. Proc., Cone Penetration--Testing and Experience, ASCE, St. Louis, Mo., Oct. 1981.
8. H.E. Stewart. The Prediction of Track Performance Under Dynamic Traffic Loading. Ph.D. dissertation, Report FRA82-292D. University of Massachusetts at Amherst, 1982.
9. H.E. Stewart, E.T. Selig, and D.R. McMahon. Maintenance Effects on Ballast Physical State. AREA Bulletin 693, Vol. 84, Oct. 1983, pp. 367-388.

Publication of this paper sponsored by Committee on Mechanics of Earth Masses and Layered Systems.

Behavior of Stabilized Layers Under Repeated Loads

LUTFI RAAD

ABSTRACT

An improved method of analysis for pavements with stabilized layers has been proposed. The method incorporates the bimodular properties (i.e., tensile modulus different than compressive modulus) of the stabilized layers and the stress-dependent behavior of granular and subgrade soils. The proposed method could be used to predict stresses, resilient strains, and deformations using a finite element representation of pavement structures. The proposed method is used to study the behavior of stabilized layers under repeated loads. Results of a limited number of split tension and flexure tests conducted on a cement-treated silty clay are presented to illustrate the bimodular behavior of the material and the influence of testing procedure and computation method on modulus values. On the basis of laboratory results it is proposed to characterize the stabilized layer in terms of its split tensile modulus, bimodular ratio, and split tensile strength. This method of characterization is incorporated in the analysis of the behavior of stabilized layers in pavements. Specifically, the influence of material characteristics on response prediction, and on fracture of stabilized layers under repeated loads, has been investigated.

Cement- and lime-stabilized layers are used in pavement structures to enhance their load-carrying capacity and improve their performance. Although shrinkage and fatigue are two common types of failure of stabilized layers, pumping and loss of foundation support are other modes of failure that could result in excessive stresses and deflections in the stabilized layer and thereby increase its rate of deterioration. Performance prediction of stabilized layers under repeated traffic loads is a soil-structure interaction problem in which the interaction between traffic loads, stabilized layer, and other soil layers in the pavement structure should be considered.

An improved method of analysis for determining the response of pavements with stabilized layers under repeated loads is presented. The proposed method uses the finite element technique to predict the stresses, strains, and deflections in the pavement section. The method incorporates the load-deformation characteristics of stabilized soils in tension and compression, the nonlinear stress-deformation behavior of granular and subgrade soils, and a failure criterion for these soils based on the Mohr-Coulomb theory. The proposed method is used to study the behavior of pavements with stabilized layers under repeated loads. Specifically, the analyses include the following:

1. The significance of materials characterization in the response of stabilized layers and
2. The fracture of stabilized layers overlying soft and stiff subgrades.

PROPOSED METHOD

The finite element method is used to determine the stresses and resilient deformations in a given pavement structure assuming axisymmetric, plane strain, or plane stress conditions. Stabilized materials in the pavement section are assumed to have bimodular properties (i.e., modulus in tension different than modulus in compression). Granular and subgrade soils are assumed to have stress-dependent moduli. For granular soils (1), the resilient modulus (M_R) is expressed as

$$M_R = K\theta^n \quad (1)$$

where

$\theta = \sigma_1 + \sigma_2 + \sigma_3$,
σ_1, σ_2, and σ_3 = principal stresses, and
K and n = material constants.

For fine-grained soils, a typical representation of resilient modulus (M_R) as a function of repeated deviator stresses ($\sigma_1 - \sigma_3$) has been proposed by Figueroa (2) and is shown in Figure 1. Similar functions proposed by others (3,4) could be incorporated in the proposed method.

The nonlinear properties of the granular and subgrade layers and the bimodular properties of the stabilized layers are included by means of a successive iteration technique. On the first iteration the modulus in tension (E_t) of the stabilized layer is set equal to the modulus in compression (E_c), whereas the moduli of the subgrade and granular layers are set equal to an assumed initial value. On successive iterations the modulus in tension is substituted in directions of principal tension for elements in the stabilized layer. Elements in the subgrade and granular layers are assigned values depending on the stress state at the end of the previous iterative step. The principal stresses in the granular and subgrade layers are modified at the end of each iteration so that they do not exceed the strength of the material as defined by the Mohr-Coulomb envelope. The procedure for stress modification has been developed by Raad and Figueroa and is presented elsewhere (5). A reasonable degree of convergence is attained in three or four iterations; and constitutive relations, equilibrium equations, and kinematic and boundary conditions are essentially satisfied.

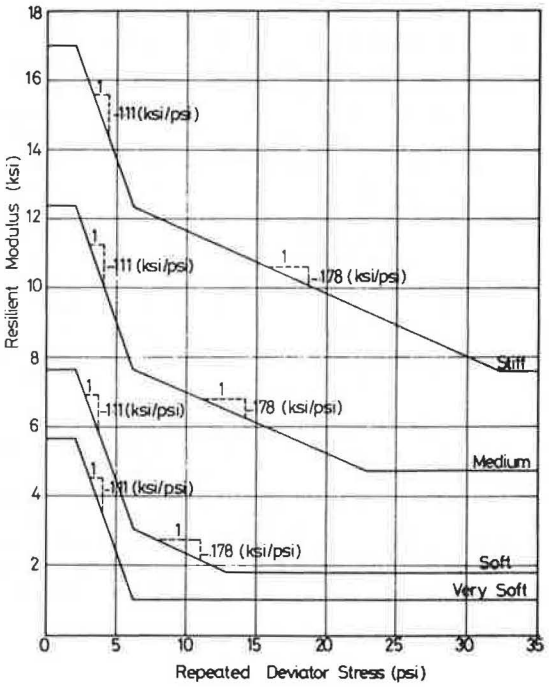

FIGURE 1 Resilient modulus of subgrade soils.

CHARACTERIZATION OF STABILIZED LAYERS

The use of advanced analytical techniques to predict the response of stabilized layers requires proper material characterization in order to obtain meaningful results. Stabilized layers are generally characterized using the flexure and split tension tests for the determination of elastic moduli and tensile strength. Analyses (6,7) indicate that elastic moduli and strength values could be different for the same material as a result of the bimodular behavior of stabilized soil as shown in Table 1. The same method of analysis would therefore yield different results depending on the input properties used for the stabilized layers. Moreover, the determination of the thickness of a stabilized layer required to carry a given traffic depends on the tensile strength used for the material if a stress criterion is chosen for design. In this case the tensile stress on the underside of the stabilized layer should be compared with the actual tensile strength of the material, which could be reasonably estimated from the split tension test according to Raad et al. (6).

TABLE 1 Correlation Between E_s/E_t and T_f/T_s as a Function of the Bimodular Ratio E_c/E_t

E_c/E_t	E_s/E_t	T_f/T_s
1.0	0.90	1.56
2.0	1.35	1.67
5.0	2.06	1.71
10.0	2.38	1.78

Note: E_s = split tensile modulus, T_s = split tensile strength, T_f = flexural strength, E_c = compressive modulus, and E_t = tensile modulus.

A limited number of flexure and split tension tests were conducted on a cement-treated silty clay (CL, PI = 12, LL = 29) to study the difference between flexural and split tensile moduli and to investigate the bimodular behavior of the material. The cement content used was 11 percent. Cylindrical specimens 4 in. in diameter and 3 in. high and beam specimens 21 in. x 6 in. x 6 in. were prepared using a drop hammer compactor and modified AASHTO compaction energy. The specimens were wrapped in polyethylene sheets and cured in a humid room for 42 days at 73° F. The compaction characteristics of the material are shown in Figure 2. At the end of the curing period, 1-in.-long SR-4 strain gauges were glued to the top and bottom of the beam specimens in the middle one-third portion. Similar strain gauges were glued on both sides of the cylindrical specimens at the center to measure lateral tensile strains (Figure 3). In both the flexure and split tension tests the load was applied through a loading head at constant rate of displacement equal to 0.0120 in. per minute. The strain gauges were monitored continuously during loading. Vertical deflections at the center of beam specimens were also monitored using a 0.0001-in. dial gauge.

Flexural modulus values $\bar{E}_f$ and E_f based, respectively, on moment-curvature relations and deflection

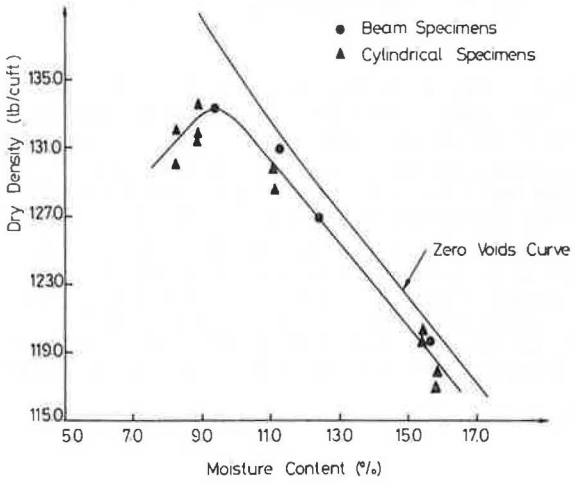

FIGURE 2 Compaction characteristics of cement-treated silty clay.

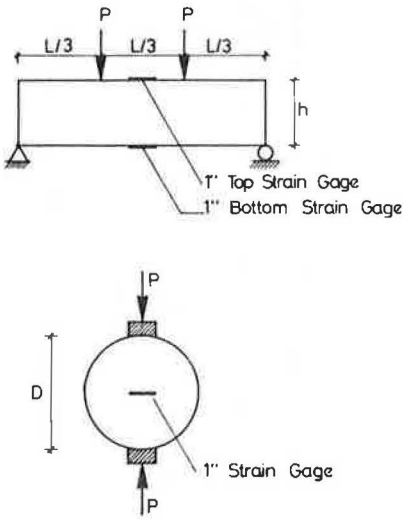

FIGURE 3 Representation of flexure and split tension tests.

at the center of the beam, were determined and compared with split tensile modulus (E_s). A summary of expressions for modulus values in the flexure and split tension tests is given in Table 2. The relationship for the split tensile modulus in terms of tensile strain (ϵ_t) at the center of the specimen has been derived using the finite element method of analysis, a Poisson's ratio equal to 0.20, and a bimodular representation of the stabilized material. The average error in this case does not exceed ± 9.0 percent for a bimodular ratio variation between 1 and 10.

TABLE 2 Expressions for Modulus Values Determined in the Flexure Test and Split Tension Test

Flexure Test	Split Tension Test
$E_f = (23/648)(PL^3/dI)$	$E_s = (P/t\Delta)(\nu + 0.2732)$
$E_f = (PL/3I)[h/(\epsilon_c + \epsilon_t)]$	$E_s = (1.65)(P/\pi Rt\epsilon_t)$

Note: P = applied load; L = length of beam specimen; d = deflection at center of beam specimen; I = moment of inertia of beam cross section; ϵ_c = compressive strain at top of beam specimen; ϵ_t = tensile strain at bottom of beam specimen or at center of cylindrical specimen; Δ = lateral deformation across diameter of cylindrical specimen; ν = Poisson's ratio; R,t = radius and thickness, respectively, of cylindrical specimens; and h = depth of beam specimen.

The variation of E_f, $\bar{E}_f$, and E_s with compaction moisture content is shown in Figure 4. Although the trend of variation with compaction moisture content is similar, values of E_f, $\bar{E}_f$, and E_s for specimens having the same dry density and compaction moisture content are different (Figure 5). Values of E_s are on the average 1.25 times greater than those of $\bar{E}_f$ but could be as much as 6 times greater than E_f.

Bimodular behavior was investigated by comparing the compressive strain (ϵ_c) and tensile strain (ϵ_t) at the top and bottom of beam specimens in the flexure test. The bimodular ratio is expressed as

$$E_c/E_t = (\epsilon_t/\epsilon_c)^2 \quad (2)$$

The bimodular ratio appears to reach a maximum value at optimum compaction moisture content (Figure 4d). Moreover, the bimodular ratio is stress dependent as shown in Figure 6. It attained values between 0.80 and 6.0. Similar observations concerning bimodular behavior of stabilized soils using flexure, direct tension, and direct compression tests show that stabilized soils exhibit bimodular ratios in the range of 1 to 10 (8,9).

Bimodular behavior could be incorporated in the analysis of pavements by using compressive and tensile moduli that correspond to the level of tensile and compressive stresses or strains in the stabilized layer. Modulus values corresponding to a stress level equal to 50 percent of the modulus of rupture in the flexure test could be used in this case.

Although the compressive modulus (E_c) and the tensile modulus (E_t) could be used to characterize a stabilized layer, an alternative approach would be to use the split tensile modulus (E_s) and the bimodular ratio E_c/E_t. If the values of E_s and E_c/E_t are known, the values of E_c and E_t are estimated from the relationship between E_c/E_t and E_s/E_t, shown in Table 1, and are then used in the analysis of the stabilized layer.

BEHAVIOR UNDER REPEATED LOADS

The behavior of pavements with stabilized layers under repeated loads has been investigated using the proposed method. Specifically, the influence of load-deformation characteristics on response and the fracture of stabilized layers under repeated loads have been studied. In all these cases the material properties used to characterize the stabilized layer include the elastic modulus (E_b), the bimodular ratio (E_c/E_t), and Poisson's ratio. E_b corresponds either to the split tensile modulus or to the flexural modulus derived from moment-curvature relations in the flexure beam test. An axisymmetric loading condition is assumed in the analyses.

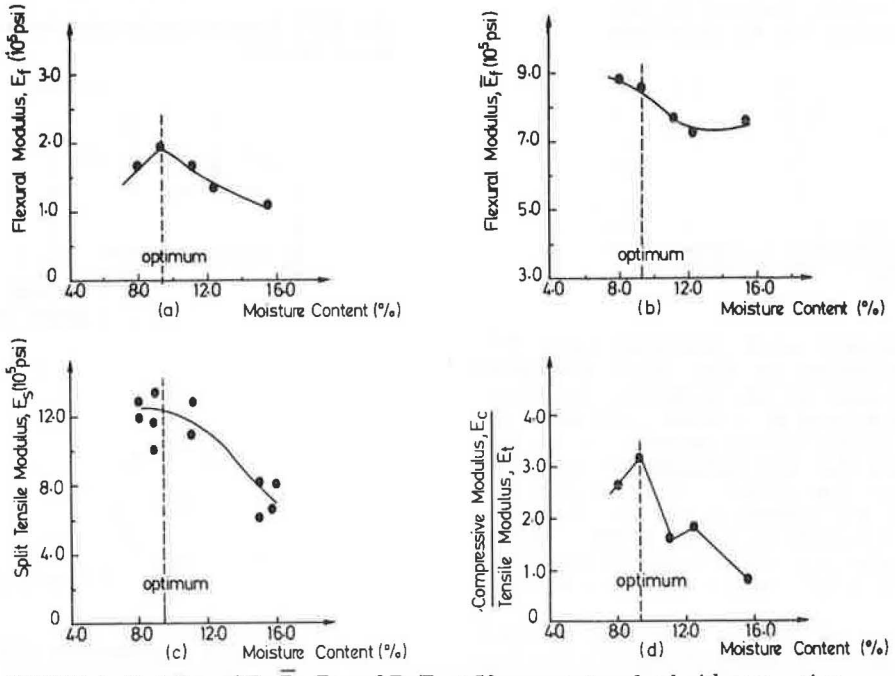

FIGURE 4 Variation of E_f, $\bar{E}_f$, E_s, and E_c/E_t at 50 percent stress level with compaction moisture content.

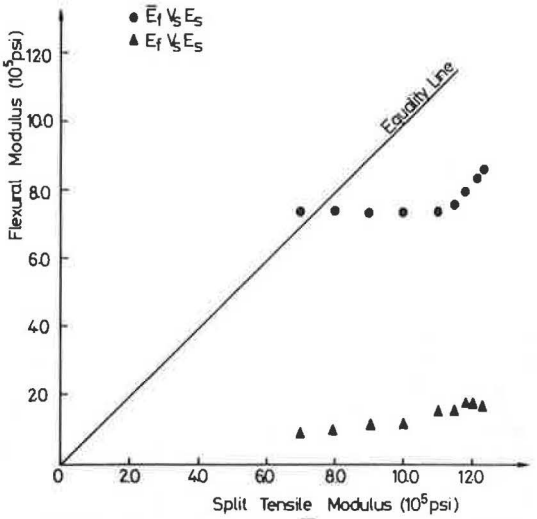

FIGURE 5 Comparison of E_f, $\bar{E}_f$, and E_s for cement-treated silty clay.

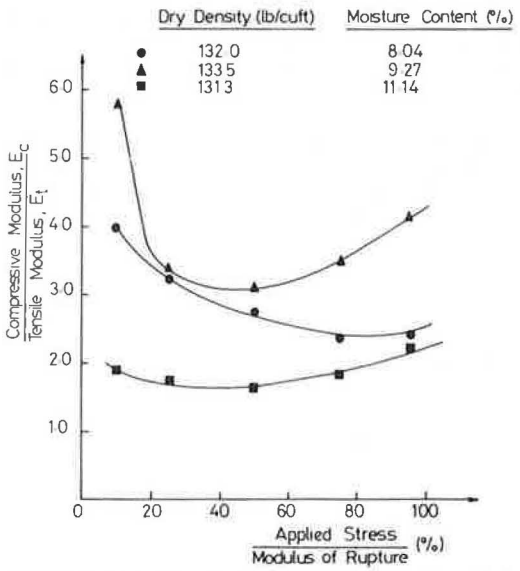

FIGURE 6 Variation of bimodular ratio with applied stress level.

Influence of Material Characteristics

The pavement section analyzed is shown in Figure 7. Two cases are considered (Table 3). In the first case the stabilized layer is assumed to be linearly elastic with a bimodular ratio equal to 1. No failure criterion is used for granular and subgrade soils. In the second case the stabilized layer is assumed to have the same elastic modulus as in Case 1, but a bimodular ratio equal to 10 and a Mohr-Coulomb failure criterion are used for the granular and subgrade layers.

Results of analysis indicate that an increase of bimodular ratio of from 1 to 10 would increase the tensile strains on the underside of the stabilized layer by 38 percent but would decrease the tensile stresses by 45 percent as shown in Figure 8. Moreover, the use of the Mohr-Coulomb failure model in the proposed approach would result in a "no tension" zone in the granular subbase. The lateral stresses predicted using the higher bimodular ratio and fail-

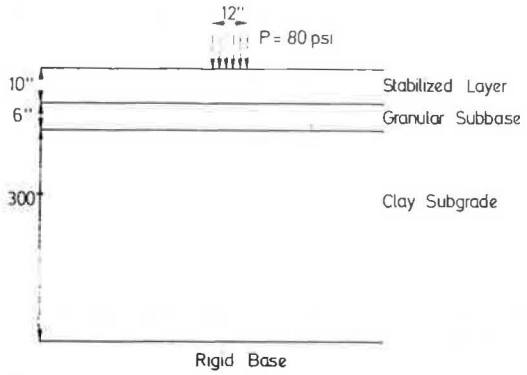

FIGURE 7 Pavement section analyzed for response prediction.

TABLE 3 Material Properties Used in Response Prediction Under Applied Load

Case	Stabilized Layer	Granular Subbase	Subgrade
1	E_b = 1.0 x 10^6 psi	K = 7000	
	E_c/E_t = 1	n = 0.35	Soft (Figure 1)
	ν = 0.20	ν = 0.35	ν = 0.47
2	E_b = 1.0 x 10^6 psi	K = 7000	Soft (Figure 1)
	E_c/E_t = 10	n = 0.35	ϕ = 0.0 degree
	ν = 0.20	ϕ = 32 degrees, C = 0.0	C = 7.0 psi
		ν = 0.35	ν = 0.47

Note: E_b = modulus of stabilized layer, E_c/E_t = bimodular ratio, ν = Poisson's ratio, C and ϕ are cohesion and angle of friction determined from Mohr-Coulomb envelope, K and n are defined in Equation 1.

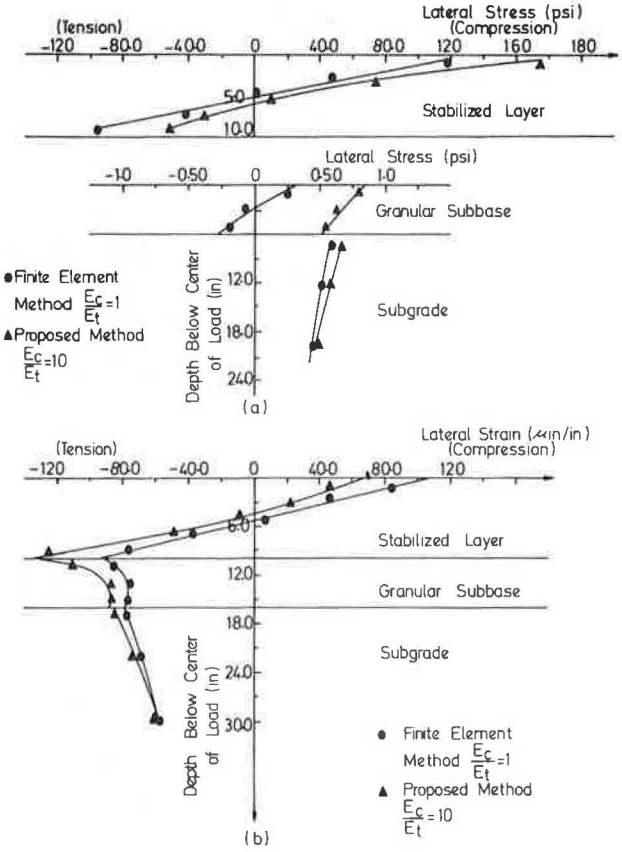

FIGURE 8 Influence of material characterization on response.

TABLE 4 Cases Studied in Fracture Analysis of Stabilized Layers

Case	Modulus of Stabilized Layer (E_b) in psi	Subgrade Stiffness	Bimodular Ratio (E_c/E_t)	Split Tensile Strength (T_s) in psi	Thickness of Stabilized Layer (h) in in.
1	3.0×10^6	Soft (Figure 1)	1 5 10	150 300	4 6 8 12 16
2	3.0×10^6	Stiff (Figure 1)	1 5 10	150 300	4 6 8 12 16
3	3.0×10^5	Soft (Figure 1)	1 5 10	50 100	4 6 8 12 16
4	3.0×10^5	Stiff (Figure 1)	1 5 10	50 100	4 6 8 12 16

ure criterion are higher but decrease with depth of the granular subbase, as shown in Figure 8.

Fracture Behavior of Stabilized Layers

The fracture behavior of two-layer systems consisting of a stabilized layer overlying a clay subgrade has been analyzed under an applied circular load that has a 12-in. diameter and a uniform surface pressure. Fracture behavior under long-term loading (i.e., 10^6 repetitions) and short-term loading (i.e., 1 repetition) has been considered. A mechanistic model for strength and fatigue based on the Griffith failure theory (10) has been used in the analysis.

For fracture behavior under long-term loading, the stress state in each element of the stabilized layer was determined and the number of repetitions required to crack the most critically stressed element was estimated. The fractured element was taken out of the system and a new stress field was determined. The number of additional repetitions required to crack a new most critically stressed element was estimated. This process was continued until the crack had propagated to the surface of the layer.

For fracture behavior under short-term loading, the load needed to crack the most critically stressed element was calculated. The fractured element was taken out and a new stress field was found. The additional load increment required to crack the next most critically stressed element was calculated. This was repeated until complete fracture of the stabilized layer had occurred.

For a given pavement system, the analysis provided a relationship between the thickness of the stabilized layer and the magnitude of load required to induce fracture. Table 4 gives a summary of the cases analyzed. In all these cases the subgrade was considered to be a layer 300 in. thick resting on a rigid base. The analyses performed lead to the following conclusions:

1. The load required to fracture the stabilized layer (i.e., ultimate load capacity) under long-term loading (10^6 repetitions) and short-term loading (1 repetition) increases with increase in layer stiffness, layer thickness, and subgrade stiffness

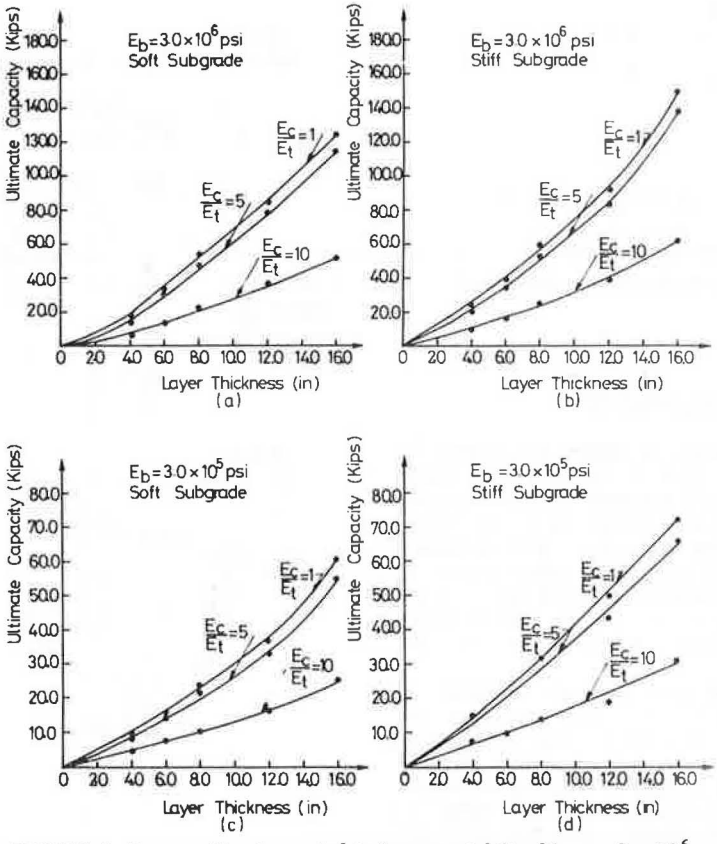

FIGURE 9 Repeated load requried to fracture stabilized layer after 10^6 repetitions.

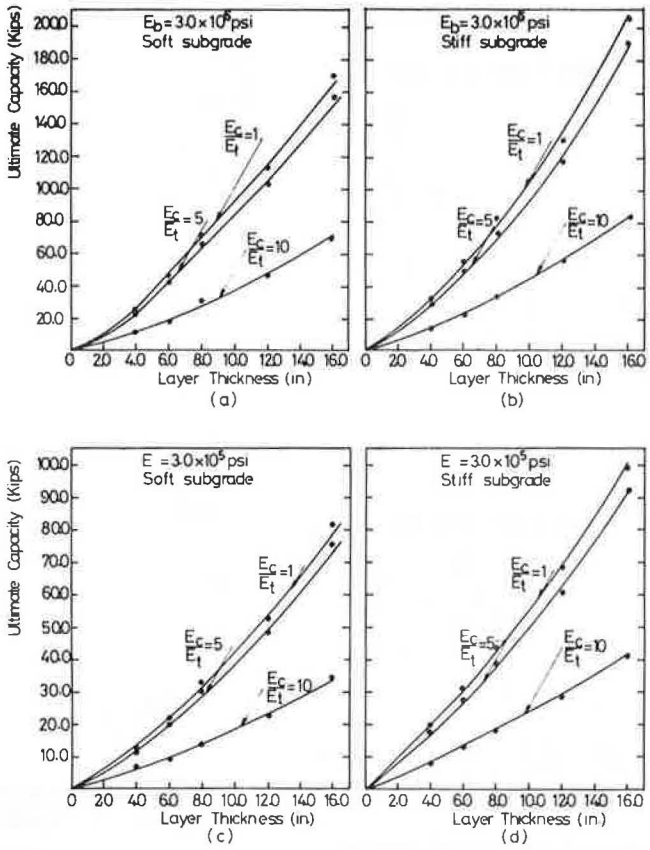

FIGURE 10 Ultimate load required to fracture stabilized layer after 1 repetition.

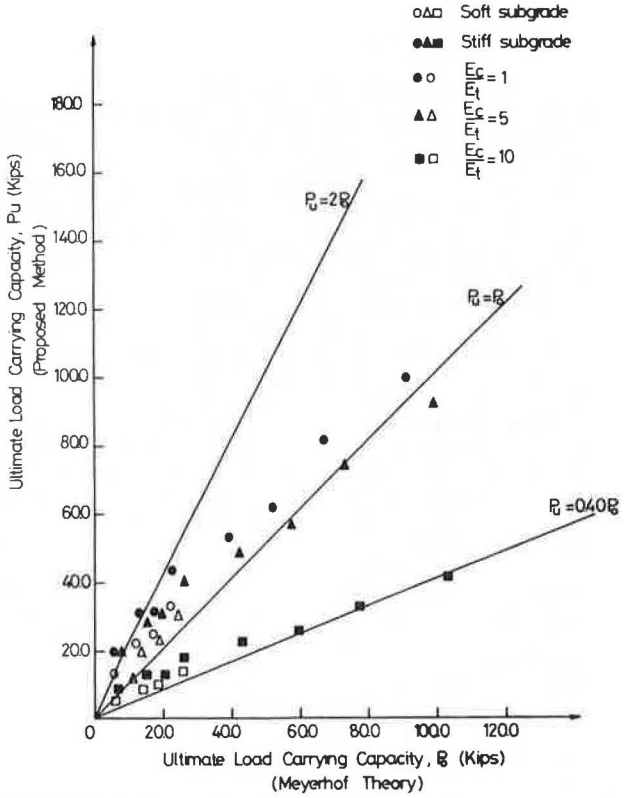

FIGURE 11 Comparison of load capacity predicted by proposed method and by Meyerhof theory.

but decreases with increase in bimodular ratio (Figures 9 and 10). The decrease is more pronounced for bimodular ratios greater than 5. Reducing the tensile strength of the stabilized layer by 50 percent leads in general to a reduction of layer capacity in the range of from 45 to 50 percent. Results shown in Figures 9 and 10 correspond to tensile strength of 300 psi ($E_b = 3.0 \times 10^6$ psi) and 100 psi ($E_b = 3.0 \times 10^5$ psi).

2. The load-carrying capacity under short-term loading (i.e., 1 repetition) (P_u) predicted using the proposed method could be greater or smaller than the ultimate capacity (P_o) predicted using Meyerhof theory (11) depending essentially on the bimodular ratio of the stabilized layer. For $E_c/E_t = 1$, P_u could approach 2 P_o, whereas for $E_c/E_t = 10$, P_u could be as low as 0.40 P_o as shown in Figure 11. Meyerhof theory tends to overestimate the ultimate capacity (P_u) for bimodular ratios greater than 5 and underestimate P_u for bimodular ratios smaller than 5. The modulus of subgrade reaction (k_s) assumed in the Meyerhof analysis was 50 psi per inch for the soft subgrade and 450 psi per inch for the stiff subgrade.

3. Experimental data presented by Suddath and Thompson (12) for ultimate capacity of lime-stabilized layers fall in the range of predicted values using the proposed method (Figure 12).

4. Comparison between load capacity under short-term and long-term loading associated with crack initiation on the underside of the stabilized layer and crack propagation to its surface is shown in Figures 13 and 14.

Results demonstrate that contrary to some current practice, which assumes that cracking of the base

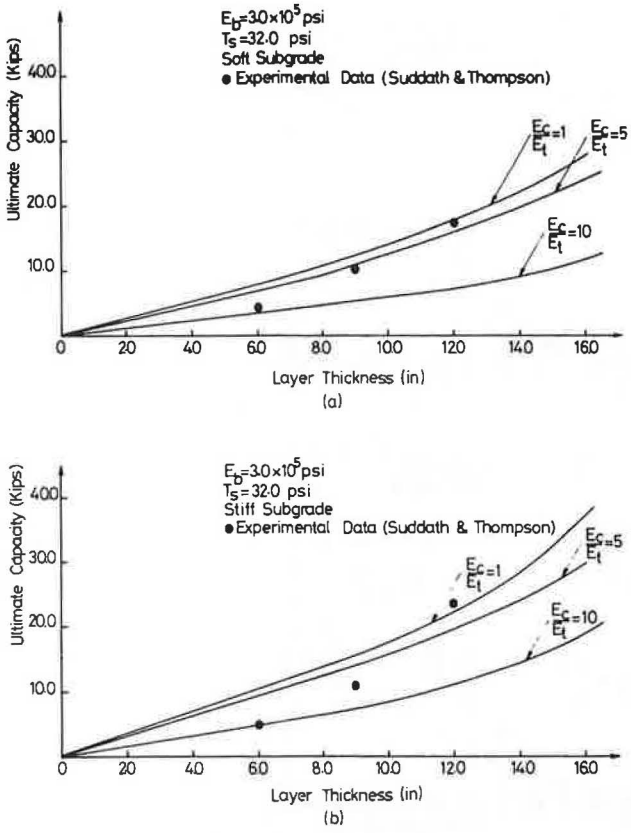

FIGURE 12 Comparison of predicted and measured ultimate capacity.

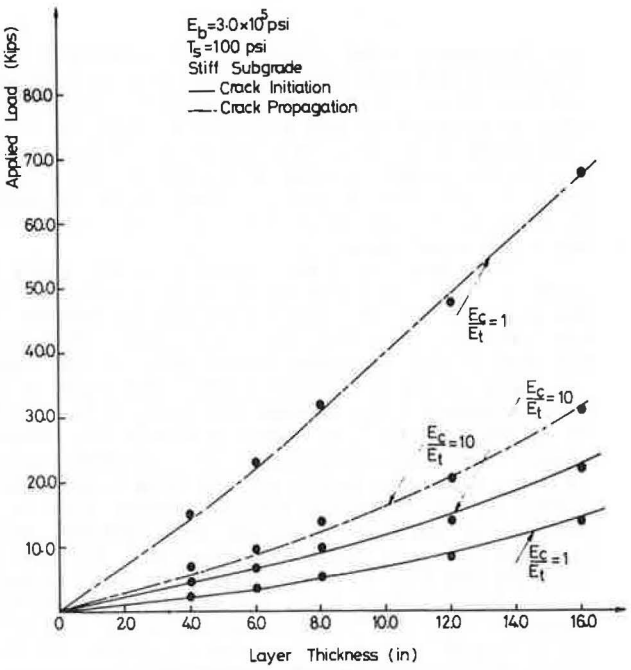

FIGURE 13 Load capacity in terms of crack initiation and propagation after 10^6 repetitions.

propagates quickly to the surface of the stabilized layer (13), the load required for crack propagation could be substantially greater than that needed for crack initiation, especially for layers with low bimodular ratios. A similar conclusion can be reached by comparing the load required to fracture

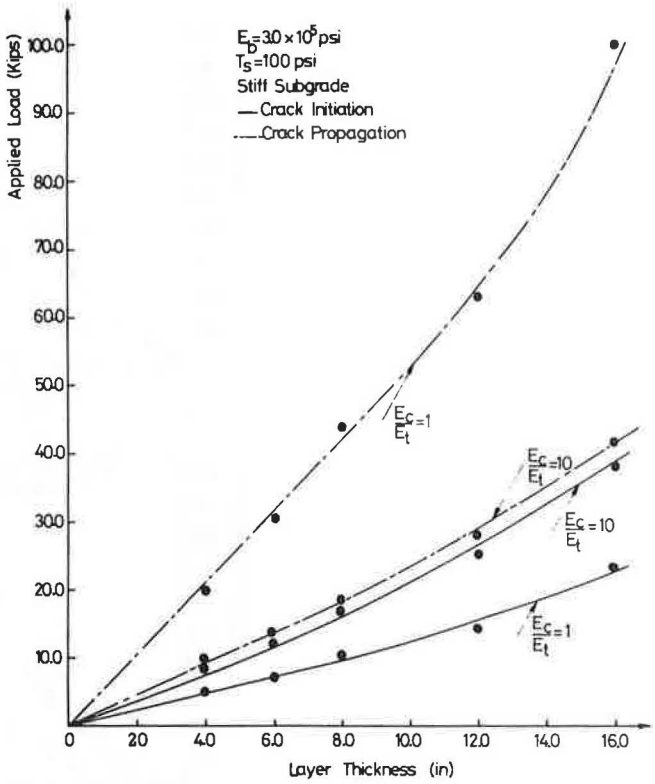

FIGURE 14 Load capacity in terms of crack initiation and propagation after 1 repetition.

the stabilized layer using Meyerhof theory with that required to induce a tensile stress at its interior (14) equal to the tensile strength, as shown in Figure 15.

SUMMARY AND CONCLUSIONS

An improved method of analysis for pavements with stabilized layers has been proposed. The method incorporates the bimodular properties (i.e., tensile modulus different than compressive modulus) of the stabilized layer and the stress-dependent behavior of granular and subgrade soils. The proposed method could be used to predict stresses, resilient strains, and deformations using a finite element representation of the pavement structure.

The proposed method has been used to study the behavior of stabilized layers under repeated loads. A limited number of split tension and flexure tests conducted on a cement-treated silty clay show that the material exhibits bimodular behavior and that modulus values computed for similar specimens are generally different and depend on testing procedure and method of computation. On the basis of laboratory results, it has been proposed to characterize the stabilized layer in terms of its split tensile modulus, bimodular ratio, and split tensile strength. This method of characterization was incorporated in the analysis to study the behavior of stabilized layers in pavements. Specifically, the influence of material characteristics on response prediction and the fracture of stabilized layers under repeated loads have been investigated.

Results of the analyses show that an increase in bimodular ratio tends to increase the tensile strains and decrease the tensile stresses on the underside of the stabilized layer. Fracture of stabilized layers, on the other hand, depends on stiffness, strength, and bimodular properties of stabilized material and on stiffness of underlying

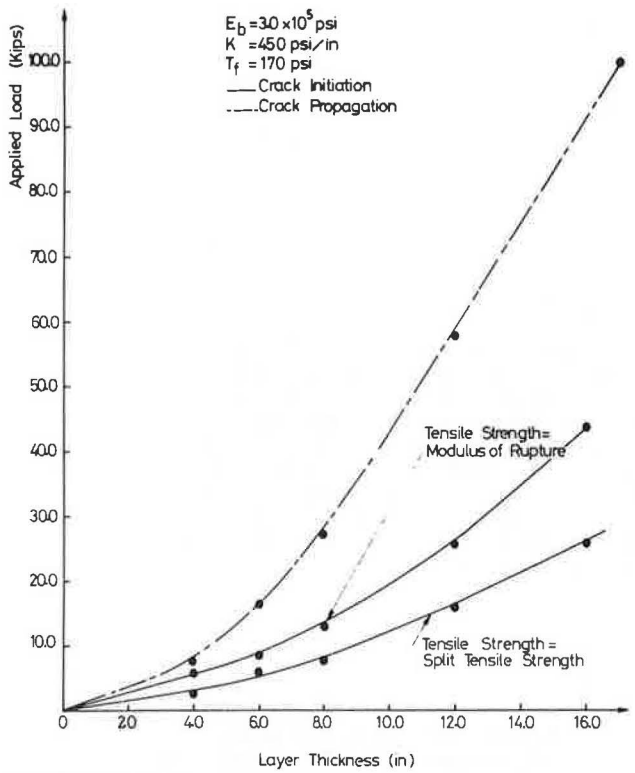

FIGURE 15 Load capacity in terms of crack initiation and propagation using Westergaard approach and Meyerhof theory.

subgrade. Agreement between predicted ultimate capacity using the proposed method and Meyerhof theory depends essentially on the bimodular ratio of the stabilized layer. Reasonable agreement between predicted capacity and experimental data has been attained within the common range of bimodular ratios of stabilized soils (i.e., E_c/E_t between 1 and 10). Results also indicate that loads associated with fracture of the stabilized layer could be substantially greater than those required for crack initiation on its underside.

ACKNOWLEDGMENT

The research presented in this paper was supported by a grant from the University Research Board at the American University of Beirut.

REFERENCES

1. J.J. Allen. The Effects of Non-Constant Lateral Pressures on the Resilient Response of Granular Materials. Ph.D. dissertation. University of Illinois at Urbana-Champaign, 1969.
2. J.L. Figueroa. Resilient Based Flexible Pavement Design Procedure for Secondary Roads. Ph.D. dissertation. University of Illinois at Urbana-Champaign, 1979.
3. M.R. Thompson and Q.L. Robnett. Resilient Properties of Subgrade Soils. Journal of the Transportation Engineering Division, ASCE, Vol. 105, No. TE1, Jan. 1979, pp. 71-89.
4. H.B. Seed, C.K. Chan, and C.E. Lee. Resilient Characteristics of Subgrade Soils and Their Relation to Fatigue Failure in Asphalt Pavements. Proc., First International Conference on the Structural Design of Asphalt Pavements, Ann Arbor, Mich., Aug. 1962, pp. 77-113.
5. L. Raad and J.L. Figueroa. Load Response of Transportation Support Systems. Journal of the Transportation Engineering Division, ASCE, Vol. 106, No. TE1, Jan. 1980, pp. 111-128.
6. L. Raad, C.L. Monismith, and J.K. Mitchell. Tensile-Strength Determinations of Cement-Treated Materials. In Transportation Research Record 641, TRB, National Research Council, Washington, D.C., 1977, pp. 48-52.
7. L. Raad and M.R. Thompson. Determination and Significance of Resilient Bimodular Properties of Stabilized Soils. In Transportation Research Record 671, TRB, National Research Council, Washington, D.C., 1978, pp. 92-98.
8. H.E. Bofinger. The Measurement of the Tensile Properties of Soil-Cement. Report LR365. U.K. Transport and Road Research Laboratory, Crowthorne, Berkshire, England, 1970.
9. J.L.M. Scott. Flexural Stress-Strain Characteristics of Saskatchewan Soil-Cements. Report 23. Saskatchewan Department of Highways and Transportation, Regina, Saskatchewan, Canada, Dec. 1974.
10. L. Raad. A Mechanistic Model for Strength and Fatigue of Cement-Treated Soils. ASTM Geotechnical Testing Journal, Vol. 4, No. 3, Sept. 1981, pp. 104-110.
11. G.G. Meyerhof. Load Carrying Capacity of Concrete Pavements. Journal of the Soil Mechanics and Foundation Division, ASCE, Vol. 88, No. SM3, June 1962, pp. 89-116.
12. L.P. Suddath and M.R. Thompson. Load-Deflection Behavior of Lime Stabilized Layers. Technical Report M-118. Construction Engineering Research Laboratory, Urbana-Champaign, Ill., Jan. 1975.
13. E. Otte, P.F. Savage, and C.L. Monismith. Structural Design of Cement-Treated Layers. Journal of the Transportation Engineering Division, ASCE, Vol. 108, No. TE4, July 1982, pp. 428-446.
14. E.J. Yoder and M.W. Witczak. Principles of Pavement Design, 2nd ed. John Wiley and Sons, Inc., New York, 1975.

Publication of this paper sponsored by Committee on Mechanics of Earth Masses and Layered Systems.

Analysis of Track Support and Determination of Track Modulus

GERALD P. RAYMOND

ABSTRACT

A design methodology that uses an approach similar to that outlined in the American Railway Engineering Association Manual for Railway Engineering for calculating the stresses below crossties of conventional railway tracks is presented. There is discussion of the practical effects of track modulus variability and its possible optimization from the point of view of both static and dynamic loading with particular reference to ballast and subgrade stress levels. These stresses are then used to estimate track deformation. Track deformation may then be used to calculate a conventional track modulus. With such a technique it is possible to calculate the effects of ballast depth variability and compressibility of crossties on track response.

The two main requirements of a stable subgrade are the provision of sufficient granular or soil-modified cover to ensure that overstressing does not occur and the provision of a granular filter blanket to prevent the piping and thus loss of subgrade fines from below the track bearing area. To ensure that overstressing does not occur, the track stresses need to be calculated. A means of calculating these stresses that follows an approach similar to that of the American Railway Engineering Association's Manual for Railway Engineering is outlined herein. Presentation of subgrade stability techniques is beyond the main scope of this work.

STATIC DESIGN OF CONTINUOUS WELDED RAIL

Talbot (1) has demonstrated that the theory of a continuous beam on an elastic support, or, more correctly, a linear spring (Winkler) foundation gives calculated bending moments for the rails close to those measured in freshly tamped track. Many investigations, including extensive ones performed by the Association of American Railways, have confirmed the validity of this theory. The American Railway Engineering Association (AREA) in its Manual for Railway Engineering (2) also endorses this method of analysis (chapter 22, article 3.2, paragraph 3.2.1, section a):

> Because of the many variables involved in tie and ballast track, the calculation of track stress and strain cannot be regarded as an exact science. However, in-service tests have shown that the track structure can be analyzed within acceptable limits of accuracy by considering the rail as equivalent to a continuous beam resting upon uniform elastic supports.

This design method results in the representative differential equation for the elastic beam (rail) subject to a vertical (wheel) load (P) of

$$EI(d^4z/dx^4) + Uz = 0 \quad (1)$$

where

- E = elastic modulus of the beam,
- I = second moment of area of the beam,
- z = deflection at a point x from the applied load,
- x = distance along the beam from the point of application of the load, and
- U = modulus of the elastic support commonly known as the track modulus (note that the track modulus as used in common practice and in the AREA manual relates to a single rail).

For a single wheel load (P) on an infinitely long beam the solutions to this equation are well known:

$$z_x = (\lambda P/2U)\ (\cos \lambda x + \sin \lambda x)\ \exp(-\lambda x) \quad (2)$$

$$M_x = (P/4\lambda)\ (\cos \lambda x - \sin \lambda x)\ \exp(-\lambda x) \quad (3)$$

where

$$\lambda = [U/(4EI)]^{0.25} \quad (4)$$

The maximum values of z and M are directly below the load at x = 0.

$$z_o = \lambda P/(2U) \quad (5)$$

$$M_o = P/(4\lambda) \quad (6)$$

These results are normally given in the form of the influence chart shown as Figure 1 in which the distance to zero moment (X_1) is used as a distance base [e.g., exhibit 1 of chapter 22, AREA manual (2)].

$$X_1 = \pi/(4\lambda) \quad (7)$$

Alternatively, but not so commonly, a deformation wavelength of $2\pi/\lambda$ is used. The rail seat loads are commonly calculated as

$$Q_x = z_x US = (1/2)\ \lambda SP\ (\cos \lambda x + \sin \lambda x)\ \exp(-\lambda x) \quad (8)$$

where S is the spacing of crossties. For a crosstie placed directly below the load (x = 0)

$$Q_o = P\lambda S/2 \quad (9)$$

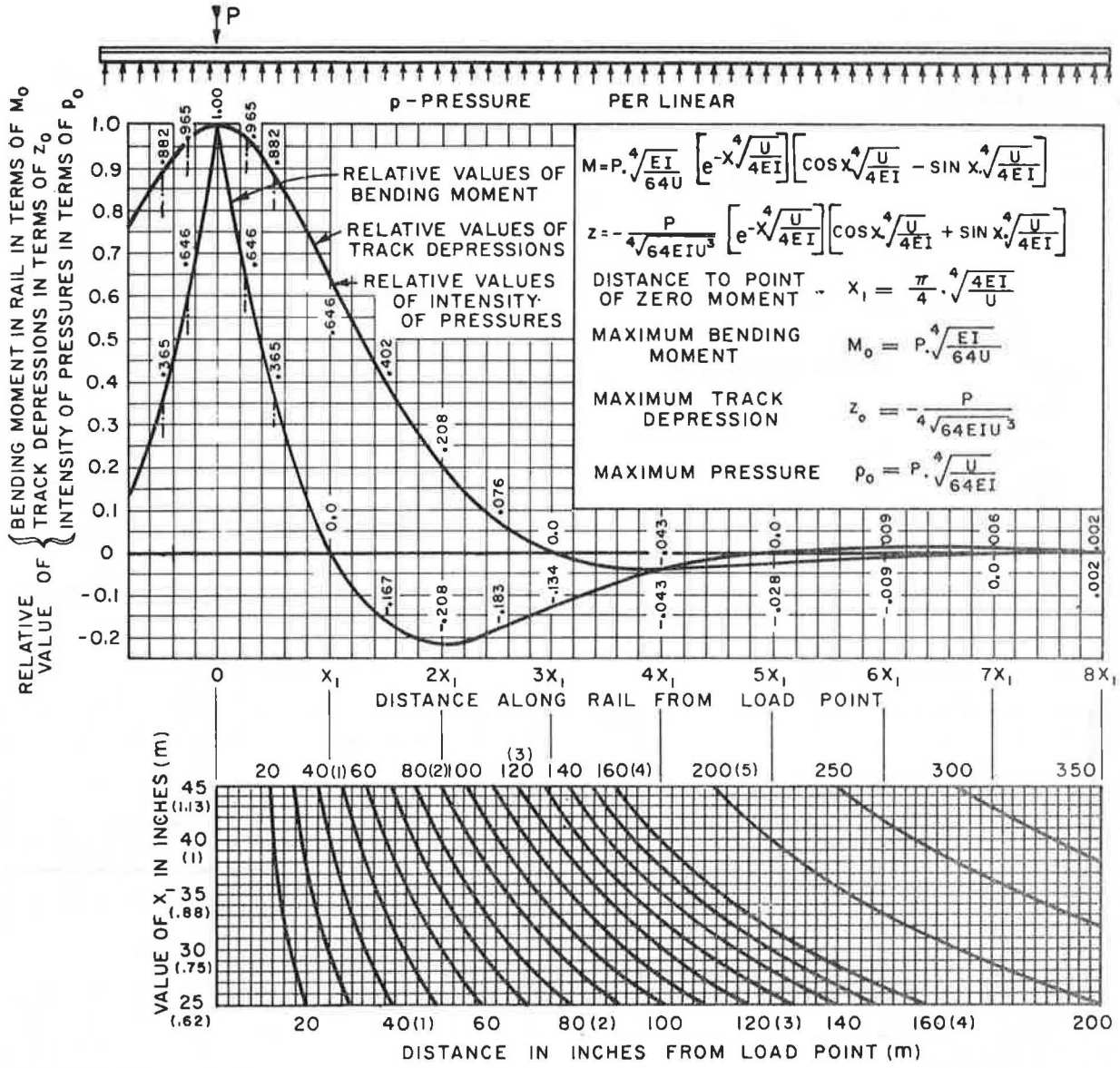

FIGURE 1 Influence chart for track design.

As an example of the effect of track modulus on rail seat loads, Figure 2 shows the variation of the rail seat loads in the vicinity of a single 147-kN (33-kip) wheel load on 68-kg/m (136-lb/yd) rail for two different crosstie spacings in which the central crosstie (crosstie 1) is directly below the load (i.e., the crosstie is positioned to produce a maximum rail seat load). Examination of Figure 2 indicates that, within the limitations of values likely to occur in practice, variation of the track modulus has a much greater influence on the rail seat load than does crosstie spacing.

EFFECT OF MULTIPLE WHEELS OR AXLES

Because the preceding theory is based on elastic response, the theorem of superposition applies and the effect of multiple wheels or axles can be simply calculated as

$$z_j = \sum z_x \tag{10}$$

$$M_j = \sum M_x \tag{11}$$

$$Q_j = \sum Q_x \tag{12}$$

where the different values of x are the distances of each wheel load from the position point j.

Example calculations of the maximum track deflection and maximum rail base bending stress are plotted on Figures 3 and 4 for both a single-axle and two coupled G-75 trucks (wheel spacing 1.78 m, 1.99 m, and 1.78 m or 70 in., 78.5 in., and 70 in.) supported by either 45-kg/m (90-lb/yd) rail or by 68-kg/m (136-lb/yd) rail. Maximum deflection occurs below the interior axles and maximum rail stresses occur below the outer axles. Examination of these curves show that as the track modulus decreases from the region of about 35 to 70 MN/m^2 (5 to 10 kips/in.^{2}) of rail there is a rapid increase in deflection or rail stress, and if the track modulus increases from this region of values a gradual reduction of deflection or rail stresses occurs. It may be concluded that for statically loaded track 35 to 70 MN/m^2 (5 to 10 kips/in.^{2}) of rail may be anticipated as an optimized value range of track modulus, at least for initial consideration.

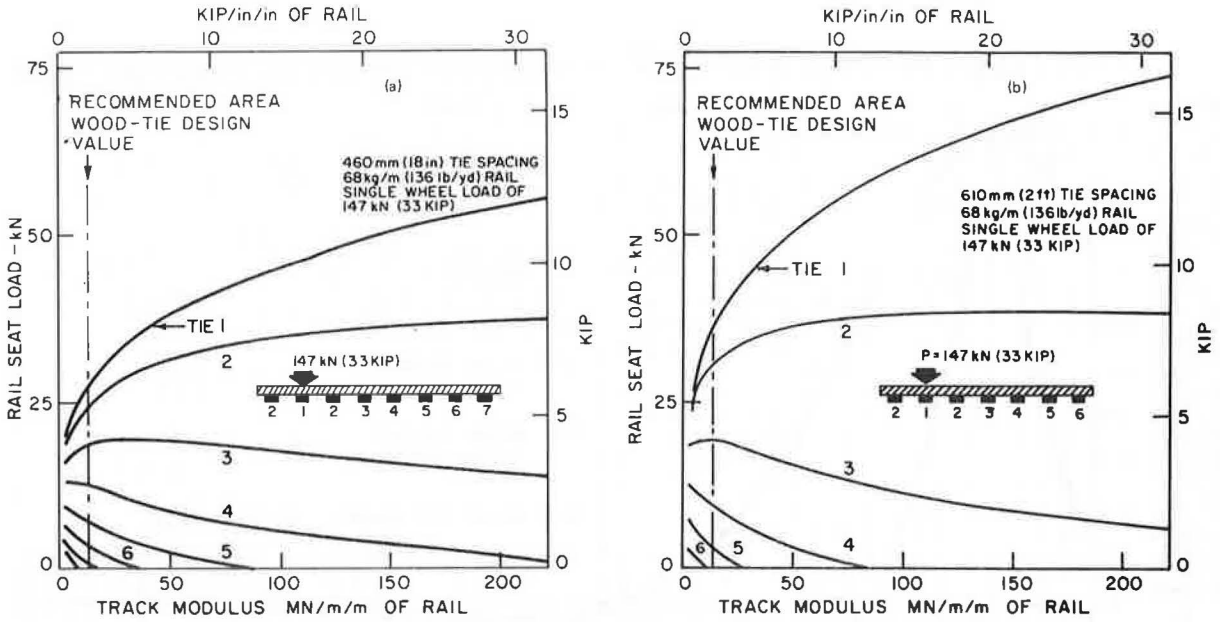

FIGURE 2 Effect of track modulus variation on rail seat loads resulting from a single static wheel or axle load: (a) 460-mm (18-in.) crosstie spacing and (b) 610-mm (24-in.) crosstie spacing.

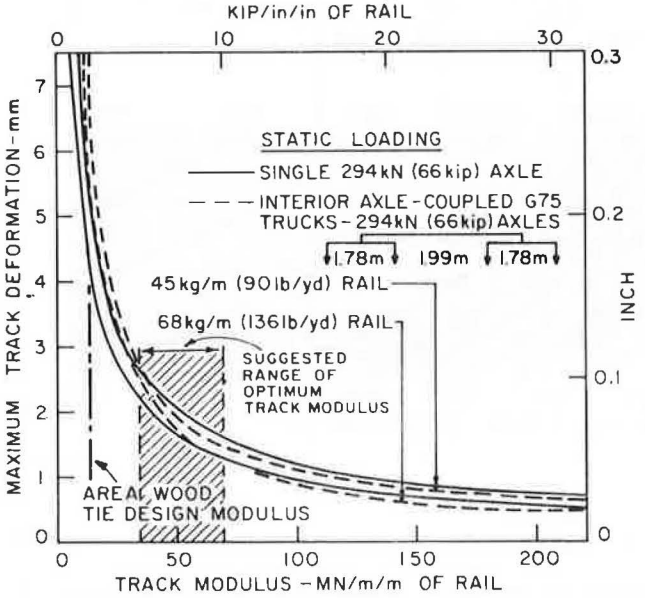

FIGURE 3 Effect of track modulus variation on maximum track deformation.

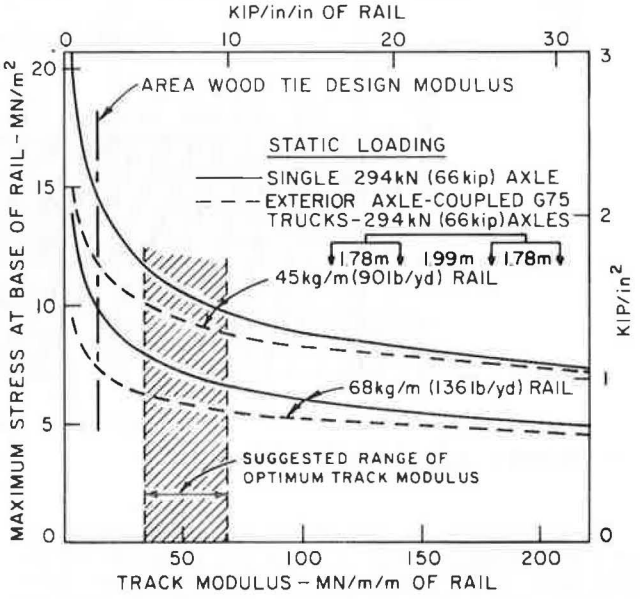

FIGURE 4 Effect of track modulus variation on maximum stress at base of rail.

CALCULATIONS OF STATIC SUBGRADE STRESSES

Similar calculations were made using Equation 12 for the determination of the rail seat loads obtained from multiple axles. The rail seat load may then be used to calculate tie bearing pressures and subgrade stresses. Sufficient evidence is available in the technical literature to show that where soils are unable to resist tensile forces the vertical stress is given by superposition of Boussinesq's solution for stresses within a semi-infinite elastic solid with surface loading. Below each rail seat the crosstie can be assumed to produce a rectangularly loaded area on the ballast. This permits the use of the solutions developed by Love (3) who extended Boussinesq's solution to a rectangularly loaded area. The area of the crosstie bearing surface per rail seat (A_b) may be calculated according to the AREA manual as

$$A_b \text{ (per rail seat)} = b(\ell - \ell_r)\{1 - [C(\ell - \ell_r)/t^{0.75}]\} \quad (13)$$

where

- b = width of crosstie,
- ℓ = length of crosstie,
- ℓ_r = distance center to center between rails,
- t = thickness of crosstie, and
- C = constant = 0.04 (0.018) if dimensions are in millimeters (inches) (note constant is dependent on units).

Alternatively, the area is assumed equal to some tamper influence distance on either side of the rail. The AREA method results in rail seat bearing areas the width of the crosstie and a length determined by the formula (Equation 13) that results in 879 mm (34.6 in) for a crosstie 178 mm (7 in.) deep by 2.55 m (8 ft 6 in.) long and 975 mm (38.4 in.) for a crosstie 178 mm (7 in.) deep by 2.70 m (9 ft 0 in.) long. For purposes of illustration two rail seat bearing lengths of 914 mm (36 in.) each below each of two rails spaced 1.50 m (60 in.) centerline to centerline apart have been assumed. This is considered the approximate distance influenced by the tamper tines.

Figure 5 shows the solution obtained using different track moduli of the underlying maximum vertical support stress resulting from a single axle load on 68-kg/m (136-lb/yd) rail and 279-mm (11-in.) crossties spaced at 610-mm (24-in.) centers. The contact pressure or vertical stress at zero depth for a single axle load may be seen to increase as the fourth root of the track modulus (i.e., an increase of track modulus by a factor of 16 doubles the contact stress). With depth the difference in vertical stress decreases slowly such that, even at 0.8 m (32 in.), the effect of track modulus variation on subgrade stresses from the single axle is considerable.

Figure 6 shows similar calculations, using the same crosstie size and spacing, for two coupled G-75 trucks having 294-kN (33-ton) axle loads. Interaction between axle loads is sufficient under the lower values of track modulus to cause a considerable increase in the contact pressure or vertical stress at zero depth. This reduces the dependence of either maximum contact pressure or maximum subgrade stress on the variation of track modulus. Using the two highest track moduli interaction actually caused

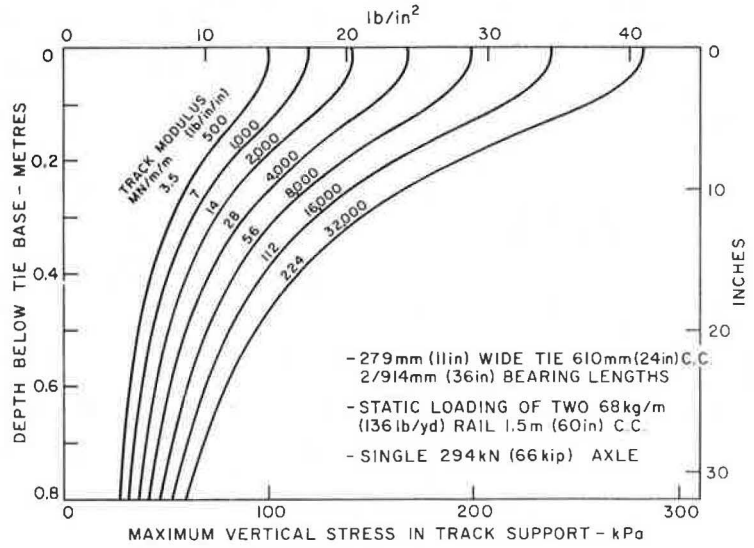

FIGURE 5 Effect of track modulus variation on maximum vertical stress in track support resulting from a single static axle load.

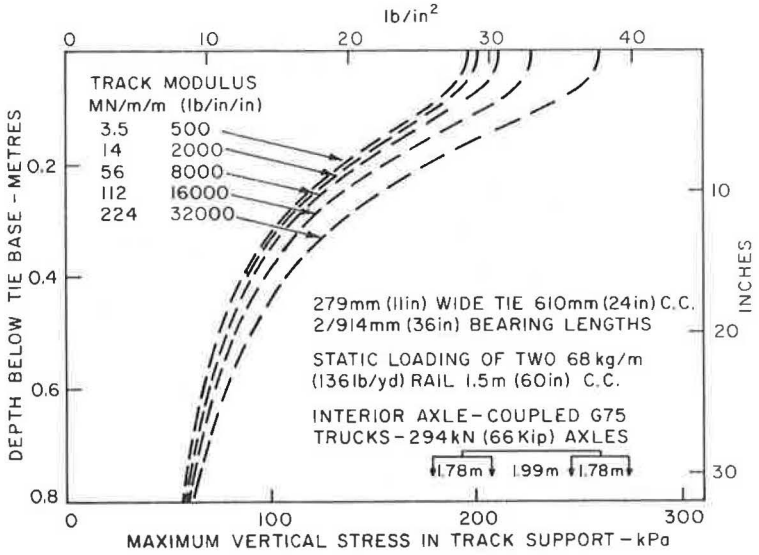

FIGURE 6 Effect of track modulus variation on maximum vertical stress in track support resulting from two coupled G-75 trucks.

a reduction in these maximum values from those calculated for a single axle.

The effect of variation of both track modulus and crosstie spacing is shown in Figure 7. In this figure is plotted the effect of using a 229-mm (9-in.) crosstie at 458-mm (18-in.) centers versus a 279-mm (11-in.) crosstie at 610-mm (24-in.) centers on track having moduli of 14 MN/m^2 (2,000 lb/in^2) of rail and 224 MN/m^2 (32,000 lb/in.^{2}) of rail with 68-kg/m (136-lb/yd) rail. If no change is made in track modulus, only about a 10 percent change in contact stress occurs for a change in specified crosstie size and spacing. On the other hand it is clearly evident from Figure 7, and from the maximum rail seat loads shown in Figure 2, that much higher support stresses result from a change in specified track modulus. This effect is more pronounced for a single axle than for coupled G-75 trucks.

In the case of a single axle on 68-kg/m (136-lb/yd) rail changing the modulus from 14 MN/m^2 (2,000 lb/in.^{2}) of rail to 224 MN/m^2 (32,000 lb/in.^{2}) of rail causes the crosstie-ballast interface stress, for the same crosstie spacing, to approximately double (i.e., 100 percent increase). Interaction of axles is more pronounced on softer track because the rail is more effective in spreading the load thus reducing the effect of track modulus change on support stresses for the coupled G-75 trucks. Changing the track modulus but retaining the same rail and crosstie size and spacing reduces the increase interface stresses to an increase of approximately 30 percent for the 229-mm (9-in.) crossties and approximately 25 percent for the 279-mm (11-in.) crossties.

In the event of changing from crossties 229 mm (9 in.) wide at 458-mm (18-in.) spacing to crossties 279 mm (11 in.) wide at 610-mm (24-in.) spacing, the effect of modulus change from 14 MN/m^2 (2,000 lb/in.^{2}) of rail to 224 MN/m^2 (32,000 lb/in.^{2}) of rail on the interface stress for a single static axle would be an increase of approximately 120 percent. Axle interaction for the two coupled G-75 trucks would reduce this increase to approximately 35 percent.

A point worth noting from Figure 7 is that as the depth increases the support vertical stresses resulting from similar wheel loadings and the same track modulus tend toward similarity. This, of course, is to be expected from "Saint Venant's principle," which says that two different distributions of force, having the same resultant acting on a small part of an elastic body, will produce the same stress except in the immediate neighborhood of the loaded part. Thus, provided the ballast is clean and of full section so it can function effectively, changes in crosstie spacing or the size of the bearing area are unlikely to affect the magnitude of the subgrade stresses but would affect the stresses in the ballast. These conclusions are verified in Figures 8 and 9 that show the distribution of support stresses for a single axle using different crosstie spacings and crosstie sizes, respectively. As previously shown, multiple axles decrease the differences shown by single axles and have been omitted from these figures.

At much greater depths than shown on Figure 5 (such greater depths are of little practical significance) the effect of modulus change would also be negligible. As far as normally anticipated ballast depths are concerned, track modulus variation is much more significant in affecting the magnitude of the subgrade stresses than variation in crosstie spacing or bearing area within the normally used limits of these variables. This is not to suggest that changes in crosstie spacing and bearing area do not affect the track modulus but rather that their effect on any change in track modulus (which is not given by the theory) has a greater influence on support stresses than their direct effect from theoretical stress distribution theory assuming no change in track modulus.

Similar calculations, done to show the effect of changing rail mass, are shown on Figure 10. Although there is some effect on the subgrade and ballast stresses for a single axle on the softer track, interaction of wheel loads for the coupled G-75 trucks reduces this difference to a negligible amount. The effect of subgrade stress reduction is much more apparent from a rail mass increase when the track is extremely stiff. This reduction occurs both for the single and the multiple axle case with maximum stresses being less for multiple axles than for single axles on extremely stiff track.

ESTIMATE OF TRACK MODULUS

The solutions developed by Love (3) for a rectangular loaded area allow for the calculation of not

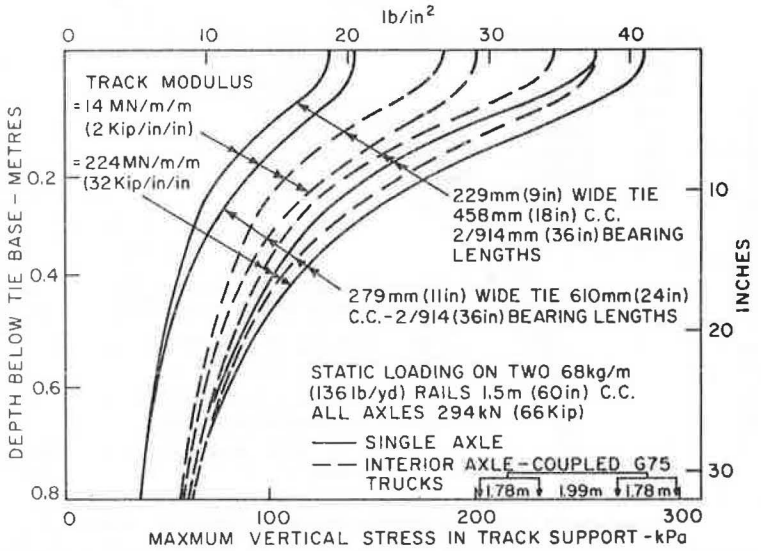

FIGURE 7 Example of effect of major increase in track modulus on maximum vertical stress in track support.

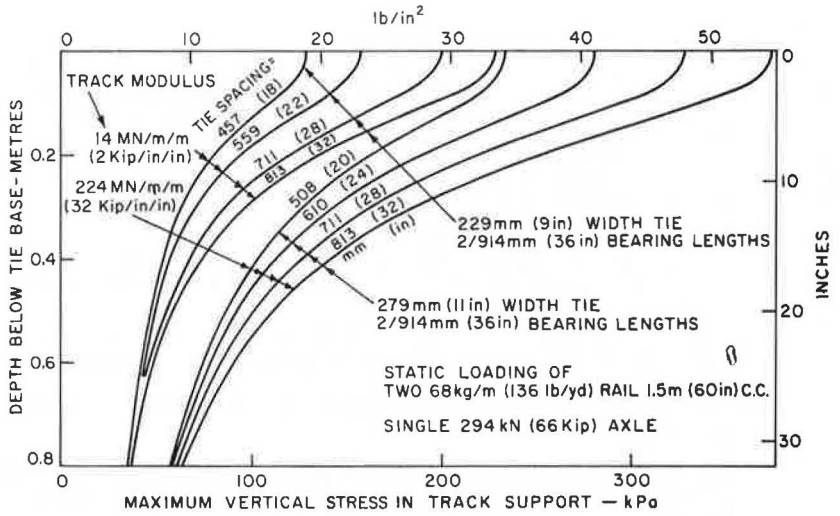

FIGURE 8 Example of effect of crosstie spacing on maximum vertical stress in track support.

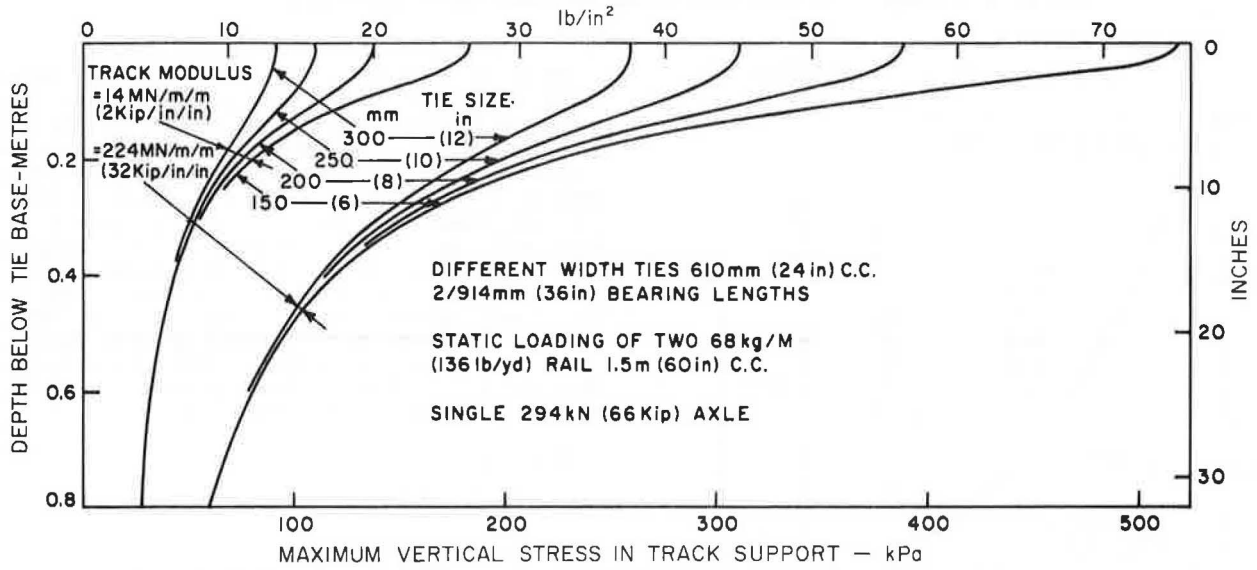

FIGURE 9 Example of effect of crosstie size on maximum vertical stress in track support.

only the vertical stress but also the six stresses (three normal and three shear) that define the state of stress at any point. Knowing the pseudoelastic parameters of the support soil allows the calculation of the strain at that point, which, by numerical integration, allows the calculation of support deformation. Addition of such deformations to those produced by the rail seat load on the crossties via the tie plates allows the total deformation to be estimated for a given set of conditions. Because different track moduli produce different calculated support stresses and rail seat loads, a series of calculations of total deformations using different track moduli is required. These results should then be compared with the deformations predicted by the "beam on elastic support" theory to determine the track modulus that defines identical deformations. It should be clearly understood that the deformation experienced by the rail at the rail seat includes not only the deformation of the track support but also that of the crosstie and its accessories. An example of the results of such a series of calculations is shown in Figure 11. These results are for a single axle loading because many field measurements of track modulus are obtained using a long loaded flatcar with two central loading jacks one above each rail. The jacks are used to apply, in increments, the equivalent of a single axle load of different magnitudes. Because of voiding below the crosstie, the modulus is calculated from the deformation recorded between about 36 kN (8 kips), the weight on an unloaded truck wheel, and 147 kN (33 kips) on each jack.

The results shown in Figure 11 were obtained using 305 mm (12 in.) of clean ballast overlying 610 mm (24 in.) of clean subballast overlying a heavily compacted silt or clay subgrade. The exact compressibility of the subgrade can be expected to vary throughout the year from negligible in extremely dry hot weather to a maximum during extremely wet or thaw conditions if subjected to freezing. Figure 11 represents calculations for extremely dry subgrade conditions. It may be seen that track on such a support constructed with concrete crossties and stiff pads would have a track modulus of about 140 MN/m^2 (20,000 lb/in.^{2}) of rail. Use of the softer

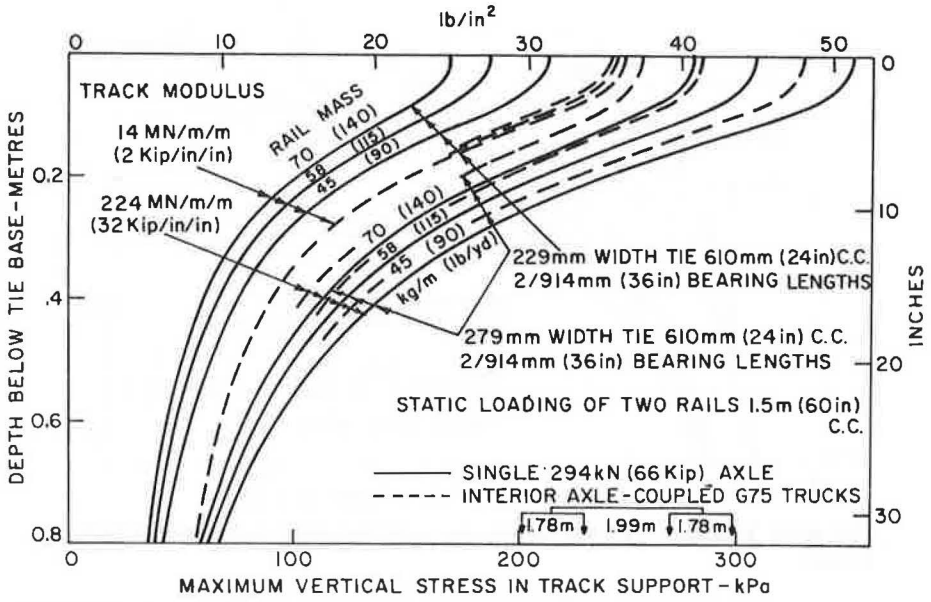

FIGURE 10 Example of effect of rail mass on maximum vertical stress in track support.

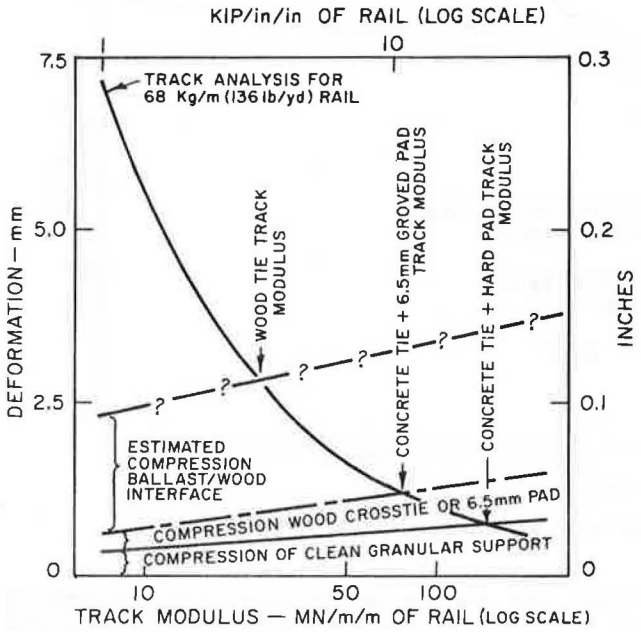

FIGURE 11 Example of estimating track modulus on the basis of pseudoelastic properties of track and support components.

grooved pads recently installed on the U.S. Northeast Corridor reduces the track modulus to about 69 MN/m² (10,000 lb/in.²) of rail. The compressibility of hardwood crossties is similar to that of the softer Northeast Corridor pads; however, the major compression observed in tests on wood crosstie track has been the elastic compression and rebound of the ballast penetration of wood or ballast-crosstie interface. The magnitude of this interface compression is shown on Figure 11 from which it is seen that wood crosstie track has a considerably lower track modulus than does concrete crosstie track. The curves plotted on Figure 11 suggest a track modulus of 24 MN/m² (3,500 lb/in.²) of rail; however, the variability of the interface compression means considerable variation from this value would not be unrealistic.

An alternative method of calculating the deformations from the support alone is to use Steinbrenner's solutions for the settlement of the corner of a rectangular loaded area extended to deal with a layered foundation. Steinbrenner's original solution assumes a homogeneous isotropic elastic layer of constant elastic parameters; thus an extension to deal with layers of different elastic parameters must be used to obtain the same results as are obtained by the use of Love's solution. Both these techniques assume that the stresses, but not the strains, are given by homogeneous elastic theory irrespective of any variations in the soil properties. When the stress distribution has been obtained, the deformations may be calculated from

$$\delta_z = \int_i [\sigma_z - \nu_i(\sigma_x + \sigma_y)]/E_i \, dz \qquad (14)$$

where

σ = normal stress,
ν_i = pseudo Poisson's ratio of the soil layer, and
E_i = pseudoelastic modulus of the soil layer.

The integration is usually done numerically by dividing the foundation into a relatively large number of soil layers and then summing the resulting layer deformations. Note that the pseudoelastic properties of granular soils vary with degree of compaction and the properties of cohesive soils with moisture content or, more correctly, soil suction. In addition, an underlying soft cohesive soil tends to prevent compaction of an overlying granular soil; thus the selection of appropriate pseudoelastic parameters requires considerable judgment. The main point, however, is that once the selection has been made the calculations are relatively simple. Results from typical calculations showing the deformation between the base of the crosstie and the given depth are shown in Figure 12 for a granular layered deposit in a loosely compacted, and in a densely compacted, state making the somewhat simple assumption that the wheel load is taken 50 percent by a central rail seat and 25 percent by adjoining rail seats. Because the calculations assume elastic response, the support deformations are directly proportional

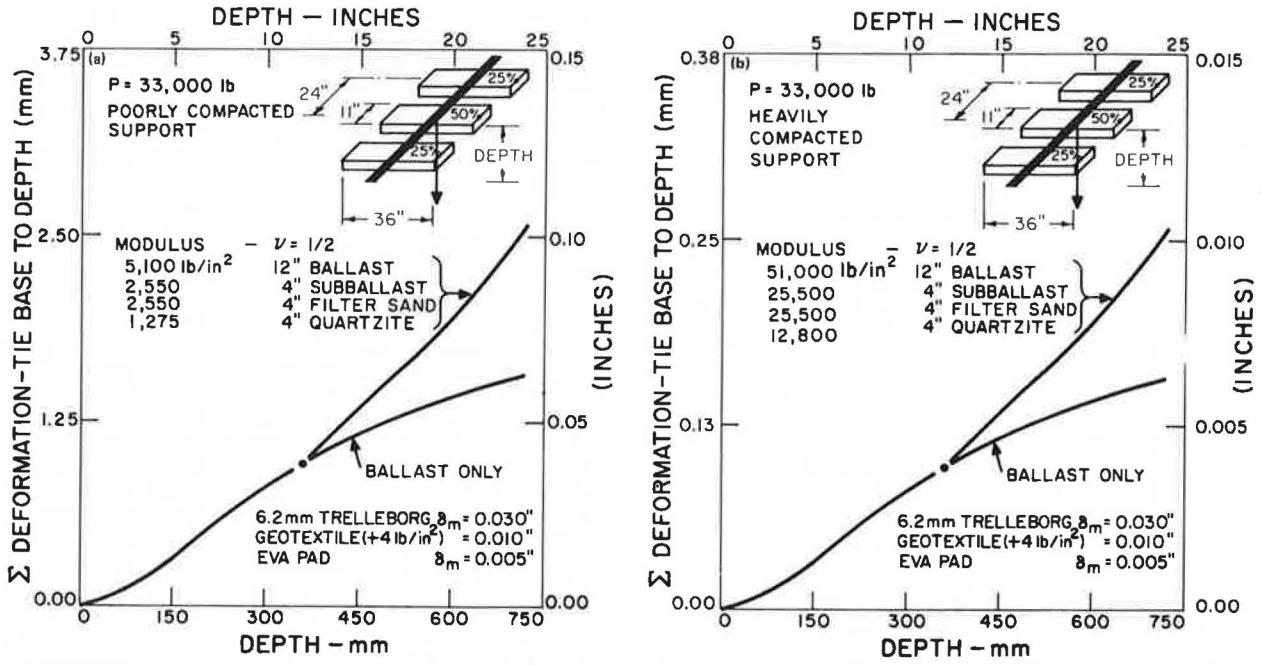

FIGURE 12 Example of simplified estimation of contribution to track deformation of support materials: (a) poorly compacted and (b) heavily compacted.

to any variation in the central rail seat load of 73.5 kN (16,500 lb). The calculations should, of course, be done for the actual distribution of rail seat loads produced by the different track moduli to obtain the best estimate of modulus.

The 50 to 25 percent load distribution does, however, permit a quick rough estimate of track modulus because, from Equation 8,

$$U = Q_o/(S\delta_o) \tag{15}$$

where Q_o is the maximum rail seat load for the single wheel load P and δ_o is the total summation of rail seat deformation at Q_o. Thus a rough estimate of U can be obtained as

$$U = P/(2S\delta_{50}) \tag{16}$$

where δ_{50} is the total deformation using 50 percent of P as the maximum rail seat load (note Figure 12 shows only the contribution to the total deformation due to the soil support of the shown 610 mm or 24 in. directly below the tie base).

CALCULATION OF DYNAMIC INCREMENT FOR CONTINUOUS WELDED RAIL

Kenney (4) has shown that on perfect track transversed by perfect wheels track forces rise extremely slowly with speed requiring a speed of about 1600 km/hr (1,000 MPH) to reach track resonance. Track irregularities or wheel irregularities are therefore the principal cause of major dynamic track forces given current (1985) speeds. Any complete theory dealing with track and wheel irregularities is clearly complex but because the track mass is much less than the unsprung mass of a wheel set it appears reasonable to neglect the track mass as a first approximation and to take the effect of the suspension spring as a steady force. The equation of motion then reduces to

$$M(dw^2/dt^2) + K\,(w + s) = 0 \tag{17}$$

where

w = displacement of the unsprung mass from the static equilibrium position,
s = amplitude of the irregularity,
M = unsprung mass, and
K = track stiffness.

Track stiffness is related to the track modulus by

$$K = (64\,E\,I\,U^3)^{0.25} \tag{18}$$

The solution to Equation 17 leads to a relationship for dynamic increment of load of the form

$$P_d - P_o = C\,s\,(M\,K)^{0.5}\,f(V) \tag{19}$$

where

P_d = dynamic wheel load,
P_o = static wheel load,
C = a proportionality parameter, and
f(V) = a function of speed.

For a well-maintained track made of continuous welded rail that is not corrugated the major track or wheel irregularity is believed to be due to wheel flats. Data on wheel flat impact obtained by the Association of American Railroads (5) on wheel flat impacts along with a first trial solution of Equation 19 are shown in Figure 13. According to Equation 19, for any given speed and weight of rail the dynamic increment should increase linearly with the irregularity depth. Because the wheel flats were carefully made as square flats, the irregularity increases with flat length as shown. This is seen as in reasonable agreement with the data considering the scatter in the results. Also from Equation 19, for any given speed the axle load should make no difference to the dynamic increment obtained from a given wheel flat and this is reflected in the theo-

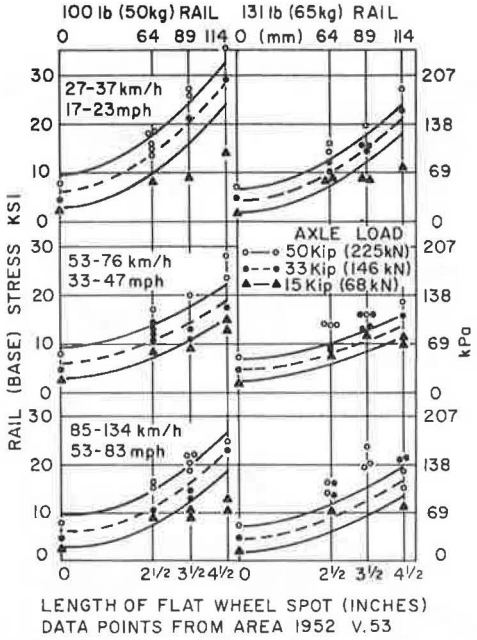

FIGURE 13 Comparison of simplified theory for flat wheel spot with experimental field data obtained by Association of American Railways.

retical curves shown. Thus, from the test data obtained, the dynamic increment for wheel flats from other vehicles and other track constructions may be obtained as

$$P_d - P_o \text{ is proportional to } M^{0.5} U^{0.375} \quad (20)$$

The data of Figure 13 were obtained using a 70-ton (net) freight car with an unsprung axle mass of 1705 kg (3,750 lb) on wood crosstie track. One hundred ton (net) cars with 20 percent heavier axle loads are in more common use today (1985). These cars have an unsprung axle mass of about 1977 kg (4,350 lb) that suggests an 8 percent increase in impact loading on wood crossties. For concrete crosstie track with stiff pads and stiff subgrades (e.g., dried out clay), the dynamic increment is estimated at an additional 98 percent, whereas soft pads would reduce this increment to 55 percent. For 100-ton cars on concrete crosstie track the increment would be 105 and 59 percent for the stiff and soft pad, respectively. However, due to the nonlinear compression of the components of the track structure, the difference in track moduli for wood and concrete crossties to be applied to the dynamic increment is probably not as numerically diverse as shown in Figure 11 because the track has been compressed by the dead load when the impact of the wheel flat occurs.

Field data in support of differences of dynamic wheel increment associated with different track stiffness, assembled from published data for passenger train wheel loading on the U.S. Northeast Corridor (NEC), are shown in Figure 14 (6,7). It may be seen that more than 90 percent of all wheels give similar loadings consistent with near-perfect wheels on track of similar roughness. The few percent of wheels having major imperfections are those, according to theory, that would show major differences in dynamic increment and this difference is seen (Figure 14) to be largest between wood crosstie track and concrete crosstie track. Although the differences in measured wheel load on concrete crosstie track are small but nevertheless measurable, the effect of a softer track on the rail seat bending moments of the differently padded concrete crossties is clearly evident. Because of the better load-spreading capability of the same rail section on softer track, the bending moments associated with softer pads are considerably less than those associated with the stiffer pads when the dynamic increment becomes large (i.e., at small occurrence levels). It is understood that the experimental results have (rightly according to theory) led to the adoption of softer pads for all further concrete crosstie installations on the NEC and the use of flat wheel detectors as an addition to the normal visual inspection that forms part of normal railroad practice for restricting the access of wheels with flats to track. It is clear

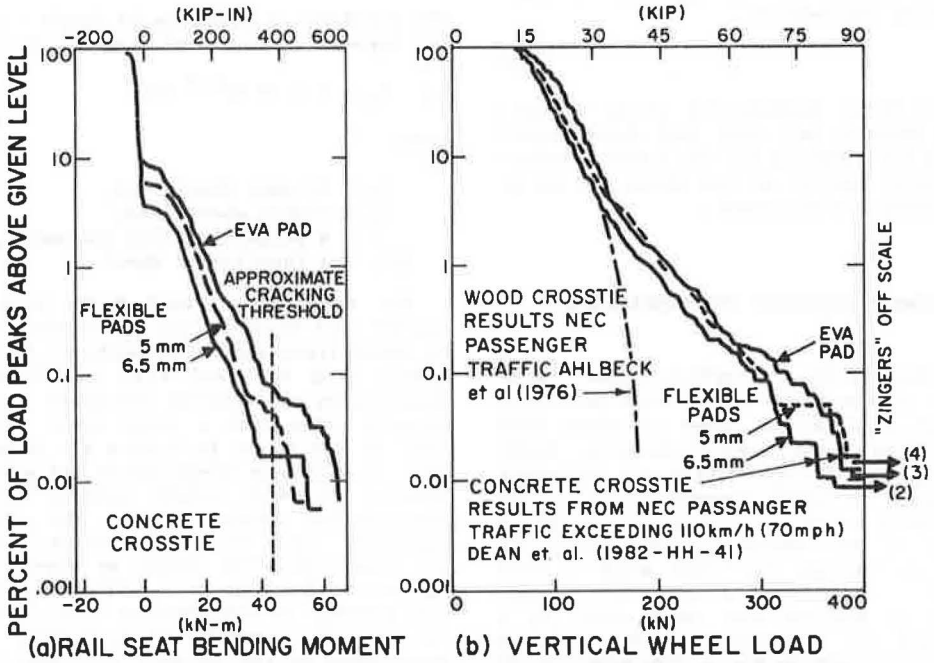

FIGURE 14 Measured dynamic wheel loads for Northeast Corridor passenger traffic (6,7).

that, although no optimization of track modulus has been established or is evident for dynamically loaded track, there is a penalty to be paid by overstiffening track that is subject to wheel and rail irregularities, which presently (1985) is occurring on North American track. Optimum track stiffness for dynamic loading is probably less than that for static loading.

TYPICAL STATIC PLUS DYNAMIC SOLUTION

Figure 15 shows results from a typical calculation based on a 51-mm (2-in.) square flat on both wheels of one inside axle of two fully loaded coupled G-75 trucks (i.e., 30-tonne or 66-kip axle load) for three track conditions. The 51-mm (2-in.) flat is the maximum permitted by Association of American Railroad (8) recommendations. The track conditions were track made from wood crossties 229 mm (9 in.) wide with 458-mm (18-in.) spacing giving an assumed track modulus of 14 MN/m^2 (2 $kip/in.^2$) of rail; track made from concrete crossties with soft pads 279 mm (11 in.) wide with 610-mm (24-in.) spacing giving an assumed track modulus of 84 MN/m^2 (12 $kip/in.^2$) of rail; and track made from similar crossties with stiff pads giving an assumed track modulus of 224 MN/m^2 (32 $kip/in.^2$) of rail.

Figure 15 shows the static loading conditions for the maximum vertical support stress along with a combination of both static and dynamic conditions. The total dynamic axle (static + increment) loads for the three assumed moduli were calculated as 294 kN (66 kips), 447 kN (100 kips), and 926 kN (208 kips), respectively. These values are likely to be higher than generally measured in track because wheel flats are never square in practice and are normally taken out of service before becoming the maximum allowable. The concrete crosstie moduli are also somewhat higher than estimated in Figure 11. These higher values were used because such values have been measured and thus the calculation illustrates the negative effect of having extremely stiff track associated with the high unsprung mass of freight vehicles.

BALLAST DEPTH DESIGN

Clearly evident from Figure 15 is the dramatic effect that a higher track modulus has on the dynamic increment. Fortunately concrete crosstie track and its higher track moduli are generally associated with firmer, and thus generally stronger, subgrades. In addition, wheels do not generally have carefully made square flats associated with "worst conditions." Thus stresses as high as the upper limit shown on Figure 15 are the exception not the rule. Typical foundation design is often based on dead load plus some percentage (often 50 percent) of the live load; the reasoning is that safe bearing stresses include some measure of safety factor and may thus be exceeded on a limited basis. As an example, the Manual for Railway Engineering of the American Railway Engineering Association (2) suggests a dynamic increment of approximately 1 percent of static loading for each 1.6 km/hr (1.0 MPH) of the maximum track speed although the writer would question the sufficiency of the recommendation for the more recently introduced stiffer concrete crosstie track. On the basis of percentage live load chosen, the limits, after proportioning, may be related to the safe bearing stress established for the subgrade soil in question to obtain the required granular (subballast plus ballast) design depth. Figure 16 shows the typical safe bearing stress values or related empirical test values developed for use in highway and airport design (9), both of which require much smaller surface deflection than do railways for good performance. Because railroads are more flexible than major highways it is this writer's opinion that the limits shown in Figure 16

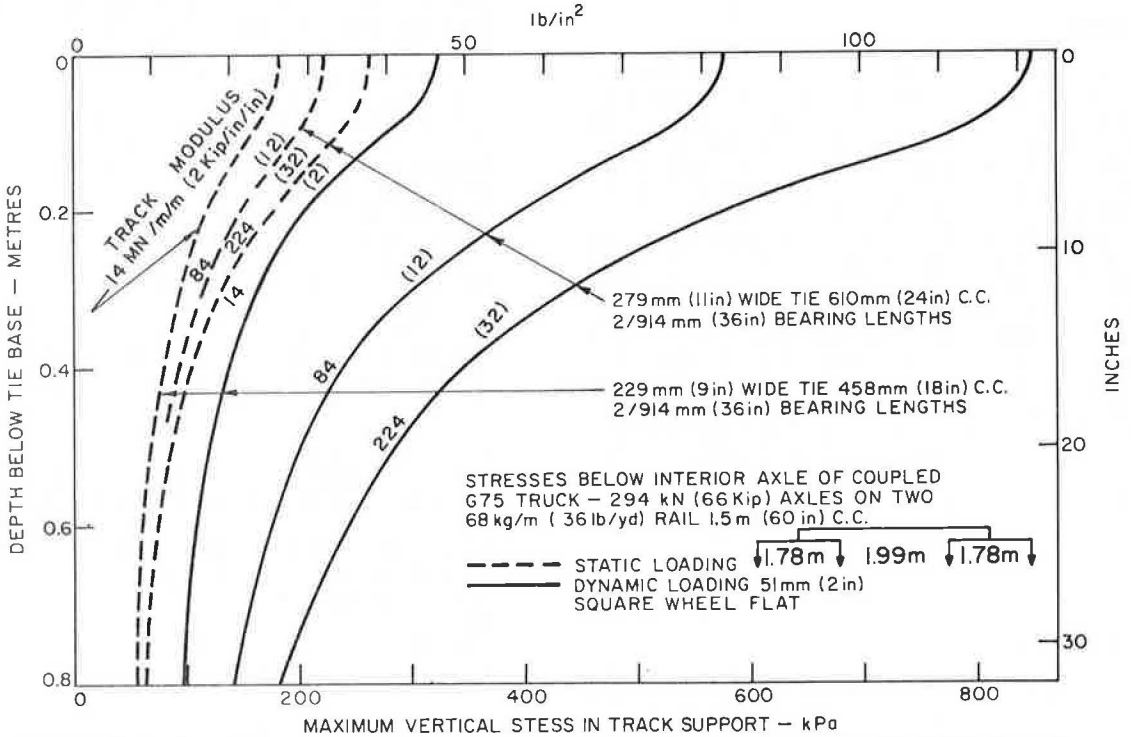

FIGURE 15 Static and dynamic loading from 51-mm (2-in.) square wheel flat effect on calculated vertical track support stresses.

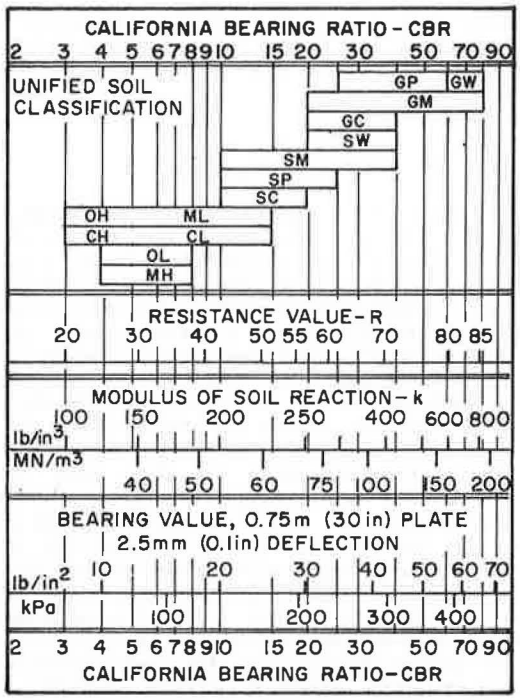

FIGURE 16 Safe bearing stresses developed for highway and airport design *(9)*.

are conservative limits for use in track support subgrade design and could probably be increased 50 percent. In addition, where climatic conditions result in freezing temperatures, minimum granular cover equal to at least half the depth of frost penetration is generally specified.

BALLAST STRESSES

It is quite obvious from the data presented that as the track modulus increases, so do the stresses in the ballast, particularly those close to the crosstie bearing area. Because a higher modulus is associated with concrete crossties than with wood crossties, it is not surprising that higher quality ballast is generally specified when concrete crossties are used. In addition, most concrete crossties are made with silica sands composed of minerals having a Mohs hardness greater than 6. To prevent mineral-to-mineral abrasion, or ballast powdering at the crosstie surface, the ballast must be composed of minerals of similar hardness. Thus ballast for concrete crossties must be obtained from hard mineral tough aggregate. This is best assured by conducting "thin section analysis" on proposed aggregate sources. Thin section analysis also enables the rejection of aggregates that have extensive micro-fractures and former fractures bonded with weak secondary minerals that weather quickly.

SUMMARY AND CONCLUSIONS

A design methodology for calculating stresses below conventional railway crosstie tracks has been presented. Rail seat loads were calculated from the beam on elastic support. The rail seat loads were assumed to cause a rectangular pressure distribution on the ballast from which stresses were calculated using isotropic elastic theory for the distribution of stresses. These stresses were used to calculate strains on the basis of pseudoelastic properties for the different soil layers. The resulting deformations that were calculated to increase with an increase in track modulus were compared with the deformations from beam on elastic support theory whose deformations decrease with an increase in track modulus. It is suggested that the best design track modulus occurs where both solutions result in the same deformations (assuming correctness of estimated component track properties). An optimum track modulus based on static loading is suggested to occur at about 35 to 70 MN/m^2 (5 to 10 $kip/in.^2$) of rail, and this is regarded as possibly too high on the basis of dynamic loading for present (1985) North American track and vehicle standards.

It is shown theoretically that the variation of track modulus has a major effect on the track component stresses and that limited field data support the theoretical conclusions.

ACKNOWLEDGMENT

The work reported forms part of general studies funded partly by Canadian Pacific Rail, Canadian National Rail, Via Rail, and Transport Canada Research and Development Centre through the Canadian Institute of Guided Ground Transport and partly by the Natural Science and Engineering Research Council of Canada.

REFERENCES

1. Stresses in Railroad Track--The Talbot Reports. American Railway Engineering Association, Washington, D.C., 1980 (reprint of Report of the Special Committee on Stress in Railroad Track, 1918-1940, A.N. Talbot, chairman).
2. Manual for Railway Engineering. American Railway Engineering Association, Washington, D.C., Vols 1 and 2, 1984.
3. A.E.H. Love. The Stress Produced in a Semi-Infinite Body by Pressure on Part of the Boundary. Philosophical Transactions of the Royal Society, Series A, London, England, Vol. 228, 1928, pp. 377-420.
4. L.T. Kenney. Steady State Vibrations of Beam on Elastic Foundation for Moving Load. Journal of Applied Mechanics, Vol. 76, 1954, pp. 359-364.
5. Effect of Flat Wheels on Track and Equipment: Abstract of Report of Mechanical and Engineering Divisions of the Association of American Railroads. Bulletin 53, American Railway Engineering Association, 1952, pp. 423-448.
6. F.E. Dean, D.R. Ahlbeck, H.D. Harrison, and J.M. Tuten. Effect of Tie Pad Stiffness on the Impact Loading on Concrete Ties. Proc., 2nd International Heavy Haul Conference, Pueblo, Colo., 1982.
7. D.R. Ahlbeck, H.D. Harrison, R.H. Prause, and M.R. Johnson. Evaluation of Analytical and Experimental Methodologies for Characterization of Wheel/Rail Loads. Interim Report PB 272 063. U.S. Department of Transportation, 1976.
8. Manual of Standards and Recommended Practice, Section G, Part II, Wheel and Axle Manual. Association of American Railroads, Washington, D.C., 1984.
9. Soil Primer Handbook. Portland Cement Association, Chicago, Ill., 1956.

Publication of this paper sponsored by Committee on Mechanics of Earth Masses and Layered Systems.

New Method of Simulating Layered Systems of Unbound Granular Material

W. O. YANDELL

ABSTRACT

The stress-strain analysis of multilayered pavements is becoming more precise--commencing with elastic solutions and developing through the more complex finite element analyses. The mechanolattice has been reasonably successful in predicting pavement performance because it takes relative plastic behavior into account. Recently, an option was developed that enables the mechanolattice to simulate any unbound granular layers in pavement. The principles of operation of the unbound simulation are described and its effects demonstrated using Sections 2 and 9 of the Pennsylvania State Test Track. The effects predicted with the "all bound" assumption are contrasted with those in which unbound layers are simulated as unbound. It is pointed out that the differences are functions of modulus ratios and the magnitude of relative plastic behavior. Many of the effects are not dependent on the absence of creep or relaxation.

Most modern pavement design and rehabilitation systems have used the theory of linearized elasticity to carry out the structural assessment of multilayered flexible pavement (1-2). Period of loading or temperature, or both, have sometimes been taken into account to simulate so-called visio-elasticity. The Council for Scientific and Industrial Research in Australia has produced investigatory stress-strain analyses such as CIRCLY and PAVAN that consider such things as cross-anisotropic materials and stress-dependent elastic moduli.

The author, recognizing the need to consider the plastic components as well as the elastic components of load-deformation behavior, developed the mechanolattice stress-strain analysis for multilayered elasto-plastic pavements (3-10). He used this to investigate the effects of the build-up of residual stresses and strains. However, the original version, like other techniques, was only suitable for bound road materials. Because some layers or the subgrade, or both, consist of unbound granular material an option was built into the mechanolattice package to enable selected layers to be treated as unbound and incapable of resisting tensile stresses.

A simple demonstration of one form of differing behavior resulting from lower layers being bound or unbound is shown diagramatically in Figure 1. A line load is applied to two-layer systems supported on rigid foundations. The upper layers are elastic and the lower are elasto-plastic. When the line loads are released there are two different outcomes. Figure 1(a), in which the lower layer is considered bound, shows a permanent deformation of the upper elastic layer with residual tension in the bottom surface and residual compression in the top. In contrast, Figure 1(b), in which the lower layer is considered unbound, shows that the elastic layer is able to spring up leaving a space under it but has no residual stress. Also, this form of behavior would obtain if both layers were bound but not bound to each other. This is of course a gross oversimplification when considering the greater realism of the mechanolattice analysis.

The mechanolattice multilayered analysis for bound material, followed by the unbound granular simulation option, is briefly described.

Comparisons are made between field observations and bound and unbound based predictions. Sections 2

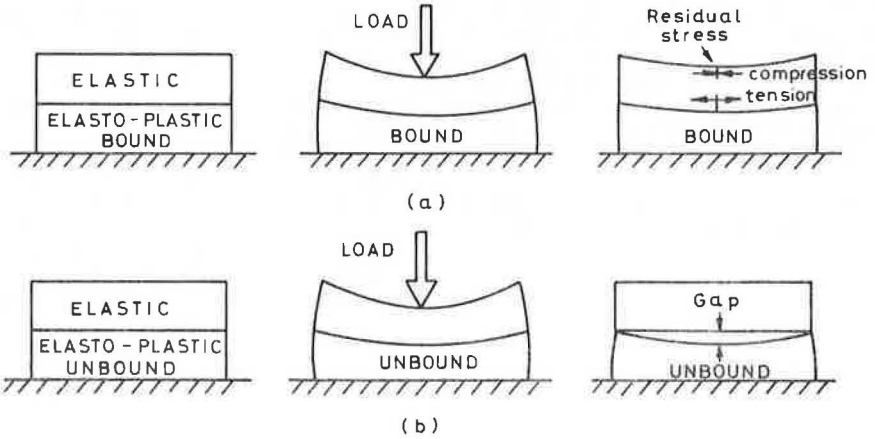

FIGURE 1 Differing behavior with bound and with unbound lower layer.

and 9 of the Pennsylvania State Test Track are used for comparison purposes.

MECHANOLATTICE ANALYSIS

The mechanolattice analysis has been described fully elsewhere (5-10). When it is applied to multilayered roads each layer is considered to be elasto-plastic. Figure 2(a) shows by broken lines the repeated loading on a load deflection plot for a hypothetical triaxial test. It will be observed that the residual deflections accumulate as repeated loading continues. To simplify computation the load-unload curves are simulated by straight lines. Possible load deflection behavior is shown in Figure 2(b).

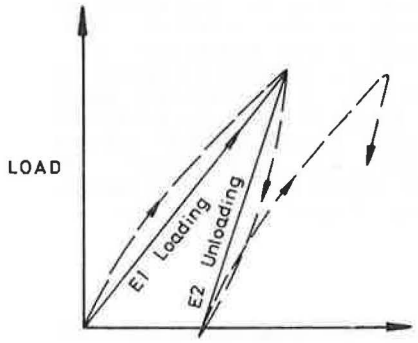

(a) Simplification of Elasto-plastic Hysteresis Loop

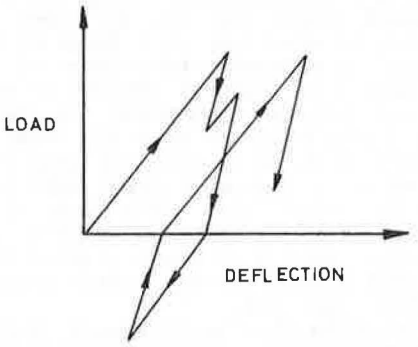

(b) Possible Load-Deflection Behavior of an Element

FIGURE 2 Elasto-plastic behavior.

To solve a problem, a type of three-dimensional mechanolattice unit was developed to simulate the behavior shown in Figure 2. The cube shaped units consist of straight line members that have different loading and unloading compliances. Figure 3 shows separately the volumetric and rectilinear elements in one view [Figure 3(a)] and the shear elements in the other [Figure 3(b)].

About 3,300 of these units are joined to simulate Section 9 of the Pennsylvania State Test Track as shown in Figure 4.

SEQUENTIAL TECHNIQUE FOR SOLUTION

Figure 5 shows a longitudinal section of the simulated pavement through the load. The units on the extreme left side, shown by broken lines, represent the initial conditions before a particular wheel pass. Elastic theory is used for predicting the

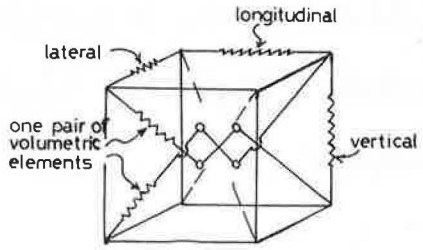

a. Volumetric and Rectalinear Elements

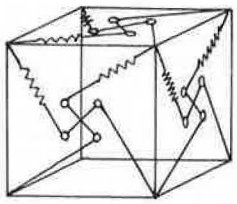

b. Shear Elements

FIGURE 3 Three-dimensional mechanolattice unit.

shape of each unit as it arrives at the simulating region from the residual no-load condition well forward of the "present" load. The consequent change in unit shape will cause the elements to change in length and therefore change their element load also. Similar things happen when the "wall" of units moves another place closer to the load. Thus, as the sequential movement of the wall of units from left to right--toward, under, and away from the load--takes place, the load-deflection history of each element is followed mathematically. This is done by calculating changes in length and changes in load with the aid of the stiffness factors. A permanent inventory of element loads is kept up to date.

Figure 5 also shows the sequential loading of a typical element of a unit as the load traverses from right to left--the three-dimensional problem is solved by imagining that the pavement structure moves from left to right with the wheel load considered to be fixed in position. For example, an element of units 1, 2, 3, and 4 has already been subjected to a loading history from previous wheel passes and as a result there is a residual stress state represented by point "a" of the inset figure of Figure 5. As the unit moves relative to the wheel from position A to position B the element becomes subject to a load level represented by point "b." Thus, as the load completely traverses the pavement, the loading of the element follows the path of a, b, c, d, e, f, and g, thus leading to a residual load. Similar behavior occurs in the other 27 elements of a unit as it moves toward, under, and away from the wheel load.

The computer program performs a similar, though more complex, task after each cycle of element length-load calculation in which the forces at each joint emanating from their attached elements are resolved into vertical, longitudinal, and lateral components. The joint is then moved in a damped manner in the direction of the unbalanced forces. The calculation damping factor is proportional to the largest force that is instantaneously out of balance at any free joint. The process is continued until all out-of-balance forces of free joints become insignificant. For this problem, between 1,500 and 2,000 computation cycles are needed. After convergence and after stresses have been calculated, the

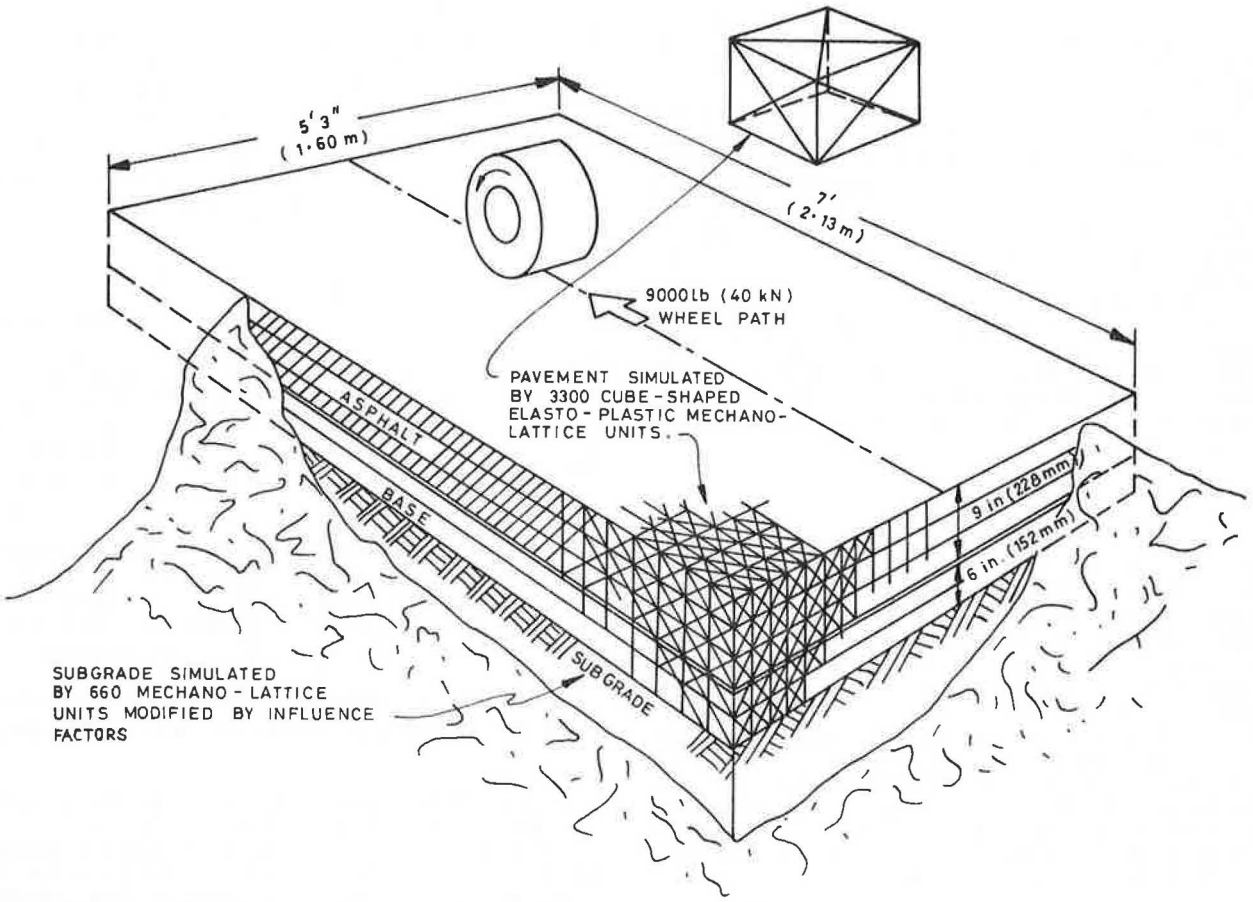

FIGURE 4 Simulation of pavements by assemblies of cube-shaped mechanolattice units.

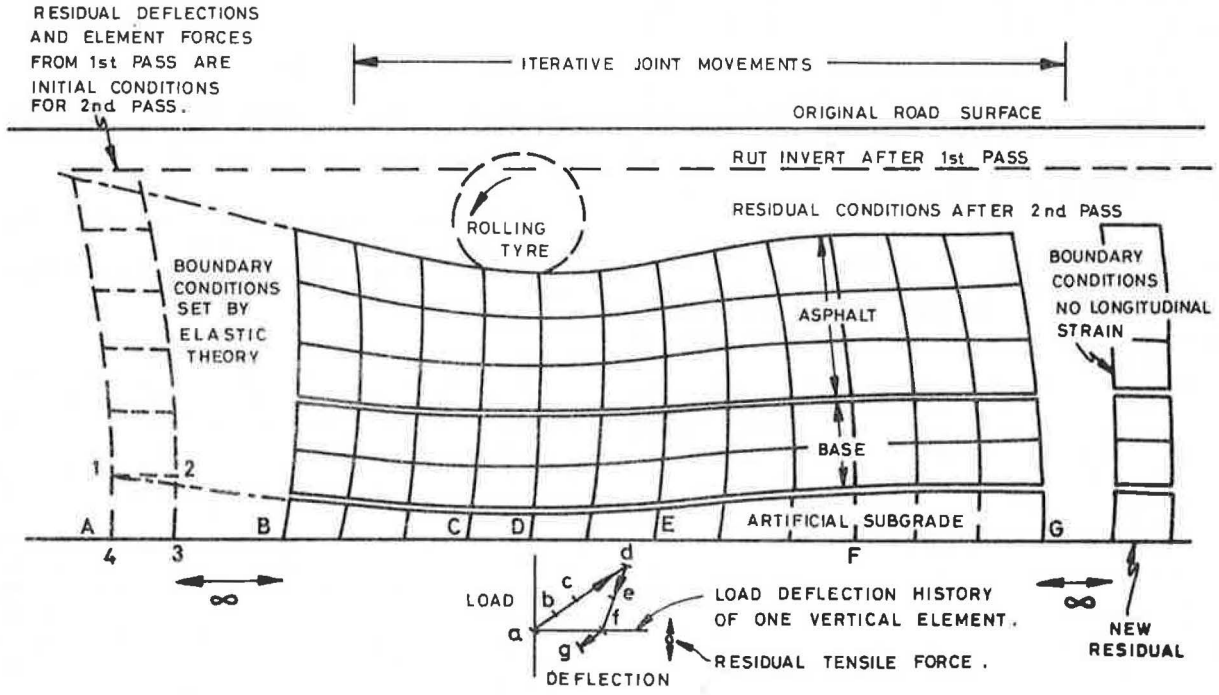

FIGURE 5 Diagramatic longitudinal section of a three-dimensional pavement analysis showing boundary conditions.

wall of units on the right of Figure 5 (in the residual condition) is used as initial conditions for the next simulated wheel pass and the process is repeated.

The foregoing techniques can be used to simulate the behavior of other materials such as elastic, perfectly plastic, and nonplastic energy absorbing material subject to gross deformation (11). The mechanolattice analysis is a rigorous technique that preserves equilibrium and has strain compatibility although some of the boundary conditions do involve approximations.

The stiffness factors of the elements are calculated by frame analysis. The loading moduli are determined from creep compliance tests (12). The unloading moduli [Figure 2(a)] are calculation expedients to set the relative plastic behavior. The plastic behavior is determined from repeated load triaxial tests (12).

UNBOUND OPTION

Although the mechanolattice technique may offend some because it does not employ classical mathematics, finite difference, or finite element techniques, it is rigorous, preserving both equilibrium and continuity. It also has a great advantage in its adaptability to a wide range of material property simulations with a minimum of extra computational effort. Thus the simulation of unbound granular material behavior is relatively simple.

The simulation will allow the material to crack when subject to tensile stress. Recompression will not start until the crack has fully closed. The incidence of cracking in a particular direction depends on the following preconditions:

1. The forces in the volume diagonals [Figure 3(a)] become tensile or the sum of the lengths of those four diagonals becomes greater than that obtained in the initial condition, or both (Figure 5). Then and only then will the forces in those diagonals be assumed equal to zero.
2. Also then and only then will the simultaneous occurrence of a tensile force in a horizontal, vertical, or lateral element lead to a crack opening in that direction.
3. Also, no increments of force can be added at the passage of an increment of time (moving from left to right in Figure 5) when condition "a" occurs cojointly with that element being longer at that instant than at the initial condition (left side in Figure 5). This ensures that recompression does not occur until the crack closes.

This logic is shown diagrammatically in Figure 6. The author has taken the liberty of assuming that shear stress can still be resisted when small cracks occur in that plane in this simulation of granular unbound material.

A pavement is analyzed by first solving the sequential multilayer problem assuming all layers are bound. The unbound criteria for base and subgrade are then invoked and an additional 1,000 iterations are made to achieve convergence once again. The cost per wheel pass is $87 on a central digital computer 76; the time required is 15 min. Cost of a full life prediction would be about $250.

Because the author is not aware of solutions to this type of problem by established finite element analysis, comparisons with it are difficult. However, finite element solutions to, for example, nonlinear problems of similar size are partly iterative and would take about 5 min. on a similar machine. Convergence of the mechanolattice is being

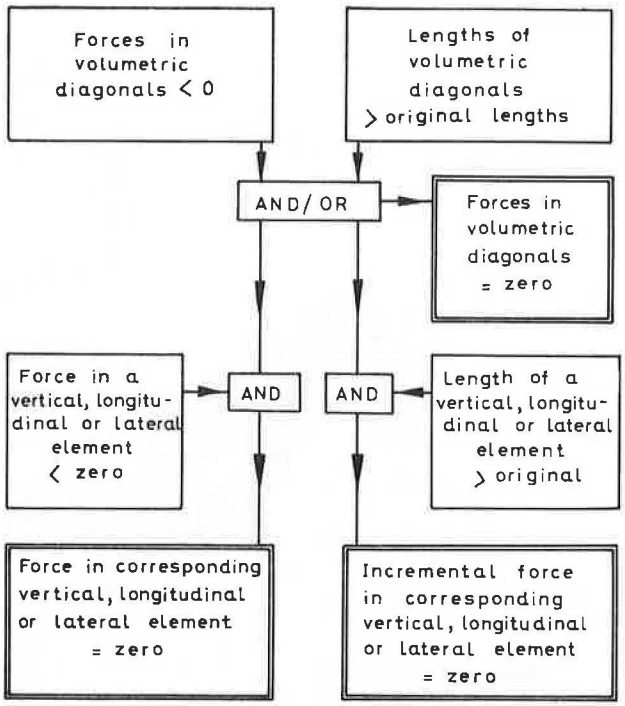

FIGURE 6 Flow diagram for unbound granular material option.

improved. Finite element analysis has the advantage of being more widely used and understood and the disadvantage of being less adaptable to pavement problems and, so far, not being able to solve this type of problem. When the loading and unloading moduli are made equal the mechanolattice gives close agreement with other elastic analyses. The analysis has been used successfully for predicting the rutting and horizontal flow behavior of an indoor test track (7), the phenomenonological investigation of asphaltic concrete (A/C) cracking (13), and the behavior of two test roads in Sydney (14,15).

EFFECT OF TREATING SOME LAYERS AS UNBOUND

Rutting and fatigue cracking behavior are compared for the two analyses of Sections 2 and 9 of the Pennsylvania Test Track as follows:

1. All three materials are considered by the mechanolattice analysis to be bound.
2. The subbase and subgrade are considered unbound.

Section 9 is obviously not a representative case because its asphaltic concrete layer acts with less plasticity than its subbase and subgrade and the difference in predicted effects between the bound and the unbound assumption is great. In contrast, Section 2 of the same test track has all layers acting with closer plasticity and the treating of some layers as unbound instead of bound has little effect on predicted fatigue and rutting. Plastic behavior for a particular layer and material may be represented here by the residual deflection shown in Figure 2(a). Such behavior is a function of the repeated stress and of the loading and the unloading modulii. In Section 2 these residual strains are of a similar magnitude for each layer whereas in Section 9 they are largest for the lower layers.

Rutting

Figure 7 shows by half cross section a comparison of rutting after a few standard axle passes predicted by (a) assuming bound material (full lines) and (b) assuming the subbase and subgrade of Section 9 are unbound (broken lines).

It will be noted that the absolute rutting (or settlement) and straight-edge rutting is less at the surface when the unbound option is used. But rutting at the top of the subgrade and subbase is much greater with the unbound option, leaving an increasing horizontal gap between the asphaltic concrete and the subbase as each wheel passes. The gap, which was due to the asphaltic concrete behaving less plastically than the subbase and subgrade, could not occur when all layers were assumed bound in themselves and to each other. The asphaltic concrete then held the subbase and subgrade up and suffered greater permanent rutting itself. Horizontal gaps or cracks similar to these were observed by the National Institute of Transport and Road Research in South Africa (C.R. Freeme, NITRR, personal communication, 1984).

Figure 8 shows a comparison between rut prediction and rut measurements for up to 1.5 x 10^6 standard axle passes. It will be noted that the straight-edge rutting for the all-bound cases is seven times as great as for the unbound case whereas the absolute rutting is only one and one-half times as great. This is because the unbound subbase and subgrade had not the tensile strength to maintain the residual curvature in the asphaltic concrete layer. Figure 9 shows a similar comparison for Section 2. In contrast to the behavior in Section 9 there is little difference between rutting predictions in the bound and unbound cases. This is due to the more uniform plasticity between layers.

Fatigue Life

A comparison of lateral stresses in half cross sections under the traveling wheel load in Section 9 is

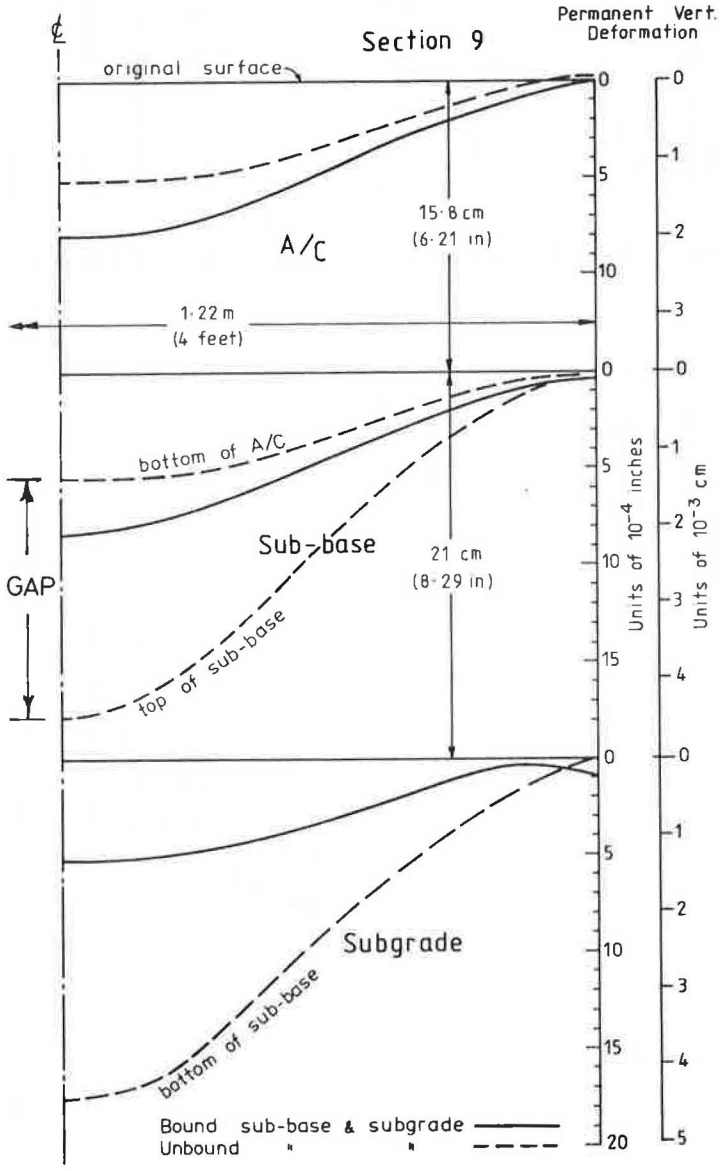

FIGURE 7 Rutting cross sections of Section 9 with bound and unbound subbase and subgrades.

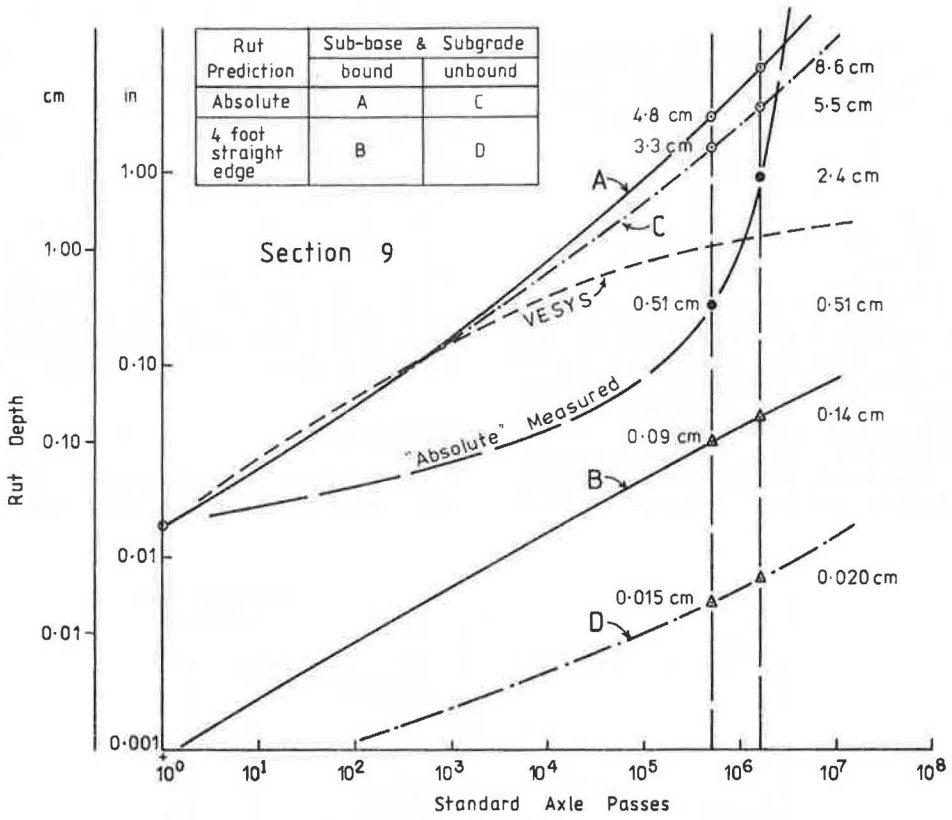

FIGURE 8 Comparison of VESYS- and mechanolattice-predicted rutting with measured rutting in Section 9.

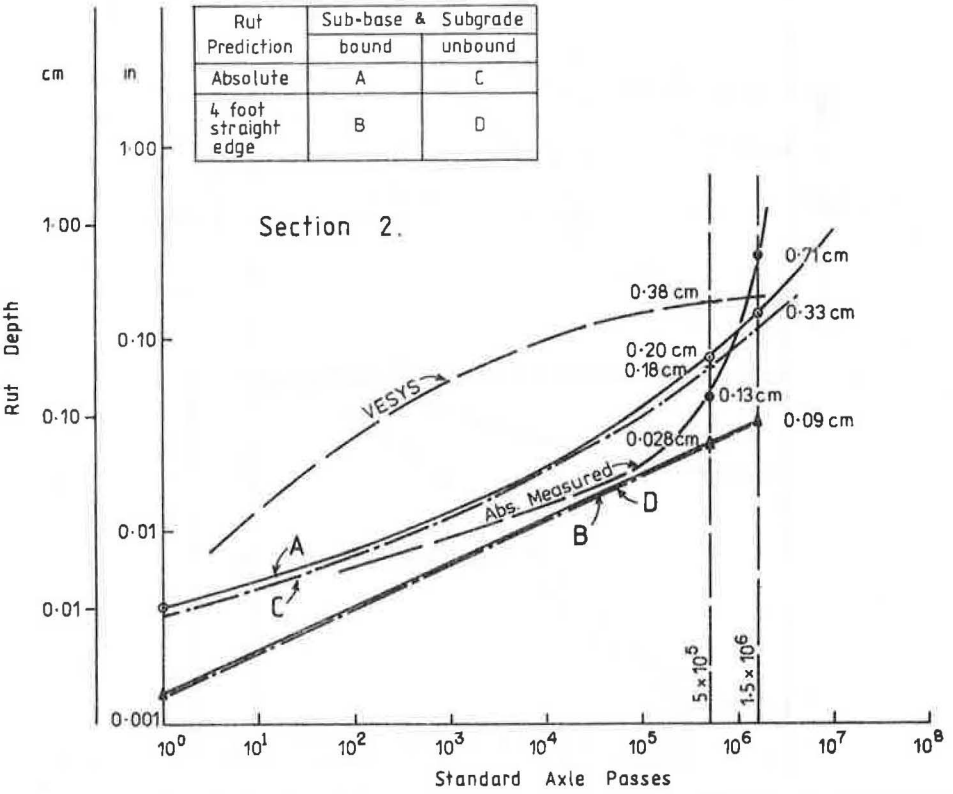

FIGURE 9 Comparison of VESYS- and mechanolattice-predicted rutting with measured rutting in Section 2.

shown in Figure 10 for the third standard axle pass. It will be noted, in the bound case, that tensile lateral stresses occur at the bottom of the subbase under the wheel path. However, as expected, no tensile lateral stresses exist in the subbase for the assumed unbound case. This means the subbase has no beam action to distribute the load laterally so the asphaltic layer has a greater imposed bending moment, increasing the bottom fiber tensile stress from 77 psi to 88 psi.

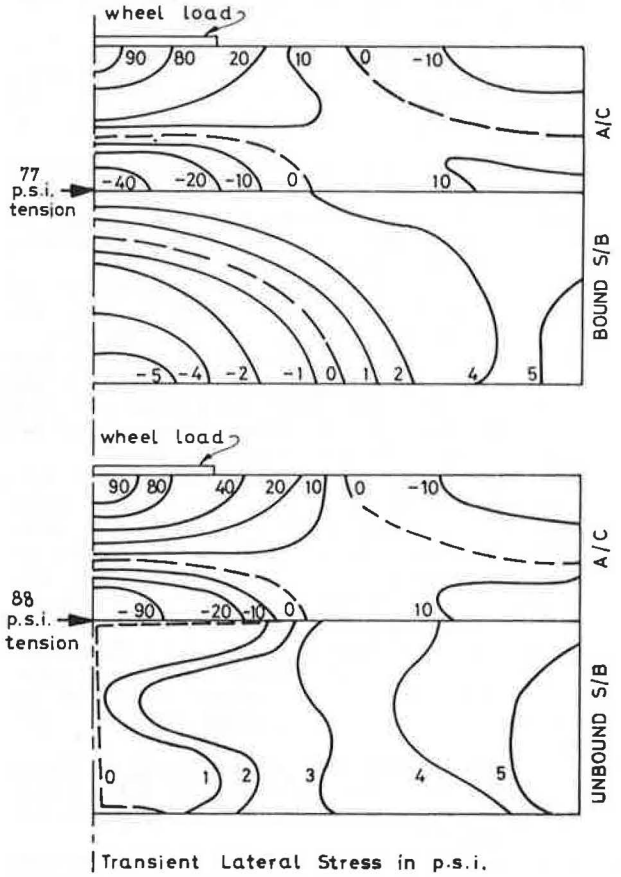

FIGURE 10 Half cross sections of transient lateral stress patterns in Section 9 under the moving load (a) with bound and (b) with unbound subbase and subgrade.

Figure 11 shows that part of the fatigue envelope chart near fatigue life end. Repeated $\log_{10}$ (lateral strain) is used as ordinate by convention. The strains are elastic equivalents to calculated stresses using the loading Young's modulus for the conversion. The radial stress at the bottom of the A/C increases with axle passes in Section 9 due to the accumulation of residual tension there, and the predicted life is thereby shortened. This is due to the A/C acting less plastically than the lower layers.

In Section 2 all layers acted with similar plasticity so small tensile residual stresses accumulated in the bottom of the A/C so the fatigue life was not shortened greatly (Figure 11). However, the fatigue life in the unbound case was shorter than in the bound case. This behavior is opposite to that of Section 9.

In Section 9, although the lateral tensile stress in the bottom of the asphaltic concrete is initially larger in the case of unbound lower layers, it increases at a lower rate because the accumulating residual tensions are less, which leads to a longer fatigue life as shown in Figure 11. This can be explained as follows: because the A/C is able to spring up after each wheel passes, it goes through greater ranges of stress and hence accumulates more residual tensile strain thus relieving accumulating tensile stresses. It will also be noted from Figure 11 that the size and shape of the contact patch have a great effect on fatigue life.

CONCLUSION

Any precision that the mechanolattice analysis may have could be partly due to its taking the elasto-plastic behavior of each material directly into account as well as to its simulating the loaded wheel as traveling in one direction. However, it was seen here that treating the unbound layers as unbound has brought this analysis closer to reality--as it would any analysis. It is ironic that having an

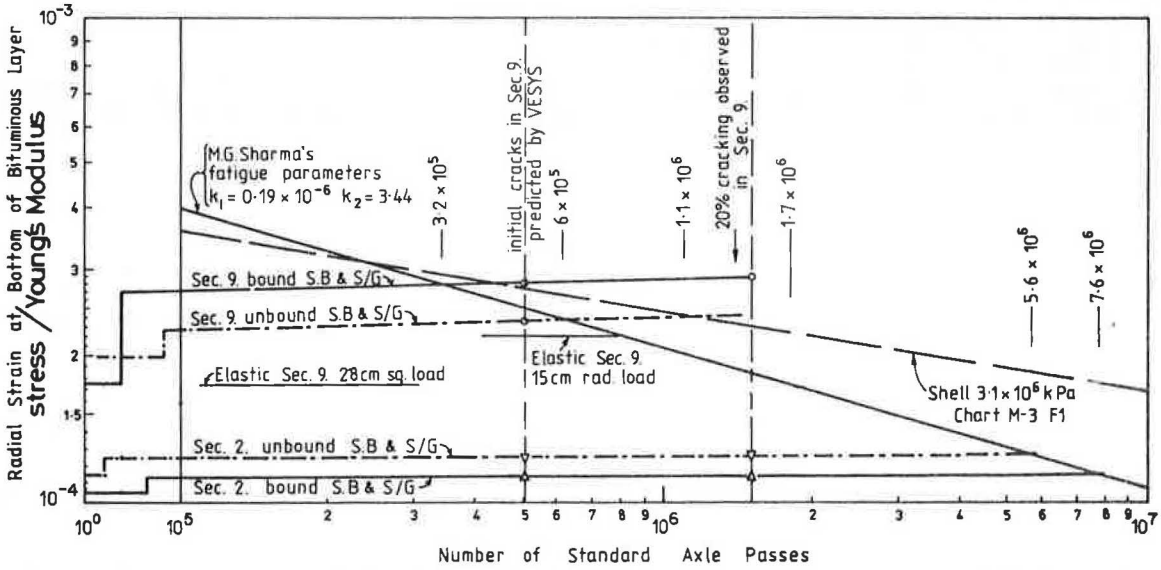

FIGURE 11 Part of the $\log_{10}$ (equivalent elastic strain in bottom of A/C) versus $\log_{10}$ (number of standard axle passes) with superimposed fatigue cracking envelope.

unbound base and subgrade in certain cases apparently extends the fatigue life of the asphaltic concrete by giving it a greater plastic behavior. However, other possible effects of these greater strain cycle ranges are unknown.

The effect of introducing the unbound option varies with the relative plastic behavior between the layers and with the modular ratios. In contrast to those of Section 9 the behavior predictions of Section 2 of Pennsylvania State Test Track were relatively insensitive to the unbound option.

It should be noted that the unusual behavior predicted in Section 9 with the unbound option of the mechanolattice analysis does not depend for its validity on the absence of creep or stress relaxation.

The computer programs used here and user manuals should be generally available by early 1985.

ACKNOWLEDGMENTS

Appreciation is extended to the Australian Research Grants Committee for the financial support of this work and to I.K. Lee for his encouragement.

REFERENCES

1. A.I.M. Claessen et al. Asphalt Pavement Design--The Shell Method. Proc., 4th International Conference on Structural Design of Asphalt Pavements, Ann Arbor, Mich., 1977.
2. W.J. Kenis. A Design Method for Flexible Pavements Using the VESYS Structural Sub-System. Proc., 4th International Conference on Structural Design of Asphalt Pavements, Ann Arbor, Mich., Vol. 1, 1977, pp. 101-118.
3. W.O. Yandell. The Prediction of the Behaviour of Elastoplastic Roads During Repeated Rolling Using the Mechano-Lattice Analog. In Highway Research Record 374, HRB, National Research Council, Washington, D.C., 1971, pp. 29-41.
4. W.O. Yandell and R.L. Lytton. Residual Stresses Due to Travelling Loads and Reflection Cracking. Report FHWATX79-207-6. Texas Transportation Institute and Texas Department of Highways and Public Transportation, College Station, Texas, June 1979.
5. W.O. Yandell and R.L. Lytton. The Effect of Residual Stress and Strain Build-Up in a Flexible Pavement by Repeated Rolling of a Tyre. Report RF4087-1. Texas Transportation Institute, College Station; American Trucking Associations, Alexandria, Va., Oct. 1979.
6. W.O. Yandell. Residual Stresses and Strains and Fatigue Cracking. Journal of the Transportation Engineering Division, ASCE, Vol. 108, No. TE1, Jan. 1982, pp. 103-116.
7. W.O. Yandell. Measurement and Prediction of Forward Movement and Rutting in Pavements under Repetitive Wheel Loads. In Transportation Research Record 888, TRB, National Research Council, Washington, D.C., 1982, pp. 77-84.
8. W.O. Yandell. Possible Effect of Relative Plastic Behavior on Pavement Life. In Transportation Research Record 930, TRB, National Research Council, Washington, D.C., 1983, pp. 86-90.
9. W.O. Yandell. The Use of the Mechano-Lattice Analysis to Investigate Relative Plastic Behavior. Proc., International Conference on Constitutive Laws for Engineering Materials, University of Arizona, Tucson, Jan. 1983.
10. W.O. Yandell. Mechano-Lattice Prediction of Pavement Performance. Proc., CAPSA, Capetown, South Africa, March 12-16, 1984, pp. 201-215.
11. W.O. Yandell. The Measurement of Surface Texture of Stones with Particular Regard to the Effect on the Frictional Properties of Road Surfaces. Ph.D. dissertation. University of New South Wales, Sydney, Australia, 1970.
12. M.G. Sharna, W.J. Kenis, T.D. Larson, and W.L. Gamling. Evaluation of Flexible Pavement Methodology Based upon Field Observations at Pennsylvania State University Test Tract. Proc., 4th International Conference on Structural Design of Asphalt Pavements, Ann Arbor, Mich., Vol. 1, 1977, pp. 158-174.
13. F. Hugo and T.W. Kennedy. New Design Considerations for Improved Asphalt Pavement Life. Proc., 4th Conference on Asphalt Pavements for Southern Africa, Vol. 1, March 1984, pp. 100-114.
14. P. Clarke. Report on the Road Trial at Church Lane, Prospect, Between 1979 and 1982. M.E.S. thesis. University of New South Wales, Sydney, Australia, 1982.
15. R.B. Smith. Comparison of Predicted Performance of Two Full Scale Crushed Rock Pavements using Mechano-Lattice Analysis with Field Performance During Initial Service Life. M.E.S. thesis. University of New South Wales, Sydney, Australia, 1984.

Publication of this paper sponsored by Committee on Mechanics of Earth Masses and Layered Systems.

Pavement Design Based on Shakedown Analysis

RICHARD W. SHARP

ABSTRACT

The realistic analysis of pavement performance requires an approach that recognizes the incremental mode of failure of such structures when subjected to repeated moving loads. The theory of structural shakedown provides such an approach. Procedures for the analysis of the shakedown of layered continua are developed. Parametric studies demonstrate the application of the analysis to representative problems, and the results of field studies are examined. It is found that pavement shakedown may be both observed and accurately predicted. A more general relationship between pavement life and shakedown predictions is formulated; the theory is applied to typical design problems, and a generalized design procedure is presented.

For economic reasons pavements are required to perform at stress levels that exceed the elastic limit of their constituent materials. Further, such stress levels may be repeated 10^6 or more times during the 15- or 20-year life of the structure. Failure, therefore, occurs by gradual deterioration not sudden collapse.

In modeling structural behavior, it is important that the analysis take into account the progressive accumulation of permanent strains during a pavement's service life. Recognition of the incremental model of failure permits the exploration of the substantial reserve of strength that exists between the elastic limit and the point of static collapse.

Many authors have recognized that repeated loading may induce failure of a body through the gradual accumulation of permanent deformation at particular locations. Ultimately, material breakdown may occur, resulting in failure by "incremental collapse." Other load sequences may instead induce yielding alternately in compression and tension, with an "alternating plasticity" failure as the final result. Alternatively, a load sequence may be such that after a certain number of load cycles no further permanent strains develop and the material subsequently responds elastically. In this case, the body is said to have undergone "shakedown" by a process of adaptation. This approach lends itself particularly to the analysis of pavements, in which incremental collapse is frequently observed. It is reasonable to expect that a pavement's life under traffic will be directly related to its resistance to incremental failure--and under ideal conditions, a satisfactory pavement will be one that shakes down.

The theory of shakedown, first presented by Melan (1), has been widely applied to discrete structures such as trusses and frames. Application to more complex structures has been confined primarily to plates (2-4), and it appears that apart from brief examinations of the problem of a long strip footing (5,6) no numerical applications of the theory to general continua have been made.

A method of analyzing the shakedown behavior of pavements is presented. Road test results demonstrate the application of this analysis to the prediction of pavement performance, and the paper concludes with a discussion of the design procedures that may be developed from such an approach.

PAVEMENT MODEL

The analysis of a general horizontally layered pavement subjected to wheel loads of varying magnitude, contact area, and spatial distribution represents a problem of considerable complexity. The following simplications have therefore been introduced:

1. The actual wheel loading (Figure 1) is approximated for plan strain pavement by a roller loading (Figure 2). In the most critical region, the vertical plane through the centerline of the wheelpath, stresses will be modeled reasonably accurately; elsewhere stresses may be somewhat overestimated. A conservative estimate of the load limit is therefore likely to be produced.

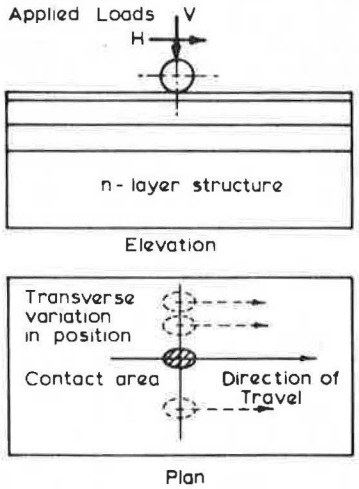

FIGURE 1 General three-dimensional pavement and loading.

2. A large number of passes of the roller may be expected to give rise to a pattern of permanent deformation that is uniform over any horizontal plane. The distributions of both permanent deforma-

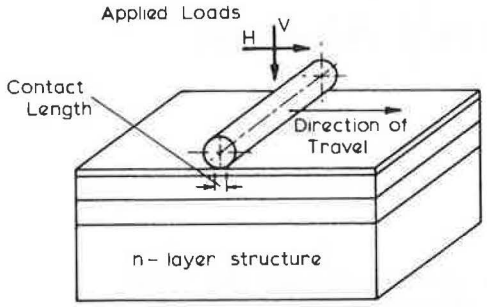

FIGURE 2 Plane strain pavement and loading.

tion and residual stresses thus become functions of depth only.

3. The observations of several authors (7-9) suggest that the longitudinal variation of normal stresses due to a pneumatic tire may realistically be approximated by a trapezoidal distribution shown in Figure 3. The distribution of longitudinal shear stresses is more variable; however, for constant wheel velocities a trapezoidal variation is again an appropriate first approximation.

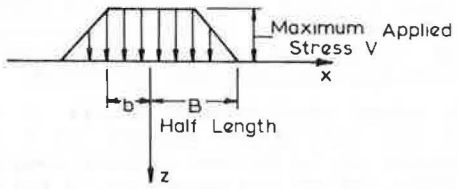

FIGURE 3 Definition of pavement loading.

4. The conventional parameters of elastic modulus (E) and Poisson's ratio (ν) serve as an adequate characterization of the stiffness of most pavement materials. More diversity of opinion exists regarding the description of material strength; the Mohr-Coulomb yield condition [parameters of cohesion (c) and angle of internal friction (ϕ)] does, however, appear to offer simplicity along with a realistic modeling of behavior. A more detailed survey and discussion are presented elsewhere (10).

SHAKEDOWN ANALYSIS OF PAVEMENTS

Algorithms for determining the shakedown limits of discrete structures have existed for some time and are generally based on the techniques of linear programming. Continuous structures, however, are not so readily treated, and a means of solution was first presented by Maier (11). This approach, which also employs linear programming, has been applied by Sharp (10) to determine the shakedown limit of a plane strain layered continuum subjected to repeated moving surface loads.

Although it represents a vast improvement over step-by-step methods of elastoplastic analysis, the linear programming approach suffers from several shortcomings when applied to continua. Most significant among these is that the computing effort is approximately proportional to the cube of the number of constraints, so program execution time increases alarmingly as the yield surface is more accurately modeled.

A method of analysis that overcomes this difficulty, and permits the true Mohr-Coulomb yield surface to be used, has been developed by Sharp (10). By considering stresses to consist of two components--elastic and residual--and adopting the convention of compressive stress positive, it is possible to reformulate the Mohr-Coulomb no-yield condition as

$$F(\sigma_{XR},\lambda) = a\sigma_{XR}^2 + 2h\sigma\lambda + b\lambda^2 + 2g\sigma_{XR} + 2f\lambda + k \geq 0 \quad (1)$$

where

λ = load factor,
σ_{XR} = residual direct horizontal stress,
$a = \cos^2 \phi$,
$h = -(\sigma_{ZE} - \sigma_{XE}) - \sin^2 \phi \ (\sigma_{ZE} + \sigma_{XE})$,
$b = (\sigma_{ZE} - \sigma_{XE})^2 + 4\tau_E^2 - \sin^2 \phi \ (\sigma_{ZE} + \sigma_{XE})^2$,
$q = -2c \sin \phi \cos \phi$,
$f = -2c \sin \phi \cos \phi \ (\sigma_{ZE} + \sigma_{ZE})$,
$k = -4c^2 \cos^2 \phi$,

and $(\sigma_{XE}, \sigma_{ZE}, \tau_E)$ represents the plan strain state of stress at Point P(x,z) due to unit applied load, c is material cohesion (≥ 0), and ϕ is material angle of internal friction ($0 \leq \phi < \pi/2$).

The region $F \leq 0$ encloses those combinations of load factor λ and residual stress σ_{XR} for which failure at P(x,z) will not occur. The boundary to this domain

$$F(\sigma_{XR}, \lambda) = 0 \quad (2)$$

may then be seen to represent a general conic section.

For analysis purposes, the region of interest at each depth zj is that common to the p sampling points $x_i : i = 1, 2...p$. That is,

$$\lambda_{zj} = \max [\lambda : F(\sigma_{XR}, \lambda, x_i, z_j) \leq 0, \ (i = 1, 2...p)] \quad (3)$$

Then the pavement shakedown limit (λ_{SD}) is given by

$$\lambda_{SD} = \min_j (\lambda_{zj}) \quad (4)$$

Figure 4 shows a number of typical domains $F(\sigma_{XR}, \lambda, x_i, z)$ and the determination of the value λ_z.

The determination of λ_{max} (x,z) may be most simply performed analytically by setting

$$d\lambda/d\sigma_{XR} = 0 \text{ in } F = 0$$

to yield

$$\lambda_{1,2} = c/(\pm\tau_E - \sigma_{ZE} \tan \phi) \quad (5a)$$

for

$$R_{1,2} = \left(c/\{\cos \phi[1 \mp (\sigma_{ZE}/\tau_E) \tan \phi]\}\right) \geq 0 \quad (5b)$$

A finite positive value of λ_{max} (x,z) = max (λ_1, λ_2) therefore exists in the region defined by ($\tau_E > \sigma_{ZE} \tan \phi$ or $\tau_E < -\sigma_{ZE} \tan \phi$). In many cases Equations 5a and 5b followed by the comparison $\lambda_Z = \min_x [\lambda_{max}(x,z)]$ are sufficient to obtain the required value. In other cases, as suggested by Figure 4, this test gives only an upper bound to λ_Z, and a simple algorithm to determine intersections of curves must be added to obtain the true value of λ_Z.

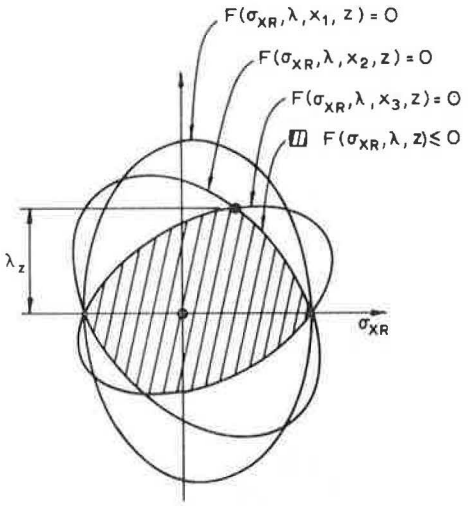

FIGURE 4 Typical shakedown domains for depth z and the determination of λ_z.

The shakedown limit for the continuum is then found by

$$\lambda_{SD} = \min_{z} (\lambda_z) \quad (6)$$

RESULTS AND GENERALIZATIONS

The analysis just presented has been used to determine the shakedown limits of a number of representative pavement structures. Results for a homogeneous half-space (various angles of friction) are shown in Figure 5. First yield and static collapse loads are included for completeness.

As a second example, Figure 6 shows values of the shakedown limit for a two-layer structure. The influence of layer thickness and relative layer stiffness on the structure's response to repeated moving loads is recorded, and the shape of the curves provides a pleasing consistency with observed behavior. For low values of surface layer stiffness, for example, little stress is attracted toward the surface, and fatigue of the subgrade tends to be the initial mode of failure. In contrast, extremely stiff surface layers themselves attract a large proportion of the stresses, caused by loading, and fatigue failure in this case is initiated within the top layer. A wide range of results is presented elsewhere (10), and further attention will be directed toward these in the discussion of design procedures that concludes this paper.

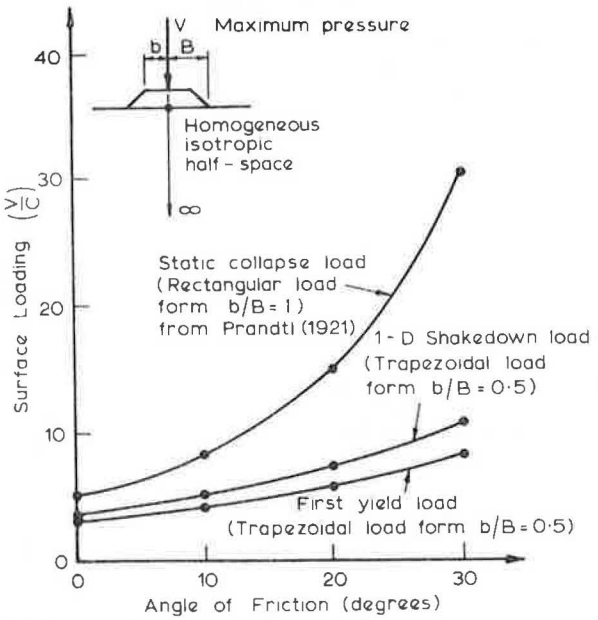

FIGURE 5 Influence of material friction angle on first yield, shakedown, and static collapse loads.

By way of verification, a more general "three-dimensional" analysis been also developed and implemented. Although this will not be given detailed attention in this paper, it should be noted that both uniform and layered continua have been analyzed using the more general approach.

It is evident from the results that the shakedown limit of a pavement derived by three-dimensional analysis may be closely related to that obtained using a plane strain approach. In this way, the approximations used in developing the latter have been shown to be appropriate. Further, the plane strain analysis not only provides a suitable approximation to the more elaborate approach but is also generally conservative in its estimates, yielding a lower bound to the true shakedown limit.

The advantages of the plane strain method are, therefore, considerable. Not only are its estimates safe and reasonably accurate, but its formulation is simpler conceptually and its execution faster. Indeed, for a typical pavement analysis, the time required in computing is of the order of one-hundredth of that consumed in a corresponding three-dimensional analysis. For parametric studies and the development of design charts, then, the plane strain approximation provides a tool of far greater convenience and is really the only practical approach.

CASE STUDY 1: THE AASHO TESTS

The AASHO Road Test, conducted in the late 1950s by the Highway Research Board (HRB) in the United States, provides a large and valuable body of data concerning pavement performance and its relationship to traffic loading and thickness design. Some of this information, fully documented in the HRB Special Reports 61, A-G (12), has been used to investigate the applicability of shakedown theory to the performance under traffic of asphaltic concrete pavements.

Table 1 gives the material strength and stiffness properties adopted for analysis, obtained from the HRB reports and an extensive testing program reported by Shook and Fang (13). Loading parameters are also included, the primary source of which information is Kent (14).

Pavement performance during the test was obtained by monitoring various indicators (rutting, cracking, patching, and longitudinal profile variations) and quantifying the measurements as a "present serviceability index" (p). The value of p may be regarded simply as a measure of pavement standard. For most pavement sections, p was found initially to be about 4.5, and the progressive deterioration of each section under traffic was reflected in declining values of p.

The performance of pavement is therefore given by the variation of p with time or number of axle applications. Failure was said to have been reached when p declined to a value of 1.5; shakedown may also be detected by a stabilizing of the value of p after a certain number of load applications. Typical performance trends, and the means by which relative performance may be defined, are shown in Figure 7.

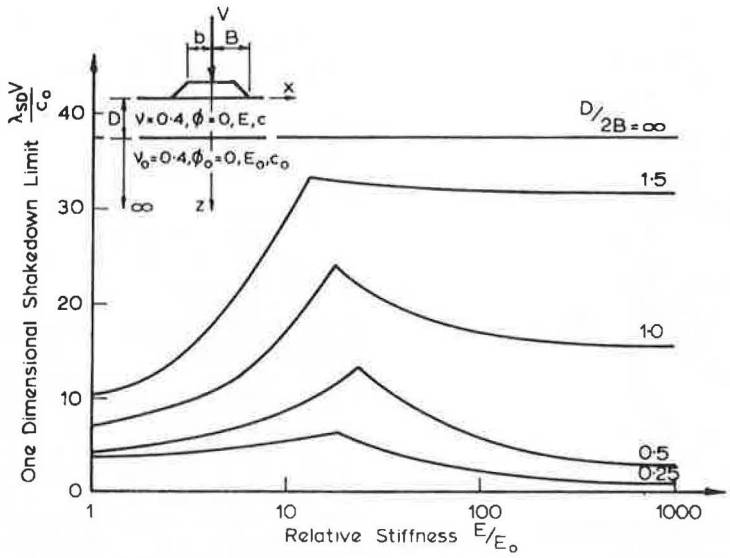

FIGURE 6 Influence of layer thickness on shakedown limit of two-layer pavement.

TABLE 1 Material and Load Parameters for AASHO Road Test Studies

Material	Elastic Parameters E MPa (ksi)	ν	Failure Parameters C kPa (psi)	ϕ°
Asphaltic Concrete	5000 (730)	0.4	4000 (580)	30
Base	85 (12)	0.3	40 (5.8)	55
Sub-base	50 (7.3)	0.3	30 (4.4)	45
Sub-grade	10 (1.5)	0.3	10 (1.5)	20

Configuration	Single			Tandem		
Load on Axle Group (tonnes)	8.2	10.2	13.6	14.5	18.1	21.8
Maximum pressure V kPa (psi)	570 (83)	570 (83)	610 (88)	530 (77)	570 (83)	610 (88)
Radius B mm (ins)	105 (4.1)	120 (4.7)	130 (5.1)	100 (3.9)	110 (4.3)	120 (4.7)

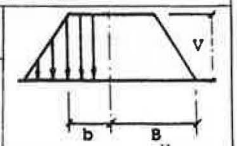

$\frac{b}{B} = 0.5, \mu = \frac{H}{V} = 0.4$

Pavement Loading (Plane Strain)

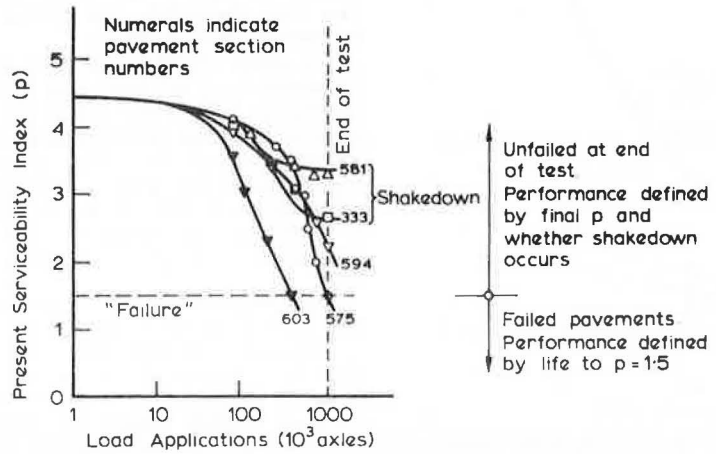

FIGURE 7 Typical performance trends—AASHO Road Test.

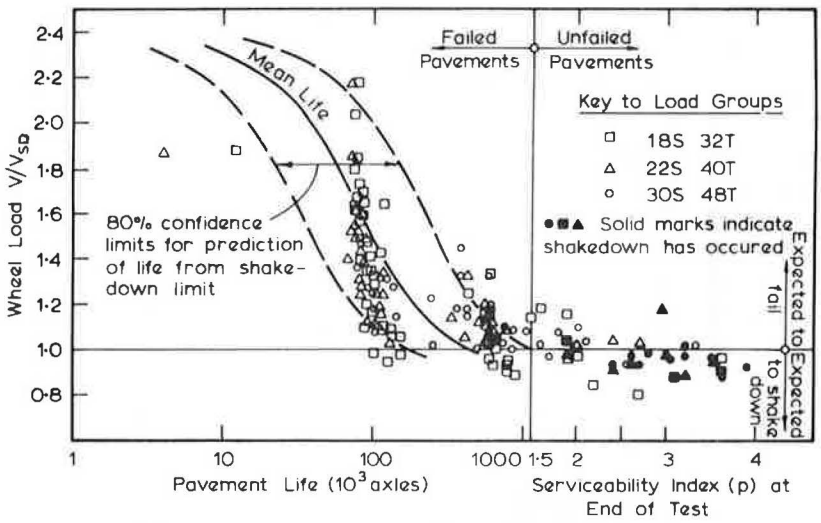

FIGURE 8 Pavement performance related to load ratio (V/V_{SD}).

Using the material and loading parameters as given, the 180 pavements comprising Loops 4, 5, and 6 of the Road Test were analyzed, and their shakedown limits, defined as the ratio of shakedown load to applied load (V_{SD}/V), determined. The shakedown limit, a measure of the fatigue strength of the pavement, may reasonably be expected to correlate with pavement life, and indeed this proved to be the case. For consistency with the S-N curves of fatigue studies, however, the approach adopted in Figure 8 was to plot dimensionless load (V/V_{SD}, the inverse of shakedown limit) against performance. Despite the scatter in the results (characteristic of fatigue tests generally and to be expected in view of typical material variability), Figure 8 clearly shows that a lighter loading or higher shakedown limit is associated with a longer life. More significant, the line $V = V_{SD}$ clearly may be used to distinguish between those pavements that failed ($V > V_{SD}$) and those that attained a stable state ($V < V_{SD}$). Also shown in the region $p > 1.5$ are those pavements that had neither failed nor reached shakedown by the end of the test; of these little can be said except that their relatively good performance is again associated with lower values of V/V_{SD}.

CASE STUDY 2: SYDNEY REGION

A second case study was undertaken with the aims of verifying the results obtained in Case Study 1, and examining the applicability of the shakedown approach to Australian conditions. The test program involved the sampling of failed pavements at 18 locations and the testing of material from each pavement layer to determine stiffness (E,ν) and strength (c,ϕ) parameters. Traffic life of the pavement was also determined from both field surveys and traffic volume records. Full documentation of the study is provided elsewhere (10).

Using the material properties and pavement profiles for each structure, a set of one-dimensional shakedown analyses was performed. Figure 9 shows these results plotted to relate pavement life to shakedown limit. The variations in results appro-

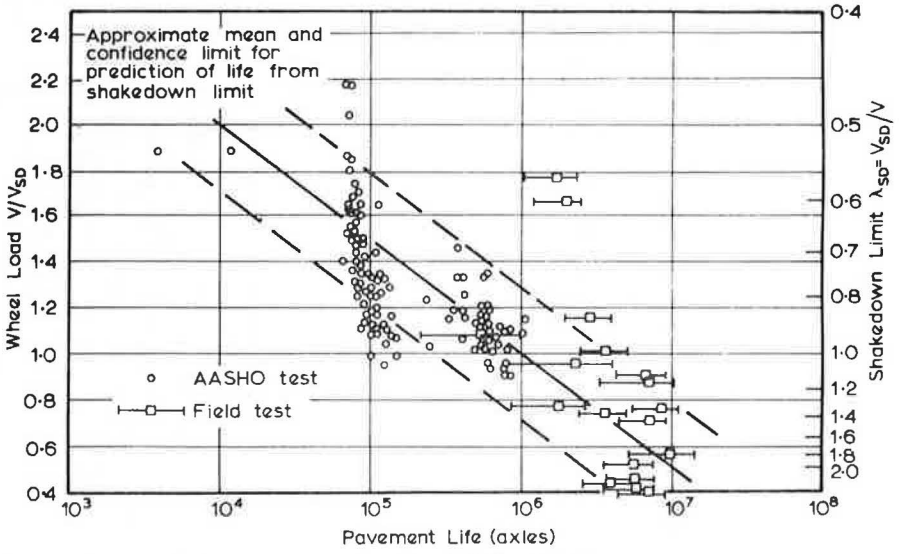

FIGURE 9 Pavement performance related to shakedown limit.

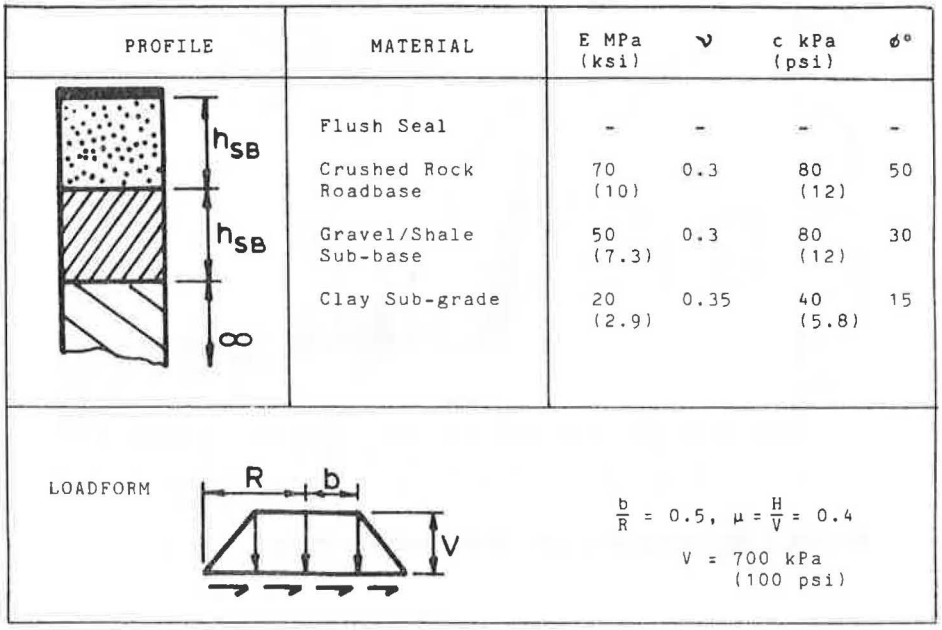

FIGURE 10 Flush-sealed pavement for development of design charts.

priate to certain sites are represented by error bars and the data from the AASHO Road Test are included for completeness. Although the possible magnitude of some errors is quite large, as might be expected for a field study of this type, the graph serves to demonstrate two important points. First, it is clear that data of this study are consistent with those of the much more controlled AASHO test. Second, Figure 9 allows an estimate of the relationship between life and shakedown limit to be made, and further permits an approximate design curve (lower bound to life) to be deduced. Despite the spread of data, it appears that this curve may be estimated with some confidence.

The study attempted to examine the relationship between the predictions of shakedown theory for pavement structures and the life of a number of local pavements under normal traffic conditions. In so doing, it demonstrated that

1. Pavement materials may be tested in the laboratory to yield useful information on both stiffness and strength properties.
2. The traffic life of a pavement may be estimated with some accuracy from readily available information. Data on heavy vehicle percentages and lane usage, both extremely important influences on life, are, however, rather limited and could benefit from further study.
3. The shakedown limit, obtained by the approximate (one-dimensional) means detailed previously, shows considerable promise as a means of estimating pavement life. Not only is the analytical approach consistent with features of normal pavement performance, but this study has shown that within the estimated limits of variation in pavement life and materials it may be used to predict the minimum expected life of a flexible pavement structure.

APPROACHES TO DESIGN

The process of engineering design involves the selection of dimensions and properties of components in order that the completed structure shall perform in a specified manner. In the case of pavement design, the properties of materials can often be defined within practical limits, and the aim of design is to select suitable layer thicknesses in order that the pavement should meet particular performance requirements. To those solutions from which satisfactory performance may be expected, a further step of optimization (economic or otherwise) may be applied.

It has already been demonstrated that the calculated shakedown limit of a pavement offers a valuable guide to its ultimate performance, expressed in terms of its serviceable life under traffic. However, the design of a pavement is complicated by the number of parameters that influence performance. Because the behavior of one particular material may be ideally described by four fundamental parameters (E,ν,c,ϕ) and pavements typically consist of three or more distinct materials, the task of formulating design procedures involves determining the influence of perhaps a dozen or more variables. This represents a considerable problem, and, in this section, some approaches to its solution are developed.

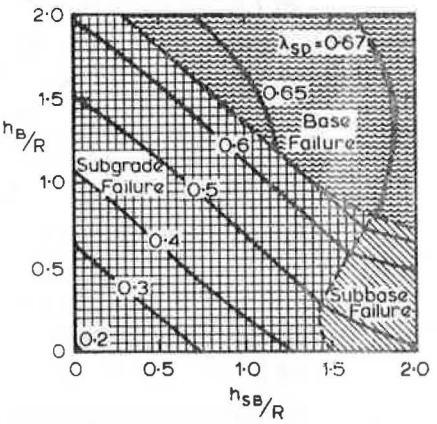

FIGURE 11 Shakedown limit of flush-sealed pavement (fixed properties) as function of thickness design.

PROFILE	MATERIAL	E MPa (ksi)	ν	C kPa (psi)	ø°
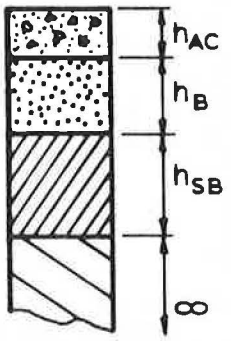	Asphaltic Concrete	2000 (290)	0.4	3000 (440)	35
	Crushed Rock Roadbase	70 (10)	0.3	80 (12)	50
	Gravel/Shale Sub-base	50 (7.3)	0.3	80 (12)	30
	Clay Sub-grade	20 (2.9)	0.35	40 (5.8)	15
LOADFORM 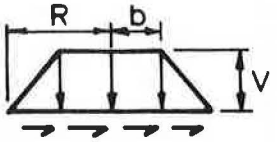					

$\frac{b}{R} = 0.5, \mu = \frac{H}{V} = 0.4$

V = 700 kPa (100 psi)

FIGURE 12 Representative three-layer pavement for development of design charts.

Two Layers on Subgrade (fixed properties)

Sharp and Booker (15) present a first step toward design employing shakedown theory, examining the case of a single layer overlying a subgrade and the influence on performance of variations in layer stiffness and strength.

By fixing material properties for a representative flush-sealed pavement (Figure 10), it is possible to explore the influence of layer thicknesses alone. With only three variables (h_B, h_{SB}, and λ), the results of the analyses lend themselves to graphic presentation using contours of constant shakedown limit (λ_{SD}) over a range of thickness combinations. Figure 11 shows the resulting design chart. For the given materials, a pavement with a shakedown limit of, for example, $\lambda_{SD} = 0.65$ may then be constructed using any one of the thickness combinations lying on that line. It may also be seen that the combination that optimizes construction cost can now be readily determined by graphic or other means.

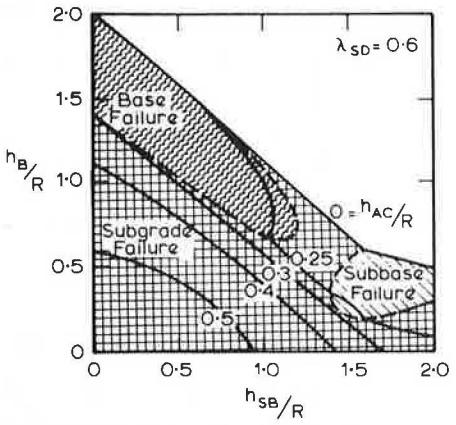

FIGURE 13 Design chart for three-layer pavement (fixed properties), performance standard $\lambda_{SD} = 0.6$.

Three Layers on Subgrade (fixed properties)

The case of three layers overlying a subgrade (Figure 12) may be treated in a similar manner. If once again material properties are known, then only four variables (h_{AC}, h_B, h_{SB}, and λ) are to be related. In this case it is preferable to keep the three thicknesses (h_{AC}, h_B, and h_{SB}) together and prepare a family of charts, each one representing a particular value of λ_{SD} and hence a particular performance standard. Figures 13 and 14 show two typical charts for the given materials, and it may be noted that, when the required performance has been selected, a single chart is capable of presenting the range of suitable thickness designs.

As before, an optimum design may then be determined. Given the applicable cost function, a small number of calculations should serve to locate the most economical design and its associated cost; if completeness is desired, superimposing contours of constant functional value will readily highlight that point at which cost is minimized.

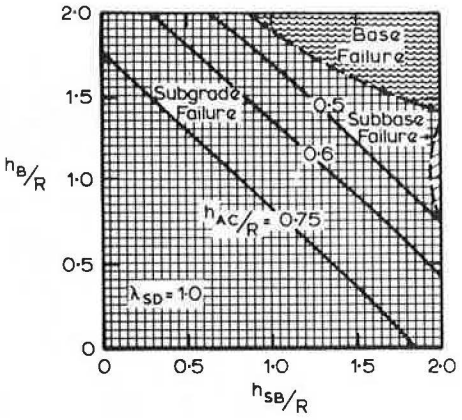

FIGURE 14 Design chart for three-layer pavement (fixed properties), performance standard $\lambda_{SD} = 1.0$.

Two Layers on Subgrade (general materials)

Many existing pavements may be idealized as two-layer structures overlying a subgrade. Clearly most flush-sealed designs fall into this category; however, many designs that include thick asphaltic concrete are also of this form. An asphalt-granular base-subgrade structure is here used as a demonstration.

With little loss of generality, typical values of Poisson's ratio (ν) and friction angle (ϕ) may be assigned to each material, leaving as variable the modulus, cohesion, and thickness of each layer, as given in Table 2.

Three further simplifications may be made at this point. First, it is shown elsewhere (10,15) that the shakedown performance of each layer may be examined individually, with results superimposed after analysis to yield the structure's shakedown limit. Attention will therefore be restricted to the subgrade; other layers may be treated in the same manner. Second, the shakedown limit may be normalized with respect to wheel load and layer cohesion. Third, pavement response is a function of modular ratios, rather than absolute values of modulus, because it is the modular ratio that determines the stress distribution within the structure. As a result the number of variables under consideration is reduced to five: (E_{AC}/E_{SG}), (E_B/E_{SG}), (h_{AC}/R), (h_B/R), and $(\lambda_{SD}V/c_{SG})$.

The detailed derivation of relationships between these variables is set out elsewhere (10). In summary, it is found that base relative stiffness (E_B/E_{SG}) and base thickness (h_B/R) both exert approximately linear influences on the shakedown limit of the pavement. This enables the original five variables to be reduced to three, with relationships formalized as

$$F_1 = \text{function } (\lambda_{SD}, E_B/E_{SG});$$
$$F_2 = \text{function } (F_1, h_B/R); \text{ and}$$
$$(h_{AC}/R) = \text{function } (F_2, E_{AC}/E_{SG}).$$

This formulation, in which the effects of the variables are isolated by simple approximations, lends itself to presentation as a multiple-intercept chart occupying three quadrants. Figure 15 is such a chart.

The dotted lines in Figure 15 demonstrate the use of the chart in designing a pavement required to have a shakedown limit (λ_{SD}) of 1.75. The pavement is to carry traffic having a representative tire load equivalent to 560 kPa on an area of radius 100 mm, and the available materials (asphalt con-

TABLE 2 Fixed and Variable Parameters for Two-Layer Pavement Design

	Material	Thickness	Stiffness	Strength
PAVEMENT	Asphaltic Concrete	h_{AC}	E_{AC} ν=0.4	c_{AC} ϕ=30°
	Granular Base	h_B	E_B ν=0.3	c_B ϕ=50°
	Sub-grade	∞	E_{SG} ν=0.35	c_{SG} ϕ=15°
LOAD	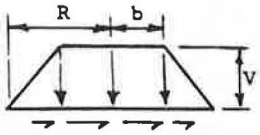		$\frac{b}{R}$=0.5 $\mu=\frac{H}{V}$=0.4 R=100mm, (4") V=700kPa (100 psi)	

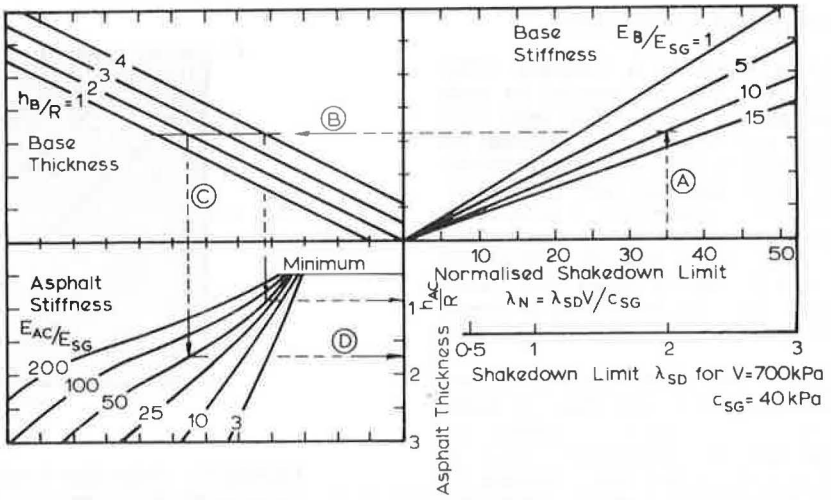

FIGURE 15 Design chart for two layers on subgrade.

crete, base course, existing subgrade) have stiffnesses of 1000 MPa, 200 MPa, and 20 MPa, respectively. The subgrade cohesion is found to be 28 kPa. Using these parameters, the normalized shakedown limit (λ_N) may be calculated as 35, and relative stiffnesses of 50 and 10 apply to asphalt and base course, respectively. Then, as Figure 15 shows, a base thickness of 200 mm requires 170 mm of asphalt, whereas a thicker base (for example, 400 mm) requires less asphalt--in this case, 90 mm. Here, 80 mm of asphalt has been replaced by 200 mm of base course. It needs to be noted, however, that this ratio of replacement (or "material equivalency") depends on both material properties and the form of structure being considered and should not be blindly applied to other pavement design processes.

When the relationship between asphalt and base thickness has been determined in this manner, considerations of construction convenience and cost may be superimposed (as previously illustrated) in order to arrive at the final pavement design.

CONCLUSIONS

The behavior of pavement structures under traffic loading is most appropriately analyzed by methods that take due account not only of finite material strength and the movement of loads but also of the gradual accumulation of plastic deformations within the structure. The theory of shakedown lends itself to this purpose.

Procedures have been developed whereby the shakedown behavior of continua such as pavements may be examined quantitatively. The results of parametic studies demonstrate the use of such procedures, and two case studies serve to confirm that pavement shakedown may be both observed and accurately predicted. A more general relationship between pavement life and shakedown predictions is then formulated.

The application of shakedown theory to a number of typical design problems follows, enabling a number of approaches to the construction of generalized design procedures to be developed.

ACKNOWLEDGMENTS

The financial support that made this work possible was provided by the University of Sydney and the Commissioner for Main Roads, New South Wales. Thanks are also due to the latter for permission to publish this paper. The guidance and suggestions of J.R. Booker and G.S. Donald are also gratefully acknowledged.

REFERENCES

1. E. Melan. Theorie statisch unbestimmter Systeme aus ideal-plastischen Baustoff. Sitzungsberichte der Akademie der Wissenschaften in Wien, Vol. IIa, 1936, pp. 145-195.
2. W.A.M. Alwis and P. Grundy. Shakedown of Plates Under Moving Loads. Proc., 7th Australian Conference on Mechanics of Structures and Materials, 1980, pp. 191-196.
3. T. Belytschko. Plane Stress Shakedown Analysis by Finite Elements. International Journal of Mechanical Sciences, Vol. 14, 1972, pp. 619-625.
4. J.A. König. Shakedown Theory of Plates. Archiwum Mechaniki Stosowanej, Vol. 21, No. 5, 1969, pp. 623-637.
5. B.L. Aboustit and D.V. Reddy. Finite Element Linear Programming Approach to Foundation Shakedown. Proc., International Symposium on Soils Under Cyclic and Transient Loading, Swansea, Wales, U.K., 1980, pp. 727-738.
6. G.N. Pande, W.S. Abdullah, and E.H. Davis. Shakedown of Elasto-Plastic Continua with Special Reference to Soil-Rock Structures. Proc., International Symposium on Soils Under Cyclic and Transient Loading, Swansea, Wales, U.K., 1980, pp. 739-746.
7. A.H.D. Marwick and H.J.F. Starks. Stresses Between Tyre and Road. Journal of Institution of Civil Engineers, Vol. 16, No. 7, 1941, pp. 309-325.
8. R.P.H. Bonse and S.H. Kuhn. Dynamic Forces Exerted by Moving Vehicles on a Road Surface. Bull. 233, HRB, National Research Council, Washington, D.C., 1959, pp. 9-32.
9. D.R. Freitag and A.J. Green. Distribution of Stresses on an Unyielding Surface Beneath a Pneumatic Tire. Bull. 342, HRB, National Research Council, Washington, D.C., 1962, pp. 14-23.
10. R.W. Sharp. Shakedown Analysis and Design of Pavements. Ph.D. dissertation. University of Sydney, Australia, 1983.
11. G. Maier. Shakedown Theory in Perfect Elasto-Plasticity with Associated and Non-Associated Flow-Laws: a Finite Element, Linear Programming Approach. Meccanica, Vol. 4, No. 3, 1969, pp. 250-260.
12. HRB Special Report 61A-G. The AASHO Road Test. HRB, National Research Council, Washington, D.C., 1961-1962.
13. J.F. Shook and H.Y. Fang. Cooperative Materials Testing Program at the AASHO Road Test. In HRB Special Report 66: AASHO Road Test Technical Staff Papers, 1961, pp. 59-102.
14. M.F. Kent. AASHO Road Test Vehicle Operating Costs Related to Gross Weight. In HRB Special report 73: The AASHO Road Test, Proceedings of a Conference Held May 16-18, 1962, St. Louis, Mo., HRB, National Research Council, Washington, D.C., pp. 149-165.
15. R.W. Sharp and J.R. Booker. Shakedown of Pavements Under Moving Surface Loads. Journal of the Transportation Engineering Division, ASCE, 1984, Vol. 110, No. TE1, 1984, pp. 1-14.

Publication of this paper sponsored by Committee on Mechanics of Earth Masses and Layered Systems.

Automated Cone Penetrometer: A Nondestructive Field Test for Subgrade Evaluation

SAFWAN A. KHEDR, DAVID C. KRAFT, and JAMES L. JENKINS

ABSTRACT

The results of a comprehensive program for the design, development, and field testing of an automated cone penetrometer are presented as an effective method for evaluating the condition of subgrade soils. Using this newly developed device, as many as 70 locations were tested at a site during an 8-hr day. The current automated penetrometer has a penetration depth of 406 mm (16 in.) and provides penetration resistance output readings at incremental 25-mm (1-in.) depths. The use of the automated cone penetrometer device, including its unique features for field use as demonstrated in a comprehensive field evaluation program conducted at Kelly Air Force Base, San Antonio, Texas, is described along with the results of a California bearing ratio (CBR) versus cone index correlation study. Analysis of the field data revealed a linear correlation between CBR and cone index with a correlation coefficient of 0.875. A parallel laboratory testing program was conducted on three fine-grained subgrade soil types obtained from the same test site. The laboratory test results were consistent with those obtained in the field. The use of the automated cone penetrometer technique and the correlation of its results to the CBR proved to be an effective, efficient, and reliable method for evaluating the subgrade soils encountered at the Kelly AFB site. The automated cone penetrometer holds promise as a good assessment tool for developing a statistical representation of subgrade conditions for fine-grained soils on both new and existing projects.

Dynamic and static cone penetration tests are widely used in deep subsurface investigations and have been adequately researched. However, penetrometers for evaluating shallow subgrade soil conditions have received little, if any, attention from researchers during the past decade, although the cone penetrometer, as an example, has proven to be a surprisingly accurate and efficient means for subgrade soil evaluation. The hand penetrometer has been used extensively especially in the military. However, the device needed development and improvement for better operation and more representative and reproducible results.

Dynamic penetration tests can be divided into two main types: constant rate of penetration and impact test. This investigation was concerned only with the first type, constant rate of penetration.

A penetrometer is basically an extremely simple device, a kind of calibrated index finger. It is a rod with a larger diameter conical tip that is forced vertically into the ground; the penetration resistance provides an indication of soil strength and is recorded as cone index (CI). The cone index is defined as the force per unit area of cone base required to push the penetrometer into the soil at a certain rate of penetration. Previous studies by Selig and Truesdale (1) and Nowatzki and Karafiath (2) have shown that CI is a function of rod size, shape, size of cone tip, and rate of penetration as well as soil type, density, and moisture conditions. On the basis of these studies and the report by Freitag (3), an automated cone penetrometer was developed as a field soil testing device.

Traditional methods of evaluating subgrade soil compaction and strength for existing and new highway projects include moisture-density, California bearing ratios (CBRs), and plate bearing tests. Although these strength tests are considered satisfactory for evaluating, directly or indirectly, the load-carrying capacity of in situ subgrade soil, the test procedures are rather lengthy, especially when conducted on poorly prepared surfaces or when conducted at certain depths below the ground surface, or both. Practically, only four to six locations can be tested for field CBR during an 8-hr workday. This presents a problem in getting statistically representative values particularly when there is some variability in soil type, moisture, and compaction conditions. Using the newly developed device, as many as 70 locations can be tested at a site each day.

The objective of this study was to develop an efficient, reliable means of subgrade evaluation, namely, the automated cone penetrometer; to establish a data interpretation process; and to correlate its results in terms of CI to a well-defined, widely used measure of soil strength.

DEVELOPMENT

The automated cone penetrometer device was developed as part of a U.S. Air Force-sponsored program designed to investigate unprepared and semiprepared soil runways as an alternative launch and recovery site for aircraft. The device developed provides the means for a quick, yet reliable, evaluation of the subgrade soil under various conditions.

The penetrometer consists of a shaft 9.4 mm (3/8 in.) in diameter with a 3.23-cm^2 (0.5-in.^{2}) base area and a 30-degree tip-angle cone at the top for shearing the soil while undergoing penetration. The penetrometer was mounted in a servo-drive electrohydraulic system that could maintain a constant rate of penetration [32 mm/sec (1.25 in./sec) was used]. The hydraulic actuator was mounted on a reaction frame that was attached to the front bumper of a

vehicle through two hydraulic jacks that were controlled by the electrohydraulic system to lower the reaction frame at the test location and retract it during vehicle travel (Figures 1 and 2). The vehicle weight provided a maximum reaction of 1,800 lb to the frame.

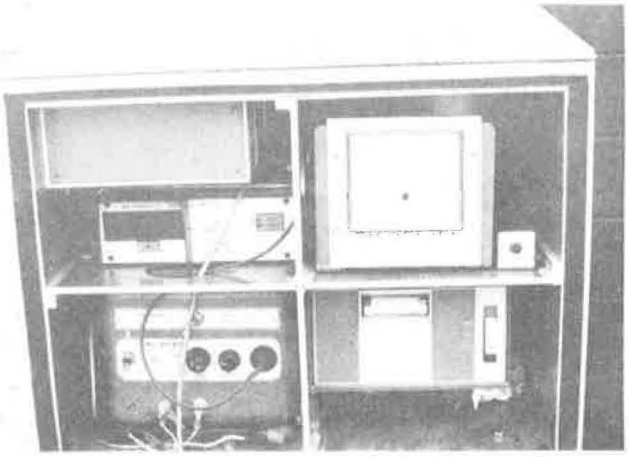

FIGURE 1 Autopenetrometer.

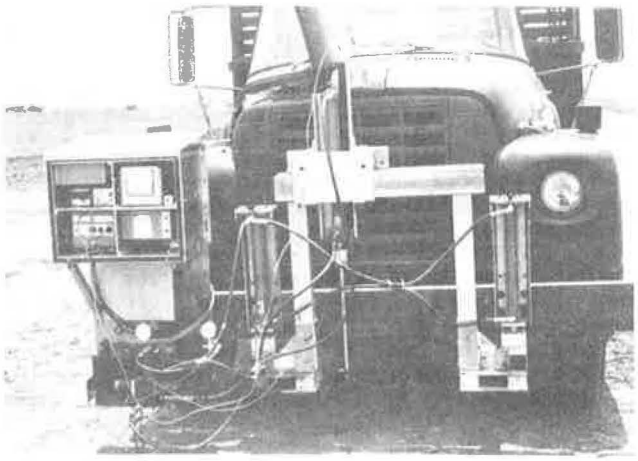

FIGURE 2 Autopenetrometer on traveling vehicle.

The penetrometer mounting arrangement permitted multiple penetration tests along the frame's cross-beam centerline at the test location without moving the vehicle. During the test program, three penetration tests, 8 in. apart, were performed at each test location. Limit hydraulic switches permitted the penetrometer to penetrate to a maximum depth of 406 mm (16 in.) measured at the base of the penetrating cone tip. Figure 3 shows the penetrometer during the test operation. Figure 4 is a schematic showing the essential features of the penetrometer.

The soil's penetration resistance force was measured through a load cell mounted between the penetration rod and the hydraulic piston. The penetration travel was measured using a linear variable differential transducer (LVDT) arrangement mounted to the hydraulic actuator. Both penetration resistance and travel were recorded on a paper tape recorder that provided a continuous printout of the results in pounds and inches, respectively. Penetration resistance in pounds was subsequently converted to cone index (CI) in psi using the cross-sectional area of 0.5 $in.^2$ of the base of the cone.

FIGURE 3 Automated penetrometer ready for testing operation.

The automated penetrometer ran on the vehicle's 12-volt DC battery, and the test operation was performed by one driver-operator.

DATA INTERPRETATION

The test data could be interpreted directly for any particular depth from the continuous recorder printout. Distinct soil stratification and layer transition, due to changes in soil type, moisture, or compaction, could be observed. In such cases it may be desirable to distinguish the results for each strength zone.

During the field testing phase of this study and during particular periods, it was observed that the upper 15 to 20 cm (6 to 8 in.) was generally of higher strength than the lower portion. Consequently, in determining cone penetration resistance, three different determinations were made:

1. Average penetration resistance (psi) for the first 8 in. of penetration,
2. Average penetration resistance (psi) for the next 8 in. of penetration, and
3. Average penetration resistance over the full 16-in. depth of penetration.

To calculate a representative penetration value for the 16-in. depth, a simple computer-programmed, statistical procedure was followed in order to eliminate data scattered beyond a defined statistical range. The procedure assumes that the penetration readings at a particular location were of a normal population with T-probability distribution. The procedure checked whether the calculated mean of the readings was within 10 percent deviance from the true mean, with 95 percent degree of confidence. The calculated mean was accepted if it met this requirement. Otherwise, readings that were more than the mean plus the standard deviation, or less than the mean minus the standard deviation, were removed, and a new mean was calculated for the rest of the data. The overall cone index for a location is the average of the three penetrations at that location.

FIELD TESTING PHASE

An extensive field testing program was conducted at Kelly Air Force Base, San Antonio, Texas. Soil

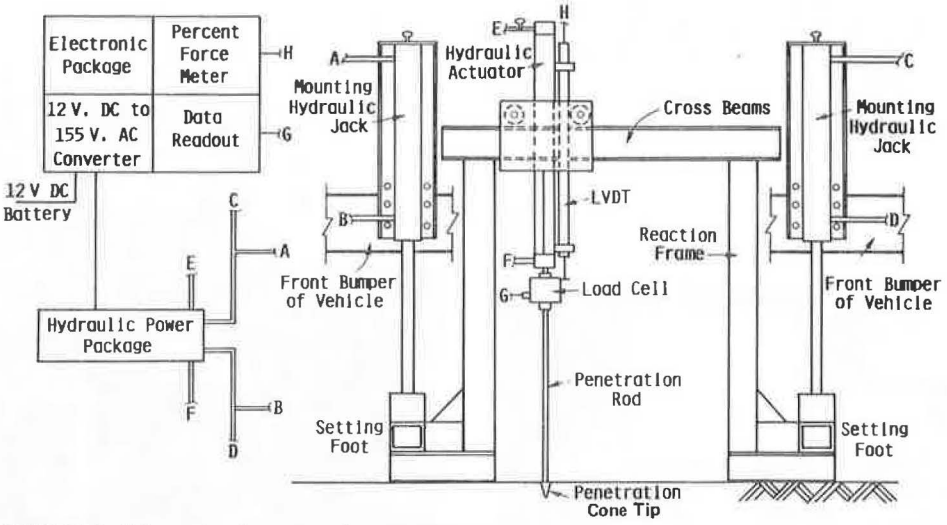

FIGURE 4 Schematic of automated cone penetrometer.

strength profile maps were made for soil runway strip and taxi areas using the automated cone penetrometer. Figure 5 shows an example of these maps. Field California bearing ratio (CBR) tests were performed at two different depths at 30 locations for which cone penetrometer results were also obtained. The penetration resistance values were taken at the depths where CBR tests were performed. However, the penetration resistance at the deepest point of the penetrometer test was taken when the depth of the CBR test was 406 mm (16 in.) or more. An average of three penetrations was used for the CBR-CI correlation analysis. The results of these field tests are given in Tables 1 and 2; Table 1 gives the tests run in June 1982 and Table 2 gives those run in July 1982.

The data in Tables 1 and 2 are for various fine-grained soils encountered on site (silty clay and clayey silt). CBR values ranged from 3.8 to 30.0 for data obtained in June (Table 1), and from 7.5 to 46.4 for the July period. The increase in strength range was due to the relatively dry weather between periods of testing.

The results in both tables are shown in Figure 6. When data in Figure 6 are fitted to a linear relationship between CBR and CI (in psi), the following relationship is obtained:

$$CBR = 0.86 + 0.015\ CI \quad \text{with correlation coefficient } r = 0.875 \tag{1}$$

It should be noted that Equation 1 is the linear regression function for data obtained for various conditions of soil type, moisture, density, and postcompaction environment. Also, unavoidable elapsed time between CBR and penetration tests during the testing program may have been responsible for some of the scatter in data.

The CI-CBR correlation previously developed by the U.S. Army Corps of Engineers (4) for the hand cone penetrometer is shown in Figure 6. It should be noted that cone tip dimensions are different from those of the one used in this study. The different trend of that correlation may be attributed to the limited capability of the hand penetrometer to main-

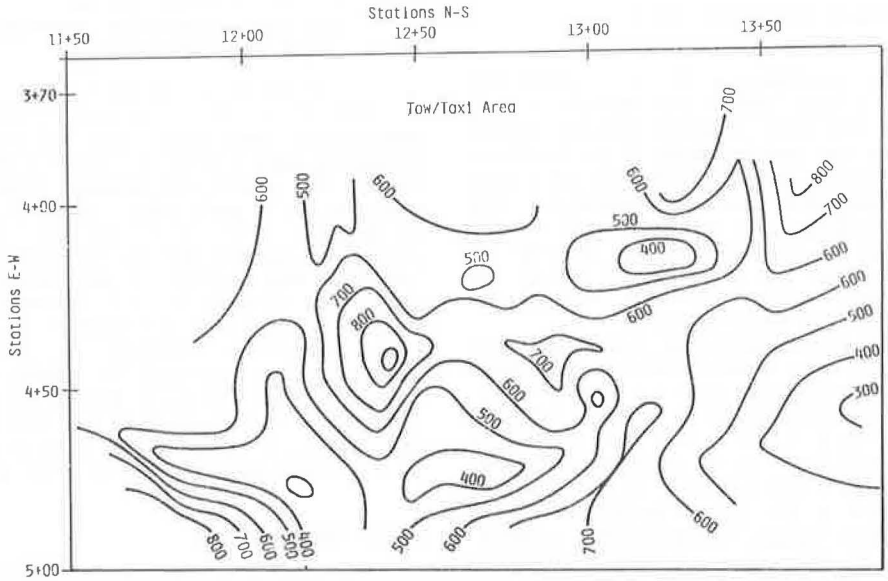

FIGURE 5 Soft soil test area strength contours, cone index (CI) in psi.

TABLE 1 CBR and CI Field Data, June 1982

Location No.	Unified Soil Classification	Average Field Moisture Content W (%)	Average Field Dry Unit Weight γ_D (pcf)	Depth of CBR Measurement (in.)	CBR (%)	CI (psi)
1	CL	26.5	90.8	5.0	7.5	390
1	CL			20.0	11.8	640
2	CL	25.9	88.05	7.0	20.5	1,044
2	CL			18.0	16.0	952
3	CL	25.0	89.1	5.5	9.2	566
3	CL			15.0	11.9	760
4		9.7	110.0	21.0	10.5	406
5		16.4	99.3	5.0	13.0	716
5				21.0	14.2	1,082
6	CL	20.0	100.2	4.5	4.9	330
6	CL			17.0	16.3	804
7	CL	25.3	88.0	9.0	3.8	178
7	CL			16.5	23.2	1,590
8		21.2	95.5	18.0	9.2	864
9		16.2	101.0	3.0	10.9	428
9				22.0	10.0	834
10	CL			5.5	9.8	314
10	CL			17.0	11.7	626
11		20.5	93.1	3.5	6.6	326
11	CL			21.0	14.6	816
12	CL	20.0	94.6	5.5	6.0	360
12	CH			15.0	8.1	454
13	CL	16.8	97.7	4.5	11.5	324
13	CL			19.0	7.8	640

TABLE 2 CBR and CI Field Data, July 1982

Location No.	Unified Soil Classification	Average Field Moisture Content W (%)	Average Dry Unit Weight γ_D (pcf)	Depth of CBR Measurement (in.)	CBR (%)	CI (psi)
14	CL	11.6	96.8	4.0	46.4	1,824
14	CL			20.5	20.7	1,270
15	CL	9.2	103.9	3.5	40.0	2,482
15	SM			19.0	12.8	712
16	CL	15.0	97.5	20.0	22.3	966
17	CL	14.1	99.5	3.5	26.3	1,548
17	CL			20.0	10.2	796
18	CL	10.3	101.8	4.0	24.2	2,004
18	CH			16.0	12.2	1,276
19	CH	8.7	100.8	5.0	33.8	1,636
19	CL			19.0	10.0	800
20		8.4	99.2	4.0	45.0	2,502
20	CH			20.0	12.0	730
21	CH			5.5	23.0	1,810
21	CH			24	7.5	1,232
22		12.3	98.5	5.0	19.5	1,482
22				16.0	18.5	1,388
23	CL	12.1	102.0	6.5	11.8	1,010
23	CL			6.5	14.2	1,010
23	CL			19.0	10.0	1,002
24		12.9	99.6	5.0	31.0	1,432
24	CH			18.0	16.8	1,430
25	SW-SM	5.1	111.6	8.0	15.8	946
26	CH	12.5	103.8	5.5	15.2	980
26	CL			18.0	23.5	1,358
27	CL	8.2	110.1	5.0	32.0	2,392
27	CL			21.0	18.7	1,182
28	CH	9.8	105.4	5.5	28.3	1,830
28	CL			16.0	13.0	1,404
30	CL	6.7	115.2	5.0	32.5	2,104
31		10.7	107.4	5.0	36.5	2,102
31	CL			20.0	11.5	1,168

tain a uniform rate of penetration when testing relatively hard soil.

LABORATORY TESTING PHASE

A parallel laboratory testing program was designed and conducted to establish the degree of correlation between laboratory CBR (as compacted ASTM D-1883) and laboratory cone penetrometer tests on similar soil specimens. CBR specimens were prepared in molds 152 mm (6 in.) in diameter and 178 mm (7 in.) high using standard Proctor compaction energy.

The penetration test was performed using a rod-and-cone penetrometer similar to that used in the field. The penetration shaft was mounted on an electrohydraulic materials testing system (Instron) shown in Figure 7. The Instron provided a constant penetration rate of 32 mm per second (1.25 in. per second). After each sample was tested for CBR, it was subjected to five penetration tests at the center and 38 mm (1 1/2 in.) off center in four locations. The penetration-resistance force results were recorded on x-y graph paper. Figure 8 shows an example of recorded test results. Zero penetration was designated at a position where the penetration cone

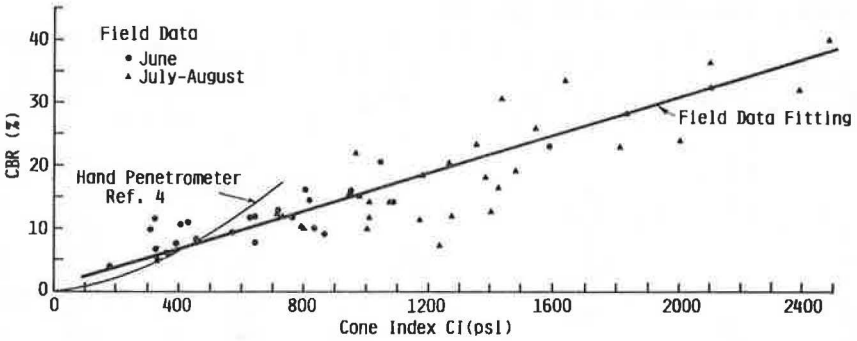

FIGURE 6 Correlation of CBR and CI from field data.

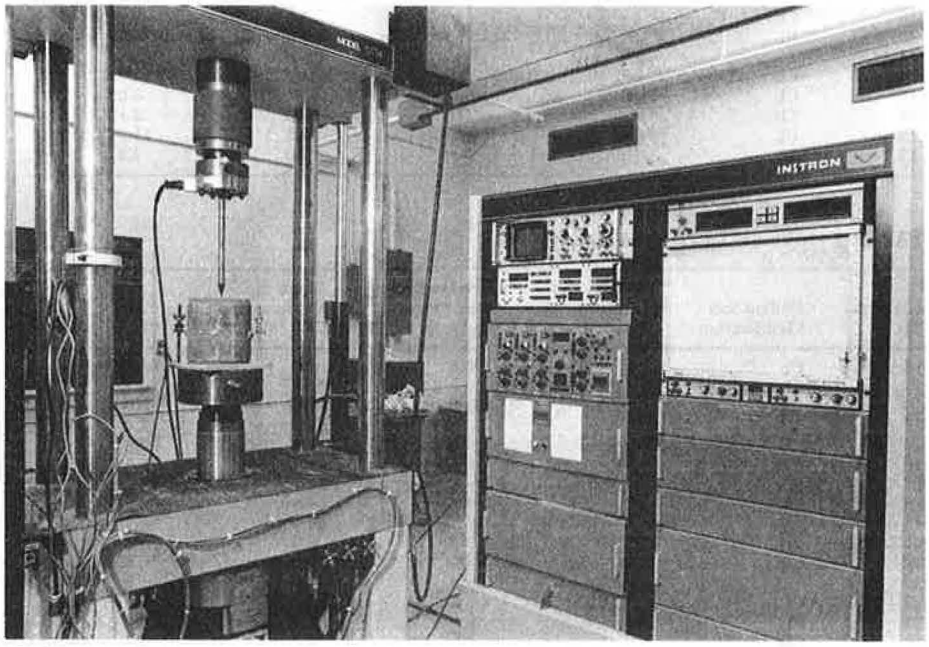

FIGURE 7 Laboratory test setup.

was set in the soil mold so that its base would be at the surface of the soil sample. The penetration test was started from that position at the specified rate for the full depth of the sample. This procedure avoided the effect of transition zones usually caused by the cone entering the soil sample and simulated the field test procedure. The penetration and resistance force were measured by an actuator-mounted LVDT and a 13.3-KN (3,000-lb) capacity load cell, respectively.

It was observed that penetration resistance varied somewhat with soil depth, reflecting soil compaction stratification in the mold. An average value was calculated to represent penetration resistance for each sample.

Four soil types encountered in the field were used in this testing phase of the study. Figure 9 shows the gradation curve for these soils, and Figure 10 shows the general relationship of CBR (as compacted) and compaction water content.

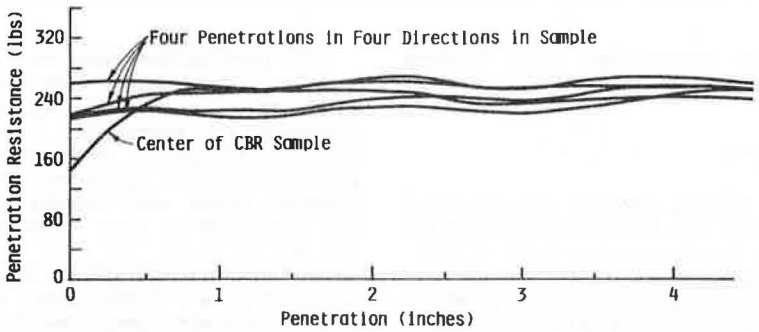

FIGURE 8 Typical penetration-resistance curves for laboratory samples.

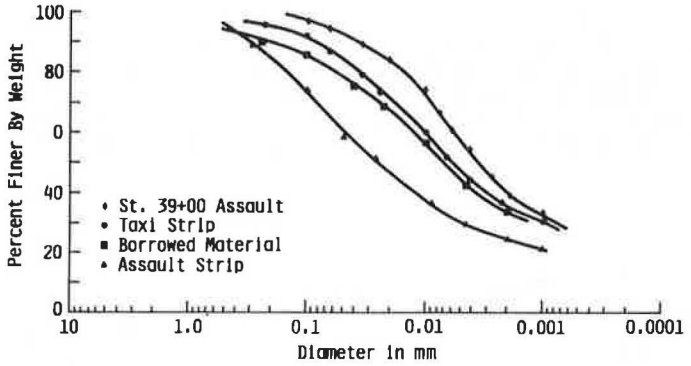

FIGURE 9 Grain size analysis results for sample soil.

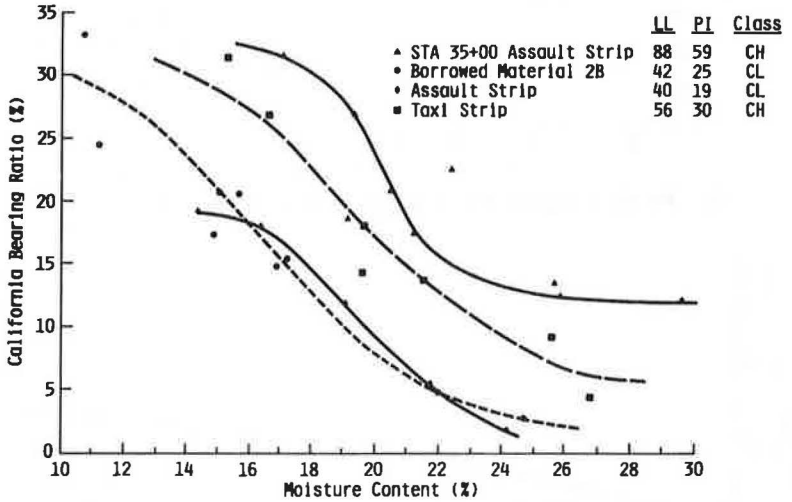

FIGURE 10 CBR versus moisture content variations for laboratory prepared soil samples.

The laboratory test results shown in Figure 11 have a general trend similar to that of the field data. The regression line developed from field data is shown in Figure 11 and illustrates that trend.

Given the nonhomogeneous nature of subgrade soils in general, Figure 6 and Equation 1 show good correlation between CI and CBR. The quick and efficient test procedure of the automated penetrometer along with Equation 1 provide the engineer with a highly reliable, effective means of evaluating fine-grained subgrade strength conditions.

EFFECT OF RATE OF PENETRATION

During the course of this study there was concern about the effect of the slower rate of penetration,

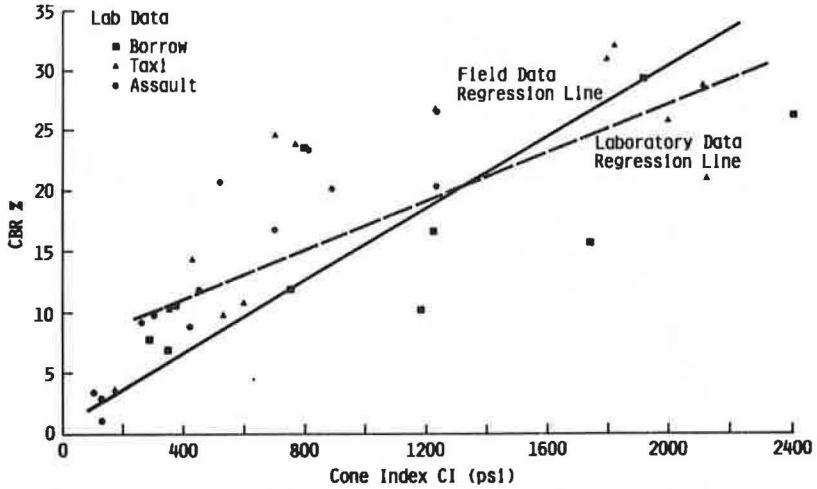

FIGURE 11 Comparison of field and laboratory CBR versus CI correlations.

which could result from relatively hard subgrade conditions, on measured penetration resistance. Different-rate penetration rate tests were performed on two soil samples in the laboratory. The penetration rate was varied between 6 mm (0.25 in.) and 32 mm (1.25 in.) per second. The results are shown in Figure 12. Freitag (3) and Selig and Truesdale (1) have investigated the same relationship in previous studies. Figures 13 and 14 show their findings. Figures 12-14 show that the measured fine-grained soil resistance to penetration varied by approximately 0 to 10 percent for a change in penetration

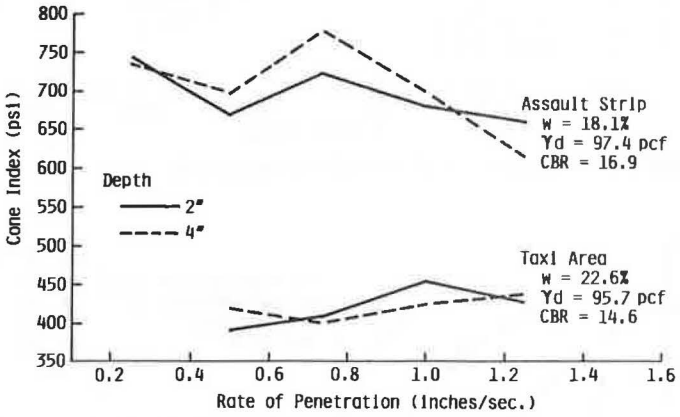

FIGURE 12 Variation of CI with cone penetration rate.

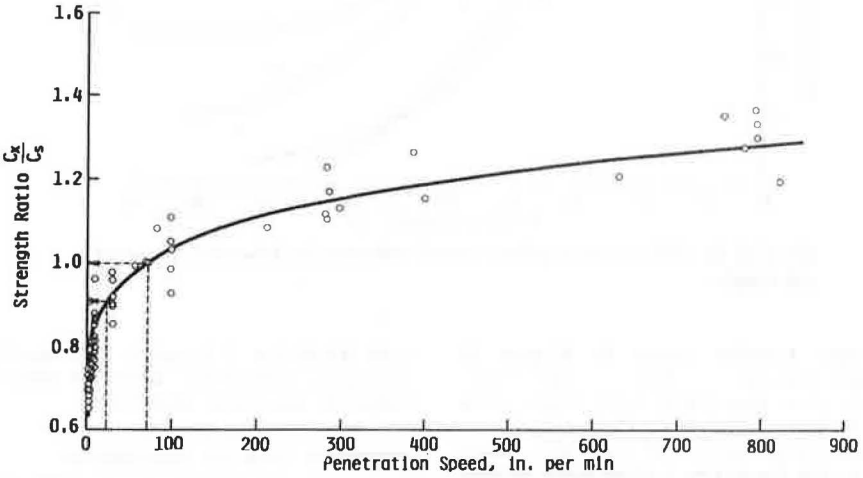

FIGURE 13 Variation in penetration resistance with penetration rate *(3)*.

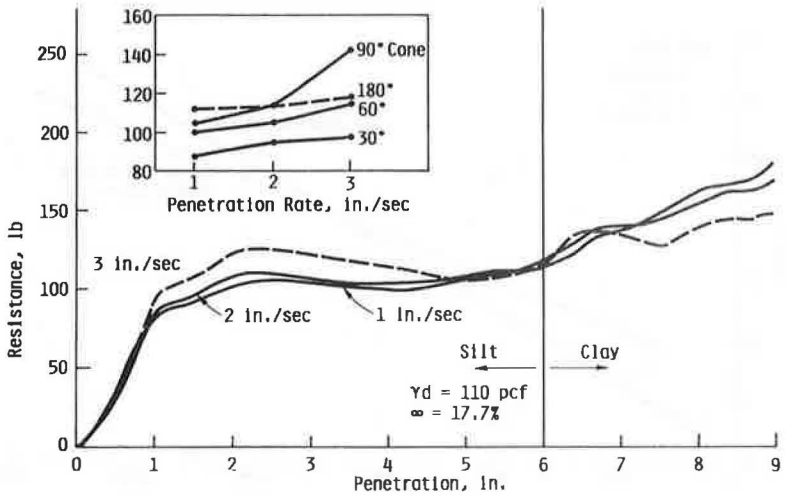

FIGURE 14 Variation in penetration resistance with penetration depth and rate *(1)*.

rate of 6 mm (0.25 in.) to 32 mm (1.25 in.) per second. However, these apparent variations in soil resistance could also be attributed to the nonuniformity of the soil, even when laboratory controlled specimens are used. The actual change in penetration rate for the automated penetrometer used in field tests was smaller than shown in Figure 12.

CONCLUSIONS

On the basis of experience gained from use of the automated cone penetrometer as a tool for assessing subgrade strength conditions at the Kelly AFB test site, and recognizing the range of soil types and strengths (CBRs between 5 and 46), the following conclusions are drawn:

1. An existing device, the cone penetrometer, has been improved through automation to evaluate subgrade soil conditions. The resulting technique and approach provide rapid, reliable, and reproducible results. The new device has a higher load capacity to test stronger subgrade soil than have existing hand-held penetrometers.
2. Results of correlation studies between the cone penetrometer tests and CBR tests indicate a consistent and definable relationship.
3. This improved test technique can be used to evaluate subgrade soil strength conditions under existing pavements as well as to provide a quality control technique for new pavement subgrade preparation.
4. The test technique does not require any special soil surface preparation and is considered nondestructive in comparison with other types of strength tests when performed at various depths below ground surface.
5. The consistency and efficiency of the test technique offer a good approach to the statistical presentation and evaluation of field data, thus ensuring a better soil strength condition evaluation to a proper depth.

ACKNOWLEDGMENT

The authors acknowledge the support and effort of the involved personnel at Wright-Patterson, Kelly, Edwards, and Tyndall Air Force Bases.

REFERENCES

1. E. Selig and W. Truesdale. An Evaluation of Field Measurements of Soil Compaction. Proc., Second International Conference of the International Society for Terrain-Vehicle Systems, Quebec, Quebec, Canada, Aug. 1966.
2. E. Nowatzki and L. Karafiath. The Effect of Cone Angle on Penetration Resistance. In Highway Research Record 405, HRB, National Research Council, Washington, D.C., 1972, pp. 51-59.
3. D. Freitag. Penetration Tests for Soil Measurements. Miscellaneous Paper 4-960. U.S. Army Corps of Engineers, Waterways Experiment Station, Vicksburg, Miss., 1968.
4. Trafficability of Soils. Technical Memorandum 3-240, first to sixteenth supplement. U.S. Army Corps of Engineers, Waterway Experiment Station, Vicksburg, Miss., March 1948 to May 1955.

Publication of this paper sponsored by Committee on Exploration and Classification of Earth Materials.

Rapid Determination of Base Course Strength Using the Clegg Impact Tester

NORMAN W. GARRICK and CHARLES F. SCHOLER

ABSTRACT

The Clegg impact tester was developed in Australia in the mid-1970s and is commonly used for density control during compaction. However, studies show that this device may be useful for measuring the strength of a wide variety of soil types. The project discussed here investigated this potential use of the Clegg impact tester. It is also part of a larger effort to develop a feasible procedure for evaluating gravel roads before paving. This device is particularly suited for the job because it is quick and simple to operate, portable, and inexpensive. Furthermore, results of this study show that Clegg impact values (CIVs) accurately predict pavement performance. In many cases CIV may be converted to an equivalent California bearing ratio value. Guidelines for testing are discussed, but additional research is required to refine the procedure.

The state of Indiana has more than 27,000 miles of gravel roads under the jurisdiction of county and town governments. In general, these roads carry small volumes of traffic in sparsely populated areas. Local governments often desire to upgrade the roadway by providing a paved surface. However, these governmental bodies usually lack the expertise to properly design and execute such projects; hence, many newly paved sections are so poorly constructed that they require frequent maintenance to remain open.

The Highway Extension and Research Project for Indiana Counties and Cities (HERPICC) at Purdue University has studied this problem and developed a simple and effective procedure for evaluating gravel roads before paving (1). A key element of this evaluation system is the determination of base course strength or load-carrying capacity. Unfortunately, most current methods for measuring strength are too cumbersome or too costly for use at this level. A potential solution to this problem is a device called the Clegg impact tester, which is quick and simple to use but largely untested in the field.

This project was conducted to assess the feasibility of measuring base course strength with the Clegg tester. The object of Part 1 of this study was to correlate Clegg impact values (CIVs) for the spring thaw period with those taken in the fall. This provides a method by which the critical value of pavement strength can be estimated for design purposes without the need for field testing in the short spring thaw period.

In Part 2 the relationship of CIV to base course thickness and to subgrade strength was investigated. This knowledge is important for interpreting laboratory studies on the Clegg tester and relating these results to field conditions. For example, CIV has been correlated with California bearing ratio (CBR) in laboratory tests, but in the field this relationship is affected by varying thickness of the gravel layer. The nature of these relationships will be examined.

DESCRIPTION OF THE CLEGG IMPACT TESTER

The Clegg impact tester has three primary components: a guide tube, a compaction hammer, and a meter (Figures 1 and 2). During testing the hammer is raised to a specified height and then allowed to fall and strike the test surface. The maximum deceleration of the hammer on impact with the surface is measured by an accelerometer in the head of the hammer. The resulting signal is sent to a recording device composed of solid-state circuits for filtering and adjusting incoming signals and a micrometer for recording the result. Each unit of CIV is equivalent to 10 gravities (g) of deceleration.

Impact values are affected by variations in the weight of the hammer, the shape of the hammer head, the height of drop, and the number of blows of the hammer. Therefore, a standard testing procedure in which each factor is specified has been adopted. The standard test for granular material specifies a 4.5-kg (10-lb) hammer and a drop height of 450 mm (18 in.). For sand and other soft material a lighter, more sensitive hammer is better. In all cases, a square-ended hammer is used and the reading is taken after the fourth blow.

REVIEW OF RELATED RESEARCH

Relationship Among CIV, Moisture Content, and Density

Good correlations have been found between CIVs and soil properties such as density and moisture content

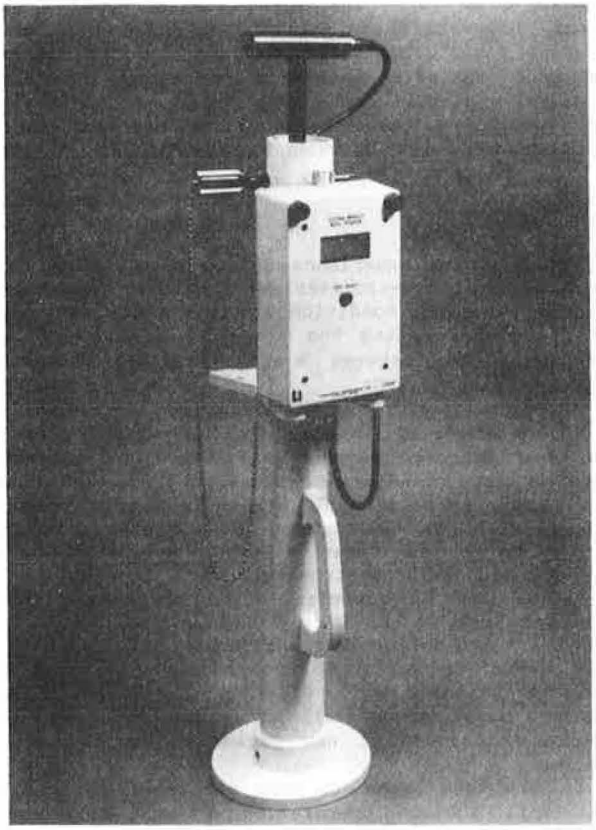

FIGURE 1 Clegg impact tester.

FIGURE 2 Clegg impact tester in use.

(2). For most soil types, CIV decreases with moisture content and increases with density until the air void is between 5 and 10 percent depending on the soil. The general form of this relationship is as follows:

$$\% \text{ modified compaction} = a\,CIV + b\,MC + c \quad (1)$$

where a, b, and c are constants and MC is moisture content. The constants vary with soil type but are in specific ranges: 0.3 to 0.4, 0.5 to 1.0, and 75 to 85 for a, b, and c, respectively. With fine sands, CIV increases with density but is not affected by changes in moisture content. Furthermore, there is no limiting air void (point of instability) at which CIV begins to decrease with increasing density.

Relationship Between CIV and CBR

Clegg impact values have also been correlated with CBR for laboratory samples, and the form of this relationship is as follows (3,4):

$$CBR = 0.07\,(CIV)^2 \quad (2)$$

In Equation 2 the CBR value used is that for unsoaked samples tested with no surcharge.

There are some data relating CIV to subjective measures of unsealed road condition. In one study (2), Clegg found that poor, satisfactory, and good performance of gravel roads corresponded to average CIVs of 30, 50, and 70, respectively.

DESCRIPTION OF FIELD TESTS

Part 1: Spring and Fall CIVs

Impact values were measured at specific points on three different county roads in April 1982 (spring thaw period) and during September and October 1982 (5). In each case, readings were measured on cross sections 50 ft apart, with nine data points on each cross section. The test sections were approximately 2,500 ft long and varied in width from 18 to 25 ft.

Part 2: CIV, Base Thickness, and Subgrade CBR

Field tests for this part of the project were conducted in May and June 1982 on the three roads used in Part 1. For each road, nine cross sections were selected on the basis of the spring CIV for the centerline position. Five cross sections with high CIV and four with low CIV were chosen to give a wide range of values in the data set. Readings were taken at both the centerline position and at a position 7.5 ft right of center.

Five readings of CIV were recorded and the average was determined for each test location. The base material was then excavated to expose subgrade material so that base thickness could be measured. Finally, the subgrade CBR was measured by a dynamic cone penetrometer (6,7). Samples of base and subgrade material were collected and analyzed for each data point.

DATA ANALYSIS

Correlation of Spring and Fall CIVs

Effect of Maintenance on Data Analysis

Maintenance crews worked on all three road sections during the interval between the spring and the fall tests. Therefore some of the changes in CIV between spring and fall resulted from either the addition or the removal of gravel during maintenance. Fortunately, it was possible to isolate the effects of maintenance because portions of the roads were left undisturbed.

An examination of the data showed a systematic pattern of change in CIV. In most cases CIV increased between the spring and the fall; however, the largest increases were found for discrete groups of data points on the same or adjacent cross sections at both edge and middle positions on the roads. Those points with a large decrease in CIV were also clustered in this manner but were located predominantly in the middle of the road. In general, the data points with the largest increase in CIV represent locations where gravel was added, and those showing a decrease in CIV were the spots where gravel was removed by grading. Consequently, the data were divided into three groups on the basis of change in CIV over the period of the study: Group 1--locations not affected by maintenance, Group 2--locations where gravel was added, and Group 3--locations where gravel was removed.

Comparison of Group 1, Group 2, and Group 3 Data

Figure 3 is a graph of average CIV by position on the cross section for Group 1, 2, and 3 data from one county road. At each position average spring CIVs were highest for Group 3 data (points where gravel was removed by grading in the summer and fall). Group 2 points had the lowest values; this was where new material was added to the road surface. If the maintenance procedure used for these roads is considered, it appears that points with the lowest CIV showed the most visible signs of distress because it was necessary to add gravel in maintenance.

These results give some insight into the relationship between CIV and pavement performance; on

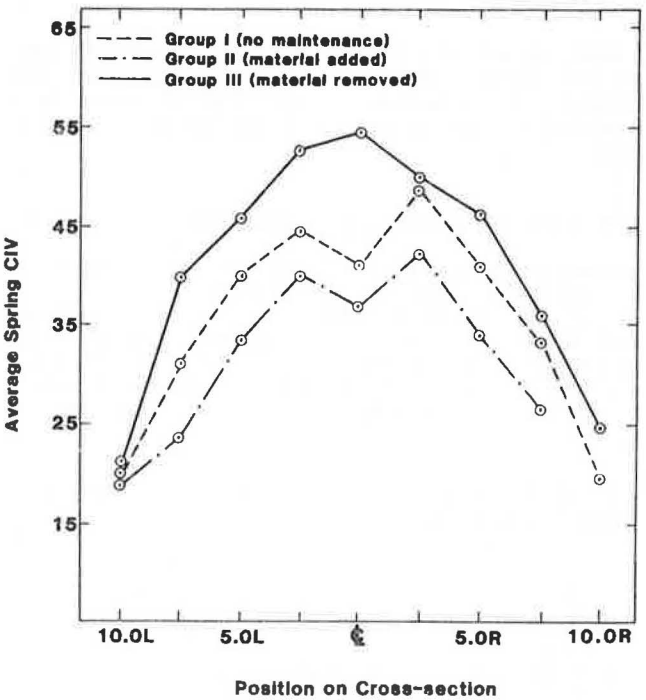

FIGURE 3 Average spring CIV by position for County Road 325 W, Tippecanoe.

the basis of the preceding discussion it may be concluded that Group 1 and 2 points (with no apparent signs of distress) gave satisfactory performances, whereas Group 3 points performed poorly. Table 1 gives the average CIV for Group 1 and 2 data (satisfactory performance) and Group 3 data (poor performance) for each of the three roads. Because traffic is concentrated in the middle of the road, values for the edge positions are atypical and were thus omitted in the computation of these averages. On the basis of these results, it appears that a minimum spring CIV of about 40 is required for satisfactory performance on these roads.

TABLE 1 Relationship Between CIV and Pavement Performance

	Average CIV for Five Interior Positions		
Pavement Performance	Co. Rd. 325 W	Co. Rd. 600 N	Co. Rd. 800 S
Poor	37.2	22.4	40.1
Satisfactory	44.5	48.2	49.9

Seasonal Variation in Pavement Strength

To obtain a true measure of seasonal variation in pavement strength it was necessary to analyze Group 1 data separately. The results for each road were almost identical; therefore, the data were pooled to give the following regression model:

$$\text{Spring CIV} = 0.973\ \text{Fall CIV} - 10.05$$
$$\text{Coefficient of determination } (r^2) = 0.93 \quad (3)$$

Thus the magnitude of strength loss due to spring thaw is of the order of 12 CIV and is virtually independent of the original impact value.

Clegg impact values were also measured in May for a number of data points. The regression model relating spring and May CIV is as follows:

$$\text{Spring CIV} = 1.03\ \text{May CIV} - 8.13$$
$$r^2 = 0.76 \quad (4)$$

Comparison of Equations 3 and 4 shows little change in CIV between May and September, implying that strength of the unsealed gravel road is almost fully restored in the first few weeks after the spring thaw.

CIV, Base Thickness, and Subgrade CBR

Regression analysis for these data shows that CIV increases with base course thickness but is not affected by changes in subgrade CBR. The six regression models relating CIV and thickness for the three roads are given in Table 2. In each case, the natural log function of base thickness gave the highest r^2 value. It should be noted that most of the values of thickness in the data were in the range of 2 to 8 in. At the upper end of this range there is little increase in CIV with base thickness. This indicates that there is some point at which increasing thickness does not result in a further increase in CIV. The limiting value of thickness appears to be about 8 in.

On all three roads the regression models give a smaller CIV for the edge position (7.5 ft to the right) than for the center position when the pavement thickness is the same. This is due to the variation in density across the roadway, caused by a concentration of traffic in the middle. The results for county road 800 S (Carroll County) are noticeably different than those for the other two roads. The regression functions for this road may be inaccurate because the data are limited to a narrow range of thickness values.

TABLE 2 Regression Models Relating CIV and Thickness for Three County Roads

Road	Position	Model	r^2
325 W Tippecanoe	Center	CIV = 16.81 ln (BT) + 19.24	0.79
325 W Tippecanoe	7.5 ft right	CIV = 16.81 ln (BT) + 13.25	0.79
600 N Tippecanoe	Center	CIV = 16.81 ln (BT) + 15.21	0.79
600 N Tippecanoe	7.5 ft right	CIV = 16.81 ln (BT) − 9.49	0.79
800 S Carroll	Center	CIV = 45.20 ln (BT) − 24.96	0.62
800 S Carroll	7.5 ft right	CIV = 30.51 ln (BT) − 11.14	0.62

Note: ln (BT) is the exponential log of base thickness.

DISCUSSION OF RESULTS

Conversion of CIV to CBR

CBR is the most widely used and accepted pavement strength parameter. As such, a method for converting CIV to an equivalent CBR value would enhance the usefulness of the Clegg tester for pavement evaluation on gravel roads. Regression models correlating CIV and CBR have been developed for laboratory samples. In most cases these models are not applicable to field test results because of the effect of base course thickness on CIV. However, where the base course thickness is greater than 8 in., CIV can be converted directly to an equivalent CBR value.

Measurement of Pavement Performance

A spring CIV of 40 appears to be the minimum required to reduce problems like rutting, potholes, and corrugations. This value depends on factors such as traffic level, traffic type, and climatic conditions. Comparable results have been obtained for gravel roads in Australia (2).

Effect of Pavement Condition on CIV

Seasonal variation in CIV can be modeled as a linear function of the original value. Thus the critical or weakest value of pavement strength can be estimated with a regression model that relates spring and fall readings. Furthermore, much of the strength is regained in the first few weeks after the spring thaw, so a conservative estimate of this value may be obtained by testing at any convenient time in the summer or fall.

In this study the loss of strength during the spring thaw was of the order of 12 CIV. This value appears to be independent of material type and of the initial CIV. However, it will fluctuate from year to year with corresponding changes in weather conditions.

The moisture content at the time of testing can significantly affect the readings. It is not practical to make a moisture content determination each time the Clegg tester is used; however, the effects of moisture may be mitigated by testing the road when the natural moisture content is at or near its lowest point. A period of about 7 days after heavy precipitation is usually sufficient for the road to dry out to this point.

Operation of the Clegg Tester

The primary advantages of the Clegg tester include its size, ease of handling, and quick and simple testing procedure. In this project, approximately 35 to 40 readings per hour were made. The Clegg tester clearly provides more comprehensive coverage of the test area than do conventional methods of evaluation. Another advantage of this device is that the readings are quite consistent when the test is conducted properly.

CONCLUSIONS

The findings of this study indicate that the Clegg tester is particularly suitable for use in the evaluation of base courses. Aside from being highly portable and simple to operate, the Clegg tester accurately measures changes in the load-carrying capacity of unsealed gravel roads. However, the readings are affected by many factors. Thus a low CIV may indicate an inadequate thickness of base course material, a poor material quality, a lack of compaction, or a combination of these factors. When the Clegg tester is used for pavement evaluation, the readings should always be supplemented by determination of soil properties and base course thickness.

Some of the findings of this project need to be investigated more extensively, but the results are generally quite encouraging. It is hoped that research will be continued so that the potential benefits of using this device will be realized in practice.

REFERENCES

1. D.G. Shurig, J.E. Hittle, E.J. Yoder, and W.H. Goetz. Field Investigation of County Road Bases and Subgrades. County Highway Series 14. HERPIC, Purdue University, West Lafayette, Ind., 1977.
2. B. Clegg. An Impact Soil Test for Low Cost Roads. Proc., Australian Road Research Board, Numawading, Victoria, Australia, Vol. 8, 1976.
3. B. Clegg. An Impact Soil Tester as an Alternative to California Bearing Ratio. Proc., Second Conference on Road Engineering, Association of Asia and Australasia, Manila, Philippines, Oct. 1978.
4. M.J. Reid. Correlation of an Impact Testing Device for Evaluating County Road Subgrades and Bases. Master's thesis. Purdue University, West Lafayette, Ind., 1978.
5. N.W. Garrick. Field Evaluation of an Impact Testing Device for Measuring Base Course Strength. Report H-83-3. Highway Extension and Research Project for Indiana Counties and Cities, Purdue University, West Lafayette, Ind., May 1983.
6. G.L. Glick and B. Clegg. Use of a Penetrometer for Site Investigation and Compaction Control at Perth, W.A. The Institution of Engineers, Australia, Civil Engineering Transactions, Vol. CE 7, No. 2, Oct. 1965.
7. D.J. van Vuuren. Rapid Determination of CBR with the Portable Dynamic Cone Penetrometer. The Rhodesian Engineer, Sept. 1969.

Publication of this paper sponsored by Committee on Exploration and Classification of Earth Materials.

Evaluation of Pavement Subgrade Support Characteristics by Dilatometer Test

ROY H. BORDEN, CECEP N. AZIZ, WESLEY M. LOWDER, and N. PAUL KHOSLA

ABSTRACT

The problem of evaluating the as-compacted or existing properties of subgrade soils is an important aspect of the design and rehabilitation of flexible pavements. The dilatometer has been shown to have significant potential for obtaining this information both reliably and economically. The relationship between the dilatometer modulus and the as-compacted California bearing ratio (CBR) for three different natural soils has been investigated. In general, the test program may be characterized as having evaluated: (a) a range of sample sizes including cylindrical molds of 6.0 in. (152 mm) and 11 in. (280 mm) diameter, a 3 ft x 4 ft (approximately 1 m x 1.25 m) chamber, and several field tests; (b) compactive efforts equivalent to AASHTO T-180, T-99, 50 percent of T-99, and a lower effort that produced a density equivalent to 90 percent of T-99 maximum dry density; and (c) a moisture content range for each soil sufficient to establish maximum dry densities at each compactive effort. The results of the laboratory and field test program lead to the following conclusions: (a) Unique relationships between dilatometer modulus and CBR were found to exist for the as-compacted A-5 and A-6 soils regardless of density and moisture content conditions. (b) A laboratory technique was developed whereby dilatometer penetration could be performed in CBR molds 6 in. (152 mm) in diameter such that both pieces of data could be obtained on the same specimen. Although the boundary conditions appear unfavorable in the small mold, the results were consistent with those obtained in an 11-in. (280-mm) mold and a chamber 3 ft x 4 ft (approximately 1 m x 1.25 m). This small mold test did not work well for the A-2-4 soil and would probably not work for any soil that was dominated by granular material with little fine-grained component. (c) Limited field tests on a compacted embankment from which one of the soils (A-6) used in the study was obtained revealed excellent correlation with the laboratory test program.

The problem of evaluating the as-compacted or existing properties of subgrade soils is an important aspect of the design and rehabilitation of flexible pavements. At present, this estimate is generally obtained by conducting in-place California bearing ratio (CBR) tests or less frequently plate loading tests. These tests involve the removal of a section of pavement large enough that a technician can work in the excavated area at the subgrade level. The flat dilatometer, a device introduced in 1975 by Marchetti (1) for the in situ investigation of soil properties, offers significant promise for providing a reliable and economical method for obtaining strength and stiffness characteristics associated with pavement design.

The flat dilatometer, shown in Figure 1, consists of a stainless steel blade with a thin, flat, circular, expandable steel membrane on one side. The body of the dilatometer has a width of approximately 3.7 in. (95 mm) and a thickness of approximately 0.6 in. (14 mm). When at rest, the external surface of the membrane, approximately 2.4 in. (60 mm) in diameter, is flush with the surrounding flat surface of the blade. The blade is jacked into the ground and when located at the desired depth the membrane is inflated by means of pressurized gas through a small control unit at the ground surface (also shown in Figure 1). A longitudinal cross section of the dilatometer is shown in Figure 2. Readings are taken of the "A" pressure required to just begin to move the membrane (related to the lateral stresses existing in the ground) and of that "B" pressure required to move its center an additional approximate 0.04 in. (1 mm) into the soil (related to soil stiffness). Movements of the membrane are measured by extensometers behind the diaphragm within the body of the device. On the basis of the assumption of linear elasticity, Marchetti (2) proposed that the lateral soil modulus be represented by the expression

FIGURE 1 Dilatometer and control unit.

$$S_o = [2\Delta pD(1 - \mu^2)]/(\pi E) \quad (1)$$

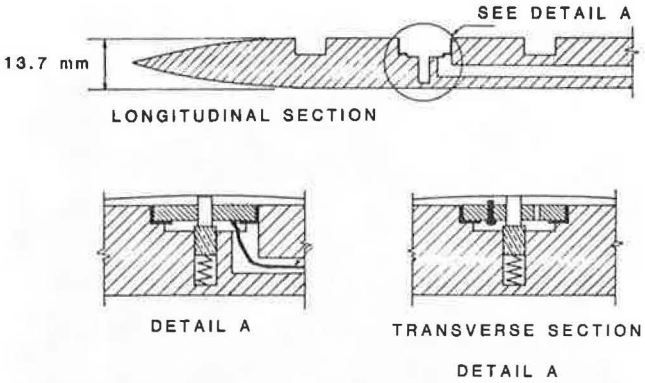

FIGURE 2 Section and details of dilatometer blade.

where S_o is the approximate 0.04-in. (1-mm) deflection of the center of the membrane, Δp is the difference in the A and B readings corrected for membrane stiffness, D is the 2.4-in. (60-mm) membrane diameter, E is Young's modulus, and μ is Poisson's ratio of the soil. The expression, $E/(1 - \mu^2)$, is then termed the dilatometer modulus (E_d).

The usefulness of lateral soil modulus data for predicting vertical stiffness has been demonstrated in a study by Briaud and Shields (3). In their study, lateral stiffness data were obtained using a small diameter pressure meter and were shown to be linearly related to pavement bearing strength as determined by McLeod plate tests.

The laboratory and field tests reported in this paper were conducted in the first phase of a research program to evaluate the use of the dilatometer for obtaining subgrade support characteristics both for pavement under construction and for those requiring rehabilitation. In the initial phase of the program, the objectives were the development of laboratory testing techniques and the establishment of correlations between dilatometer moduli and CBR values for a range of soil types and moisture-density conditions. Field verification tests were also conducted in a newly compacted subgrade as were preliminary tests in an existing pavement system. In one instance, the dilatometer was hydraulically pushed through an asphalt pavement with the 7,500-lb. (33.4-kN) capacity of a Mobile drill rig. Research is continuing on developing field testing techniques for use beneath existing pavements and on correlating the lateral soil modulus obtained from the dilatometer with resilient modulus and constrained modulus response.

EXPERIMENTAL PROGRAM

To evaluate the potential usefulness of the dilatometer for determining pavement subgrade support characteristics, an experimental program was designed using the three natural soils the characteristics of which are given in Table 1. These soils were chosen for their range of properties and significance as locally encountered materials. Most notably, the first soil has a significant mica content, the second has a higher silt-clay content, and the third has an extremely high sand content. Because the primary goal of this first phase of the research program was to identify the potential for predicting in-place subgrade characteristics (as indicated by CBR value) from the dilatometer modulus, it was deemed important to evaluate the significance of soil type on the functional relationship. It was also anticipated that the insertion of the dilatometer blade into a laboratory scale sample could produce results different from those that would be obtained in the field due to boundary effects. The experimental program evolved because the findings on the first soil tested influenced the subsequent procedures. In general, the test program may be characterized as having evaluated (a) a range of sample sizes including cylindrical molds 6 in. (152 mm) and 11 in. (280 mm) in diameter, a chamber 3 ft x 4 ft (approximately 1 m x 1.25 m), and several field tests; (b) compactive efforts equivalent to AASHTO T-180, T-99, 50 percent of T-99, and a lower effort that produced a density equivalent to 90 percent of the T-99 maximum dry density; and (c) a moisture content range for each soil sufficient to establish maximum dry densities at each compactive effort.

TABLE 1 Soil Characteristics

	Soil 1	Soil 2	Soil 3
Percentage passing no. 4 sieve	88	97	100
Percentage passing no. 40 sieve	77	84	40
Percentage passing no. 200 sieve	43	65	18
Liquid limit (%)	46	37	26
Plasticity index (%)	3	15	4
γ_d max (pcf)	102.4	111.0	118.0
wopt (%)	20	16.8	12.5
γ_d max (pcf)	110.4	123.0	–
wopt (%)	16.8	12.2	–
Specific gravity	2.77	2.78	2.70
AASHTO classification	A-5	A-6	A-2-4

Note: Dashes indicate not conducted.

The standard preparation technique for all samples involved the air drying of soil, followed by an increase in moisture content by means of a combination of hand and rotary mixing. All samples were then sealed in plastic bags and placed in a 100 percent humidity room for at least 72 hr to enhance moisture equilibration. All specimens 6 in. (152 mm) in diameter were compacted using an automatic drop weight device fitted with a sector-shaped hammer head. Standard AASHTO compaction procedures were used. A fresh batch of soil was used for each compaction test. This eliminated the question of any residual fabric effects that can arise in some soils from the reuse of previously compacted material.

For practical reasons it was not deemed feasible to compact the specimens 11 in. (280 mm) in diameter with the same drop weight procedure. Static compaction using an MTS loading frame was employed to compress layers of soil to the desired density. In this way densities could be obtained that corresponded to the densities (T-180, T-99, and so forth) from the impact tests. Three layers were used to make specimens approximately 13 in. (330 mm) to 13.8 in. (350 mm) in height. After the last layer was compacted, three CBR tests were conducted in the top layer. The dilatometer test was performed once in each layer with the dilatometer positioned in such a way that the center of the membrane was approximately at the middepth of each layer.

The CBR tests for each of the lower layers were performed after carefully removing the soils on top of them. The final wet unit weight of the compacted soil was determined as the ratio of the weight of soil in each layer divided by its final volume (taking into consideration the densification of the lower layers due to placing of the upper layers).

To more clearly identify the influence of sample size that resulted from the presence of constraining boundaries, an even larger laboratory sample was used in the first test series. A test chamber with plan dimensions of 3 ft x 4 ft (approximately 1 m x 1.25 m) and a height of 3 ft (approximately 1 m) was constructed. Soil for this sample was brought to the

desired moisture condition by mixing in a concrete mixer. A layer of sand was placed and compacted in the bottom of the chamber, followed by compacted layers of soil approximately 5 in. (125 mm) thick. Each soil layer was compacted using a hand-held mechanical field compacter. The dilatometer was pushed into the sample by means of a hydraulic piston mounted on an overhead frame. The use of pressure-compensating flow control valves allowed the dilatometer to be inserted at a controlled rate. When the center of the dilatometer membrane was approximately at middepth of the first layer, the penetration was stopped and the membrane inflated. On completion of the test, the dilatometer was advanced to middepth of the next layer. This procedure continued until all three layers had been tested, with the sand layer providing a "cushion" to ensure that the tip of the dilatometer did not strike the bottom of the chamber when penetrating to the bottom layer. After the completion of numerous dilatometer insertions, the box was excavated allowing for (a) conducting "field" CBR tests at the middepth of the compacted layers and (b) an actual measurement of the as-compacted layer thickness and moisture content distribution.

Finally, for the second soil tested, a local field site was identified where a compacted embankment for a bridge abutment had recently been constructed. A series of field density tests, field CBR tests, and dilatometer tests was conducted. The CBR tests were conducted using the loaded reaction truck shown in Figure 3, which was jacked off of its springs and supported on concrete cylinders. The dilatometer was hydraulically inserted by using the Mobile drill rig shown in Figure 4. Only minor modifications in the coupling of the union were required to attach the dilatometer to the existing equipment.

FIGURE 3 Field CBR test.

RESULTS

The results of the laboratory and field tests conducted in this study are presented in the sequence in which the three soils were tested because intermediate conclusions were reached and these findings influenced subsequent testing procedures. During the initial stages of the testing program special attention was focused on answering the following questions:

1. If specimens are made in a larger diameter mold, will differences in specimen preparation technique substantially influence the density-CBR and the CBR-dilatometer relationships?
2. How large does the mold into which the dilatometer is pushed need to be in order to reduce boundary effects to a minimal level for compacted soils?
3. Can a unique relationship between dilatometer modulus (E_d) and CBR be found, regardless of soil density or moisture content conditions, for each soil tested?

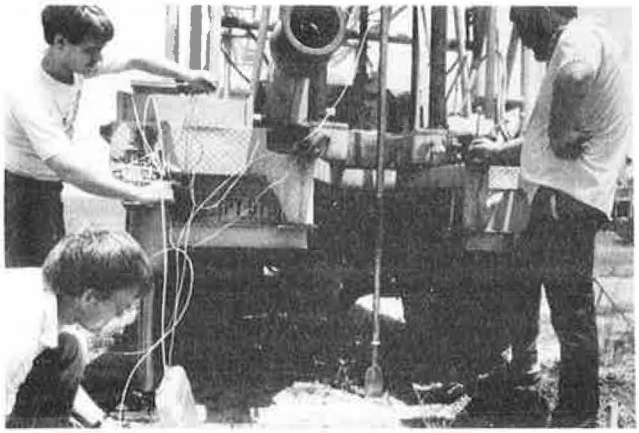

FIGURE 4 Insertion of dilatometer with drill rig.

It was obvious that moisture-density relationships and CBR data would need to be developed in standard molds with conventional compaction procedures. However, it was initially believed that the dilatometer would probably need to be inserted into specimens that had a minimal diameter of the 11 in. (280 mm).

Figures 5 and 6 show the compaction characteristics and unsoaked CBR response, respectively, for the A-5 soil. For the lower moisture contents, the effect of increased compactive effort is to increase the CBR value. At higher moisture contents, the as-compacted CBR values are lower for the specimens compacted with the highest energy level. This is due to the increased initial degree of saturation and resultant influence on the effective stress state during penetration.

On the basis of the results of the impact-compacted specimens reported in Figures 5 and 6, and

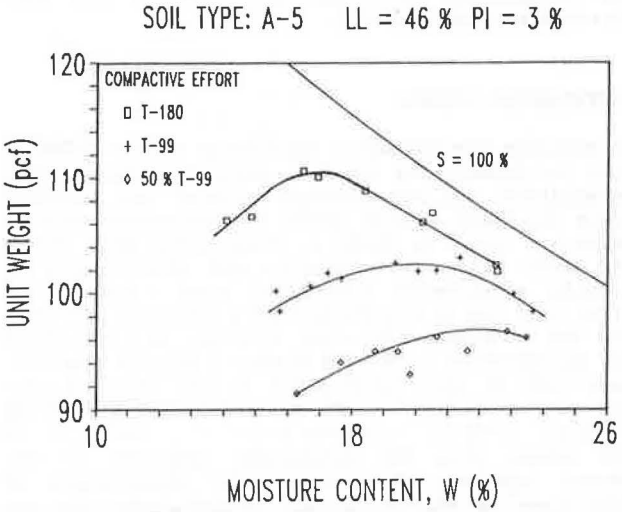

FIGURE 5 Moisture content versus unit weight for A-5 soil.

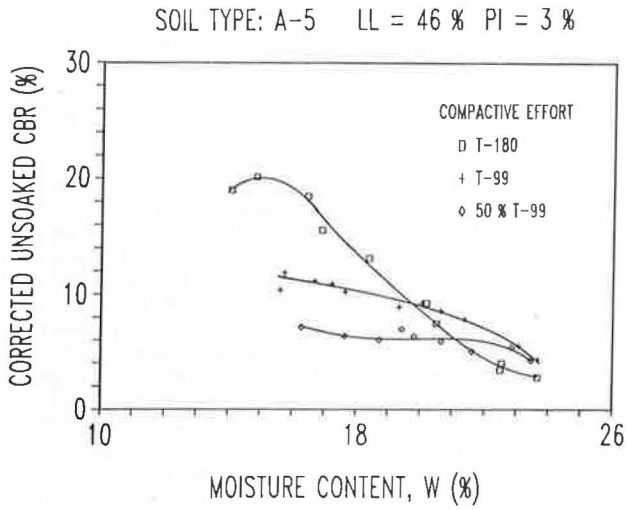

FIGURE 6 Moisture content versus corrected unsoaked CBR for A-5 soil.

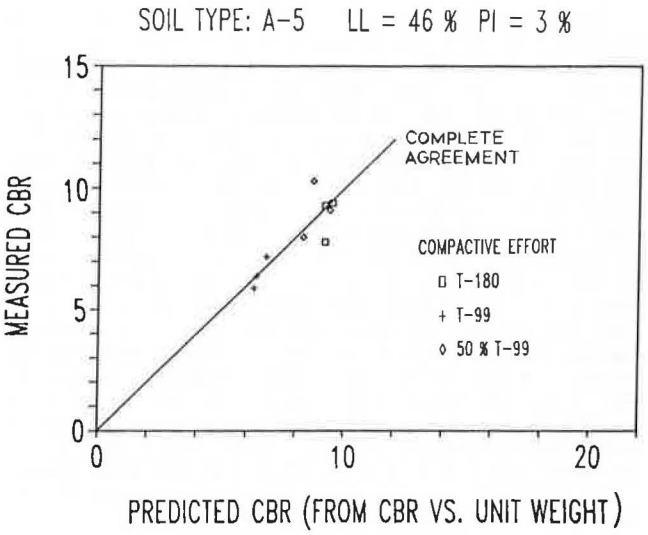

FIGURE 8 Predicted CBR versus measured CBR for A-5 soil.

using the smooth curves fit through the data, Figure 7 was constructed (4). From this figure, the as-compacted CBR value can be predicted for any combination of moisture content and dry density. This allowed a comparison to be made between the CBR values obtained from tests on statically compacted samples and standard impact-compacted samples. The dry density and moisture content of the statically compacted sample were determined by excavating the sample after testing. When these two values had been determined, the predicted CBR value was found from Figure 7 and compared with the value obtained from the CBR test on the statically compacted sample. The degree to which these data agree is some measure of the similarity of the specimens. The results of this comparison are shown in Figure 8 with several typical values noted. The 45-degree line indicates complete agreement and the comparison is seen to be quite good. Although this is no guarantee that fabric or structural differences between impact-compacted and statically compacted specimens do not exist to any degree, it is an indication that they are not significant near the optimum moisture content where the statically compacted specimens were prepared.

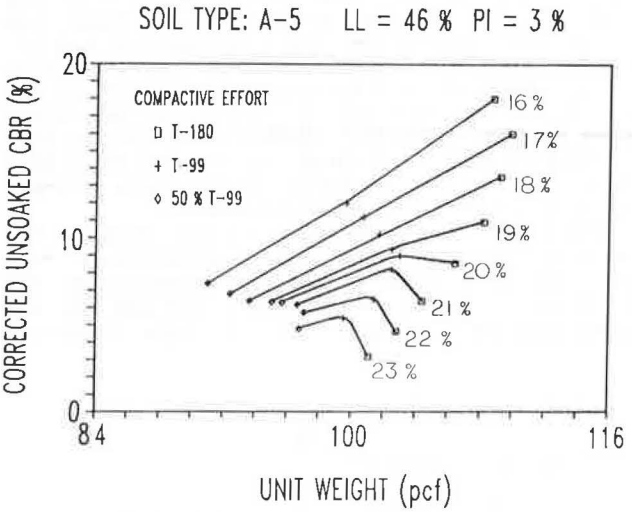

FIGURE 7 Unit weight versus corrected unsoaked CBR for A-5 soil.

Figure 9 shows a summary plot of the CBR versus dilatometer modulus data for the tests conducted in the statically compacted specimens, the large test chamber previously described, and several tests conducted in a mold having the same diameter as the standard CBR mold but that was considerably taller and allowed the impact compaction of a specimen 12 in. (approximately 300 mm) thick. CBR tests were conducted on the surface and the dilatometer was inserted down to midheight of the mold. A linear regression was performed using all data points except those circled; this resulted in the regression coefficients a = 0.07, b = .041, and an R^2 value of 0.86. With an insignificant loss in predictive capability, the expression could be more simply stated as

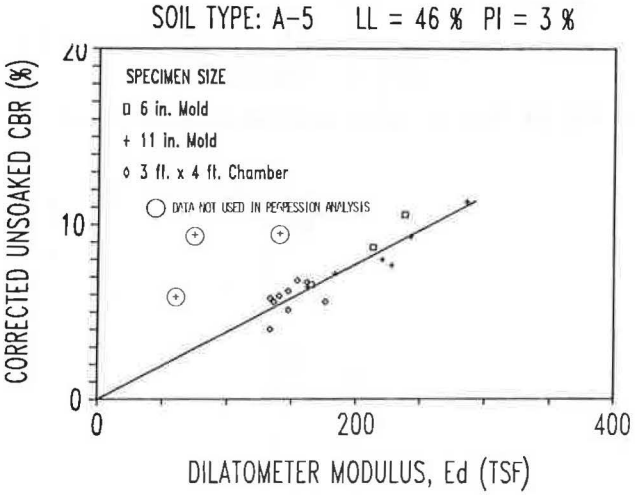

FIGURE 9 Dilatometer modulus versus corrected unsoaked CBR for A-5 soil.

$$CBR = 0.041\ E_d \quad (2)$$

with the CBR value expressed as a percentage and the E_d value in tsf.

The three values that are circled in Figure 9 represent dilatometer data obtained in the top layer of the statically compacted three-layer specimens. In each case the top layer was approximately 4 in. (100 mm) thick and the dilatometer membrane 2.4 in. (60 mm) in diameter was only 0.8 in. (20 mm) to 1.2 in. (30 mm) below the soil surface. It appears that the insertion of the blade created enough disturbance of the adjacent soil to cause a loss of lateral support. This was noted by visual observation. In subsequent tests on the third soil (predominated by its sand component) actual bearing capacity failures with significant uplifted zones were noted in some specimens. The data from the large box actually represent the average of two or three dilatometer modulus values within a 10-in. (254-mm) radius of the three CBR tests conducted in the center of each of the three layers. The CBR tests were conducted along the centerline of the box at the one-quarter, one-half, and three-quarter points on the plan area.

An analysis of the data shown in Figure 9 resulted in two important conclusions:

1. The modulus data obtained in the 6-in. (152-mm) mold (standard CBR mold diameter) provided data consistent with the larger mold and large box although the boundary conditions are obviously less favorable and
2. The 0.8- to 1.2-in. (20- to 30-mm) penetration of the dilatometer diaphragm below the 11-in. (280-mm) mold surface was not sufficient.

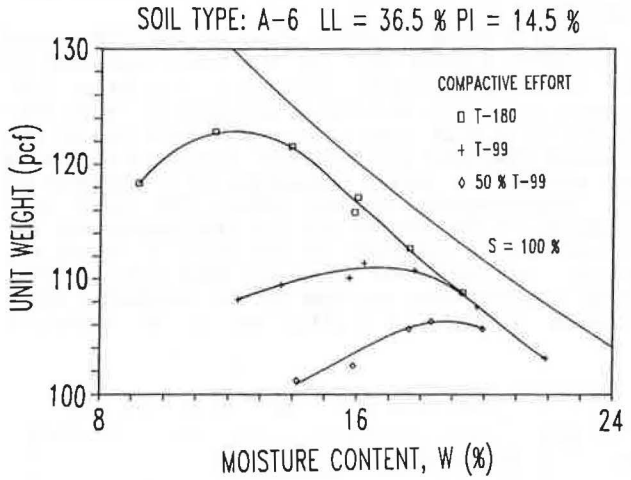

FIGURE 10 Moisture content versus unit weight for A-6 soil.

The similarity of the results obtained in the three different size test specimens was not anticipated. It was postulated that the compression of the soil adjacent to the dilatometer membrane during insertion of the blade must have been essentially the same in each environment. This could explain the consistent lateral stiffness observed. The densification that occurred at distances away from the dilatometer may well have been a function of specimen size, but this behavior was not investigated.

Therefore, two modifications were incorporated in subsequent testing. First, a technique was developed whereby the CBR mold could be used as a specimen for dilatometer testing after the CBR test was conducted. Simply stated, the surcharge weights were removed, the top volume of the mold was filled with sand, the base plate was then disassembled and attached to the top of the mold, the mold was inverted, and penetration was made from the opposite end. This allowed for the generation of a large number of CBR and dilatometer data on identical specimens over a wide range of moisture and density conditions. Second, the layer thickness in the large mold was altered to provide a thicker top layer. All subsequent 11-in. (280-mm) mold tests were conducted on specimens with lower layers approximately 3.9 in. (100 mm) thick and a top layer of approximately 5 in. (125 to 130 mm). With the penetration of the dilatometer to near the bottom of the top layer, the top of the membrane was now approximately 2.4 in. (60 mm) (or one diaphragm diameter) below the free surface. Because the dilatometer modulus did not appear to be influenced by sample size, it was determined that the large test chamber would only be used if future results indicated the presence of a size influence when data generated in the 6-in. (152-mm) and 11-in. (280-mm) molds were compared.

The compaction characteristics and unsoaked CBR response for the second soil, classification A-6, are shown in Figures 10 and 11, respectively. The correlation between the results obtained in the impact-compacted CBR molds and the larger statically

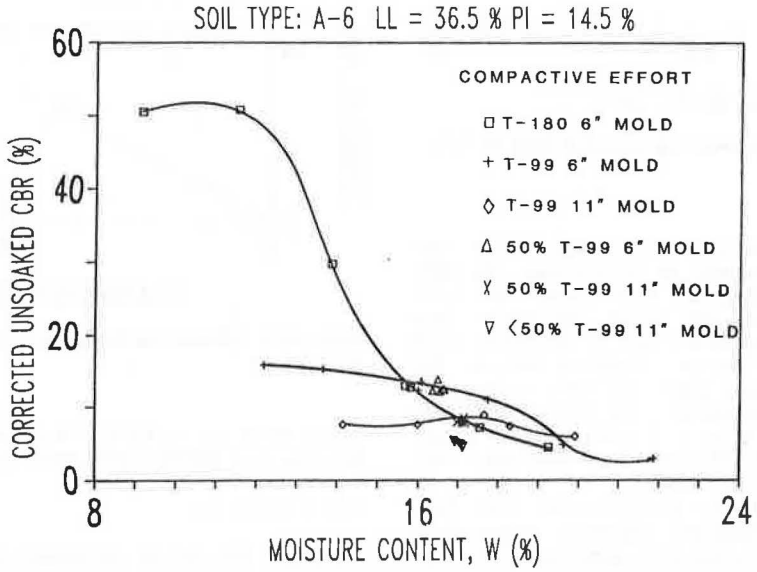

FIGURE 11 Moisture content versus corrected unsoaked CBR for A-6 soil.

compacted molds was excellent. Although plots similar to Figures 7 and 8 for soil 1 were developed, the degree of agreement is clearly shown in Figure 11. The lower compactive effort data were generated in the 11-in. (280-mm) mold by statically compacting the soil at the optimum moisture content (for the T-99 compactive effort) to a density representative of approximately 90 percent of the T-99 dry density. Figure 12 shows the dilatometer data generated for this soil. The linear regression coefficients utilizing all the laboratory data are a = 0.16, b = 0.052, and an R^2 value of 0.89. As with the first soil tested, the intercept value is negligible and the relationship may be expressed as

$$CBR = 0.052\ E_d \quad (3)$$

with the CBR value expressed as a percentage and the E_d value in tsf.

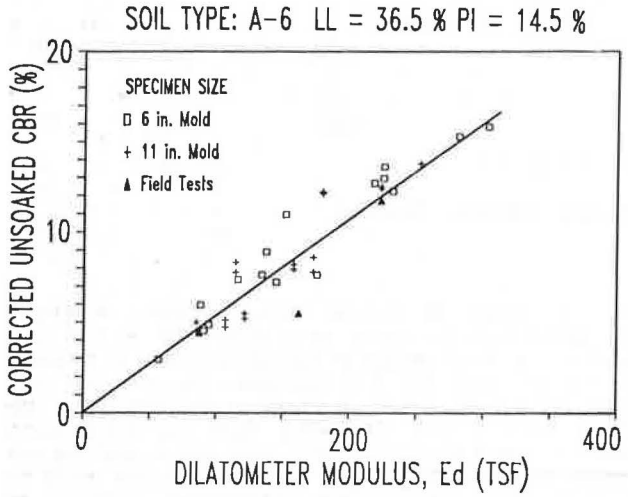

FIGURE 12 Dilatometer modulus versus corrected unsoaked CBR for A-6 soil.

In all but one instance two CBR tests were conducted on each of the three layers of the three 11-in. (280-mm) specimens. In order that the consistency of the CBR data might be shown, each of the values obtained was plotted versus the single dilatometer reading from that layer. It is also notable that the data furthest to the left of the regression line were again those obtained from the top of the 11-in. (280-mm) mold, although the magnitude of the difference was not as observable as it was with the first soil. It appears that the increased depth of membrane insertion (to one membrane diameter) in these tests helped solve the problem identified previously. However, because a loss of lateral support due to dilatometer insertion has clearly been identified as the reason for low readings in previous tests, it may be suspected that this factor is still operating to some degree in these tests.

Finally, the compaction characteristics and the unsoaked CBR response for the third soil, an A-2-4, are shown in Figures 13 and 14. Due to the extremely high density and corresponding high CBR values for the T-99 compacted specimens, it was deemed more interesting from a practical point of view to evaluate a lower compactive effort in place of the previously used T-180. Several high compactive effort specimens were prepared with moisture contents of 10 and 12 percent with resulting CBR values in excess of 50. However, none of these specimens could be penetrated with the 5,000-lb. (22.2-kN) capacity of

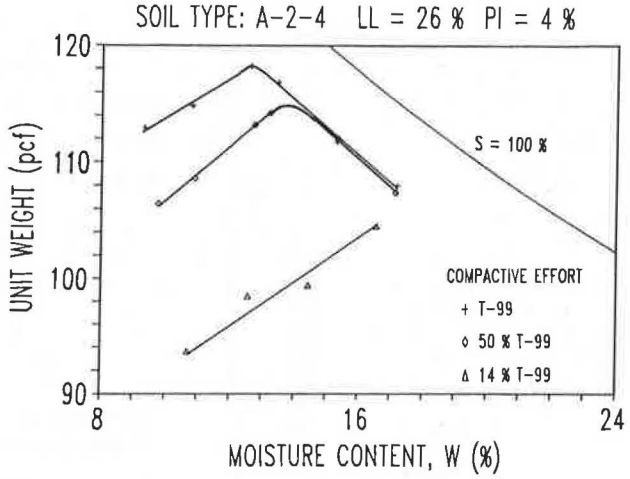

FIGURE 13 Moisture content versus unit weight for A-2-4 soil.

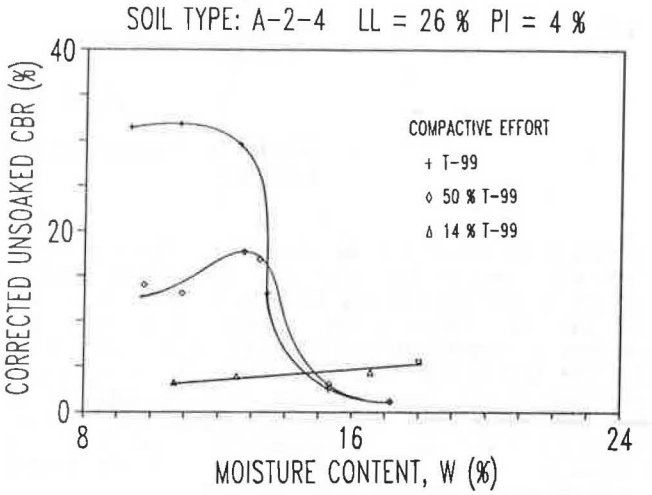

FIGURE 14 Moisture content versus corrected unsoaked CBR for A-2-4 soil.

the laboratory hydraulic piston used for dilatometer insertion.

The CBR-versus-dilatometer relationship shown in Figure 15 exhibits significant scatter. The symbols used in Figure 15 differ somewhat from those used previously in order to illustrate several significant points. First, in numerous instances the insertion of the dilatometer into this soil resulted in obvious heaving of the surface; in some instances wedges of soil lifted from the molds resulting in a loss of lateral support. This response was seen for both the 6-in. (152-mm) and the 11-in. (280-mm) molds. All of these points are circled in Figure 15 and were not used in the subsequent regression analysis. In one instance, in the 11-in. (280-mm) mold test on the T-99 compacted specimens, no dilatometer data were obtained for the top layer due to the amount of soil displaced during penetration. Second, the data obtained in the lower layers of the 11-in. (280-mm) mold appear to be consistent. The limited capacity of the laboratory hydraulic piston prevented penetration of the dilatometer in several instances. For example, only the top layer of the T-99 compacted specimen could be penetrated, but no dilatometer data were obtained as previously mentioned; for the 50 percent of T-99 specimen, the first and second layers were penetrated, but the

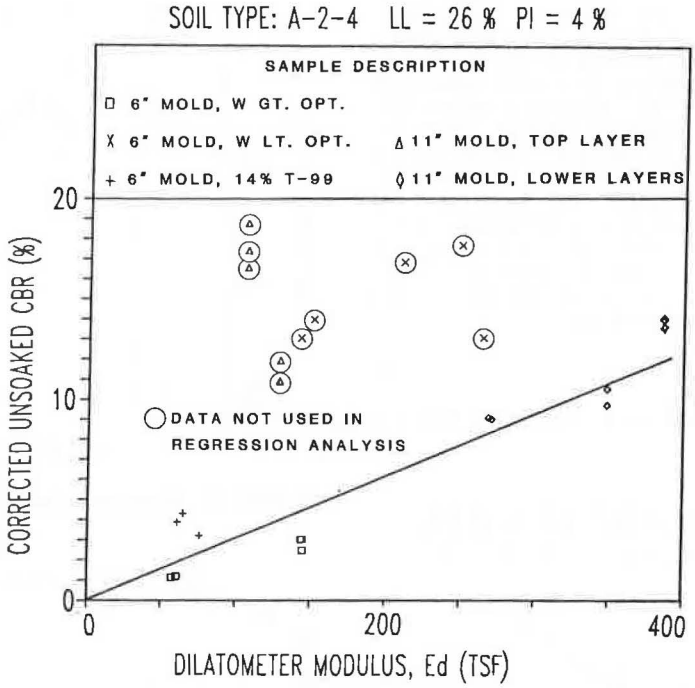

FIGURE 15 Dilatometer modulus versus corrected unsoaked CBR for A-2-4 soil.

lowest layer could not be penetrated. The top layer data are shown in Figure 15 with CBR values between 16 and 19 and with a low dilatometer modulus of 100 due to soil heaving. The middle layer data are plotted at approximately a dilatometer modulus of 400 tsf and a CBR value of 16.5. Penetration was achieved in all layers of the lower density specimen, and apart from the top layer data (E_d approximately 125 tsf and CBR between 10.5 and 12), the bottom two layers appear consistent with the middle layer of the 50 percent T-99 specimen.

A linear regression on the data from the lower layers in the 11-in. (280-mm) molds and that from tests conducted on lower density specimens and those compacted wet of optimum yielded the following coefficients: a = 0.19, b = 0.031, and R^2 = 0.89. Simplifying, as before, yields the expression

$$CBR = 0.031\ E_d \quad (4)$$

with the CBR value expressed as a percentage and the E_d value in tsf. The inclusion of the 6-in. (152-mm) mold data on the lower compactive effort specimens and those compacted wet of optimum was done because no visual observations were made that indicated that they should be discarded. The observance of surface heaving in numerous tests indicated that the results of small mold tests and unconfined near-surface tests in compacted soils that are predominately sand with little cohesive component must be viewed with caution.

FIELD TESTING

In an effort to validate the results of the laboratory study reported in this paper, field tests were conducted at the location of a new bridge structure that was under construction in the Research Triangle Park area of North Carolina. This location served as the borrow site for the A-6 soil used in the laboratory study. In cooperation with the Geotechnical Unit and Materials and Test Unit of the North Carolina Department of Transportation (NCDOT), field CBR and field density tests were conducted on the surface layer of a compacted embankment that will serve as the approach for the overpass. Because the surface had not been cut to final grade, the three in-place density and CBR tests were conducted at a depth of approximately 8 in. (200 mm) below the existing surface. No attempt was made in this study to evaluate the near-surface dilatometer response by varying the depth of penetration. The dilatometer was hydraulically pressed into the compacted fill using the Mobile drill rig shown in Figure 2 at locations approximately 12 in. (300 mm) away from the CBR and density tests. The dilatometer was pushed until the center of the diaphragm was at the desired 8 in. (200 mm) depth. Subsequent advances were made in 8-in. (200-mm) increments through the fill to a maximum depth of approximately 20 ft (6 m). However, because CBR and density data were only obtained at the surface, the rest of the dilatometer data are not presented in this context.

The results of the field CBR and dilatometer tests are presented with the laboratory data previously discussed in Figure 12. Although the data are limited, the correlation with the many laboratory tests is encouraging. The time required to conduct the field dilatometer tests was on the order of 1 min per test when near-surface data were being gathered. For the approximately 20-ft (6-m) penetrations, readings were taken at every 8 in. (200 mm) for a total of 29 readings. The assembly and disassembly of rods increased the average time to approximately 1.5 min, or a total of 45 min. This indicates the great economy that can be achieved in obtaining subgrade support characteristics compared with in-place CBR tests.

SUMMARY AND CONCLUSIONS

The problem of evaluating the as-compacted or existing properties of subgrade soils is an important aspect of the design and rehabilitation of flexible

pavements. The dilatometer has been shown to have significant potential for obtaining this information both reliably and economically. In this paper, the relationship between the dilatometer modulus and as-compacted CBR for three different natural soils has been investigated. Current research is extending this work to include resilient modulus and one-dimension compression modulus (constrained modulus) correlations.

On the basis of the results of the laboratory and field test program reported herein, the following conclusions are advanced:

1. Unique relationships between dilatometer modulus and CBR were found to exist for the as-compacted A-5 and A-6 soils regardless of density and moisture content conditions. The relationships were found by linear regression to be CBR = 0.041 E_d for the A-5 soil and CBR = 0.052 E_d for the A-6 soil. The data for the A-2-4 soil yielded the relationship CBR = 0.031 E_d, although many more tests were found unacceptable due to heaving of the soil surface and loss of lateral support. Reasonable data were obtained when the dilatometer diaphragm was at a depth of approximately 7 in. (175 mm) or more below the mold surface.
2. A laboratory technique was developed whereby dilatometer penetration could be performed in CBR molds 6 in. (152 mm) in diameter such that both the dilatometer modulus and CBR value could be obtained on the same specimen. Although the boundary conditions appeared unfavorable in the small mold, the results were consistent with those obtained in an 11-in. (280-mm) mold and a chamber 3 ft x 4 ft (approximately 1 m x 1.25 m). It was postulated that the compression of the soil adjacent to the dilatometer blade during penetration was essentially the same in each of the specimens. Thus the stiffness of the soil within the zone of influence for the 0.04-in. (1-mm) diaphragm expansion was observed to be similar. This small mold test did not work well for the A-2-4 soil and probably would not work well for any soil that was dominated by granular material with little fine-grained component.
3. Limited field tests on a compacted embankment from which one of the soils (A-6) used in the study was obtained revealed excellent correlation with the laboratory test program. The economical use of the dilatometer was shown in the ability to obtain data at a given location in approximately 1 min per test point desired. A 3.3-ft (1-m) penetration with five tests conducted at depth increments of approximately 8 in. (200 mm) took a total of about 5 min. This was in sharp contrast to the time that it took to obtain the limited CBR data. In addition, the problems of surface preparation, equipment alignment, and maintaining constant CBR penetration rates are eliminated.

ACKNOWLEDGMENTS

The research reported herein was supported by the North Carolina Department of Transportation through the Institute for Transportation Research and Education in cooperation with the Federal Highway Administration, U.S. Department of Transportation.

A technical advisory committee chaired by George Wells, Manager of Highway Design, and including Harold Landrum, John Ledbetter, Dick Reaves, and Pat Strong from the NCDOT and John Wadsworth from the Federal Highway Administration aided in the coordination of the research project.

Thanks are also due to Billy Brantly and Njoroge Wainaina of the Materials and Test Unit and to Dave Bingham and Bill Moore of the Geotechnical Unit of the NCDOT who made valuable contributions in the field portion of this project.

The authors wish to thank Harvey Wahls and David Johnston of the Civil Engineering Department of North Carolina State University who provided many helpful suggestions with regard to the testing program and construction of the large test chamber. The assistance of Bill Dunleavy, also of the Civil Engineering Department of North Carolina State University, who provided the technical support for all of the project instrumentation needs, is also appreciated.

All of these individuals have been most helpful in the formulation, guidance, and conduct of the research reported herein.

REFERENCES

1. S. Marchetti. A New In Situ Test for the Measurement of Horizontal Soil Deformability. Proc., Conference on In Situ Measurement of Soil Properties, ASCE Specialty Conference, Raleigh, N.C., Vol. 2, June 1975, pp. 255-259.
2. S. Marchetti. In Situ Tests by Flat Dilatometer. Journal of the Geotechnical Engineering Division, ASCE, Vol. 106, No. GT3, March 1980, pp. 299-321.
3. J.L. Briaud and D.H. Shields. Use of Pressure Meter Test to Predict Modulus and Strength of Pavement Layers. In Transportation Research Record 810, TRB, National Research Council, Washington, D.C., 1981, pp. 33-42.
4. H.E. Wahls, C.I. Fisher, and L.J. Langfelder. The Compaction of Soil and Rock Materials for Highway Purposes. Research Report ERD 197-25. Department of Civil Engineering, North Carolina State University, Raleigh, 1966.

Publication of this paper sponsored by Committee on Exploration and Classification of Earth Materials.

Flat Dilatometer and Lateral Soil Modulus

E. SABRI MOTAN and MUHAMMED A. GABR

ABSTRACT

Changes in the lateral stress condition in soil in the immediate vicinity of the blade of the flat dilatometer during the penetration of the device were experimentally investigated in a laboratory study. Lateral separation that takes place during the penetration of the blade was simulated by horizontally advancing a rectangular aluminum block instrumented with a dilatometer diaphragm against sand specimens prepared in a testing tank at different relative densities. A cantilever beam-type deflection transducer mounted in the chamber behind the diaphragm made it possible to obtain a continuous record of pressure-diaphragm center deflection. For purposes of comparison, a standard flat dilatometer was used in a series of penetration tests conducted concurrently with the lateral separation study. Also, the effect of repeatedly expanding the diaphragm on the pressure-diaphragm center deflection curve was considered. The results of the study point out factors that are thought to be of importance in a meaningful interpretation of the dilatometer data and the assessment of the lateral soil modulus.

An extensive array of penetration devices has been developed during the last half-century as a result of a need to profile subsoil conditions more accurately than conventional methods of drilling and intermittent sampling allow. Some of these devices, such as the standard penetration and cone penetration tests, have been widely accepted and used in a range of geotechnical and highway engineering problems. In highway engineering, in addition to their use in solving typical foundation soil bearing capacity problems, penetrometers have been used as quality control tools during the construction of compacted embankments.

The flat dilatometer, first introduced in this country in the mid-1970s (1) is basically a penetrometer that is also capable of measuring the soil stiffness with the help of an expandable, circular steel diaphragm attached on a stainless steel blade 14 mm (0.550 in.) thick. The blade is jacked into the soil using a penetrometer rig. A nylon tube that runs through the penetrometer rods connects the dilatometer control unit with a chamber behind the diaphragm. A steel wire passing through the nylon tube completes the electrical circuit that is used to detect specific positions of the diaphragm center as it is expanded against the soil. A spring-loaded displacement sensor mounted inside the pressure chamber behind the diaphragm is adjusted to close the circuit and keep a buzzer on the dilatometer control unit activated when the diaphragm center is at two specific positions: (a) flush with the blade surface and (b) deflected by 1 mm against the soil. During penetration of the blade, the diaphragm is kept flush with the surface of the blade by the lateral soil pressure acting on it. As soon as the desired depth is reached, the diaphragm is inflated by pressurized gas. The first pressure reading is taken at the instant the outward movement of the diaphragm is initiated. This is indicated by the silencing of the buzzer on the control unit. The second pressure reading is taken when the diaphragm center has deflected by 1 mm (0.039 in.), at which instant the buzzer is activated again. These readings, which must be corrected for diaphragm stiffness, are used to compute soil index parameters that correlate with in situ soil type and characteristics.

Previous applications of the flat dilatometer include profiling of subsoil conditions and estimation of a number of soil parameters such as at-rest lateral earth pressure; overconsolidation ratio; coefficient of volume compressibility; and, in saturated sands, assessment of liquefaction susceptibility (2-4). By virtue of its construction, the flat dilatometer is capable of obtaining lateral soil stiffness data in a nearly continuous manner in both cohesive and cohesionless soils. It can, therefore, be employed as an alternative to the methods currently used in assessing soil response during lateral loading of pile foundations.

Differences in the soil strains resulting from dilatometer penetration and pile driving, however, present difficulties in extrapolating the dilatometer data for use in the analysis of laterally loaded pile behavior. This study was designed to

1. Obtain the soil response against the expansion of the diaphragm in the form of a continuous pressure-diaphragm deflection curve and evaluate the significance of such a relationship and
2. Investigate the changes in the lateral pressure in the immediate vicinity of the dilatometer in response to penetration of the dilatometer blade.

The scope of the work presented covers the possible use of flat dilatometer data in estimating the stiffness of cohesionless soils for laterally loaded pile analyses. The results presented are of a preliminary nature. However, the data obtained, which should be substantiated by calibration studies on laterally loaded full-scale piles, indicate a potential for effective use of the flat dilatometer in securing field data for such analyses.

LATERAL SOIL STIFFNESS

A number of techniques and related equipment are available for the evaluation of lateral soil stiffness. These include, in addition to the flat dilatometer, full-scale lateral pile loading tests (5-9), plate-loading tests (10,11), triaxial testing (12,13), consolidation test (14), pressuremeter

(15,16), Iowa stepped blade (17), standard penetration test (18,19), and empirical correlations with other soil properties (10,20,21). A primary source of difficulty in interpreting the test results--with the exception of full-scale pile load testing--has been the significant differences in deformation modes imposed on soil during the tests and those that occur as a result of pile installation and subsequent lateral loading. Therefore, the majority of the techniques listed previously will not work satisfactorily under all circumstances. Also, discontinuous profiling of the soil, in relation to the lateral stiffness parameters, has a tendency to increase the statistical margin of uncertainty of the analysis. Therefore, short of conducting in-place full-scale lateral loading tests on prototype piles, much remains to the judgment of the engineer in extrapolating the field data, which are often obtained in the form of standard or cone penetration test results, far enough to make reasonable estimates of the lateral soil stiffness parameters.

During a dilatometer test the lateral stresses acting on the blade are measured at approximately 20-cm intervals as the blade penetrates the soil under static or impact loading. The mode of deformation imposed on the soil is similar to that resulting from the penetration of a driven pile, and dilatometer data may be used in a subgrade reaction type of analysis of piles under lateral loading. Because of the difference in the lateral soil separation that results from dilatometer and pile penetration, however, the soil disturbance condition, at which the soil stiffness is obtained by the dilatometer, is intermediate between undisturbed state and remolded conditions as imposed by the cross-sectional dimensions of the driven pile and the pile-soil friction. This leaves the task of extrapolating the dilatometer data backward to zero lateral strain condition to obtain the undisturbed soil stiffness and forward, within reason, to estimate the pressure-displacement relations for driven piles of substantially larger cross sections than that of the dilatometer blade. Another factor to be remembered in the analysis is the dependence of the subgrade reaction coefficient on the dimensions of the loaded area.

Marchetti (3), assuming linear elasticity, defined a "dilatometer modulus" $(E/(1 - \mu^2)$ that can be calculated with the data obtained during the expansion of the diaphragm against soil:

$$E/(1 - \mu^2) = (2D\Delta p)/(\pi S_o) \quad (1)$$

where

E = elastic modulus of soil,
μ = Poisson's ratio of soil,
D = diaphragm diameter,
S_o = deflection of the diaphragm center, and
Δp = difference between two pressure readings corrected for diaphragm rigidity: the first reading is taken immediately after the outward movement of the diaphragm has been initiated (p_0), and the second at 1-mm lateral deflection of the diaphragm center (p_1).

The dilatometer modulus correlates with the soil compressibility and the lateral soil stiffness. If the generally nonlinear stress-strain response of soils is considered, however, the dilatometer modulus in Equation 1 is actually a secant modulus. In this study, a suitably placed deflection transducer mounted to be in contact with the inside surface of the diaphragm was used to obtain a continuous record of the deflection of the diaphragm center as a function of inflation pressure.

Ideally, a field calibration test can be conducted on a driven pile instrumented with a number of stress cells or dilatometer blades mounted flush with the surface (S. Marchetti, personal communication, 1982). Another dilatometer can be used to profile the soil in the vicinity of the pile and to establish correspondence with the pile response observed under lateral loading. However, by most standards, this technique is time consuming and relatively cost prohibitive to implement as a routine field test.

EXPERIMENTAL STUDY

The laboratory study to be described was carried out under controlled conditions and concentrated primarily on (a) the form of the pressure-diaphragm deflection curve when the diaphragm is inflated against soil and (b) the effect of the wedging action, which takes place as a result of dilatometer penetration, on the lateral soil pressure conditions in the immediate vicinity of the blade.

The present design of the flat dilatometer yields two pressure readings that necessarily require the assumption of ideally elastic soil behavior in calculating the dilatometer modulus. With a standard dilatometer, however, a gradually decreasing p_1 obtained by repeated pressurizing of the diaphragm and the fact that on the release of the pressure following the first inflation of the membrane the buzzer is not activated again are indicative of inelastic behavior as well as permanent soil deformations effected by previous pressurizing.

To obtain the pressure-deflection curve in a continuous form, a leaf-type cantilever beam deflection sensor, instrumented with a half-bridge strain gauge arrangement, was used behind the dilatometer diaphragm. The cantilever deflection sensor had a maximum tip travel of approximately 1.13 mm (0.044 in.). No significant creep was observed in deflection readings during the experimental program. Both the deflection sensor and the diaphragm were mounted on an aluminum block, 150 mm (6 in.) long, 100 mm (4 in.) wide, and 25 mm (1 in.) thick. Experimental work was carried out in a steel bin (Figure 1). A pipe section 25 mm (1 in.) in diameter was attached to the backside of the block and was extended out through a hole on the short side of the bin. Dilatometer pressure line and deflection sensor wires were taken out through the pipe. A sand composed of angular particles was used during the experiments, and the test specimens were prepared at initial relative densities of 15, 30, and 45 percent.

Increasing lateral separation of soil as a result of dilatometer penetration was simulated by laterally forcing the aluminum block against the soil using a trailer jack mounted rigidly on a steel frame that, in turn, was welded to the short side of the bin. Overburden stress was simulated by applying a vertical force through a hydraulic jack on a rigid steel plate placed on the sand surface. The steel plate was purposely not extended over the aluminum block in order to avoid damaging the block as the vertical pressure was applied. The vertical force was measured by a load cell mounted between the steel plate and the hydraulic jack. Before the start of each test, overburden load was applied, and, through a hole cut in the steel plate, a standard dilatometer was introduced to the same depth as the aluminum block, diaphragms facing each other. Readings of p_0 and p_1 were taken by the standard dilatometer after 7 mm (0.275 in.) lateral movement of the aluminum block. The inflation pressure was measured by an electronic pressure transducer mounted on the dilatometer control box at a distance of approxi-

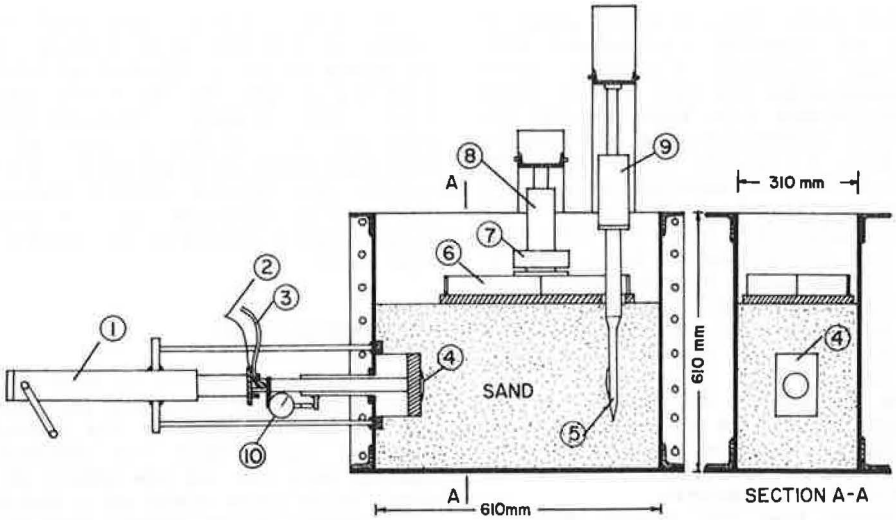

FIGURE 1 Experimental setup: 1, trailer jack; 2, deflection sensor leads; 3, pressure line; 4, aluminum block; 5, flat dilatometer; 6, pressure plate; 7, load cell; 8 and 9, hydraulic jacks; and 10, dial gauge.

mately 750 mm (30 in.) from the dilatometer block along the pressure line.

Initially, the pressure versus diaphragm center deflection curves were taken at 0-, 2-, 4-, and 7-mm lateral movement of the aluminum block. One such group of curves (a) is shown in Figure 2, which was redrawn by tracing over experimental curves. However, it was later discovered that inflating the diaphragm at 2- and 4-mm lateral penetration substantially decreased p_1 taken at 7-mm penetration. Therefore, a new series of experiments was performed in which the full inflation curves were obtained at 0- and 7-mm lateral penetration values only. At intermediate penetration values of 2, 3, 4, and 5 mm, only the p_0 readings were taken. Repeated pressurizing of the diaphragm (five times) was performed in the majority of tests at 7-mm lateral movement of the block (Curve b in Figure 2). The diaphragm calibration curves were taken several times during the experimental study by inflating the diaphragm against atmospheric pressure before the sand specimens were prepared inside the bin (Curve c in Figure 2). The net pressure-diaphragm deflection curves can subsequently be obtained with reference to this calibration curve.

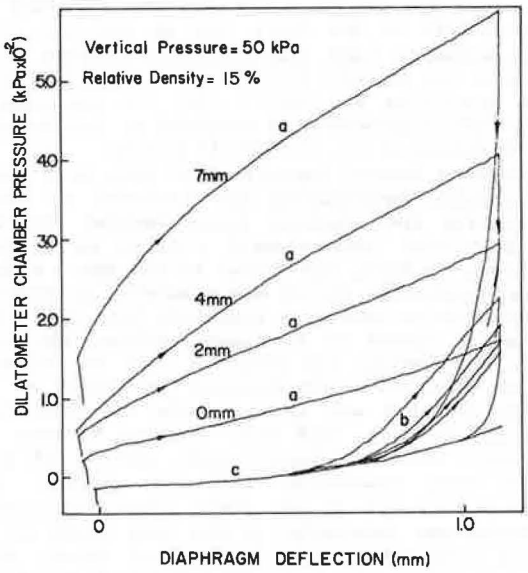

FIGURE 2 Block dilatometer chamber pressure-diaphragm center deflection curves: a, initial inflation curves; b, repeated pressurizing curves; and c, diaphragm calibration curve.

EXPERIMENTAL RESULTS AND DISCUSSION

Pressure-Diaphragm Deflection Curves

An increasingly nonlinear relationship between the pressure and the diaphragm center deflection was observed as the aluminum block was gradually forced horizontally against the soil. Curve family (a) in Figure 2 illustrates this behavior. The full inflation curves at intermediate lateral penetrations of 2 and 4 mm were taken during the first series of experiments only. At all three initial relative densities, however, within the 0- to 1-mm deflection range of the diaphragm center, no significant nonlinearity was observed on the pressure-deflection curves taken before the lateral movement of the aluminum block. This indicates that, if the diaphragm inflation were to be started at at-rest earth pressure condition, the deflection range of the diaphragm would be inadequate to detect the nonlinearity in the pressure-diaphragm deflection curve that would definitely occur at larger deflections.

If, however, the point of interest is specifically the soil stiffness for the small-strain lateral response analysis of cast-in-place piles, a relationship to be obtained between the dilatometer modulus and the modulus corresponding to lateral loading beginning with at-rest earth pressure conditions will be convenient. One such relation, shown in Figure 3, indicates linear dependence between the two modulus values. The resulting relationship is evidently independent of the relative density and overburden stress conditions. A relation of this nature should be useful in estimating the Young's modulus of the soil for possible use in formulas relating the modulus of elasticity of the soil to the lateral coefficient of subgrade reaction (12). Further testing is presently under way to investigate whether the slope of the line in Figure 3 is significantly dependent on soil type. Also, for

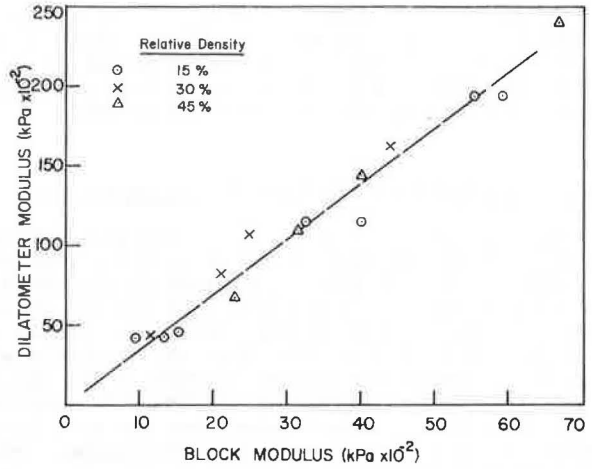

FIGURE 3 Standard dilatometer modulus versus at-rest condition block dilatometer modulus.

seismic analyses, a plot of this type is expected to yield reasonably accurate values for the small-strain shear modulus of the soil in situ if a reasonable assumption about the Poisson's ratio can be made. If the shear modulus at still smaller strains were needed, the continuous pressure-diaphragm deflection curve obtained by the cantilever beam attachment would have to be used.

In the majority of the experiments, the secant value of the dilatometer modulus calculated from the pressure-deflection curve using Equation 1 yielded reasonable average values for the modulus within the 0- to 1-mm range of lateral soil displacements. However, the tests also indicated that the initial tangent dilatometer modulus can be as much as 50 percent higher than the secant modulus. This points to the possibility of a substantially lower actual modulus value if the inflation curve is extrapolated significantly beyond the 1-mm point, or a substantially greater modulus at lateral displacements of less than 1 mm.

During the experiments, p_0 and p_1 values obtained with a standard dilatometer blade were found to be consistently less than the corresponding values obtained after laterally penetrating the aluminum block 7 mm toward the soil. Figure 4 shows the difference for 30-kPa vertical pressure at initial relative densities of 15, 30, and 45 percent. This is interpreted as reflective of the effect of vertical shear deformations accompanying lateral separation of soil during the penetration of the standard dilatometer. No such action took place as the aluminum block was forced against the soil laterally. Table 1 gives a comparison of these readings for the second test series.

Because of the lack of a provision for continu-

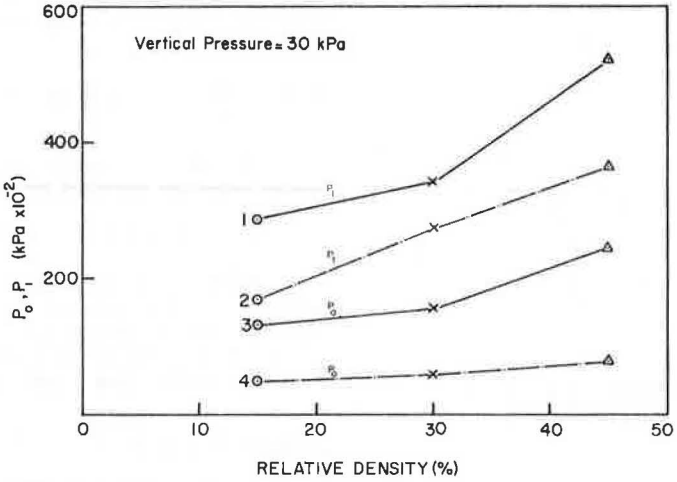

FIGURE 4 Values of p_o and p_1 obtained by standard dilatometer and the dilatometer block as a function of the initial relative density: Lines 1 and 3, aluminum block; Lines 2 and 4, standard dilatometer.

TABLE 1 Dilatometer Block and Standard Dilatometer Diaphragm Inflation Data

Initial Relative Density (%)	Vertical Pressure (kPa)[a]	Dilatometer Block (at rest)		Dilatometer Block (7 mm)		Standard Dilatometer	
		p_0 (kPa)	p_1 (kPa)	p_0 (kPa)	p_1 (kPa)	p_0 (kPa)	p_1 (kPa)
15	12.5	10	35	80	190	38	147
	30	10	50	130	285	48	167
	50	75	180	350	610	93	393
	100	110	255	460	820	133	638
30	12.5	20	50	100	265	38	152
	27	30	85	155	340	58	273
	50	45	110	235	475	78	358
	100	80	195	395	695	148	572
45	12.5	5	65	145	375	68	243
	30	27.5	110	245	520	78	363
	50	45	150	300	625	123	498
	100	85	260	445	1050	218	843

[a] 1 kPa = 0.145 lb/in.^{2}.

ously recording the movement of the diaphragm on the standard flat dilatometer, it is not possible to assess the effects of repeated pressurizing of the diaphragm on the lateral soil stiffness. The pressure to reach 1-mm deflection gradually decreases with successive cyclings of pressure. However, because the exact position of the diaphragm cannot be determined when the pressure is reduced to zero, the term S_o in Equation 1 is unknown and a new value of the dilatometer modulus cannot be determined. Continuous measurement of pressure and diaphragm deflection, however, indicated increased soil stiffness for repeated cyclings of pressure (curve group b in Figure 2), although beyond the second cycling of the pressure the change observed in the dilatometer modulus was minimal (Figure 5). Residual deformation, however, continued to build up with continued cycling of pressure. The initial upward curvature recorded on the cycling curves is thought to be due to the receding of the diaphragm by a small amount from the soil following the depressurizing of the chamber. On repressurizing, when the diaphragm-soil contact was established, the curves became significantly steeper.

It is thought that the cycling curves can be used in estimating the buildup of permanent deformations in soil surrounding piles laterally loaded in a repetitive manner. However, a viable method of establishing correspondence between the test data and the actual pile response has yet to be devised.

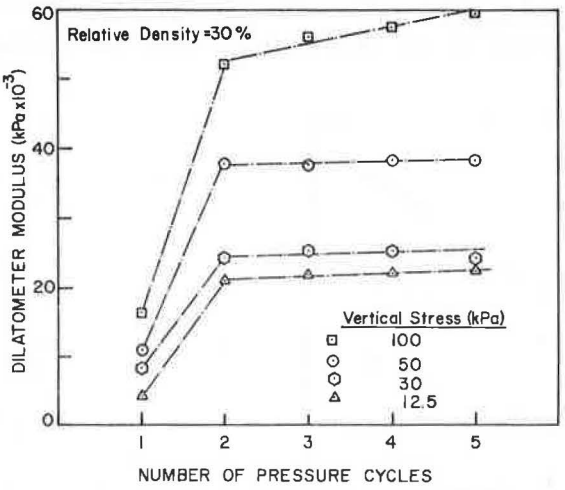

FIGURE 5 Dilatometer modulus values obtained as a function of the number of pressurizing cycles of the diaphragm.

Lateral Pressure as a Function of Soil Separation

The lateral pressure necessary to start the outward movement of the diaphragm on the block (p_0), plotted as a function of the lateral movement of the block, yielded approximately a straight line for all three relative densities and vertical pressures. Figure 6 shows two such curves. The slope of a continuous curve of p_0 versus the lateral movement of the block should indicate the coefficient of subgrade reaction of the soil for an object separating the soil laterally--in this case, the flat dilatometer. The present flat dilatometer design does not allow for obtaining such relationships in field applications. However, it would be enlightening to see if the diaphragm pressurization data taken after 7 mm of lateral deflection might be of any use in determining the value of the slope of this curve. For this, consider the curves in Figure 6. If linearity is assumed, between 0- and 7-mm lateral separation values the lateral coefficient of subgrade reaction would be

$$k_h = [(p_{0(7)}) - (p_{0(0)})]/d \quad (2)$$

In Equation 2, d is the half-thickness of the dilatometer blade. The numerical data in Figure 6 yield, for the upper curve,

$$k_h = [(245 - 27.5)/0.007] = 31\ 070\ kN/m^3$$
$$(114.3\ lb/in.^3)$$

With the block width of 100 mm (4 in.), the subgrade reaction modulus becomes

$$k = 31\ 070 \times 0.1 = 3107\ kN/m^3\ (450\ lb/in.^3)$$

A "diaphragm subgrade reaction coefficient" was defined for the purpose of comparing the soil stiffness values obtained by Equation 2 and during the inflation of the dilatometer diaphragm through Equation 1. Rearranging Equation 1 in the form

$$\Delta p/S_o = (\pi/2D)[E/(1 - \mu^2)] \quad (3)$$

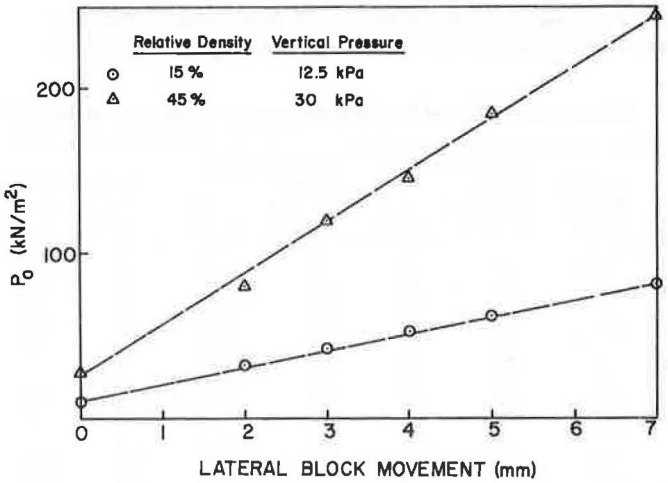

FIGURE 6 p_o versus lateral block movement curves obtained by the aluminum block.

yields the ratio of the difference between two corrected pressure readings to the diaphragm center deflection and has the same units as the subgrade reaction coefficient. Both Δp and S_o are quantities measured during a dilatometer test, and the ratio $\Delta p/S_o$ can be calculated without knowledge of the terms on the right-hand side. The data obtained by a standard dilatometer for this particular test yielded approximately 285 000 kN/m^3 (1,046 lb/in.^{3}) for the diaphragm subgrade reaction coefficient. A comparison indicates that this value is an order of magnitude greater than the lateral coefficient of subgrade reaction obtained previously.

One possible way of interpreting the difference is that, as the block penetrates laterally, yielding of the soil in the vicinity of the edges takes place, whereas, when the diaphragm is inflated, it is forced against the part of the soil that was densified by the wedging action of the dilatometer blade without yielding significantly. The difference is also believed to be partly a typical display of the dependence of the subgrade reaction on the contact area and the difference in the modes of deformation imposed by the blade, in the form of lateral penetration of a rectangular object, and by the diaphragm, as essentially axisymmetric loading of a thin plate.

A first-approximation value of the lateral subgrade reaction modulus can be computed with Equation 2 using p_0 obtained by a standard dilatometer and assuming zero in situ lateral stress. For the same initial relative density (45 percent) and the simulated overburden pressure (30 kPa) conditions considered previously, the data yielded

$$k_n = (78/0.007) = 11\ 142\ \text{kN/m}^3\ (41.0\ \text{lb/in.}^3)$$

This value, also, is substantially lower than the dilatometer subgrade reaction coefficient calculated on the basis of the diaphragm inflation data.

Because of the soil disturbance resulting from the penetration of the blade, the values of the average coefficient of subgrade reaction obtained by the standard dilatometer were substantially different from those obtained by the block. Given that the lateral subgrade reaction obtained by the block will be more representative as a design value in the case of cast-in-place piles, it is interesting to note that these two values plot approximately as a straight line at small overburden pressures with evidently little dependence on relative density (Figure 7). The slope of this line is defined here as the "disturbance index" and represents the correction factor by which the standard dilatometer subgrade reaction coefficient value should be divided to obtain a disturbance-free lateral subgrade reaction coefficient. With increasing overburden pressure, however, the effect of relative density becomes more pronounced, and, also, the straight line approximation does not remain valid (Curves a, b, and c in Figure 7). At this point it is not known whether the relationship is significantly dependent on the type of sand. In the case of piles constructed in sand, a sample of the soil can be tested in the laboratory using a setup similar to that in Figure 1 to obtain, for subsequent analyses, an approximate value of the disturbance index and, if necessary, a complete group of curves similar to those of Figure 7.

Schmertmann (22) suggests that a first approximation of the value of the lateral subgrade reaction coefficient can be obtained as the ratio of the difference between the standard dilatometer p_0 reading and the at-rest lateral earth pressure to the half-thickness of the dilatometer blade (Line c in Figure 8). Here the at-rest lateral pressure is to be estimated through a statistical relationship presented by Marchetti (3). However, as discussed previously, because of the disturbance that results from the insertion of the dilatometer blade, the undisturbed p-y relationship (Curve a in Figure 8) may be significantly different from the value calculated as the slope of Line c in Figure 8. Nevertheless, this assumption may have merit in assessing the lateral stiffness of the soil around driven piles because of the significant soil disturbance associated with the pile installation techniques.

For cast-in-place piles constructed without substantial remolding of the soil in the vicinity of the pile, a better value of the lateral subgrade coefficient can probably be obtained by dropping the in situ lateral pressure term from the calculation scheme. Although theoretically incorrect, ignoring this term will have an improving effect on the calculated value of the subgrade reaction coefficient because the remolding of the soil around the dilatometer already results in too low a value for p_0.

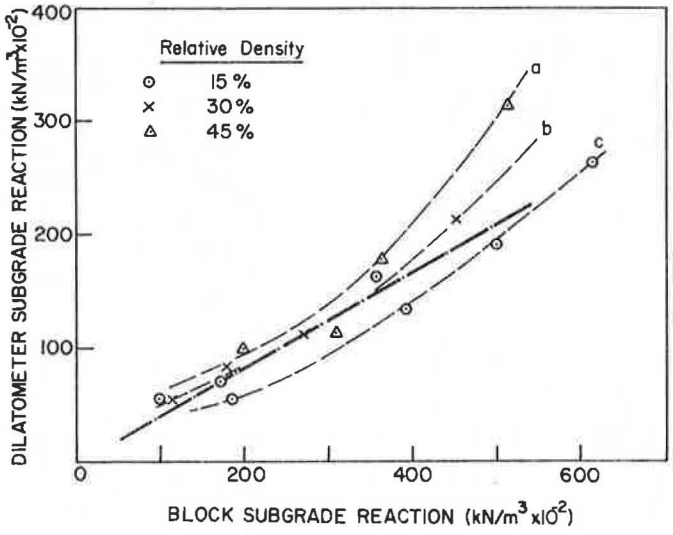

FIGURE 7 Relationship between average values of dilatometer and block subgrade reaction calculated over a separation distance of 7mm.

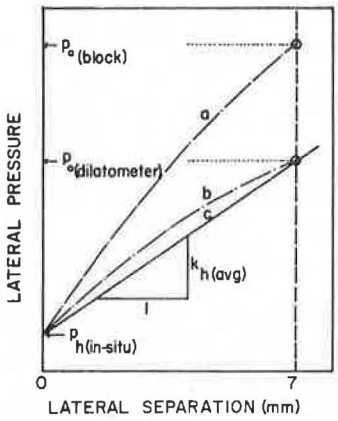

FIGURE 8 Qualitative comparison of the block and standard dilatometer lateral separation-pressure curves and the lateral subgrade reaction coefficient ($k_{h,avg}$) as suggested by Schmertmann *(22)*; p_h is the at-rest lateral earth pressure.

This argument assumes that the p_0 value obtained by the dilatometer is always less than what it would be if lateral soil separation were not accompanied by vertical shear deformations around the blade during penetration, which implies contractive soil behavior. The effect of possible delative behavior is not known at present and further work is planned to clarify this point.

A case study on a pier foundation 1370 mm (4.5 ft) in diameter and 4500 mm (15 ft) long constructed in a silt soil yielded good agreement between the measured lateral pier-top displacement and the computed value obtained by using the subgrade reaction coefficient corrected according to Figure 7. In the analysis, the slope of the initial straight line portion of p-y curves (6) was computed on the basis of the corrected subgrade reaction coefficient. An extensive field calibration study, however, appears to be absolutely necessary to evaluate the potential of the flat dilatometer for securing data for use in pile analyses under lateral loading, especially if a strong nonlinearity is present in the lateral response characteristics of the soil.

The test results presented indicate that the direct use of the diaphragm subgrade reaction coefficient (as defined in Equation 3) in analyses will probably result in a substantial overestimation of the actual soil stiffness for the pile dimensions considered. It should, however, also be stressed that the laboratory study was conducted on a sand. At the present time, the writers do not have data on this aspect of the behavior of cohesive soils.

CONCLUSION

The results obtained, although preliminary in nature, point out some of the factors that have to be considered and the questions that need to be answered in order to realize the full potential of the flat dilatometer. The potential certainly exists for using dilatometer data in estimating the subgrade coefficient of soils for lateral loading. In its present form, the flat dilatometer is capable of yielding an average soil modulus instead of a complete description of the lateral stress-displacement (p-y) relationship, and the modulus value obtained will probably reflect the soil stiffness within a small deflection range.

This study points out a viable procedure for obtaining representative values of soil stiffness for piles constructed in place with little disturbance to the soil in the immediate vicinity. The subgrade reaction modulus obtained by a standard dilatometer can be corrected for soil disturbance to give a representative value for the disturbance-free soil stiffness. However, the more general problem of relating the data to the actual soil stiffness as a function of the pile cross section and the method of pile installation is presently the primary obstacle that has to be removed through further study. Research should also address the question of whether the dilatometer modulus can effectively be combined with the subgrade reaction modulus obtained by Equation 2 to substantiate data on the lateral stiffness of a soil (e.g., evaluating nonlinear effects).

REFERENCES

1. S. Marchetti. A New In-situ Test for the Measurement of Horizontal Soil Deformability. Proc., Conference on In Situ Measurement of Soil Properties, ASCE, New York, Vol. 2, 1975, pp. 255-259.
2. S. Lacasse and T. Lunne. Penetration Tests in Two Norwegian Clays. Proc., Second European Symposium on Penetration Testing, Amsterdam, The Netherlands, Vol. 2, 1982, pp. 661-670.
3. S. Marchetti. In Situ Tests by Flat Dilatometer. Journal of the Geotechnical Engineering Division, ASCE, Vol. 106, No. GT3, 1980, pp. 299-321.
4. S. Marchetti. Detection of Liquefiable Sand Layers by Means of Quasi-Static Penetration Tests. Proc., Second European Symposium on Penetration Testing, Amsterdam, The Netherlands, Vol. 2, 1982, pp. 689-696.
5. J.M.O. Hughes, P.R. Goldsmith, and H.D.W. Fendall. Full Scale Laterally Loaded Pile Test at the Westgate Freeway Site, Melbourne, Australia: Load Deflection Predictions and Field Results. Report 190. Department of Civil Engineering, University of Auckland, Auckland, New Zealand, 1979, 80 pp.
6. H.G. Poulos. Behavior of Laterally Loaded Piles: II-Pile Groups. Journal of the Soil Mechanics and Foundations Division, ASCE, Vol. 97, No. SM5, 1971, pp. 733-751.
7. L.C. Reese, W.R. Cox, and F.D. Koop. Analysis of Laterally Loaded Piles in Sand. Paper UTC 2080. Presented at the Fifth Annual Offshore Technology Conference, Houston, Tex., 1974.
8. L.C. Reese and R.C. Welch. Lateral Loading of Deep Foundations in Stiff Clay. Journal of the Geotechnical Engineering Division, ASCE, Vol. 101, No. GT7, 1975, pp. 633-649.
9. L.C. Reese, W.R. Cox, and F.D. Koop. Field Testing and Analysis of Laterally Loaded Piles in Stiff Clay. Paper OTC 2312. Proc., Seventh Offshore Technology Conference, Houston, Tex., 1975.
10. B.B. Broms. Lateral Resistance of Piles in Cohesive Soils. Journal of the Soil Mechanics and Foundations Division, ASCE, Vol. 90, No. SM2, 1964, pp. 27-63.
11. K. Terzaghi. Evaluation of Coefficient of Subgrade Reaction. Geotechnique, Vol. 5, No. 4, 1955, pp. 297-326.
12. A.S. Vesic. Bending of Beams Resting on Isotropic Elastic Solid. Journal of the Engineering Mechanics Division, ASCE, Vol. 87, No. EM2, 1961, pp. 35-53.

13. A.S. Vesic. Beams on Elastic Subgrade and the Winkler's Hypothesis. Proc., 5th International Conference on Soil Mechanics and Foundation Engineering, Paris, France, Vol. 1, 1961, pp. 845-850.
14. A.J. Francis. Analysis of Pile Groups with Flexural Resistance. Journal of the Soil Mechanics and Foundations Division, ASCE, Vol. 90, No. SM3, 1964, pp. 1-32.
15. F. Baguelin and J.F. Jezequel. Further Insights on the Self-Boring Technique Developed in France. Proc., ASCE Specialty Conference on In-Situ Measurement of Soil Properties, Raleigh, N.C., Vol. 2, 1975, pp. 231-243.
16. L. Menard. Rules for the Calculation of Bearing Capacity and Foundation Settlement Based on Pressuremeter Tests. Proc., 6th International Conference on Soil Mechanics and Foundation Engineering, Toronto, Canada, Vol. 2, 1965, pp. 295-299.
17. R.L. Handy, B. Remmes, S. Moldt, A.J. Lutenegger, and G. Trott. In Situ Stress Determination by Iowa Stepped Blade. Journal of the Geotechnical Engineering Division, ASCE, Vol. 108, No. GT11, 1982, pp. 1405-1422.
18. D.J. D'Appolonia, E. D'Appolonia, and R.F. Brisette. Discussion of Settlement of Spread Footings on Sand. Journal of the Soil Mechanics and Foundations Division, ASCE, Vol. 96, No. SM2, 1970, pp. 754-762.
19. I. Yoshida and R. Yoshinaka. A Method to Estimate Modulus of Horizontal Subgrade Reaction for a Pile. Soils and Foundations, Vol. 12, No. 3, 1972, pp. 1-17.
20. M.T. Davisson. Lateral Load Capacity of Piles. In Highway Research Record 333, TRB, National Research Council, Washington, D.C., 1970, pp. 104-112.
21. A.W. Skempton. The Bearing Capacity of Clays. Building Research Congress, Institution of Civil Engineers, Division 1, Part 3, 1951, pp. 180-189.
22. J.H. Schmertmann, ed. DMT Digest 4. GPE, Inc., Gainesville, Fla., 1984.

Publication of this paper sponsored by Committee on Soils and Rock Instrumentation.

Abridgment

Pavement Failure Investigation: Case Study

VISHNU A. DIYALJEE

ABSTRACT

An investigation of pavement distress occurring along a major two-lane roadway 5 years after its construction is presented. The primary objective of the study was to determine the probable cause or causes of the pavement distress. The investigation involved a condition survey and an examination of the pavement structure and subgrade through soil borings. The condition survey showed that outer wheel path rutting and associated cracks were severe on both lanes and covered about 68 percent of the overall length of the roadway. The soils investigation revealed that the bank gravel subbase was saturated and the bituminous base course had deteriorated to a virtually cohesionless material that could be easily removed with the fingers. Distinct rapid seepage of water was observed at the interface of the base and subbase layers and within the subbase. On the basis of the findings of the investigation, it was concluded that the major factor causing distress was free water trapped within the pavement structure. This water, it was reasoned, infiltrated the pavement through cracks and a porous surface but because of the poor drainability of the subbase was unable to leave the pavement through the shoulders. This situation resulted in the pavement existing in a "bathtub" condition.

Most, if not all, flexible pavement structures undergo some form of distress during their design life. Investigation of the cause or causes of distress is required for successful pavement rehabilitation and to provide data for improving or modifying design methods, construction techniques, and job specifications.

An investigation undertaken to determine the probable cause or causes of continually occurring pavement distress along a major two-lane roadway is described.

BACKGROUND

The roadway investigated is located in Trinidad, West Indies, an island with a uniform average yearly temperature of 26° C (79° F) and annual rainfall of

1.5 to 3.0 m (5 to 10 ft). This roadway, situated in the Southern Basin, was constructed in 1975 as a connector road between a major four-lane divided highway and a secondary road at the southern extremity of the four-lane highway.

The cross section of the connector road consisted of two 3.66 m (12 ft) travel lanes with 1.22-m (4-ft) shoulders. The design pavement thickness was 267 mm (10.5 in.) under the travel lanes and consisted of 127 mm (5 in.) of asphaltic concrete pavement overlying 140 mm (5.5 in.) of down-graded bank gravel subbase with a maximum size of 38 mm (1.5 in.) and 25 percent passing the 0.074 mm (No. 200) mesh. The shoulder design consisted of 89 mm (3.5 in.) of chip-sealed asphaltic concrete overlying the bank gravel subbase.

Outer wheel path ruts, longitudinal cracks, and pavement distortions along both lanes of the roadway prompted an investigation to be undertaken in June 1980. The investigation included a pavement condition survey and a subsoil investigation. Before this investigation, isolated areas had been overlaid but the previous distress recurred.

CONDITION SURVEY

This survey, done by the guidelines outlined in the Manual for Condition Rating of Flexible Pavements (1), indicated that the major pavement distress manifestations were

1. Outer wheel track rutting and associated fatigue cracks,
2. Pavement distortion, and
3. Longitudinal cracks and depressions along the shoulders.

These distress manifestations were predominant along the eastbound lane where only about 6 percent of the pavement surface was free from major defects.

SUBSOIL INVESTIGATION

Test Holes

Five boreholes, including two groundwater observation holes, and three test pits were sunk at locations shown in Figure 1. During the drilling, the following were observed:

1. Rapid seepage of water at the interface of the asphaltic base course and bank gravel layers and through the bank gravel itself. The quantity of flow was measured as roughly 76 cm^3 (0.003 ft^3) per second in Borehole 1.
2. Seepage or "bleeding" of water through cracks in the pavement surface.
3. Deterioration of the asphaltic concrete base course. This layer was found to be deficient in asphalt and extremely brittle. In Borehole 2, for example, the base course had deteriorated into an almost cohesionless material that could be easily removed with the fingers.

Groundwater Conditions

No groundwater was encountered in the test holes or in the two observation boreholes sunk off the edge of the shoulder. The observation holes were drilled to a depth of 5 m (15 ft) relative to the elevation of the carriageway at the test boring locations and observed over a period of 2 weeks following the site investigation.

Soil Profile

The profile deduced from the boreholes consisted of structural pavement layers overlying a silty clay subgrade soil. The thickness of the structural pavement varied between 300 and 584 mm (12 and 23 in.) and consisted of 120 to 406 mm (5 to 16 in.) of asphaltic concrete pavement. The subbase course consisted of bank gravel varying in thickness between 127 and 180 mm (5 and 7 in.).

SOIL CHARACTERISTICS

Atterberg limits, shear strength, and standard Proctor compaction results for the subgrade soil are shown in Figures 2 and 3, and California bearing ratio (CBR) test results are summarized in Table 1.

The subgrade soil was mainly of the CH type and exhibited very high potential expansiveness (Figure 4) as determined from Williams' chart (2).

Although swelling of the subgrade soil can contribute to pavement failure, there was no consistent evidence from the condition survey and the soils investigation that the distress along the carriageway was caused by subgrade volume change.

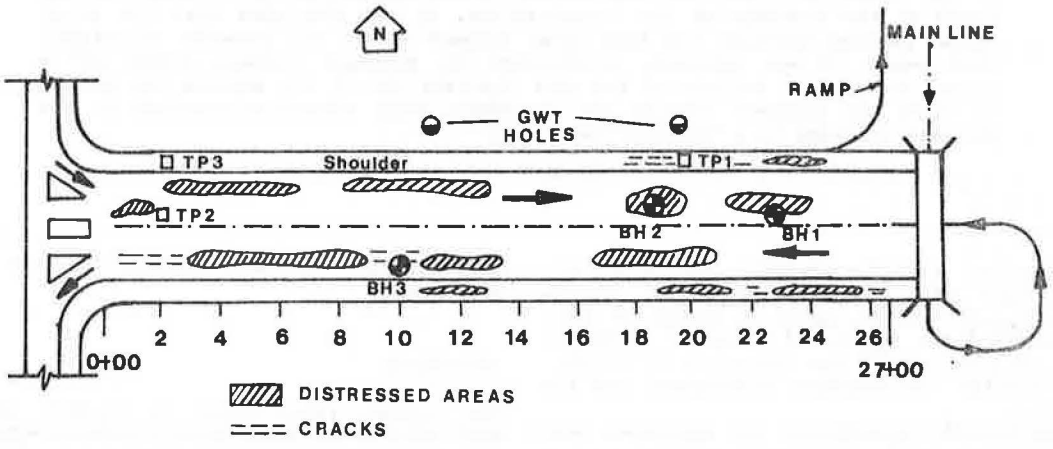

FIGURE 1 Plan of connector road.

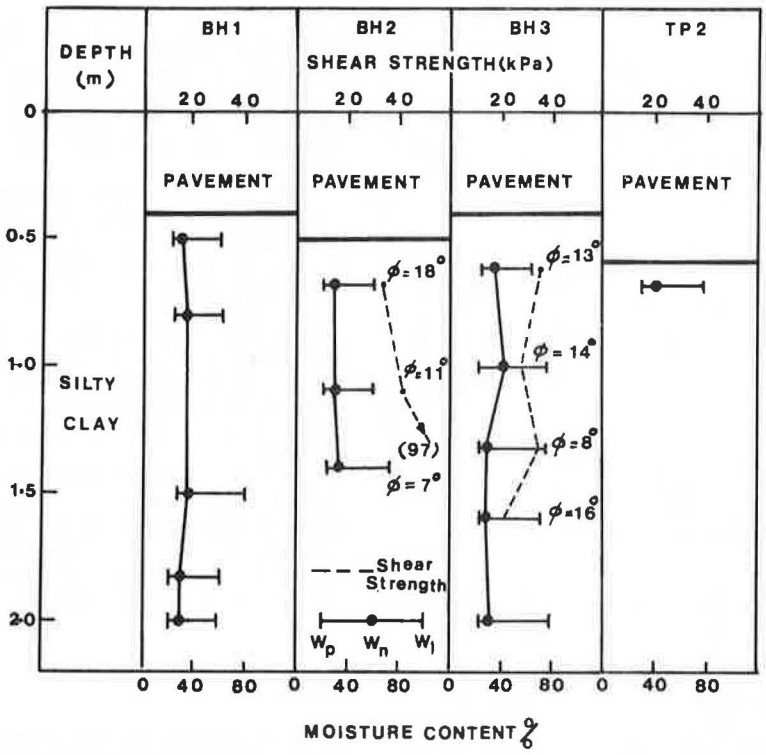

FIGURE 2 Moisture content and shear strength versus depth.

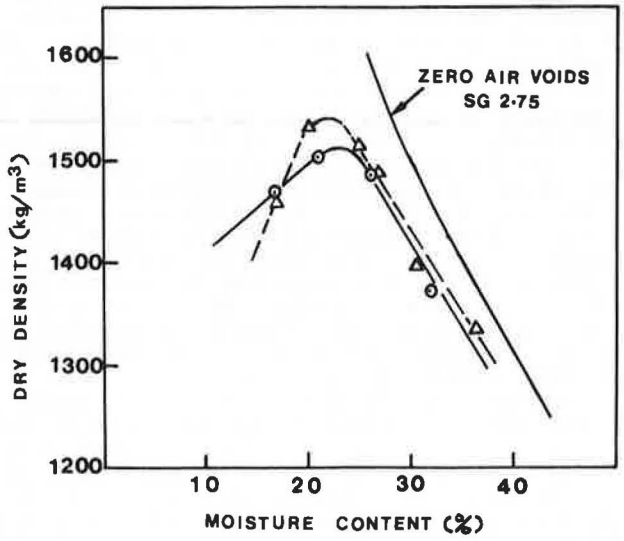

FIGURE 3 Moisture-density relationship of subgrade soil.

TABLE 1 Summary of California Bearing Ratio Test Results

Test Pit	Bulk Density in kg/m³ (lb/ft³)	Dry Density in kg/m³ (lb/ft³)	MC (%)	CBR[a] (%)	Swell (%)	Remarks
1	1902 (119)	1514 (94)	25.6	6.8		Remolded
		1538 (96)	22			Standard Proctor optimum
1		–	–	3.2	2.5	4-day soak
2	1891 (118)	1458 (91)	32	6.6		In situ
3	1869 (117)	1506 (94)	24	7.1		Remolded
		1510 (94)	23			Standard Proctor optimum
3				2.5	2.6	4-day soak

[a]Average of CBR values obtained from testing both top and bottom of specimen.

SUBGRADE STRENGTH

For pavement design, the strength of the subgrade in tropical climates is normally assessed in terms of the California bearing ratio. Using shear strength parameters, c = 36 kPa (5.22 psi) and ϕ = 14 degrees, and average of values within the top 0.6 m (2 ft) of subgrade in Boreholes 2 and 3, an estimated in situ CBR value of 6.3 percent was obtained (3). This value compares favorably with 6.6 percent obtained from laboratory tests on an in situ sample, (Table 1).

Although several criteria have been proposed for determining the soil strength to be used for design purposes (4-6), the 4-day soaking period is considered the most appropriate for soils exhibiting appreciable swell and for climates in which annual rainfall exceeds 245 mm (9.6 in.) (6). Therefore, the CBR of 2.9 percent rounded to 3 percent was considered appropriate for design.

DESIRABLE PAVEMENT THICKNESS

As a first step in pinpointing the cause of the pavement failures, the adequacy of the pavement design of the connector road was checked using the National Crushed Stone Association method of design (7). This method was chosen in the absence of actual traffic data.

Using a CBR of 3 percent, pavement thicknesses of 533 mm (21 in.), 610 mm (24 in.), 660 mm (26 in.), and 762 mm (30 in.) were obtained for four categories of traffic loadings--medium, medium heavy,

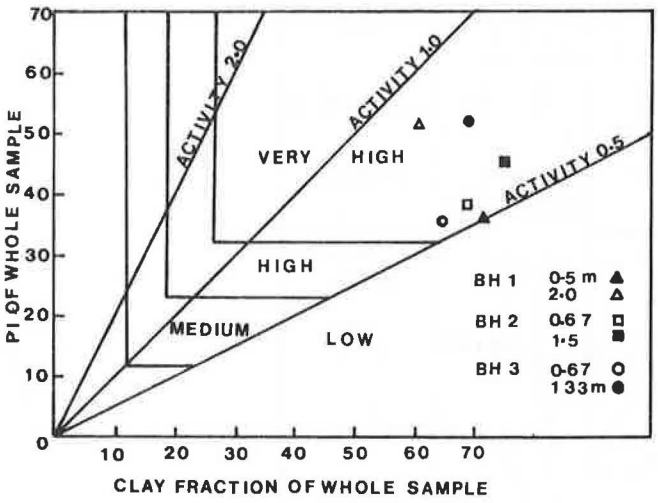

FIGURE 4 Plasticity index versus minus 2μ fraction.

heavy, and very heavy. These pavement thicknesses are considerably greater than is the design pavement thickness of the roadway.

Except for the design pavement thickness of 267 mm (10.5 in.) for the connector road, no information could be found on the "thickness design" of this roadway. However, for the adjoining main-line (four-lane) highway the design pavement thickness was 394 mm (15.5 in.). This thickness was determined using the Asphalt Institute's method of design (8), a design CBR of 2.5 percent, design traffic number of 82, and a 20-year design life (1970 to 1990). This pavement was made up of 234 mm (9.2 in.) of asphaltic concrete pavement overlying 140 mm (5.5 in.) of downgraded bank gravel.

The pavement thickness of the connector road was considerably less than that of the main line. However, when the in situ thickness of the connector road at the time of investigation is considered, the average pavement thickness as well as asphalt pavement thickness far exceeded the design thickness of the main line.

Because the connector road was only 5 years old at the time of this investigation, the design thickness of 267 mm (10.5 in.) should have been adequate for a design traffic intensity similar to that of the main line using planned stage construction for a specified period (8).

It is of interest to note, however, that in a recent 20-year design (1980 to 2000) of the south extension of the main line, a pavement thickness of 851 mm (33.5 in.) was recommended. This design was based on a design traffic of 2 to 6 million standard axles and a subgrade CBR of 2 percent. The design pavement was to be made up of 76 mm (3 in.) of asphaltic concrete surface and leveling courses, 150 mm (6 in.) of asphaltic concrete base course, 200 mm (8 in.) of crushed rock base course, and 425 mm (17 in.) of stone and sand-free clay surface coatings.

Compared to the 1970 and 1975 main-line and connector road designs, this recent design suggests a large escalation in axle loads that could probably not have been anticipated during the previous designs. This increase in traffic was due to the increased off-shore exploration along the south coast of Trinidad and the increasing sales of commercial and passenger vehicles caused by a booming economy--the spin-off of increased world market oil prices in the mid 1970s. In 1979, for example, the waiting period for a new vehicle was about 3 years.

On the basis of the foregoing, it can be readily concluded that both the connector and the main line were seriously underdesigned. On the other hand, because the connector road with an in situ asphaltic concrete pavement of 406 mm (16 in.) and an overall pavement thickness of 583 mm (23 in.) still suffered failures, it is questionable whether inadequate pavement thickness was the principal cause of distress.

Corroboration that inadequate pavement thickness was not the principal factor was provided by an investigation of the northbound carriageway of the main line in areas where seepage through the pavement surface was noted. In such areas the only external evidence of pavement distress was short discontinuous longitudinal cracks concentrated along the inner and outer wheel paths. Investigation of these areas showed pavement seepage and deterioration of the asphaltic base course similar to that found during the investigation of the connector roadway.

On the basis of these observations, it was concluded that the major factor influencing distress along travel lanes of the connector road was water trapped within the pavement section. Inadequate pavement thickness, although identified, was not considered a significant factor.

DISCUSSION

It is surmised, in the absence of detailed information on the history of construction or postconstruction performance of this roadway, that this water entered the pavement from surface infiltration through cracks and a porous asphalt surface. This conclusion was reached because there was no evidence of groundwater seepage in any of the test holes or groundwater observation holes. That the roadway section investigated was entirely on fill ruled out the possibility of lateral seepage as well. It should be noted that, up to the time of this investigation, crack sealing was not normally carried out in Trinidad as part of the routine maintenance of roadways.

The loss of serviceability of the base course as a result of the presence of water is readily appreciated on examination of the base course. As mentioned previously, this layer has been reduced to an almost cohesionless material. It is the author's opinion that the drainage of the entrapped water occurs only by "bleeding" through the pavement surface as noted during the investigation.

Bleeding occurs through cracks in the pavement surface and is encouraged by repeated traffic loadings and thermal changes. Bleeding was noted to occur principally during the warmer portion of the day. The effect of increased temperature is to heat the air entrapped in the pavement and thereby give the water a "lift."

Good lateral drainage of the pavement structure, a factor considered essential to pavement longevity, could only have occurred through the bank gravel subbase course. However, the bank gravel used was moderately plastic (liquid limit 29 percent, plastic limit 18 percent). In addition, properly compacted bank gravel has a low permeability due to the high percentage of minus 0.074 mm (No. 200) fraction. Low drainability of the subbase was substantiated by the following observations:

- The amount of water observed to be contained within the carriageway on removal of the asphaltic layers and
- Water standing for a day or two on the surface of the subbase material after a period of rainfall.

The combination of the poor drainability of the subbase and the presence of water caused the pavement section to exist in a "bathtub" condition (9).

CONCLUSION

An investigation of the cause of pavement distress along a major two-lane roadway has been described. The results of this study have shown that the major factor affecting pavement performance was free water trapped within the pavement section. Overall, this study demonstrates the influence of water on pavement performance and the necessity for providing good drainage within the pavement structure in climates with moderate to heavy rainfall.

ACKNOWLEDGMENTS

The work described was undertaken by the author during employment as Civil Engineer, Soils, in charge of the Soils and Materials Branch of Ministry of Transportation and Communications, Trinidad. The use of the information presented is gratefully acknowledged. The author also acknowledges the assistance of Joanne Donnelly in typing this manuscript.

REFERENCES

1. Manual for Condition Rating of Flexible Pavements--Distress Manifestations. Research and Development Division, Ministry of Transportation and Communications, Toronto, Ontario, Canada, Aug. 1975.
2. A.A.B. Williams. Discussion of The Prediction of Total Heave from the Double Oedometer Test by J.E.B. Jennings and K. Knight. Transactions, South African Institution of Civil Engineers, Vol. 8, No. 6, 1985, pp. 123-124.
3. W.P.M. Black. The Calculation of Laboratory and In-Situ Values of California Bearing Ratio from Bearing Capacity Data. Geotechnique, Vol. 11, No. 1, March 1961, pp. 14-21.
4. K. Russam. The Prediction of Subgrade Moisture Conditions for Design Purposes. Moisture Equilibria and Moisture Changes in Soils Beneath Covered Areas, Butterworths Publishing, Ltd., Sydney, Australia, 1965.
5. M.P. O'Reilly and R.S. Millard. Road Materials and Pavement Design on Tropical and Sub-Tropical Countries, Report LA279. Transport and Road Research Laboratory, Crowthorne, Berkshire, England, 1969.
6. E.J. Yoder and M.W. Witczak. Principles of Pavement Design, 2nd ed. John Wiley and Sons, Inc., New York, 1975.
7. Flexible Pavement Design Guide for Highways. National Crushed Stone Association, Washington, D.C., April 1975.
8. Asphalt Institute Method of Design Manual Series 1 (MS-1). Asphalt Institute, College Park, Md., 1969.
9. H. Cedergren. Drainage of Highway and Airfield Pavements. John Wiley and Sons, Inc., New York, 1974.

Publication of this paper sponsored by Committee on Subsurface Drainage.